Dissertation
submitted to the

Combined Faculty of Natural Sciences and Mathematics
of the Ruperto Carola University Heidelberg, Germany
for the degree of
Doctor of Natural Sciences

Presented by
M.Sc. Molecular Biotechnologist
Verena Martina Rickert-Zacharias
born in Aschaffenburg, Germany

Oral examination: 06.09.2018

Design, synthesis characterization and application of FRET probes for the detection of channel-activating protease (CAP) activity

Referees: Dr. Anne-Claude Gavin
Prof. Dr. Ralf Bartenschlager

Table of Contents

I Abbreviations

aa	amino acids
AEC	airway epithelial cells
a.u.	arbitrary units
AMC	7-amino4-methyl-coumarin
ASL	airway surface liquid
A1AT	alpha-1-antitrypsin
BAL	bronchoalveolar lavage
ENaC-Tg	ENaC-overexpressing
equi.	equivalents
CAP	channel-activating protease
CTSB	cathepsin B
CTSS	cathepsin S
CF	cystic fibrosis
CFTR	cystic fibrosis transmembrane conductance regulator
Cou343	Coumarin343
COMU	(1-Cyano-2-ethoxy-2-oxoethylidenaminooxy) dimethylamino- morpholino-carbenium-hexafluorophosphate
CPP	cell-permeable peptide
DCM	dichloromethane
DIPEA	diisopropylethylamine
DMF	dimethylformamide
DNA	deoxyribonucleic acid
D/A	donor/acceptor
ENaC	epithelial sodium channel
ESI	electrospray ionization
FACS	fluorescence activated cell sorting
Fmoc	fluorenylmethoxycarbonyl
FRET	Foerster resonance energy transfer

GPI	glycosylphosphatidylinositol
HAI	Hepatocyte growth factor activator inhibitor
HAT	human airway trypsin-like protease
HBTU	2-(1H-Benzotriazole-1-yl)-1,1,3,3-tetramethyluronium hexafluorophosphate
hNEC	human nasal epitheiial cells
IPF	idiopathic pulmonary fibrosis
h/m	human/murine
HL-60	neutrophil-like cell line
mTEC	murine tracheal epithelial cells
MetOCou	7-amino methoxy coumarin
Mtt	4-Methyltrityl
NE	neutrophil elastase
HPLC	high-pressure liquid chromatography
LPS	lipopolysaccharide
LUT	look up table
MeOCou	7-amino- 4-methoxy-coumarin
MMP	matrix-metalloproteinase
Palm	palmitic acid
Peg	polyethylenglycol
RNA	ribonucleic acid
SD	standard deviation
SEM	standard error of the mean
ST-14	suppressor of tumorigenicity- 14
SPLUNC	short-palate lung and nasal epithelial clone
TAMRA	5,6-carboxytetramethylrhodamine
TBTA	1-hydroxybenzotriazole
TFA	trifluoroacetic acid
TMPRSS	transmembrane protease, serine
TRIS	tris(hydroxymethyl)-aminomethan
WT	wild type

II List of Figures

III List of Tables

IV Abstract

The epithelial sodium channel (ENaC) and the proteolytic processing of its alpha- and γ-subunits by channel-activating proteases (CAPs) play a crucial role in sodium transport across different epithelial membranes, including the airways, and in airway surface liquid (ASL) homeostasis. The loss of ion transport homeostasis results in various diseases, including one of the most frequent lethal genetic disorders: Cystic fibrosis. The fundamental cause of the disease is a mutation of a chloride channel, resulting in loss or reduction of chloride secretion. Not only the chloride transport is affected, but also the sodium transport *via* ENaC which is increased in CF. It has been shown that CAP expression is elevated in primary bronchial epithelial cultures of Cystic Fibrosis (CF) patients compared to tissue from healthy subjects. However, the impact of CAPs on ENaC activity and ASL regulation in the CF lung disease is unknown.

In order to study the role of CAPs in CF lung disease and their regulation in the disease context, substrate-based Förster Resonance Energy Transfer (FRET) probes were developed for measuring protease activity. In contrast to most commercial substrates, the probes presented in this work, are equipped with two fluorophores. Proteolytic cleavage of the probe resulted in a loss of FRET, giving a ratiometric readout reflecting enzyme activity. The attachment of a lipid anchor enabled the detection of membrane-associated enzyme activity in a spatially resolved manner. Different substrate sequences and fluorophore combinations were synthesized and tested towards their physical and biochemical properties. Not only extension or contraction in the amino acid sequence between both fluorophores affects the efficacy of FRET and maximal fold change of the ratio upon full cleavage of the probe, but also the identity of the flanking amino acids significantly contributes. For the lipidated probes, the combination of Coumarin 343 and TAMRA turned out to be the best working combination.

Probes based on different substrate sequences have been evaluated with respect to selectivity for CAPs over other proteases. *In vitro* characterization using recombinant enzymes as well as cell-based characterization using broad-spectrum inhibitors identified the probe based on the CAP cleavage site in the human ENaC γ-subunit as the most selective one towards CAP activity. Probes based on the autoactivation cleavage site of CAP3, however, also have sufficient specificity and perform better with respect to localization and dynamic range compared lipidated versions. Furthermore, the fluorophore combination and potentially the insertion of the lipid anchor significantly affect the specificity.

As proof of concept, the probes were successfully tested in primary human nasal epithelial cells and primary murine tracheal epithelial cells. Application of the probes to a small cohort of CF patients and a healthy control showed that the novel FRET probes are able to detect increased CAP activity in nasal cells from CF patients compared to healthy control samples. Murine tracheal epithelial cells of βENaC-transgenic mice, a mouse model for CF lung disease, however, have significantly reduced CAP activity compared to cells isolated from wild type mice.

Both experimental sets suggested that our FRET probes are a useful tool to measure CAP1 and CAP3 as potential biomarkers in human specimens for different diseases as well as research tools for further investigation of CAP activity in chronic lung diseases, including CF, idiopathic pulmonary fibrosis and lung cancer.

V Zusammenfassung

Epitheliale Natriumkanäle (ENaC) und die proteolytische Prozessierung der α- und γ-Untereinheiten durch Kanal aktiviernde Proteasen (CAPs) spielen eine wichtige Rolle beim Natriumtransport über verschiedene epitheliale Gewebe, einschließlich der atemwege, und der Homöstase des Atemwegsflüssigkeit. Der Verlust des Ionentransport-Gleichgewichts führt zu verschiedenen Erkrankungen, einschließlich einer der häufigsten, genetischen lethalen Erkrankungen: Zystische Fibrose (Mukoviszidose, CF). Die grundlegende Ursache der Erkrankung ist eine Mutation in einem Chloridkanal, die zu einem Verlust oder der Reduktion der Chloridsecretion führt. Es ist jedoch nicht nur der Chloridtransport betroffen, sondern auch der Natriumtransport über ENaC, der in CF erhöht ist. Es wurde gezeigt, dass die Expression von CAPs auf primären Bronchienepithel-Kulturen von CF – Patienten gegenüber Gewebeprobe von gesunden Probanden erhöht ist. Die Bedeutung der CAPs auf die Aktivität von ENaC und die Regulation der Atemwegsflüssigkeit im Zusammenhang mit der CF-Lungenerkrankung ist bisher unklar.

Um die Rolle der CAPs bei der CF Lungenerkrankung und ihre Regulation in diesem Zusammenhang zu untersuchen, wurden Substrat-basierte Förster- Resonanzenergietransfer (FRET)-Sonden entwickelt, mit dem Ziel, die Enzymaktivität zu messen. Im Gegensatz zu den meisten kommerziell erhältlichen Substrasten wurden die Sonden, die in dieser Arbeit präsentiert werden, mit zwei Fluorophoren ausgestattet, so dass ein ratiometrisches Auslesen die Enzymaktivität wiederspiegelt. Das Anhängen eines Lipidankers ermöglicht die Detektion der Membran-assoziierten Enzymaktivität mit räumlicher Auflösung. Verschiedene Substratsequenzen und Fluorophorkombinationen wurden hergestellt und auf ihre phyikalischen und biochemischen Eigenbeschaften hin untersucht. Nicht nur die Verlängerung oder Verkürzung der Aminosäuresequenz zwischen den Fluorophoren beeinflussen die Effizienz des FRET und die maximale Änderung des Verhältnisses bei vollständiger Spaltung, sondern auch flankiernde Aminosäuren tragen signifikant dazu bei. Für die lipidierten Sonden zeigte sich die Kombination aus Coumarin 343 und TAMRA als beste Fluorophor-Kombination.

Sonden, basierend auf verschiedenen Substratsequenzen, wurden hinsichtlich ihrer Spezifität für CAPs über andere Proteasen untersucht. Sowohl die Charakterisierung *in vitro* mit Hilfe rekombinanter Enzyme, als auch die Zell-basierte Untersuchung unter Verwendung von Breitspektrum-Inhibitoren identifizierten die Sonden, die auf der Schnittstelle der γ-Untereinheit von ENaC basieren, als die spezifischste für CAPs. Die Sonden, die auf der Schnittstelle für die Selbstaktvierung von CAP3 basieren, weisen eine ausreichende Spezifität auf und funktionieren als lipidierte Sonden besser hinsichtlich ihrer Lokalisierung und der dynamische Breite. Außerdem ist zu

bemerken, dass die Fluorophorkombination sowie möglicherweise das Anhängen des Lipidankers signifikant zur Spezifität beitragen.

As Nachweis der Machbarkeit wurden die Sonden erfolgreich auf primären humanen Nasenepithel-Zellen und murinen Luftröhren-Zellen getestet. Die Auswertung einer kleinen Kohorte von CF-Patienten und gesunden Kontrollen konnte zeigen, dass die neuartigen FRET-Sonden in der Lage sind, die erhöhte CAP activity in Nasenzellen von CF-Patienten gegenüber gesunden Kontrollen zu messen. Murine Luftröhren-Zellen von βENaC-transgenen Mäusen, ein Mausmodell für die CF-Lungenerkrankung, zeigen signifikant verringerte CAP activity im Vergleich zu Zellen, die aus Wildtyp-Mäusen isoliert wurden.

Beide Experimente schlagen unsere neuen FRET-Sonden sowohl als Messinstrument für CAP1 und CAP3 als mögliche Biomarker bei humane Proben für verschiedene Krankheiten, als auch als Werkzeug für die Forschung vor, um die Regulation von CAPs in chronischen Lungenerkrankungen wie CF, idiopathische Lungenfibrose oder Lungenkrebs zu untersuchen.

1. Introduction

1.1 Ion transport defects in cystic fibrosis

Cystic fibrosis (CF) is among the most common lethal genetic disorders in the Caucasian population with 1 case per 2500 newborns in Germany. It is caused by mutations in the cystic fibrosis transmembrane conductance regulator (CFTR) gene, resulting in dysfunctional chloride channels in of many epithelial tissues. This leads to reduced transport of chloride and hydrogen carbonate ions across the apical membrane into the airway surface liquid[3]. Although CF affects many organs, the major cause for morbidity and mortality is the severe lung disease[4-5]. The following discussion focusses on CF lung disease.

Numerous mutations in the CFTR gene are known and they have various effects on CFTR function and consequently on the severity of the disease. In general, the lack of functional CFTR leads to reduced transport of chloride and hydrogen carbonate ions across the apical membrane into the airway surface liquid[3].

In healthy tissue, anion transport is coordinated with sodium absorption across epithelial sodium channels (ENaC). As consequence of the sodium absorption, the transport of water across the apical membrane is regulated. A balance of chloride secretion and sodium absorption control the level of hydration of the airway surface liquid (ASL) which is maintained at a physiological thickness of ~ 7 µM. In response to drying, chloride is secreted to increase the water transport. Soluble factors such as extracellular adenosine are highly important for the coordinated ion transport[3] (Figure 1).

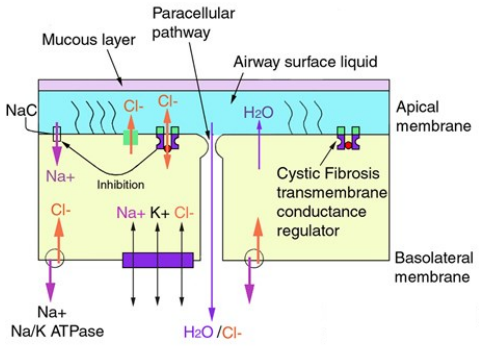

Figure 1: Ion transport processes in healthy lung epithelium

Chloride is secreted *via* CFTR and sodium is absorbed into the epithelial cells *via* ENaC across the apical membrane counteracting the release of sodium *via* tight junctions. Water is transported *via* a paracellular pathway from the apical to the basolateral side of the cells. The transport is further affected by soluble and membrane-bound factors that modulate CFTR and ENaC activity.

Figure from http://www.cfmedicine.com/htmldocs/cftext/basicproblem.htm on 01.06.2018, 13:00

In CF, the coordination of chloride and sodium transport is lost due to the mutated CFTR. The absorption of sodium and water from the ASL is not stopped at the physiological level so that the ASL is continuously dehydrated, leading to the collapse of ciliary beating and mucus clearance[3]. *In vivo*, although there are compensatory mechanisms, the lack of mucus clearance results in increased

bacterial load, chronic inflammation and finally in lung destruction by a number of proteases. The importance of sodium transport for the CF lung disease was also shown using a mouse model with overexpression of β-ENaC. The animals show a similar pulmonary phenotype compared to human CF lung disease[6].

1.2 The epithelial sodium channel and its proteolytic regulation by channel-activating proteases

Epithelial sodium channels are rate-limiting in sodium transport across airway epithelial cells[2]. ENaC is a heterotrimer, consisting of an α-, β- and γ-subunit. After channel formation, the β-subunit is not further processed. The α- and γ-subunits contain inhibitory fragments and are subjected to proteolytic processing. Upon proteolytic cleavage, the fragments are released to activate ENaC[2,7] (Figure 2).

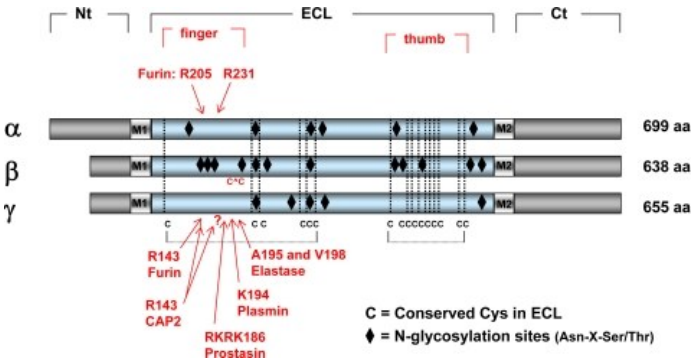

Figure 2: Proteolytic activation of ENaC

Whereas the β-subunit of ENaC is not processed, the α-subunit is processed by furin in the finger domain of the large extracellular loop (ECL). The γ-subunit can be processed by various proteases including prostasin and channel-activating protease 2 (CAP2)

N-terminal (*Nt*), C-terminal (*Ct*) tails, first (*M1*) transmembrane domain, second (*M2*) transmembrane domain, amino acid (aa)

Figure from [2]

The α-subunit is processed in the trans-Golgi network by the serine protease furin during the biosynthetic pathway. The cleavage by furin releases an inhibitory tract which increases the activity from low to moderate level. The γ-subunit is partially cleaved by furin. The release of the inhibitory fragment however requires cleavage by a second protease and leads to highly active channels. Channels with the inhibitory tract of the γ-subunit still in place can be transported to the plasma membrane as silent channels with reduced opening probability compared to fully processed channels[2,8].

Depending on the tissue, different proteases are able to fully activate ENaC. In the following, several proteases are described in more detail. This is however not an exhaustive list and many serine proteases might be able to cleave and activate ENaC in a similar manner[2].

1.2.1 Channel-activating protease 1: Prostasin

One of the most relevant ENaC-activating proteases is serine protease prostasin, also called CAP1. It was first identified in seminal fluid and its active site is closely related to other trypsin-like serine proteases including trypsin itself, hepsin, kallikrein and coagulation factor XI[9]. Its expression is not limited to the prostate gland, but the enzyme is also found in significant abundance in other epithelial tissues in lung, kidney, colon, pancreas, salivary glands etc., and these tissues are also affected in CF. It is glycosylphosphatidylinositol (GPI)-anchored in the plasma membrane. As a trypsin-like protease, CAP1 recognizes basic amino acids, especially arginine residues, in the position N-terminal of the cleavage site and is inhibited by many serine protease inhibitors such as aprotonin, leupeptin or camostat mesilate[9-11].

Prostasin and its target ENaC are involved in many physiological and pathophysiological conditions, including regulation of blood pressure, sodium and potassium homeostasis in the colon or regulation of the airway surface liquid volume in the lung[11-14].

Murine knockout models revealed that prostasin is indispensable for survival. A constitutive, systemic knockout is embryonically lethal due to placenta defects. An epiblast-specific knockout enabled embryonic development but due to severe skin defects, the mice die within few days after birth[15-16]. Interestingly, the importance of prostasin for embryonic and postnatal survival is independent of its enzymatic function. Mice with a systemic catalytic knockout, where the serine of the catalytic triad had been mutated to non-functional alanine, developed a normal skin barrier and do not show impaired survival[17].

In 1997, it was reported that prostasin can cleave the inhibitory tract in the γ-subunit of epithelial sodium channels and significantly increases their activity in the *Xenopus* cell line A6. Further it was shown that ENaC is regulated by a protease expressed on the surface on the same cell. However, prostasin can also be released from the membrane[18].

Airway-specific knockout of prostasin revealed its role in the activation of ENaC in airway-epithelial cells under physiological conditions. In the absence of prostasin in the alveolar epithelial cells decreased ENaC-mediated sodium currents by 40%[19]. Furthermore, RNA and protein levels of prostasin have been found to be increased in cystic fibrosis cell lines as well as primary human airway epithelial cells of CF patients[20-22]. To summarize, prostasin (CAP1) seems to be one of the central mediators of increased ENaC activity and sodium transport in CF.

1.2.2 Channel-activating protease 2

TMPRSS4 or CAP2 is a type II transmembrane serine protease that is very closely related to CAP1. Studies with murine enzymes expressed in *Xenopus* oocytes showed that CAP2 is able to activate ENaC in a similar manner as CAP1[23-25]. The activation is dependent on its proteolytic activity[26]. A murine knockout model did not reveal any physiological role of CAP2 on the activation of ENaC. Furthermore, the mice were viable, fertile and without any obvious phenotype[27]. The lack of importance to sodium transport in the lung is likely due to its very low expression in healthy conditions, both in mouse and human[28-29]. The spectrum of its targets remains largely unknown and so does its physiological role[27]. Recently however, TMPRSS4 has come to forefront in cancer research, as it is suggested to be involved in different cancer types including lung, prostate, breast and many more. In disease state, TMPRSS4 (CAP2) seems to be strongly upregulated and involved in tumor signaling, proliferation and disease progression[28, 30-33].

1.2.3 Channel-activating protease 3: Matriptase

Channel-activating protease 3 (CAP3), also called matriptase or suppressor of tumorigenicity-14 (ST-14), was first identified in conditioned medium of breast cancer cells[34] and in colorectal cancer tissue[35]. As described for prostasin, matriptase is expressed in many epithelial tissues, including lung, skin and kidney. *In vitro* co-expression with ENaC in *Xenopus* oocytes revealed the ability of matriptase to cleave the γ-subunit of the sodium channel and activate to similarly to CAP1 and CAP2[26].

ENaC is the only well characterized substrate of CAP3. A constitutive knockout of CAP3 in mice is characterized by early postnatal death within 48 h after birth due to severe defects in epithelial barrier formation. This leads to fatal dehydration of the newborn mice[36]. The mice are born with an altered lipid composition and the loss of proteolytically processed filaggrin, one of the major epidermal proteins that is required for keratin aggregation and the formation of the cornified envelope, a protective barrier at the inner leaflet of the cell membrane in korneocytes. In the stratum corneum, filaggrin is completely decomposed to hygroscopic amino acids that maintain epidermal hydration in wildtype animals. The N-terminal S-100 filaggrin fragment is believed to be transcriptional regulator during late stratum corneum differention[37].

In order to further investigate targets and the physiological role of CAP3, hypomorphic mice have been created that show a 100-fold reduction in epidermal CAP3 mRNA levels and consequently reduced, but not fully depleted protease activity. Unlike the CAP3 knockout mice, the hypomorphic mice are viable, fertile and develop a skin disease mimicking autosomal recessive ichthyosis

described for humans with a mutation in the ST-14 gene. This mutation also results in reduced CAP3 activity. The phenotype of CAP3 hypomorphic mice is most likely due to reduced amounts of processed profilaggrin[38]. However, not only the skin of these mice is affected by the reduction of proteolytic activity of CAP3, but they are also characterized by reduced barrier formation in the gut where only 1 % of the normal matriptase mRNA level was detected. The transepithelial electrical resistance is significantly reduced, suggesting impaired formation of tight junctions. In matriptase hypomorphic mice, the turnover of Claudin-2, a tight junction protein that has been associated with permeability, is reduced although matriptase does not directly process it[39].

Although most CAP3 research is focused on its major physiolocigal role in the skin, matriptase has also been associated with idiopathic pulmonary fibrosis (IPF) where it has been found to be upregulated, like CAP2, and described as a trigger of fibrosis[29,40]. Matriptase hypomorphic mice are not susceptible to IPF, indicating the central role of matriptase in the context of this disease[40]. In CF however, matriptase does not seem to be upregulated[21].

1.2.4 Other relevant or potential ENaC-activating proteases

Apart from the channel-activating proteases CAP1-3 described above, many more proteases are involved in proteolytic processing of ENaC.

As mentioned above, proteolytic cleavage of ENaC by furin is absolutely crucial for channel function. Furin is a subtilisin-like proprotein convertase that is ubiquitously expressed in many tissues. It is mostly located in the Golgi apparatus where it is involved in the proteolytic processing of many different proteins in the secretory pathway. Furin is a calcium-dependent serine protease that recognizes a very similar amino acid sequence to the CAPs: arginine residues in the P1 and P4 position. Further, it prefers repeated basic amino acids in P1 and P2[41].

Proteolytic cleavage by furin in the α-subunit of ENaC releases an inhibitory fragment so that ENaC is partially activated. Together with other CAPs, furin-mediated cleavage also leads to the release of an inhibitory fragment in the γ-subunit[42].

Until now, furin was believed to exclusively act intracellularly in the Golgi network where it processes most of its targets. Recent studies, however, suggest that in CF airway epithelial cells excessive furin activity might also be located at the plasma membrane[43].

In other tissues than the lung, ENaC is activated under physiological conditions by a number of other serine proteases that are closely related to CAP1-3. For example, in the kidney, the urinary tissue kallikrein has been shown to cleave ENaC in the same position as prostasin and thereby increase its

activity[44-45]. In pathophysiological circumstances like proteinuria, urinary plasminogen is converted to active plasmin, another ENaC activator in the kidney[8,46].

Human airway trypsin-like protease (HAT) is very closely related to CAP2 and CAP3. It is also a transmembrane trypsin-like serine protease that is expressed in airway epithelial cells, mostly in the trachea and lower airways[47]. In contrast to prostasin and matriptase, the mouse analog of HAT is dispensable in embryonic development, postnatal survival and skin integrity[48]. So far, the physiological role of HAT remains unclear but it might be related to some specific regulatory processes. Based on the substrate specificity, HAT might be able to activate ENaC, but this has not been shown so far. The latest publications suggest that HAT is upregulated in pulmonary fibrosis, as CAP2 and CAP3, but it seems to have protective role rather than contributing to disease progression[49]. Up to now, HAT has not been linked to CF.

In CF, a number of additional proteases have been described to be potential ENaC activators in the lung. CF lung disease is characterized by a severe, chronic neutrophilic inflammation which finally leads to the destruction of lung tissue and emphysema[50]. Neutrophil elastase (NE), one of the neutrophil serine proteases, is found in high amounts in the CF lung and is correlated with the severity of the CF lung disease[51]. The enzyme has been found to be a potential activator of near-silent ENaCs, cleaving the inhibitory tract of the γ-subunit close the physiological CAP cleavage site[52-53]. Activation of ENaC by NE, however, requires prior processing of the channel by furin so that furin inhibition prevents the activation by NE. This observation is in contrast to the inhibition of CAPs which does not affect the activation by NE[43]. Other proteases that are released by macrophages like macrophage elastase (MMP-12), matrix-metallopreptidase (MMP-) 9 or by neutrophils like cathepsin G or proteinase 3 have never been linked to ENaC activation so far.

Furthermore, increased amounts of the cysteine protease cathepsin S have been found in the bronchoalveolar lavage (BAL) fluid of CF patients, independent of *Pseudonomas aeruginosa* infection[54] as well as in cultured airway epithelial cells of healthy and diseased origin[55]. *In vitro* data show that cathepsin S is able to proteolytically process and activate epithelial sodium channels. The putative cleavage sites in the γ-subunit are identical to the ones suggested for NE, in both cases distal to the CAP cleavage site[56]. The physiological role of cathepsin S in ENaC activation remains unclear so far.

Similarly to cathepin S, the cysteine protease cathepsin B has been shown to be expressed in cultured airway epithelial cells[55] and increase ENaC activity in the airway. So far, the precise cleavage site has not been identified, but the polybasic recognition motive that is also required for cleavage by CAPs and chymotrypsin also seems to be necessary for cathepsin B[57-58].

Both cathepsins B and S favor acidic conditions for optimal enzyme activity, in contrast to CAPs which have been shown to have higher activity in basic conditions. In CF, due to reduced hydrogen carbonate transport via CFTR, the airway surface liquid is slightly acidified which might both increase the activity of cathepsins as well as decrease the activity of CAPs[57].

1.3 Interplay between CAP1 and CAP3, models of altered protease-antiprotease balance and increased ENaC-activity in CF airways

CAPs 1 and 3 are most relevant for ENaC activation under physiological conditions. Interestingly, murine knockout models suggested that these enzymes are tightly coupled together in a highly complex system, including their natural inhibitors hepatocyte growth factor activator inhibitor (HAI)-1 and -2. CAP1- and CAP3- deficient mice have an identical phenotype, apart from the embryonic lethality of the constitutive CAP1 knockout[59]. Both enzymes are synthesized as inactive zymogens that require proteolysis to get activated. At least in mice, they have been shown to be co-localized in the skin[59] and in human airway samples, both enzymes are found to be expressed[21]. Matriptase-deficient mice lack proteolytically processed CAP1[59] and *in vitro* studies revealed that CAP1 triggers CAP3 zymogen activation[60]. CAP3 activation does not require prostasin catalytic activity as matriptase undergoes auto-activation *via* proteolytic cleavage[61]. Catalytically inactive CAP3 cannot be activated by direct proteolysis of CAP1[60].

In vivo, the activity of CAP1 and CAP3 is strongly regulated by their endogenous inhibitors HAI-1 and HAI-2. Similarly to constitutive knockouts of the proteases, complete deficiency of one of the inhibitors or haploinsufficiency of both are lethal in murine models[62-63]. Strikingly, the developmental deficits, due to HAI-1 and HAI-2- deficiency, were rescued by reduced CAP1 activity[64].

To summarize, a balance between CAP1 and CAP3 activity is required for crucial biological processes; deficiency in any of the factors is associated with severe defects and lethality.

Many diseases are associated with an impaired protease- antiprotease balance[42], including pulmonary fibrosis[65-66] and cystic fibrosis. For the neutrophil serine proteases, the break of the antiprotease shield sets the stage for lung destruction in CF[67]. Limiting CAP activity is one the major regulators for epithelial sodium transport *via* ENaC which seems to contribute to the ion transport imbalance in the CF airways. In the airways, the regulation of proteolytic cleavage of ENaC is coupled to the change in airway surface liquid volume which is dependent on the osmotic force created by sodium absorption and chloride secretion[68].

In normal airways, a fraction of ENaC is transported to the plasma membrane as “near-silent” channels that require proteolytic cleavage by CAPs for full activation. In the airway surface liquid,

soluble endogenous CAP inhibitors like HAI-1[69], HAI-2[21] and bikunin[70] are present that are able to limit proteolytic activity. A model suggests that increasing ASL volume reduces the concentration of soluble inhibitor, resulting in increased protease activity. Consequently, ENaC activity is increased, leading to increased sodium and water absorption until the physiological volume and ASL height are reached. By restoring the protease-antiprotease balance, the secretion and absorption processes return to their physiological levels. In case of reduction in the ASL, the concentration of soluble inhibitors increases so that the proteolytic activity of CAPs is reduced. Therefore, absorption goes down and secretion of water from the epithelial cells overweighs the absorption – the ASL increases to its physiological volume[21,68] (Figure 3 A-B).

In CF however, this regulation process is disrupted (Figure 3 C-D). Interestingly, CF airway epithelial cultures do respond more strongly to the exogenous inhibitor aprotinin whereas they are less affected by the addition of exogenous trypsin. This suggests that CF airway epithelial cells have less endogenous inhibitor, more constitutively active sodium channels and less near-silent, inactive channels. Consequently, CF airway cultures have less possibility to limit sodium and water absorption[21,68]. Furthermore, data from CF airway cultures suggest that the expression of CAP1 is significantly increased compared to normal tissue[21].

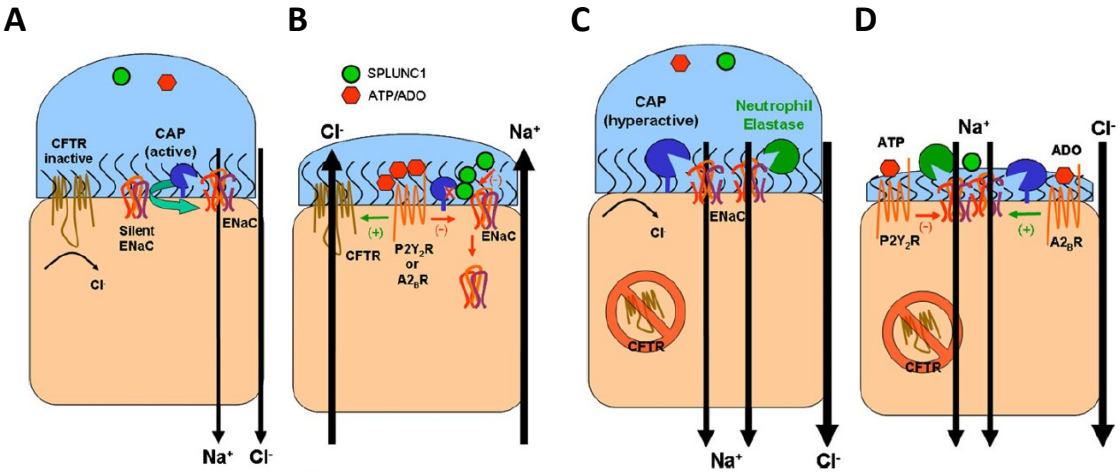

Figure 3: Regulation of ASL height by activation and inactivation of ENaC in normal and CF epithelium

In normal epithelium, high airway surface liquid volume leads to the activation of ENaC by active CAPs (A). Consequently, the sodium transport increases and the ASL volume decreases. At low ASL volume, the soluble inhibitor SPLUNC1 prevents ENaC activation and extracellular ATP increases CFTR function so that the volume is restored (B). In CF, hyperactive CAPs as well as inflammatory proteases like NE are present in epithelial cells (C).

Figure from [1]

In the airways, ENaC activity is also regulated by its allosteric modulator short-palate lung and nasal epithelial clone 1 (SPLUNC-1). In contrast to HAI-1 and HAI-2, SPLUNC-1 does not affect protease activity but causes the internalization of α- and γ- subunits of ENaC, reducing the amount of active

channel on the cell surface. Furthermore, it increases the ubiquitination of the α-subunit by Nedd-4-2, an E3 ubiquitin-protein ligase[71-72]. Interestingly, SPLUNC-1 has been shown to be inactive under acidic conditions, such as CF airways, due to highly pH-sensitive salt bridges in the molecule. Reduced activity of SPLUNC-1 might also contribute significantly to increased ENaC activity in CF airways[73].

To summarize, it remains a question of debate which key factors contribute to the impaired ion transport balance in CF and more tools are required to obtain further insight on the pathophysiological mechanisms.

1.4 Basic principles of fluorescence and fluorescence energy transfer

Fluorescence is a type of luminescence in which the absorption of photons causes the transition of an electron from its ground electronic level to an excited singlet level. Within nanoseconds, the electron falls back to a lower excited state and subsequently to the ground state, emitting light with lower energy, corresponding to a longer wavelength compared to the excitation light. In contrast to phosphorescence, the spin electron remains paired with the ground state electron during the whole process. The loss of energy is caused by non-radiant, vibrational relaxation between the excited states. This process is essential for the existence of fluorescent properties of a molecule. The difference between excitation and emission wavelength is called Stokes shift[74].

Fluorescence microscopy is based on molecular fluorescence. In molecules with more complex electronic systems, the energy level of the ground and excited levels is not discrete but is spread to energy bands. This results in the typical absorption and emission spectra of fluorophores. All fluorophores share the property that they contain conjugated double bonds which allow the electrons to be displaced in a rigid and planar molecule. The larger is the conjugated electron system, the higher the emission and absorption wavelength [74].

In the past decade, the variety and quality of fluorophores available for biological applications have increased enormously. Nowadays, there are fluorophores available throughout the whole spectrum of visible light as well as UV-excited and infrared dyes. Improvements towards sharp excitation and emission spectra as well as high extinction coefficients and high quantum yields have been made by chemical modifications of older fluorophores like fluorescein and rhodamine or completely new designs[75].

In biological experiments, fluorophores are frequently used to monitor the location of specific labeled molecules or proteins. In more advanced settings, they are very useful tools to monitor dynamic processes, e.g. the activity of a protease. Most commercially available protease substrates

are designed as fluorogenic substrates that become fluorescent at a distinct wavelength upon cleavage of the fluorophore from the peptidic recognition motive.

Foerster Resonance Energy Transfer (FRET) describes a process in which a donor fluorochrome transfers its energy to another fluorophore or quencher without emission of light. For the energy transfer, the two molecules, so called donor and acceptor, must be in a very close proximity (several nanometers), the Foerster radius[75]. In case of protease substrates, donor (D) and acceptor (A) fluorophores are linked by a peptidic recognition sequence for the enzyme. As long as the molecule is still intact, the energy absorbed by the donor fluorophore is transferred to the acceptor, FRET occurs. The donor fluorophore is almost fully quenched whereas the acceptor fluorophore emits fluorescent light. Upon cleavage the donor fluorescence increases significantly whereas the acceptor fluorescence decreases and the change in D/A ratio is a measure of enzyme activity (Figure 4).

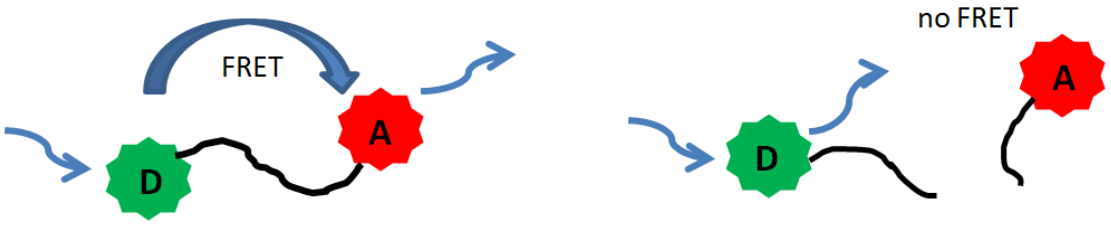

Figure 4: Principle of FRET probe design and readout

Similar ratiometric probes have been successfully established for MMP-12 and NE[76-77].

1.5 Aims of the project

The development and use of personalized drugs requires fundamental understanding of the pathophysiological processes combined with comprehensive characterization of the phenotype of each individual patient. In CF research, the strongest research focus is typically characterization and modulation of CFTR function. Nowadays, a number of CFTR modulators and correctors are on the market and more research is ongoing. ENaC and proteases as therapeutic targets have been neglected for a while even though there are promising studies showing improvements in the phenotype after inhibition of the ENaC/protease axis[43, 78-79]. One of the reasons might be the lack of tools to investigate protease activity to identify biological processes as well as protease activity levels in patients. Up to now, soluble fluorogenic peptides, RNA and protein quantification were the limited available tools to quantify enzyme activity in patient samples or mouse tissue. Therefore, I wanted to develop tools that facilitate enzyme activity quantification in murine and human samples.

From experience in the Schultz and Mall research groups, it is known that ratiometric FRET probes which insert themselves into the plasma membrane because they bear lipid side chains, are useful tools to detect and quantify membrane-bound enzyme activity[76-77]. In the past, the focus was on inflammatory cell-derived proteases that are responsible for the destruction of lung tissue. In this project, we aimed to develop probes for the quantification of channel-activating protease activity in human and murine samples. As described, the proteases seem to be redundant because one can replace another in the task of ENaC activation. Therefore, we did not aim to develop a probe which is able to dissect the activity of several channel-activating proteases from each other but rather to measure the sum of them.

A suitable CAP probe should thus fulfill the following criteria:

1. Stable insertion of the lipidated probe into the plasma membrane with no or very low internalization in the time frame of our experiments, varying from 2 to 10 hours
2. High dynamic range of the FRET signal to enable quantification of small differences in enzyme activity
3. Applicability to murine and human samples
4. Selectivity towards proteases that cleave ENaC in a similar manner

After successful design and characterization, the probes undergo initial proof of concept experiments to determine whether they are useful tools and/or suitable biomarkers that can be used in *ex vivo* with CF patient samples.

2. Results

2.1 Representative purification and identification of peptide-based probes after solid-phase synthesis

All FRET probes were synthesized by partially automated, fluorenylmethoxycarbonyl (Fmoc)-based solid phase peptide synthesis (SPPS) as described in the methods section. After cleavage from the resin in acidic conditions, the probes were purified by HPLC. All chemical structures are shown in the Material and Methods section (6.2.2) and on the addendum. The detailed synthetic procedures are described in the Material and Methods section (6.2.2).

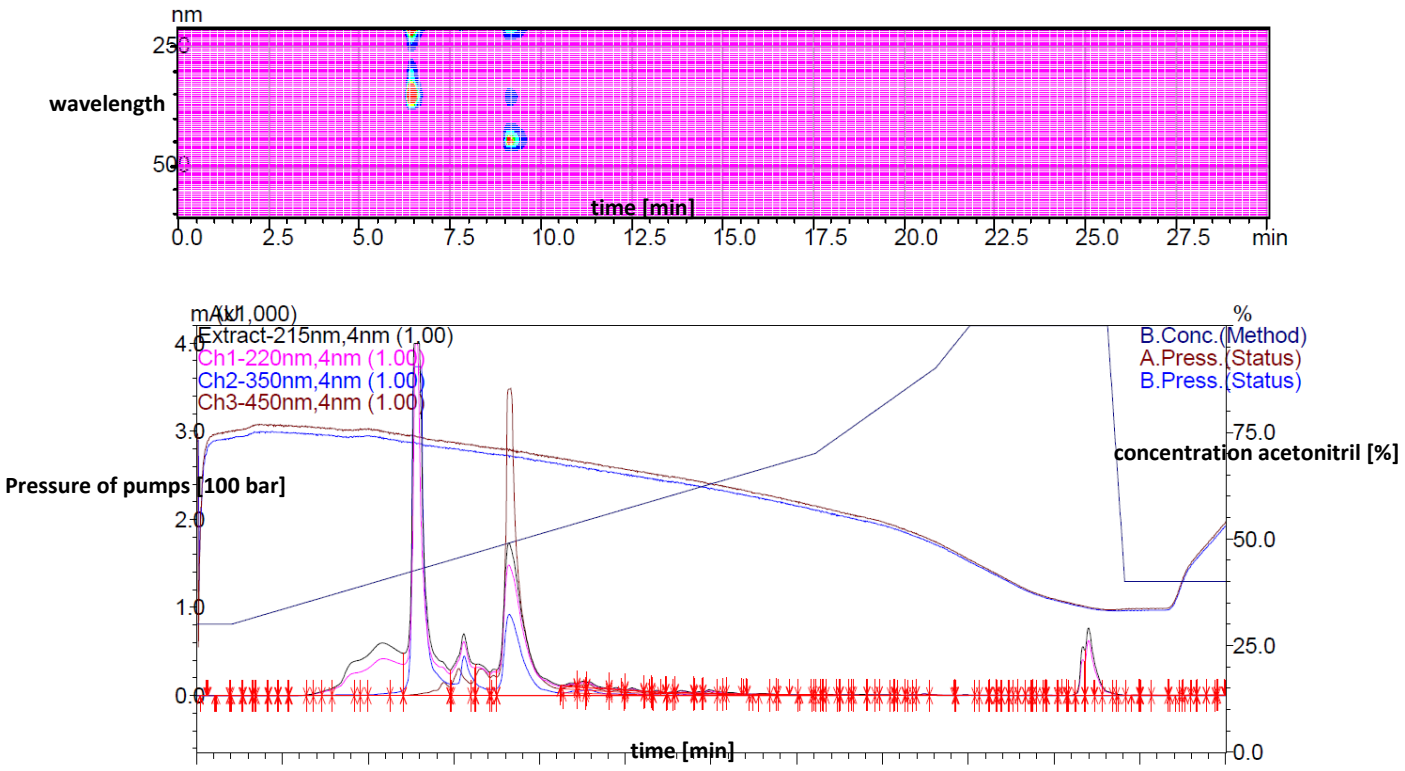

Figure 5: Representative preparative HPLC trace of CAPRee1 during purification

Part A shows the full spectrum of the wavelengths detected over time. At about 6 min, a molecule was detected absorbing at low wavelength (220 nm, peptidic part) and at 350 nm (MetOCou). This represents the byproduct containing only the donor fluorophore. At 8.5-9 min, the desired compound, absorbing at all three wavelengths 220 nm (petidic part, Ch1), 350 (MetOCou, Ch2) and 450 nm (Cou343 Ch3), was eluted. Part B shows the chromatogram at selected wavelengths, the concentration of acetonitrile (right hand side).

In Figure 5, a representative preparative HPLC trace of the soluble probe CAPRee1 after cleavage from the resin is shown during purification. For the majority of soluble probes synthesized, the peptide sequence was fully synthesized, but the coupling of the fluorophores was achieved in lower

yield. Therefore, as byproducts during the synthesis, probes bearing only one of the fluorophores were obtained.

Compounds absorbing at 220 nm, 350 nm (7-amino-4-methoxycoumarin (MetOCou)) and 450 (Coumarin343 (Cou343)) nm were collected and submitted to analytical HPLC with coupled mass spectrometry to check purity and mass.

In case of lipidated probes, the synthesis efficiency was affected by the lipid chain which had been coupled in the second step of synthesis. The detailed synthetic steps are described in Material and Methods (6.2.1 and 6.2.2). Therefore, more byproducts with aborted peptide chains were observed in some cases. Peaks with absorbance at 220 nm, 450 (Cou343) nm and 550 (TAMRA) nm were collected and checked by mass spectrometry. Keeping in mind that TAMRA had been used as a mixture of two isomers during synthesis, successfully synthesized compounds showed up double peaks in the analytical HPLC with identical mass. As control molecules for the expected localization of the fragments after cleavage, the fragments after peptide cleavage were also synthesized independently for selected probes. Apart from HPLC and mass spectrometry, these were further analyzed by NMR. All analytical data and chromatograms are shown in the appendix.

After purification and removal of the solvents, the samples were dissolved to stock solutions in DMSO in millimolar concentration. We observed that Coumarin343 is not stable in dry conditions at -20 °C, most likely due to remaining TFA from the solvents used in HPLC (Figure 4). Purification without acid or formic acid instead for TFA failed due to worse separation of the compounds. Compounds stored in DMSO or water were not prone to degradation and proved stable for at least 2 years of storage at -20°C (Figure 6). The concentration was measured by absorbance of Cou343 in ethanol (ε=44100 $L*mol^{-1}*cm^{-1}$)[76].

After purification and quality check, the samples were submitted to characterization by high resolution mass spectrometry at the Mass Spectrometry Facility @OCI, University of Heidelberg.

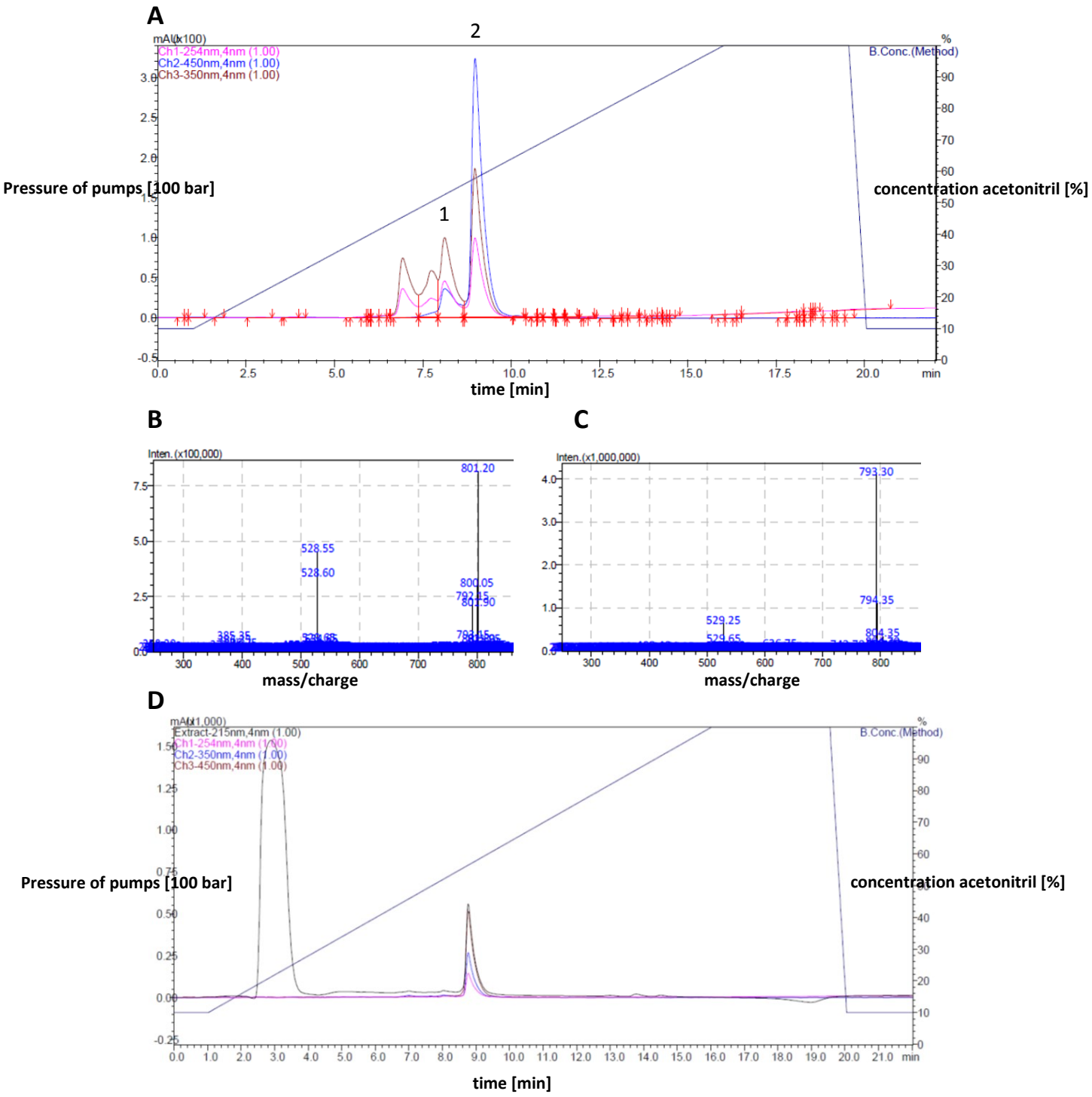

Figure 6: Stability of CAPRee1 as lyophylized powder and in DMSO solution

Part A shows the purity of CAPRee1 after 7 months of storage as lyophilized powder. Part B is the mass corresponding to peak 1, C to peak 2. Most likely due to remaining traces of TFA in the powder, Cou343 was degraded significantly. The mass of the compound lacking Cou343 absorbance increased by 16 Da, which might suggest the addition of an oxygen atom somewhere on the ring system which destroys the conjugated system. The exact structure could not be solved as NMR is difficult for molecules of this size and requires comparably large amounts of probe which were not available. In contrast, storage in water or DMSO prevents degradation of the fluorophore (D). The large solvent peak is due to DMSO. Consequently, all probes were stored in DMSO solution after purification.

2.2 Characterization of CAP probe based on autoactivation cleavage site of matriptase

For CAPRee1-3, the amino acid (aa) sequence is identical to the sequence of the autoactivation cleavage site of CAP3 (R^{611} – G^{618}) and related to the amino acid sequence of the commercial substrate sold by R&D systems (Cat# ES014) for CAPs 1 and 3[80]. For the soluble probe, the donor fluorophore was added to the N-terminal part of the molecule, the acceptor on the side chain of a C-terminal lysine residue. The lipidated probes were designed with the acceptor fluorophore at the N-terminal, basic and hydrophilic part of the molecule and the donor fluorophore and the lipid anchor at the more hydrophobic, C-terminal part of the peptide sequence. The water soluble acceptor part diffuses away after cleavage while the hydrophobic donor part remains attached to the plasma membrane. Therefore, a dual read out of the cleavage is achieved: first, FRET is lost due to separation of the fluorophores to distances higher than the Foerster radius and second, we observe the loss of colocalization of the fragments.

In Figure 7, the common chemical structure of the CAP3-based probes is shown. The detailed structures of all probes are shown in the Methods Section (6.2.2). For the different CAPRee probes, the fluorophores (R) and linkers (X) and their positions were modified as well as single point mutations in the amino acid sequence.

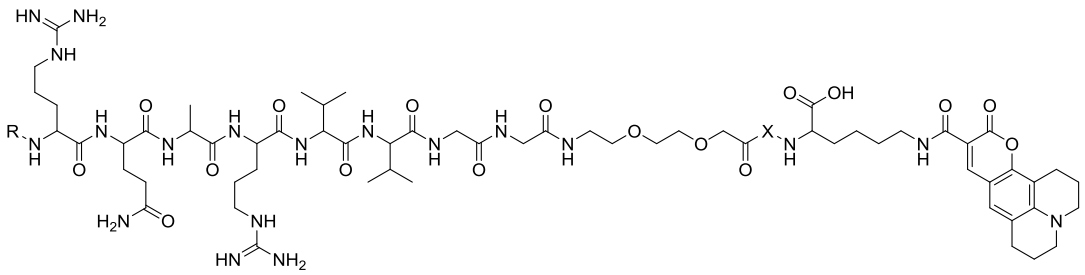

Figure 7: Common structure of all CAP3-based CAPRee probes

All CAP3 based CAPRee probes share the common recognition sequence which is derived from the autoactivation cleavage site of CAP3. One fluorophore, Cou343, is coupled to a C-terminal lysine. In position R, different fluorophores were used to optimize the performance of the probe. In position X, a lysine with palmitoic acid could be coupled to obtain lipidated probes.

2.2.1 Physical properties of soluble and lipidated probes CAPRee1-3

From experience, it was known that having at least one polyethylenglycol (peg)-linker moiety adjacent to the aa sequence is crucial for solubility in water. All soluble probes are equipped with 7-amino-methoxycoumarin (MetOCou, donor (D)) and Coumarin343 (Cou343, acceptor (A)) as the fluorophore pair as this has been established to give good FRET efficiency in solution[76-77].

For CAPRee1, the D/A ratio does not change in the absence of enzyme, indicating good solubility of the probe and no unspecific loss or gain of FRET (Figure 6 A and B). The initial D/A ratio calculated from the emission wavelength scan between the maximal donor (400 nm) and acceptor fluorescence (490 nm) is 0.56 ± 0.027 (average ± SEM, calculated by linear regression), independent of the concentration of the probe varying between 0.5 µM and 4 µM. Murine CAP3 cleaved CAPRee1 over time (C and D) as quantified by the ratio of MetOCou and Cou343. The normalized trace is calculated by division of the D/A ratio value by the average of the negative control, calculated from Fig. 6 B.

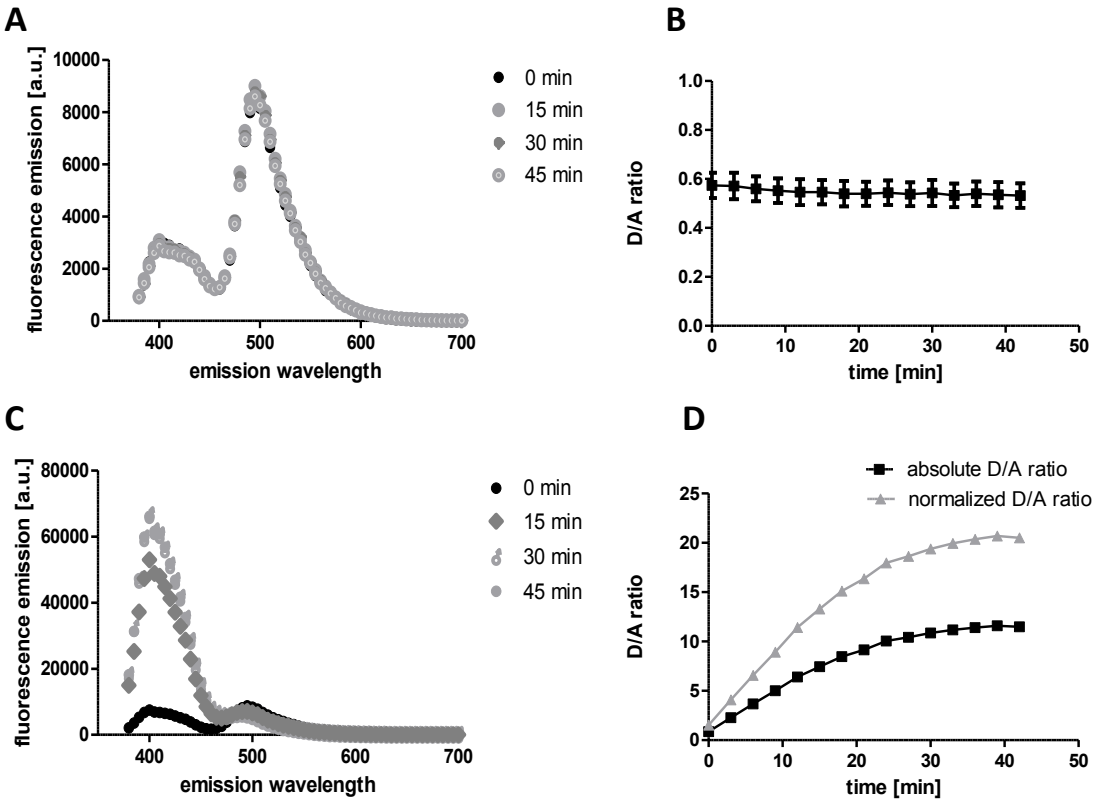

Figure 8: Behavior of CAPRee1 in absence or presence of enzyme

A emission wavescan of CAPRee1 in absence of enzyme with excitation wavelength 350 nm
B quantification of the ratio at 400 nm and 490 nm over time in absence of enzyme, n=5, plotted as mean ± SEM
C emission wavescan CAPRee1 in presence of 5 nM mCAP3 with excitation wavelength 350 nm
D quantification of the ratio at 400 nm and 490 nm over time in presence of 5 nM mCAP3. The normalized D/A ratio was calculated by division of each absolute D/A ratio value by the average D/A ratio value in absence of enzyme.

The assay was performed in 50 nM Tris-HCl and 0.05 % Brij-35 in water at neutral pH. Each curve, except B, was shown as representative curve for n=1. A was measured in five replicates. Positive and negative controls were included in all experiments.

In general, the normalized D/A ratio shows the dynamic range (maximal fold change) that is reached for a distinct probe which makes it very useful for the comparison of different probes. For the application on human or murine specimen later on, the calculation of the fold change is not always possible due to experimental requirements as described later. To be consistent throughout, all quantification was done without normalization unless indicated otherwise. Upon cleavage by mCAP3, the D/A ratio increases both by increase in donor fluorescence and decrease in acceptor fluorescence. When the assay was performed in basic conditions, as recommended by the supplier of the recombinant enzymes, the D/A ratio peaked and decreased afterwards, indicating that at least the donor fragment precipitated after cleavage. Consequently, all further experiments were performed at neutral pH, where the D/A ratio enters a plateau upon complete cleavage (Figure 9). The behavior of the probe in different pH was observed in more than 100 traces of each condition with different probe and enzyme concentrations as well as for different enzymes.

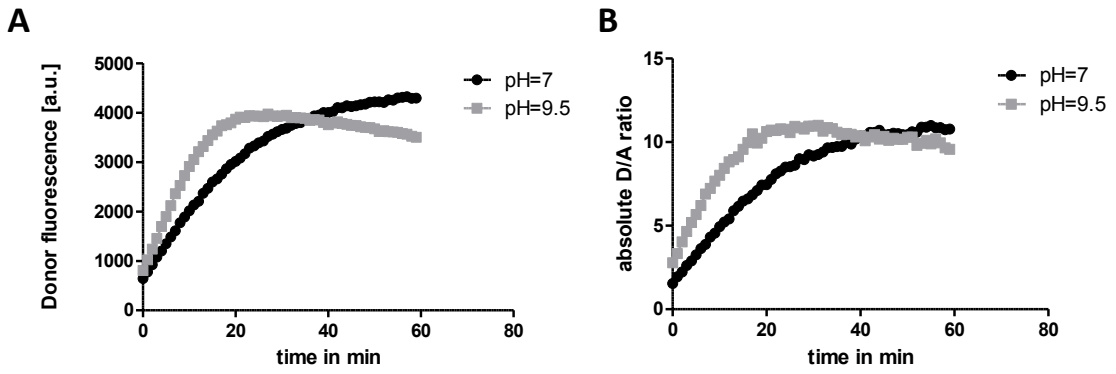

Figure 9: pH-sensitivity of donor fluorescence and absolute D/A ratio change

The assay was performed with 10 nM mCAP3 in 50 nM Tris-HCl and 0.05 % Brij-35 at the given pH, adjusted by addition of NaOH. The curves are plotted as representative traces with n=1.

The lipidated probe was designed for the detection of enzyme activity on the surface of cells and inserts into the outer leaflet of the plasma membrane, as can be seen by confocal microscopy (include images to demonstrate the localization). For the characterization, the probes are tested *in vitro*. In previous studies, liposomes had been used to provide an artificial membrane into which the probe can insert[76-77]. Therefore, liposomes approximately 320 nm in size were generated in CAP assay buffer. In contrast to MMP12 and NE which had been tested before, the insertion into these small liposomes drastically impaired proteolytic cleavage by human and murine CAP3. Consequently, liposomes could not be used for the *in vitro* characterization of the lipidated probes (Fig. 10A). As alternatives, a neutrophil-like cell line, HL-60, which is handled in suspension, was tested as well as the use of pure buffer. Undifferentiated HL-60 cells do not express relevant serine proteases on their

surface. Comparison of pure buffer and usage of HL-60 cells as membrane supply did not show significant differences in cleavage rate, and the cleavage was much faster compared to liposomes (Fig. 10 B). Because of the good solubility of the lipidated probes, the use of cells as support is not required. Therefore, the characterization was done in pure buffer; the composition was enzyme-dependent as described in the methods section.

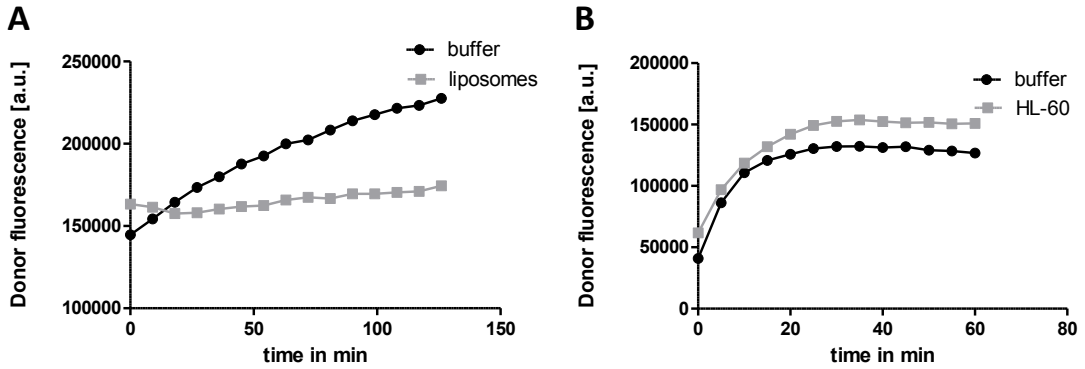

Figure 10: *In vitro* cleavage of CAPRee3 in buffer, on liposomes or HL-60 cells

The assay was performed with 2 µM of CAPRee5, in A 10 nM mCAP3 and B 50 nM mCAP3. The HL-60 cells were handled in PBS, buffer and liposomes in 50 nM Tris, 0.05 % Brij-35. The traces are exemplary and were measured as single measurements over time. For B, the experiment was performed for eight different enzyme concentrations and three different probe concentrations (total n=24).

The lipidated CAPRee probes are equipped with a different set of fluorophores because the combination of MetOCou and Cou343 is not suitable for imaging on cells. First, standard microscopes do not have a laser or lamp which is able to excite MetOCou at 350 nm. Second, continuous excitation of the fluorophores with UV light is not compatible with live cell imaging over longer time periods. Therefore, the combination of fluorophores has to be shifted to higher excitation and emission wavelength. Previously, Cou343 and TAMRA had been chosen for lipidated probes. The performance of such a probe, CAPRee3, is presented in Fig. 11. As expected, the donor fluorescence is quenched by the acceptor fluorophore as long as the molecule is intact, but the initial FRET is lower compared to the soluble probe CAPRee1. In absence of enzyme, the D/A ratio is constant. Furthermore, the lipidated probes are cleaved much more slowly, which is not unexpected and has been observed before also for MMP12 and NE sensors[76-77]. For enzyme quantification, a comparison between recombinant enzymes, which are composed of the catalytic subunit and lack the membrane-anchoring and regulatory regions, and cell-bound endogenous enzymes is not possible so that absolute values for enzyme concentration cannot be concluded. Most likely, the activity of recombinant and endogenous enzymes will differ significantly.

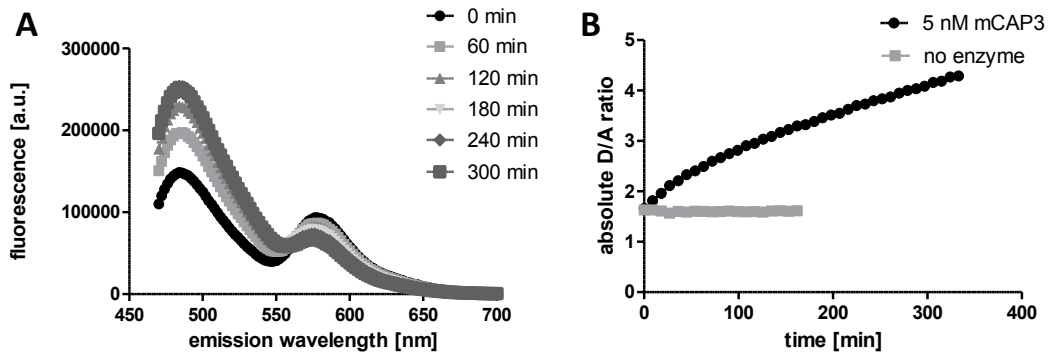

Figure 11: *In vitro* cleavage of CAPRee3 in presence of 10 nM mCAP3

The experiment was performed in 50 mM Tris-HCl with 0.05 % Brij-35 at 2 µM probe concentration.

In order to optimize FRET, several modifications have been tested towards their effect on FRET efficiency and also specificity (described in 3.2.2). The detailed modifications are listed in Table 1 together with the resulting initial D/A ratio of the intact molecule.

Table 1: Modifications of CAPRee1

CAPRee1: MetOCou- RQARVVGG peg K(Cou343)

#	Modification	Initial D/A ratio
CAPRee1_a	R in P1 -> K in P1	0.4
CAPRee1_b	3 additional C-terminal aspartic acid residues	1.3
CAPRee1_c	additional peg linker in P5	1.9
CAPRee1_d	Additional C-terminal lysine residue	2.4

The replacement of the arginine in position P1 of the peptide does improved the FRET efficiency and the initial D/A ratio. CAPRee1_a was further tested for its specificity as described later. CAPRee1_b was synthesized to check the effect of additional, negatively charged amino acids without modifying the two-dimensional distance between the fluorophores. Potentially, the lipidated probe might be internalized into the cell due to its overall positive charge. However, the mechanism of internalization of lipidated peptides is not known. The intial FRET ratio increased significantly, suggesting that the probe, despite its small size, occupies a 3-dimensional structure which is affected by the addition of negative charges. This might also be the case for the lipidated probe where the dynamic range is already dramatically reduced compared to CAPRee1. Therefore, the addition of negative charges is not favored. The insertion of a second peg-linker N-terminally of the arginine in

P4 in CAPRee1_c increased the distance between the fluorophores by approximately 1 nm in the 2-dimensional model, which resulted in a strong loss of FRET in the intact molecule. The effect was tested for 8 concentrations between 20 µM to 0.02 µM in absence and or presence of enzyme. For all, the dynamic range remained very poor, with a maximum of 3.5 for 1.25 µM probe concentration. Similarly, in CAPRee1_d where an additional lysine residue was inserted between the fluorophores, the initial FRET ratio is significantly increased (Fig. 12).

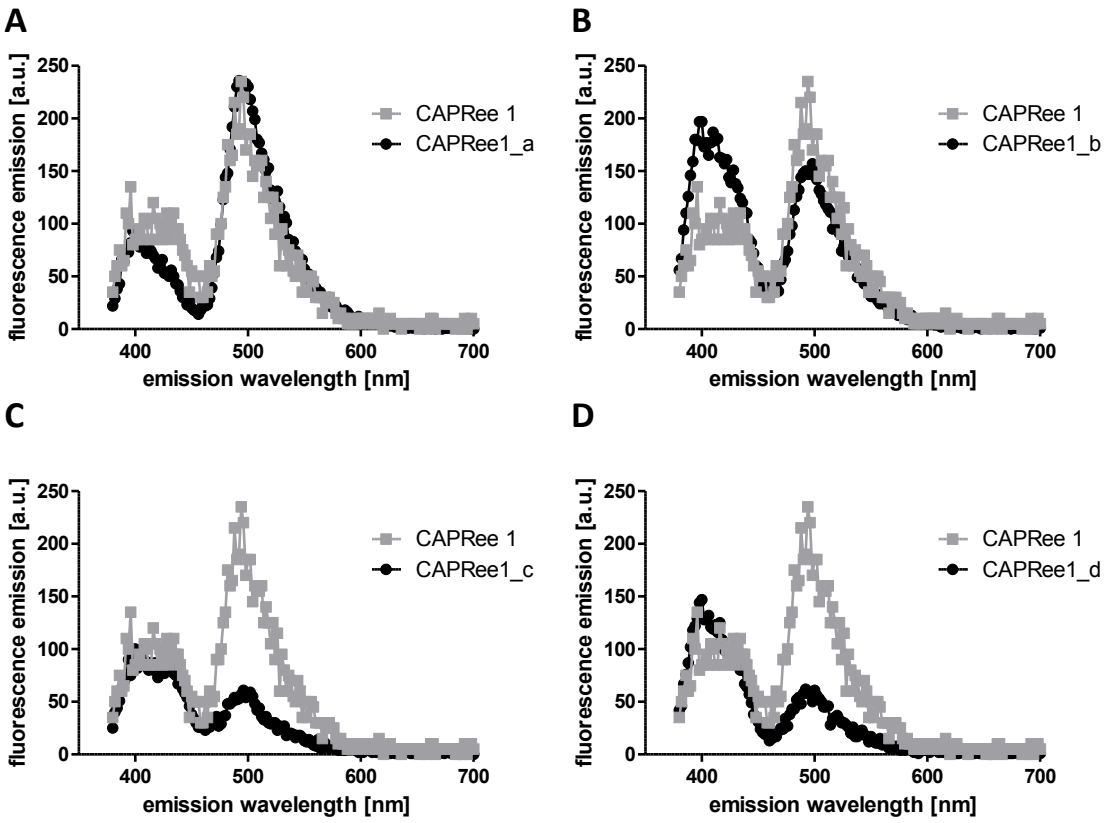

Figure 12: Modifications of CAPRee1 and their effect on initial D/A ratio

The experiment was performed in 50 mM Tris-HCl with 0.05 % Brij-35 at 2 µM probe concentration in the absence of enzyme. Each trace was measured individually, replicates were renounced for A, B and D as the probes or the described modifications were not further used, except C. C was repeated once with an additional concentration series from 20 µM to 0.02 µM.

The maximal D/A ratio change for the lipidated probe CAPRee2 was poor compared to that of the soluble probe CAPRee1. Therefore, the combination of different fluorophores with Cou343 was tested. The choice of fluorophores was based on the overlap of the excitation spectrum with the emission spectrum of Cou343 and a large red shift for the emission of the acceptor fluorophore as well as high extinction coefficient and quantum yield. Furthermore, the fluorophore should have minimum absorbance at 405 nm, where Cou343 is usually excited in the microscope. In addition, the price of purchasing the fluorophores is not negligible because for the synthesis, large amounts are

needed compared to labelling techniques. Therefore, advanced dyes like Alexa variants are not an option so far, especially not during the phase of establishment of a new probe.

Initially, the lipidated probe (which one) was synthesized with a similar structure to that of the soluble probe CAPRee1, i.e. with one peg linker (state how long this is – two ethylene glycol units I think). For insertion into the plasma membrane, a lysine which was palmitoylated on the side chain was added between the C-terminal donor fluorophore and the peg-linker (Figure 7, position X). In the probes CAPRee2_a and CAPRee2_b, TAMRA was replaced by Cy3 and Dy485-XL (Figure 7, position R). These fluorophores were chosen because it was hoped that Cy3 would be a better quencher compared to TAMRA, because of its 3x higher extinction coefficient. The quantum yield, however, is much lower compared to TAMRA. Dy485-XL is coumarin-based, with a large Stokes shift and its absorbance spectrum has perfect overlay with the emission of Cou343. As the combination of two coumarins works very well for the soluble probe this was thought to offer good possibilities for the lipidated probe. The structures of the dyes are shown in Figure 13.

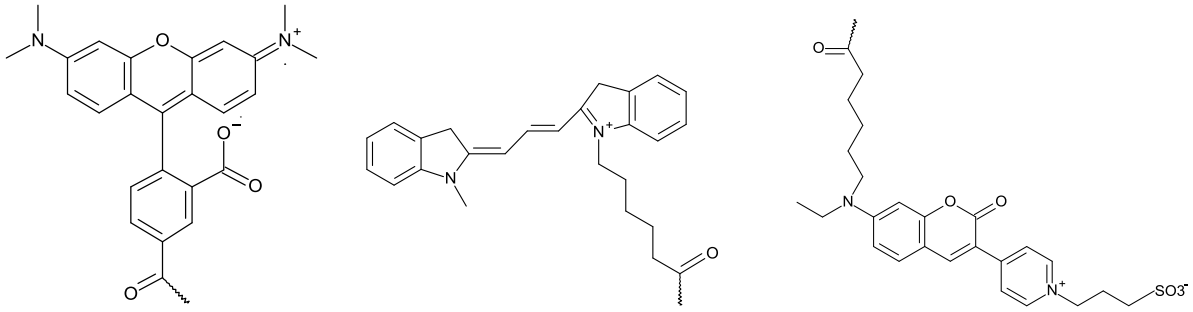

Figure 13: Structures of different acceptor fluorophores tested for lipidated CAPRee probe

TAMRA was incorporated in CAPRee2 CAPRee2_a and CAPRee3, Dy485_XL in CAPRee2_b and Cy3 in CAPRee2_c.

CAPRee2 with TAMRA as second fluorophore had an initial D/A ratio of about 1.35, which is as expected for this combination of dyes[76-77]. Upon addition of 50 nM mCAP3, the probe was cleaved slowly over time and was not fully cleaved after 5 h (Figure 14). CAPRee2_c which contains Cy3 had a similar initial D/A ratio but was cleaved faster and reached a higher final D/A ratio. However, this variant was also not fully cleaved after 5h of incubation. For CAPRee2, the D/A ratio did not increase further even when acceptor fluorescence remained. Potential reasons will be discussed later. Dy485-XL did not improve the initial D/A ratio, but decreased it significantly. The FRET in the intact molecule

is rather poor. This might be due to the low extinction coefficient of the dye or an unfavorable orientation of the dyes in the molecule.

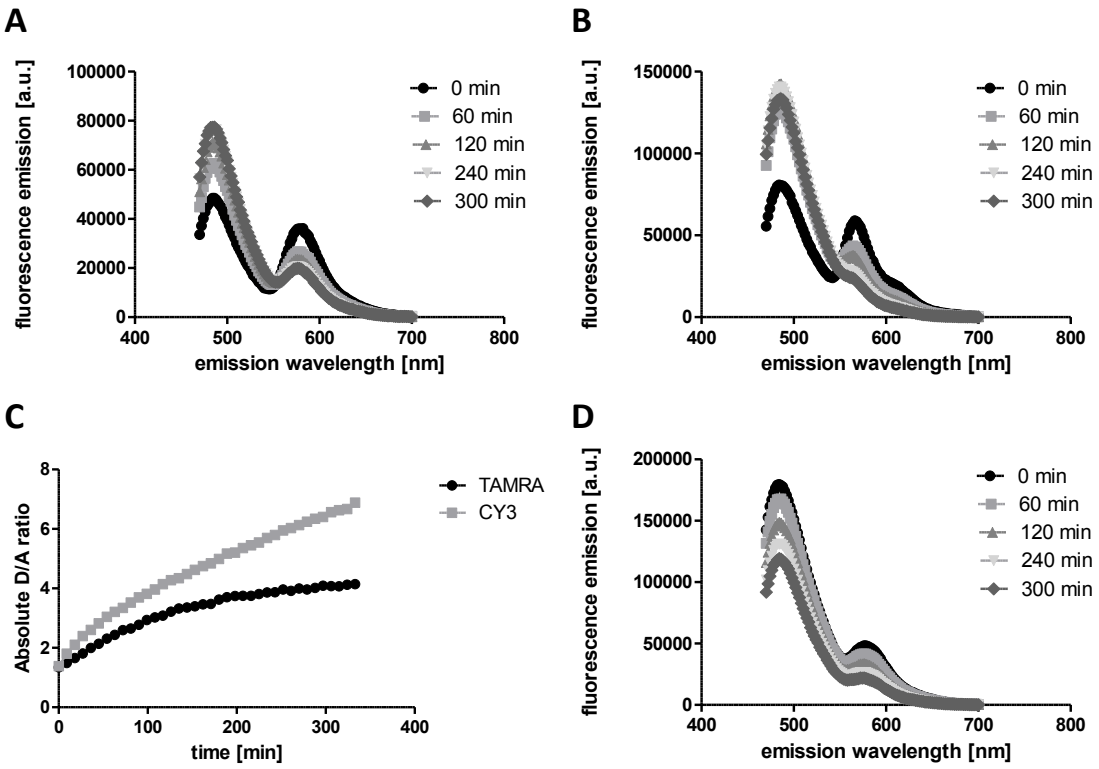

Figure 14: Effect of different acceptor fluorophores on lipidated CAPRee probes CAPRee2, CAPRee2_b, CAPRee2_c

CAPRee2 is synthesized with TAMRA as acceptor fluorophore (A). Compared to CAPRee1, the acceptor of the lipidated probe is not as efficient in quenching the donor fluorophore. Therefore, the initial ratio is 1.35 for CAPRee2 (C). CAPRee2_c has a Cy3 derivative instead of TAMRA (B). Spectrum of CAPRee2_b with Dy485-XL instead of TAMRA. (D) The assay was performed in presence of 50 nM mCAP3 in assay buffer. The traces are shown as representative traces for n=1.

The use of the sensor on primary cells requires the application of rather high concentrations due to the experimental setup. Therefore, a variant of CAPRee2 with an additional peg-linker between the aa sequence and the N-terminal fluorophore was synthesized to increase aqueous solubility (CAPRee3, detailed structure in appendix). In contrast to the soluble probe CAPRee1, where the addition of a second peg-linker with a total length of 4 ethylene glycol units did strongly affect the FRET in the intact molecule, the increase in the 2-D distance between the fluorophores in the lipidated probe CAPRee3 did not have a major impact on the D/A ratio. This behavior of the probe suggests that it indeed takes a certain shape so that the increase in the theoretical two-dimensional length between the fluorophores does not result in increased distance between the fluorophores. The results from the *in vitro* experiments might not directly translate to the behavior on the cell

surface because the probe will be embedded in a dense network of surface proteins, and the close proximity to the hydrophobic plasma membrane might also affect the structure and FRET efficiency.

2.2.2 Kinetic properties and specificity towards CAPs over other proteases

For the development of useful tools for the quantification of protease activity, the specificity of the probe is fundamental. The specificity of the CAPRee probes was tested towards a number of proteases that have been published to be relevant in the context of CF lung disease[54, 57, 81-82]. In this context it is worth mentioning that there are no small molecule inhibitors available that enable the distinction between different CAPs so it is to be expected that the design of a substrate selective for one of them might not be possible. Due to redundancy of the CAPs in mediating ENaC activation, this was also not the focus of this work.

The specificity of the synthesized probes was tested for human and murine enzymes. As previously described, the D/A ratio was affected by the pH of the assay buffer so it was set to neutral conditions irrespective of what was recommended for the enzyme. Furthermore, absolute quantification of selectivity was not possible because of the high variability of enzyme activity which is reported for specific substrates. Being natively membrane-bound enzymes, the reduction to the catalytic subunit will not be comparable to the native enzyme with respect to the activity. Furthermore, recombinantly expressed enzymes lack regulatory domains, which will also have significant effect on the activity of the enzyme.

To normalize enzyme activity for semi-quantitative specificity data, the activity of each enzyme was determined for the substrate recommended by the manufacturer or the commercial CAP substrate of R&D systems with a similar recognition sequence.

To prove that CAPRee1 was exclusively cleaved in the expected cleavage site, the peptide was redesigned with a D-arginine in the putative cleavage site (CAPRee1*). Enzymes do not recognize unnatural D-amino acids as substrates so that CAPRee1* should not be cleaved by mCAP3 or hCAP3 (Figure 15A). The expected cleavage site was further confirmed by mass spectrometry (mass expected for acceptor fragment 872.94 Da, mass found 871.9 Da).

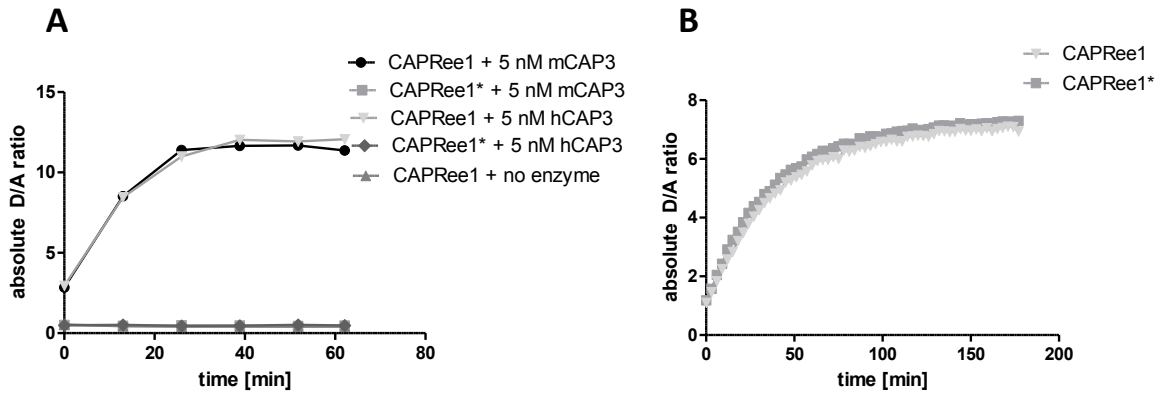

Figure 15: Modification of CAPRee1 – D-arginine in P1

The assay was performed with 2 µM of the given probe in presence or absence of mCAP3 or hCAP3 (A). In B, 6.5 ng/ml hNE were added. Each trace was measured as single trace within a dilution series. The cleavage rate was enzyme concentration dependent for CAPRee1 in presence of NE, human or murine CAP3 and furthermore concentration dependent for CAPRee1* in presence of NE. The cleavage of CAPRee1* in presence of NE was done for 12 different NE concentrations, showing a concentration dependent cleavage rate.

Remarkably, this is not the case for neutrophil elastase (NE) which cleaves CAPRee1* with identical cleavage rate compared to CAPRee1 (Figure 15 B). NE does not recognize arginine in the cleavage site but small aa residues like valine[77]. It was confirmed by mass spectrometry that neutrophil elastase cleaved between the valine residues in P1' and P2' and therefore, a D-arginine in P1 did not prevent cleavage by NE (Figure 15 B). The cleavage by NE is of no major concern as long as the probe is applied to activity measurements in epithelial cells, which do not express NE. However, it has to be kept in mind for the application in samples such as sputum supernatants where high NE activity is to be expected. To determine CAP activity in such samples selective NE inhibitors like sivelestat[83] can be used to block NE activity. Sivelestat is not expected to block CAP activity[84].

Enzymatic reactions can be described by the Michaelis-Menten model of enzyme kinetics. The Michaelis-Menten equation is as follows:

$$v_0 = \frac{v_{max}[S]}{k_M + [S]}$$

with v_0 being the initial reaction rate, v_{max} the maximal reaction rate, $[S]$ the substrate concentration and k_M the Michaelis constant. According to the model, the reaction rate is dependent on the substrate concentration[85]. For murine CAP3, the corresponding data is shown in Figure 13. Based on the donor fluorescence emission, the cleavage exactly followed Michaelis-Menten kinetics. The reaction rate was dependent on the substrate concentration until saturation was reached and the initial reaction rate could no longer increase. Remarkably, the D/A ratio did not follow this trend but, in a concentration range from 50 nM to ~ 3 µM, the increase was independent of the substrate

concentration (Figure 16 D and F). This is highly advantageous for the application of our probe which is used in this concentration range. In contrast to commercial substrates, CAPRee probes cannot be used in the saturation range, i.e. [S]>> k_M, due to solubility problems. On the cell surface, the concentration cannot be measured exactly. Therefore, it is crucial that the increase in D/A ratio exclusively depends on the enzyme concentration and is not affected by the probe concentration, which might vary due to loading efficiency. For high concentrations, i.e. [S]> 3 µM, the increase in D/A ratio was not independent of the probe concentration. The maximal D/A ratio as well as the rate of its increase decreased with increasing probe concentration (Figure 16 E). This might be due to intermolecular effects or product inhibition effects. For low concentrations, i.e. [S]< 50 nM, the increase in D/A ratio was also concentration-dependent and decreased with decreasing probe concentration. The range in which the increase in D /A ratio was concentration independent, was similar for all enzymes tested, i.e. CAP1 and CAP3 (human and murine). K_M values were also comparable for the different enzymes in the low µM range.

For CAPRee1, the maximal fluorescence intensity and maximal D/A ratio upon full cleavage were independent of the enzyme concentration. They are only dependent on the substrate concentration (Figure 17 A-B). This was expected as the maximal fluorescence intensity is dependent on the amount of fluorophore present in the sample. The amount of unquenched MetOCou determines the intensity detected at 400 nm. This should be independent of how fast the maximum is reached, i.e. independent of the enzyme concentration.

Upon cleavage of CAPRee3 by hCAP3, the maximal fluorescence intensity (Figure 17 C) and dynamic range of the D/A ratio (Figure 17 D), seem to be partially be dependent of the enzyme concentration in the range between 3 nM and 50 nM hCAP3. For higher concentrations of enzyme, the maximum fluorescence intensity of the donor as well as the dynamic range were independent of enzyme concentration. For HAT, no concentration dependence of the D/A ratio increase was observed (Figure 17 E). For mCAP3, the concentration dependence of the maximal donor fluorescence intensity was most pronounced (Figure 17 F).

All experiments were performed for four different substrate concentrations. The behavior was independent of the substrate concentration, so that precipitation at a certain concentration of the fragments is unlikely. Most likely, this effect is due to product inhibition which depends on the specific enzyme and might vary significantly. More experiments would be required to definitively answer this question.

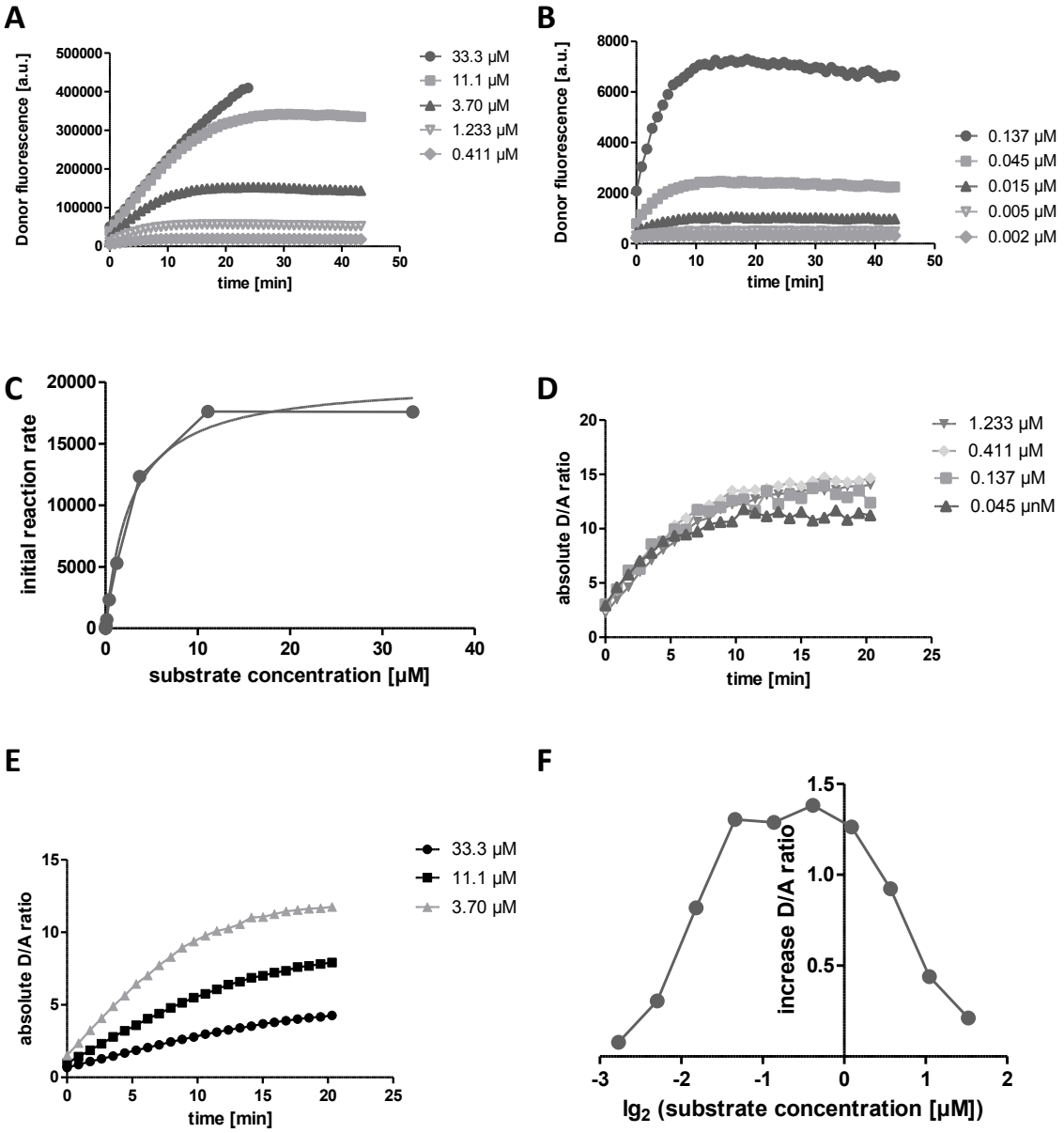

Figure 16: Determination of CAPRee1 kinetics with mCAP3

The assay was performed with 10 nM mCAP3. The probe concentration varied between 33.3 µM and 2 nM.
A: donor fluorescence for difference probe concentrations. B: donor fluorescence for very low probe concentrations.
C: kinetic plot, initial slopes of A and B vs. probe concentration. D and E: D/A ratio or different probe concentrations.
F: slope of D/A in the first 10 min vs. lg_2 of the probe concentration [µM]
Each trace was measured once, the traces are plotted for n=1. Identical experiments were performed for four different enzyme concentrations.

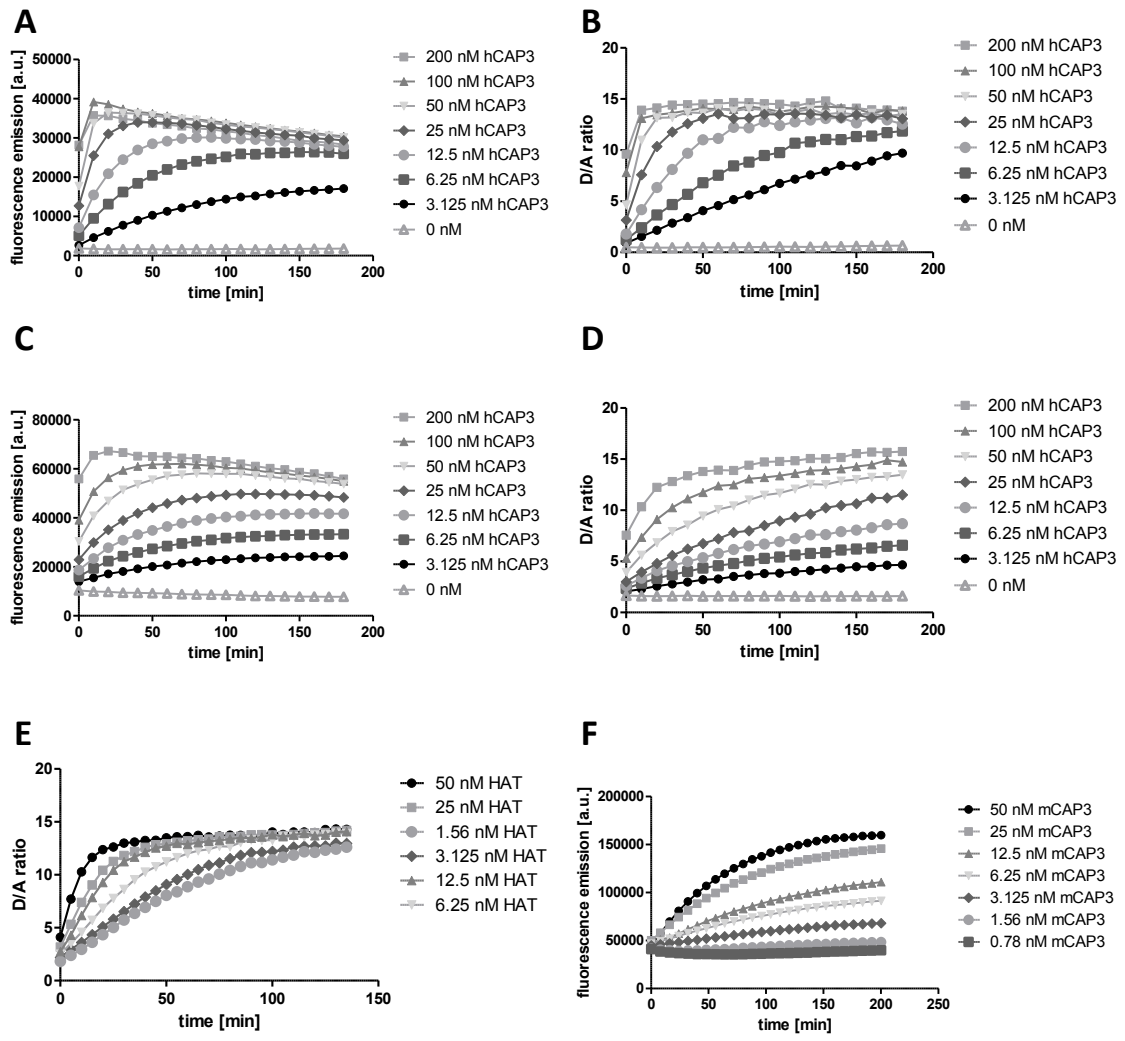

Figure 17: Behavior of donor fluorescence and D/A ratio of CAPRee3 upon cleavage by hCAP3, mCAP3 and HAT

The experiments were performed in identical buffer conditions (50 mM Tris-HCl, 0.05 % Brij-35). The traces are representative for CAPRee1 at 4 µM (A and B) and CAPRee3 in 1 µM concentration (C-F). The effects described are however independent of the substrate concentration which was varied between 0.5 µM and 4 µM (i.e. 0.5 µM, 1 µM, 2 µM, 4 µM). The numerical values of donor fluorescence emission were probe concentration dependent. Each substrate concentration was tested once for all given enzymes and concentrations thereof as controls. A-E are performed with human enzymes, F with murine CAP3.

Due to this behavior, the analysis of kinetic curves had to be reconsidered. The quantification of donor fluorescence seems not to be ideal because it is heavily influenced by numerous factors. The quantification of enzyme activity based on D/A ratio changes is much more robust. Over a set of 100 kinetic measurements, the D/A ratio curves were either fitted by linear regression in the first minutes or by non-linear regression fitting an inverse exponential function, calculating half-life and plateau height. Analysis revealed that the half-life did not significantly correlate to enzyme concentration, due to the behavior described that the maximal fluorescence and/or D/A ratio are not independent of enzyme concentration. Therefore, the plateau height was also an objective measure because this was not the case for all enzymes. The linear slope gave highly significant ($p<0.001$) correlation to the

enzyme concentration in all cases and was therefore the measure for all following experiments. The normalization to 1 as initial ratio at timepoint 0 is only possible if a negative control is available. For primary cells this would increase the number of experiments significantly or is partially even impossible. In case of murine tracheal epithelical cells or human nasal epithelial cells, it is not possible to obtain negative control and kinetic data from one sample due to technical limitations. Based on *in vitro* data, this normalization is not required for the read out of enzyme activity.

The cleavage of CAPRee1 was assessed for the following human proteases: CAP1, CAP3, HAT, furin, CTSS, CTSB, MMP12 and NE (Figure 18).

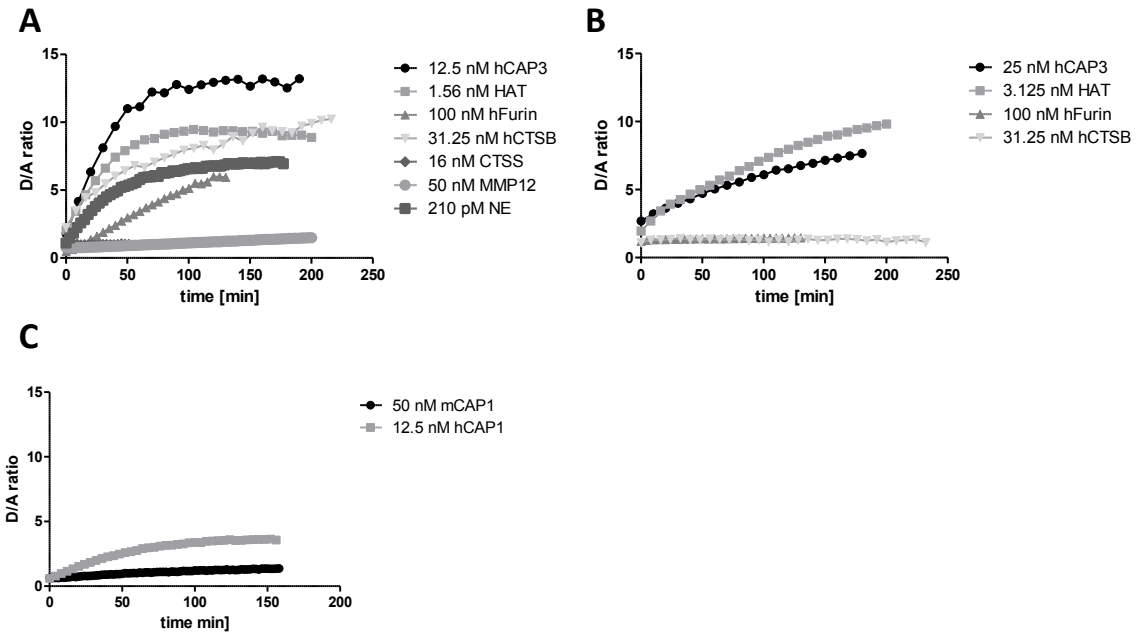

Figure 18: Cleavage of CAPRee1 and CAPRee3 by different recombinant enzymes

The assay was performed with the given enzyme concentration for CAPRee1 (A) and CAPRee3 (B). Probe concentration was 2 µM. The buffer composition was adapted to the enzyme. Enzyme concentration was normalized to cleavage of the respective commercial substrate sold for the enzyme. CAP1 could not be normalized to the other enzymes due to very low cleavage of the commercial substrate. (C) shows the cleavage of CAPRee1. All enzymes were tested in 8 or 12 different enzyme concentrations and 4 different substrate concentrations. The graphs show representative traces. All enzymes cleaved their respective commercial substrate from R&D systems as positive controls. The reaction rate for CAPRee1 and CAPRee3 was enzyme concentration dependent. Each concentration was measured once (n=1), for a total n of 32-48 combinations per enzyme and substrate.

Murine and human CAP1 are not included in the common graph due to comparably low enzyme activity. An activity comparable to the other enzymes could not be achieved.

To summarize, CAPRee1 was not only cleaved by CAPs, but also significantly by HAT, as expected, NE, cathepsin B and furin to some extent. The lysine in the cleavage site of CAPRee1_a prevented

cleavage by CTSB. CAPRee1 was not cleaved by cathepsin S and MMP12 at all. Interestingly however, the lipidated probe CAPRee3 was not cleaved by cathepsin B and furin at all. Cathepsin S and MMP12 were not further tested. For murine enzymes, the situation was comparable, i.e. the soluble probe CAPRee1 was cleaved by furin and cathepsin B, but not the lipidated probe CAPRee3. So far, the lipidated probe had not been carefully characterized[76-77]. It is expected in the protease field that the amino acid sequence is crucial for recognition as a substrate, but adjacent fluorophores should not significantly affect the specificity. However, this data shows that the modification from the soluble to the lipidated probe was not without effects on specificity. Further investigation is required to understand whether the fluorophores or the lipid anchor affect the binding to certain enzymes. On the cell surface, the lipid anchor will most likely not affect the recognition because it is expected to be hidden in the membrane. However, cleavage might be affected by the distance of the cleavage site from the membrane as well as the distance and flexibility of the catalytic subunit of the enzyme from the membrane.

2.2.3 Specificity of CAPRee1 on cell lines

Because the soluble probe was shown to be rather unspecific in experiments with recombinant enzymes, two relevant cells lines, i.e. human bronchial epithelial cells (CFBE41o$^-$) and murine kidney collecting duct cells (M-1), were tested with broad spectrum inhibitors that inhibit certain classes of enzymes. Serine proteases were blocked by Pefabloc SC, an irreversible, less toxic phenylmethylsulfonylfluorid (PMSF) derivate, metalloproteases by complexing agents like ethylenediaminetetraacetic acid (EDTA), cysteine proteases by E-64 and aspartic proteases by pepstatin A. The concentration was varied in the range recommended by the supplier of the inhibitor and incubated in DMEM + Hepes buffer to maintain neutral pH at atmospheric CO_2 20 min before addition of the substrate. After preincubation with the inhibitors, CAPRee1 was added at 2 µM concentration in DMEM + Hepes and the given inhibitor concentration. Except for Pefabloc SC, the inhibitors did not affect the cleavage of CAPRee1, whereas the serine protease inhibitor completely abolished cleavage on M-1 cells (Figure 19 A). On CFBE cells, camostat and Pefabloc SC significantly reduced the cleavage of CAPRee1, but did not abolish it completely (Figure 19 B). Interestingly, incubation with EDTA increased the cleavage rate, which might be explained by the fact that divalent cations have been published to inhibit regulate CAP1 activity[10]. Therefore, CAP1 activity might increase upon incubation with EDTA. Cleavage by proteases other than serine protease is not relevant on the respective cell lines. From this data, epithelial cells do not express NE or cathepsin B on their surface. Therefore, CAPRee1 was specific enough to exclusively detect serine protease activity. It was however not possible to distinguish between HAT and CAPs as HAT is also blocked by camostat mesilate and Pefabloc SC.

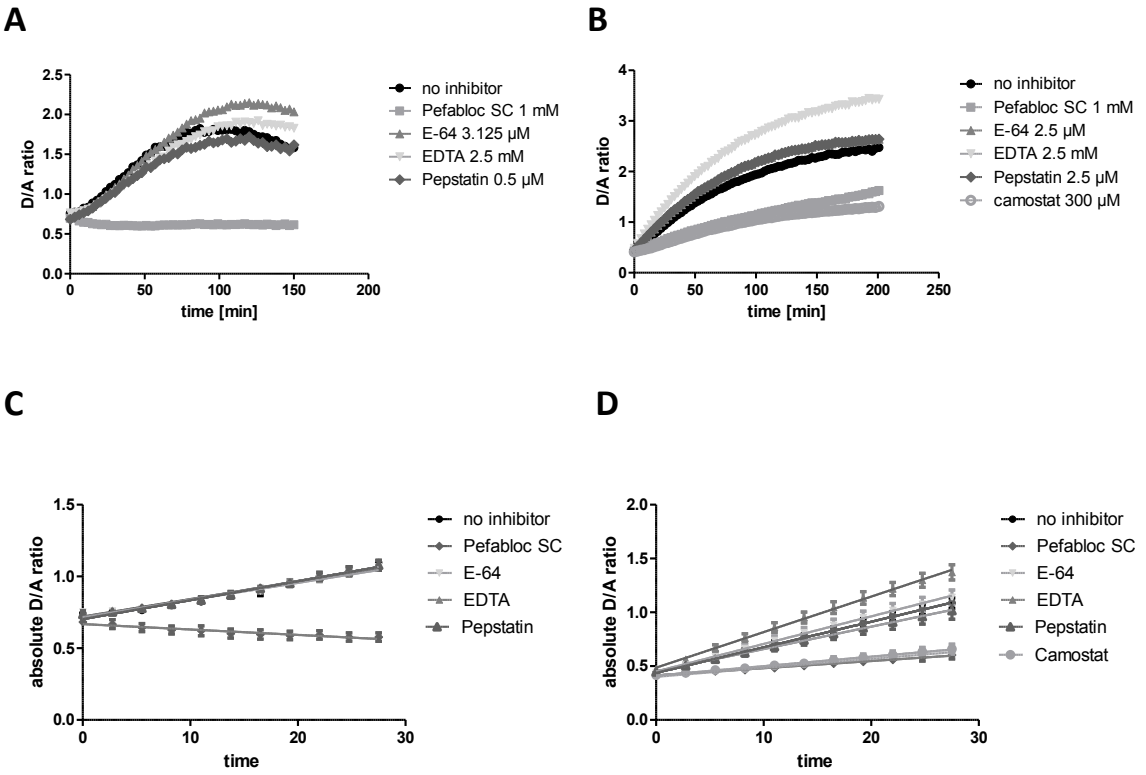

Figure 19: Specificity of CAPRee1 on M-1 and CFBE cells with broad spectrum inhibitors

To exclude cleavage by other than serine proteases, M-1 (A) and CFBE41o$^-$ (B) cells were seeded into 96-well multititer plates, incubated with the inhibitors for 20 min and afterwards incubated with CAPRee1. The cleavage was measured over time. A and B show representative traces, C and D show the linear increase in the first 30 min as mean ± SEM for an n=3. For M-1 cells, only incubation with Pefabloc SC is significantly different from the inhibitor control and all other inhibitors ($p<0.001$), but not different from zero. For the CFBE cells, none of the curves was not significantly different from zero. Pefabloc SC, camostat and EDTA were significantly different from no inhibitor ($p<0.0001$). Statistics was calculated by One-way ANOVA and Bonferroni Post Test.

2.2.4 Characterization of lipidated probes on murine and human cell lines

Apart from physical and biochemical properties of the probe as described above, the behavior of the CAPRee2 and CAPRee3 probes on the surface of cells is crucial for an utilizable probe. Internalization of the intact probe is a disqualifier because the probes are aimed to detect surface-bound protease activity. Furthermore, the separation of the fluorophores after cleavage is indispensable, i.e. only the donor fragment may remain attached to the membrane and the acceptor fragment should diffuse away from the cell surface. Ideally, the donor fragment would be internalized after cleavage to obtain a memory effect. The mechanism however, how the MMP12-probe LaRee is internalized after cleavage, remains unknown. Therefore it is unclear, how probes need to be designed to achieve this behavior. In case that the behavior is sequence-dependent, it cannot be designed on purpose as the recognition motive of the target enzymes mostly determine the sequence.

The experiments were performed on a Leica SP8 confocal microscope. For localization experiments in submerged conditions, the cells were seeded the day before the experiment into 8-well LabTek® dishes. Initially, the experiments were performed using the 405 nm- UV laser light for donor fluorophore excitation. After working out that the CAP activity is rather low which requires long imaging times in live cell imaging, the experimental conditions were changed and for later experiments, the 458 nm laser line of the Argon laser was used. The little red shift of the excitation light reduced energy-associated cell damage and improved survival of the cells. The signals of donor and acceptor fluorophores were collected in the Leica Hybrid Detectors. After initial adjustments for the experimental setup (i.e. submerged or air-liquid-interface), the gain was kept without further modifications. The intensity of the excitation light was adjusted according to signal intensity for every individual experiment. All experiments with human cells and cell lines were performed with a 40x or 63 x oil objectives. For the imaging of murine tracheal epithelial cells, a 20x water objective was used.

As proof of concept, HEK293 cells which do not have endogenous CAP activity were seeded into a LabTek® chamber and incubated with CAPRee2. Imaging was started immediately after addition without washing. The probe localizes exclusively to the plasma membrane. After 20 min of imaging, recombinant human trypsin, which cleaves CAPRee2 very efficiently, was added to the cells and imaged for another 20 min (Figure 20 A). Before the addition of exogenous enzyme, no change in the D/A ratio was observed. Similarly, murine CAP3 cleaves CAPRee2 on the surface of HEK cells (Figure 20 B). After addition, the D/A ratio increased rapidly upon cleavage. CAPRee2 is not significantly internalized after cleavage (Figure 20 C).

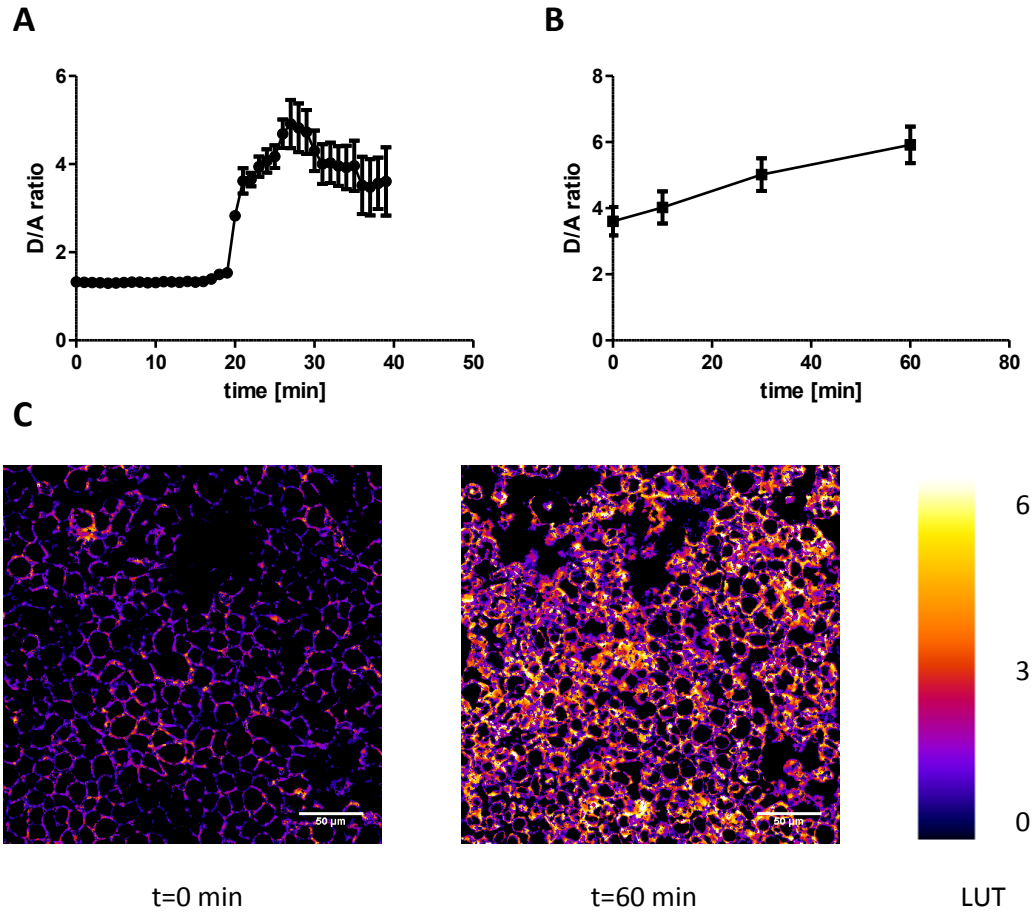

Figure 20: CAPRee2 on HEK293 cells

HEK cells do not express serine proteases capable of cleavage of CAPRee2 on their cell surface. A Addition of 5 nM recombinant human trypsin after 20 min. B mCAP3 enzyme addition at t=0. Images were taken after 10, 30 and 60 min of incubation C localization of CAPRee2 and ratio change represented as colour change according to look up table (LUT).

In A, 15 positions with each 11-40 cells were imaged (total n=366) and plotted as mean + SD over time. In B, each time point was measured individually. The plot represents mean ± standard deviation (SD). For t=0 min, n=131, for t= 10 min, n=883, for t=30 min, n=46, for t=60 min, n= 74. n equals number of cells quantified.

To summarize, CAPRee2 could be cleaved on the surface of cells by exogenous enzymes. Next, endogenous enzymes expressed on the surface of cells have to be able to cleave the probe. As model systems for human enzymes, the human bronchoepithelial cell derived from a CF patient, CFBE41o$^-$, was chosen. The cell line expresses all relevant CAPs and is homozygous for the most frequent CFTR mutation ΔF508. For murine systems, a lung cell line with CAP expression was not available. Therefore, the popular renal cortical collecting duct cell line M-1 was used for our experiments. The cell line expresses all relevant CAPs as well as ion channels including ENaC and CFTR and is heavily used in this field of research[86-89].

Similar to HEK cells, CAPRee2 localized to the plasma membrane of M-1 cells (Figure 21 A). In contrast to HEK cells, M-1 cells express proteases on their surface that cleave CAPRee2 over time. The cleavage could be blocked by the addition of 10 µM camostat mesilate (Figure 21 B). The D/A

ratio increased from about 3-4 up to a plateau around 6.5 (Figure 21 C). As shown for the soluble probe CAPRee1, the cleavage of CAPRee2 of the surface of M-1 cells could be fully blocked by the serine protease inhibitor camostat mesilate.

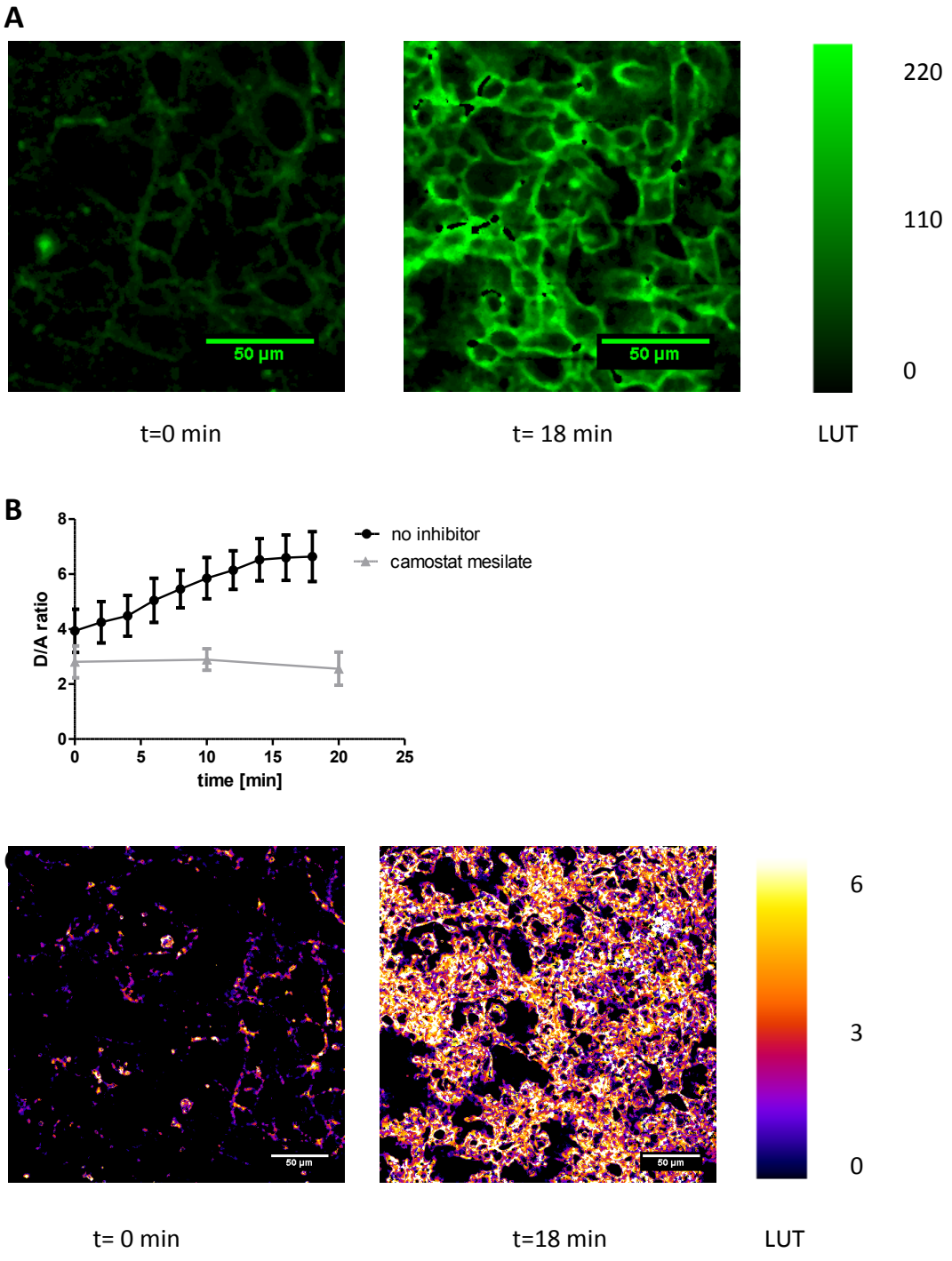

Figure 21: CAPRee2 on M-1 cells

2 µM CAPRee2 is incubated on M-1 cells in phenol red-free and serum-free DMEM at 37 °C and 5 % CO_2. A shows a representative image of the donor fluorescence signal after addition and after 18 min. B represents the quantification of the D/A ratio over time in absence of inhibitor, represented as mean ± SD (n=92 cells). The inhibitor, 10 µM camostat mesilate, was incubated for 20 min before addition of the probe (n=21 cells). C represents representative images of the mean D/A ratio after addition and after 18 min in absence of inhibitor.

To test CAPRee2 for the application in human systems, CFBE41o$^-$ cells were seeded into Lab-Tek chambers and cultured overnight. Typically, the cells grow in islets which impedes immediate homogenous staining and which is only achieved after several minutes of incubation. CAPRee2 localizes to the plasma membrane and remains there for several hours. CFBE41o$^-$ cells express CAPs so that the probe is cleaved over time, shown as increased brightness of the donor channel (Figure 22).

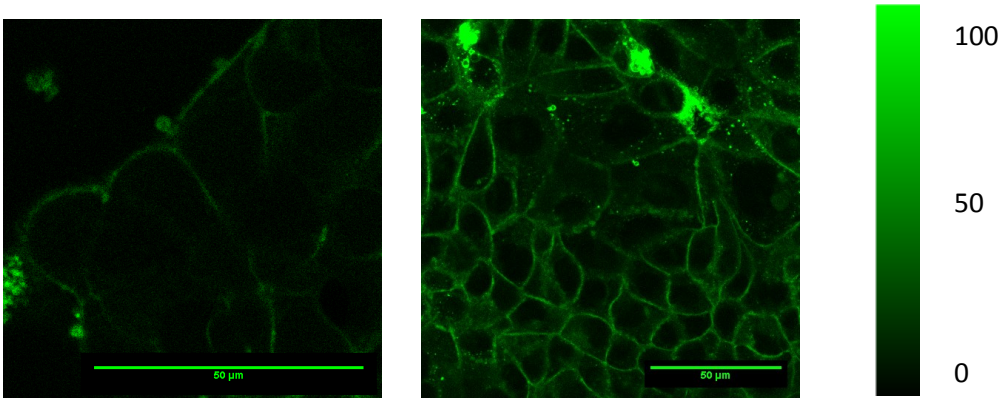

Figure 22: Localization of CAPRee2 on CFBE41o$^-$

The cells were seeded in LabTek^{tM} dishes over night and incubated with 2 µM CAPRee2. The images represent the Cou343 fluorescence directly after addition and after 3 h of incubation. The images show representative images from a dataset of 15 different positions.

Both *in vitro* and cell-based assays revealed that the maximal ratio change obtained from CAPRee2 is rather low. To test whether a modification does improve the maximal fold change, M-1 cells were stained with the probes in suspension and spinned on glass slides either directly after addition of the probe ("uncleaved") or after incubation with 2 nM trypsin for 1 h ("cleaved"). This results in the maximal fold change that is to be obtained (Table 2). As the cells could be carefully washed, acceptor fragments that are non-covalently attached to the plasma membrane could be washed off (Figure 23). First, the probe was modified so that the position of Cou343 and lipid were interchanged so that the theoretical distance between the fluorophores was reduced (CAPRee2_c). The modification however did not improve the performance but decreased the maximal fold change compared to the original probe CAPRee2 on fixed M-1 cells. Therefore, the modification of the acceptor fluorophore was done on the original backbone of CAPRee2.

Table 2: Modifications of CAPRee2 and maximal D/A ratio fold change

#	Acceptor fluorophore	Modification compared to CAPRee2	fold change
CAPRee2	TAMRA	-	6.5
CAPRee2_a	TAMRA	Position of Cou343 and lipid interchanged	5.9
CAPRee2_b	Dy485-XL	-	2.5
CAPRee2_c	Cyanin-3	-	8.0
CAPRee3	TAMRA	Additional peg-linker between TAMRA and N-terminal Arg	3.1

Next, the acceptor fluorophore was modified. As described above, TAMRA was replaced by a Dy485-XL- and a Cyanin-3 derivative. The structures are shown in Figure 10. If not indicated otherwise, the images shown are representative images from M-1 cells. However, there was no significant difference observed in the localization of the probe on the different cell lines. The cleavage of the probe was faster on M-1 cells so that they were chosen for the comparison experiments.

First, the large stokes-shift dye Dy485-XL was tested for its performance as acceptor fluorophore. It is a coumarin-based dye which should be less sticky compared to cyanin-3 as well as less prone to form stacks compared to TAMRA. Additionally, the excitation spectrum of the dye has perfect overlap with the emission spectrum of Cou343 which might significantly improve the quenching of the donor. The extinction coefficient of Dy485-XL however is rather low and in the range of Cou343. Due to additional sulfonate groups on the dye, it should be very hydrophilic. *In vitro* testing however already revealed that the dye did not improve the performance of the probe. Potentially, either the orientation of the dyes towards each other is not ideal or the low extinction coefficient and quantum yield are not sufficient for a well performing acceptor fluorophore. The observation was confirmed by cell-based experiments. The D/A ratio in the intact molecule was very high compared to CAPRee2. The maximal ratio change obtained in ideal conditions with fixed cells is about 2.5 which was very poor compared to the previously described probes CAPRee2 and CAPRee2_a. (Figure 23). Life cell imaging did not improve the D/A ratio change, but did show a second unfavorable feature of the probe. The acceptor fragment seems to localize to vesicles after cleavage (Figure 24). Consequently, CAPRee2_b was not further characterized because it did not show any improvements compared to CAPRee2.

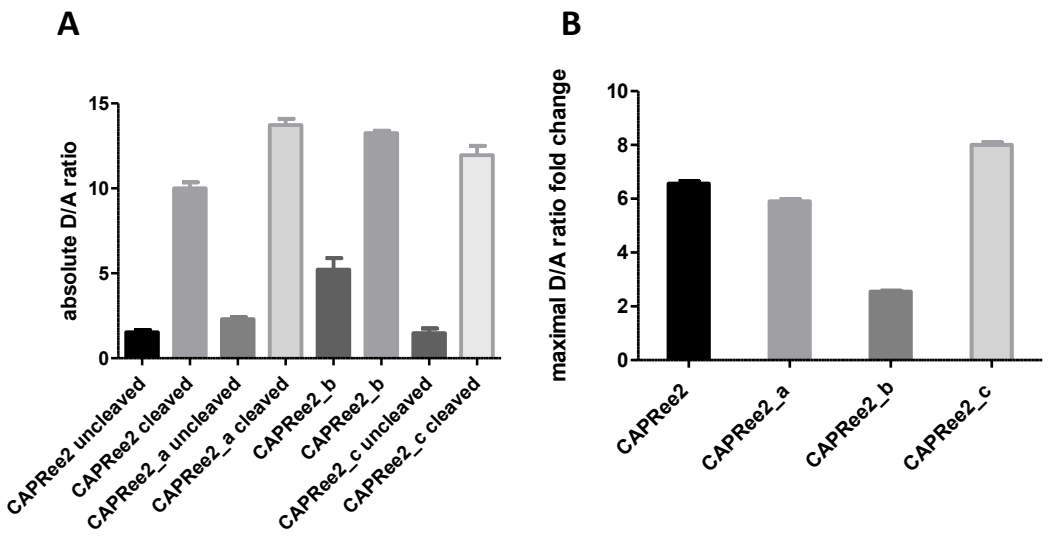

Figure 23: CAPRee2 and derivatives on fixed M-1 cells

A absolute D/A ratio on fixed M-1 cells with 1 µM of the respective probe, fixed with 4 % paraformaldehyde in PBS.
B maximal D/A ratio fold change normalized to D/A ratio of the uncleaved samples. Data as mean ± SD.

n=17 positions for all expect, CAPRee2 cleaved (n=14) and CAPRee2_c cleaved (n=34). Within one position, the mean was averaged. Each position contained about 50 cells.

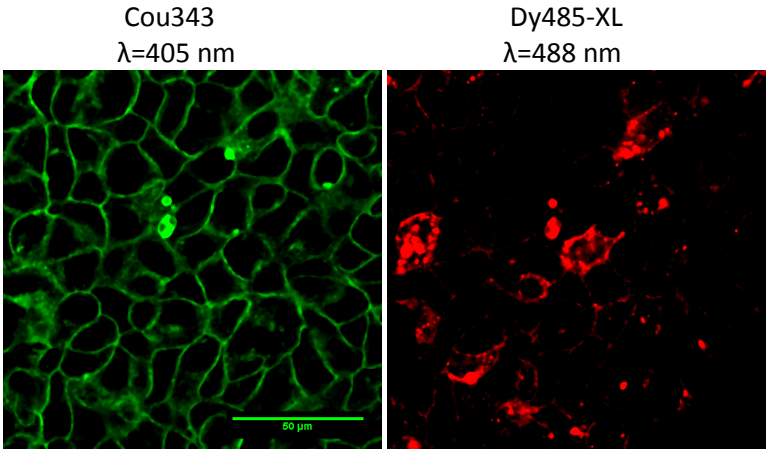

Figure 24: Localization of CAPRee2_b on M-1 cells after 3 h

The cells were incubated with 4 µM CAPRee2_b for 3 h and imaged. The donor localizes to the plasma membrane whereas the acceptor is localized to dot-shaped structures. The cells were imaged in phenol red-and serum-free DMEM at 37 °C and 5 % CO_2. 10 different positions were chosen and imaged. The image is representative.

Cyanin-3 has a higher extinction compared to TAMRA which might increase the quenching effect in the intact molecule. *In vitro*, the performance with respect to maximal D/A ratio change was improved, which was even further confirmed by experiments on fixed cells stained in suspension (Figure 20 A-B). Live cell experiments however revealed a critical feature of cyanin-3 as acceptor fluorophore: the dye was very sticky towards membranes so that the acceptor fragment did not diffuse away but remained attached to the cell in dot-shaped structures, potentially vesicles (Figure

25 A). There was a very clear difference in localization of donor and acceptor signal which indicates that this happened to the cleaved probe and not the intact molecule. The donor remained attached to the plasma membrane whereas the acceptor was obviously localized to vesicles. This only happens in case of loading the intact molecule. When the donor and the acceptor are separated by cleavage of the probe before addition, only the donor fragment loads onto the cells whereas the acceptor does not efficiently bind to the cell membrane due to the lack of lipid anchor (Figure 25 C). This property is highly disadvantageous in case where the cells cannot be washed during imaging which is the case in all relevant applications of the CAPRee probes. This resulted in a strongly decreased maximal D/A ratio change of about 2 in live-cell imaging conditions (Figure 25B). However the difference to the inhibitor control was still highly significant ($p< 0.0001$).

A second probe was synthesized with Cy3 as acceptor with an additional peg-linker to increase the solubility of the acceptor fragment, but it did not significantly change the behavior of the fragment compared to CAPRee2_c. To conclude, cyanin-3 is not an adequate acceptor fluorophore for the CAPRee probes.

The modification of acceptor dyes did not improve the overall behavior of the lipidated probe compared to TAMRA. CAPRee2 might not be hydrophilic enough for some relevant applications. For cells that are grown in air-liquid-interface (ALI) conditions, the application of high volumes to the apical “air” side of the cells might be detrimental. On the other hand, the cell density is extremely high compared to submerged conditions. The cells were seeded with 5x higher density compared to LabTek^{TM} dishes and cultured for several weeks instead of hours. Therefore, the amount of cell membrane to be stained is much higher compared to submerged conditions. Consequently, a probe with very good water solubility was required which can be loaded in high concentrations up to 20 µM in aqueous solution without precipitation. This enabled the application of low volumes with sufficient loading of the probe onto the cell membrane. Furthermore, the volume to which the acceptor fragment will diffuse after cleavage is extremely low in ALI condition, i.e. about 20 µl. Therefore, an additional peg-linker was inserted between the acceptor fluorophore and the arginine in P4 to obtain increases aqueous solubility (CAPRee3). As shown in the *in vitro* characterization, the insertion of the linker did not significantly affect the maximal ratio change for CAPRee3. On fixed cells, the difference seemed to be higher but in live cell imaging conditions, the probe did give a sufficiently high ratio change. The probe initially localized to the plasma membrane and did not internalize significantly. There was no membrane staining detectable for the acceptor after cleavage. The probe has similar localization compared to CAPRee2 on M-1 and CFBE cells as well as similar cleavage behavior (Figure 26). The quantification of the D/A ratio change in live cell conditions will be presented later.

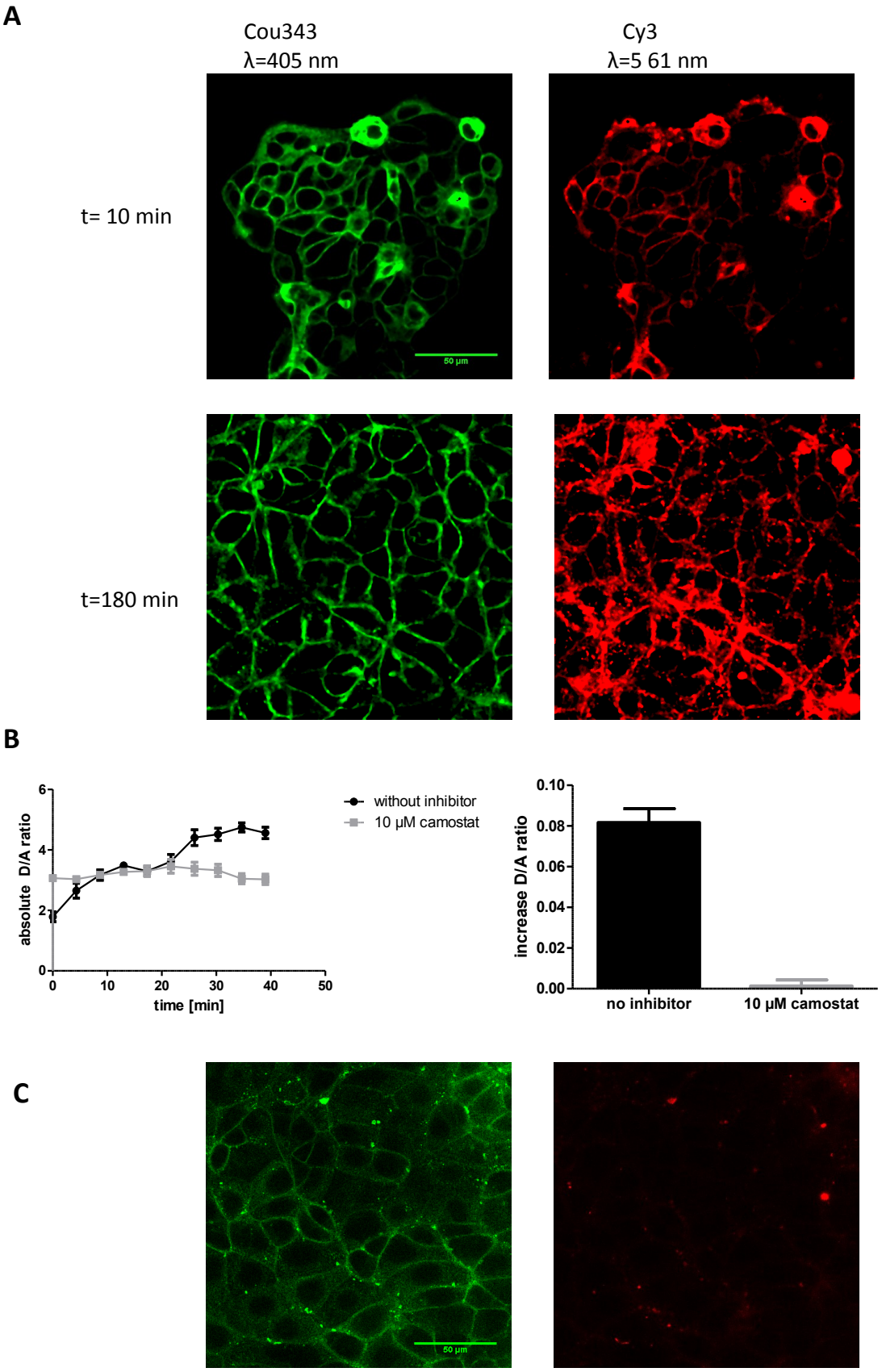

Figure 25: Localization and cleavage of CAPRee2_c on M-1 cells

The cells were incubated with 4 µM CAPRee2_c for 10 min and imaged right after incubation and after 3 h in phenol red- and serum-free DMEM at 37 °C and 5 % CO_2. For part A, the contrast and brightness was adjusted individually to show the localization. In B, the cells were preincubated with 10 µM camostat mesilate before the addition of the probe, data as mean ± SEM. 5 positions were imaged and averaged, with each 50-100 cells. Although the ratio is higher in total, the increase in the D/A ratio is not significantly different from 0 for the inhibitor control. The given wavelengths are the respective excitation wavelength for the image.

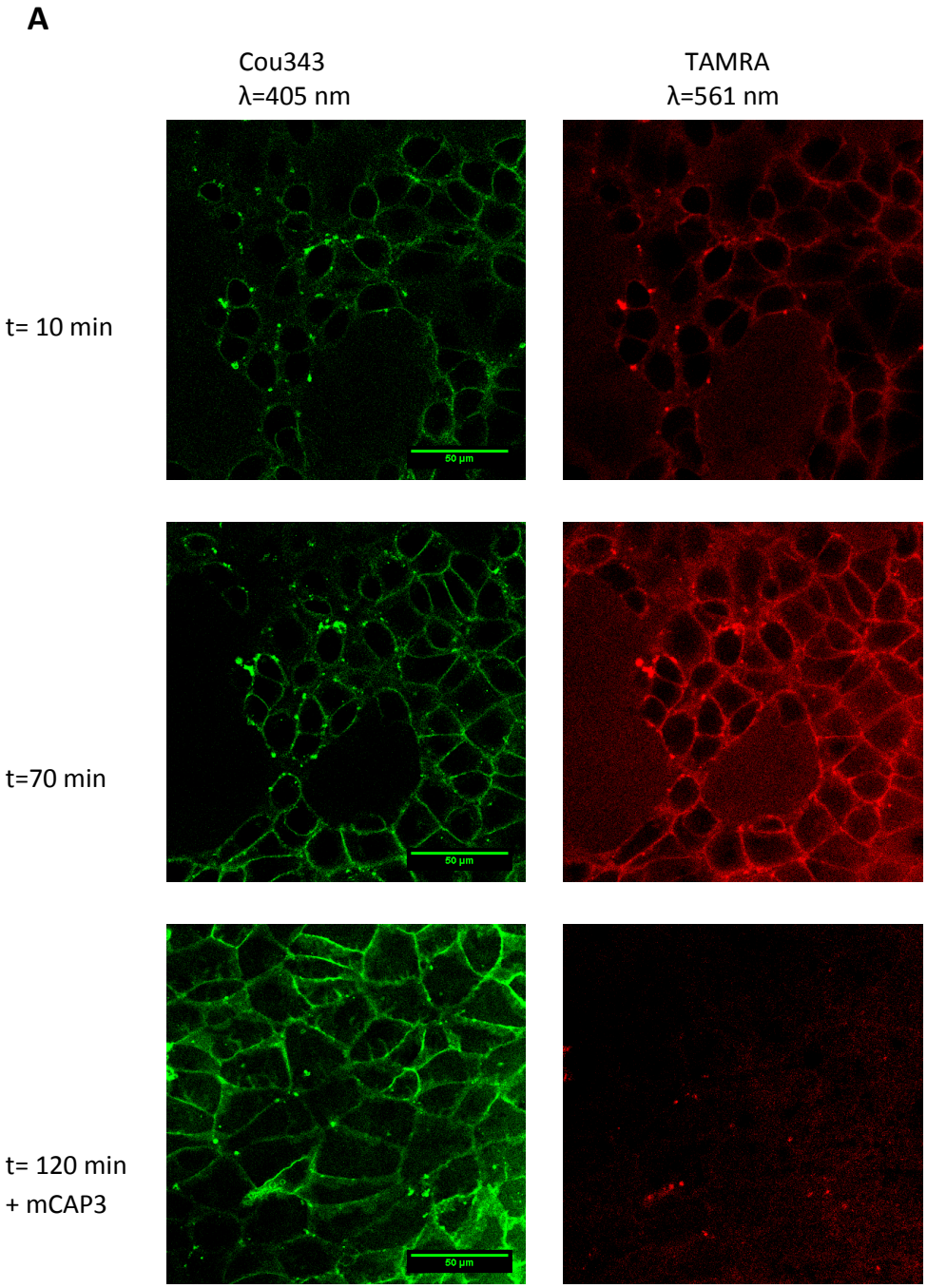

Figure 26 A: Localization of CAPRee3 on M-1 cells

The cells were incubated with 2 µM of the probe and, where indicated with 50 nM mCAP3. The cells were imaged for 2 h, the images are representative for each time point. Cou343 is the donor fluorescence, TAMRA acceptor fluorescence. For each condition, 10 positions were imaged with similar cell density.

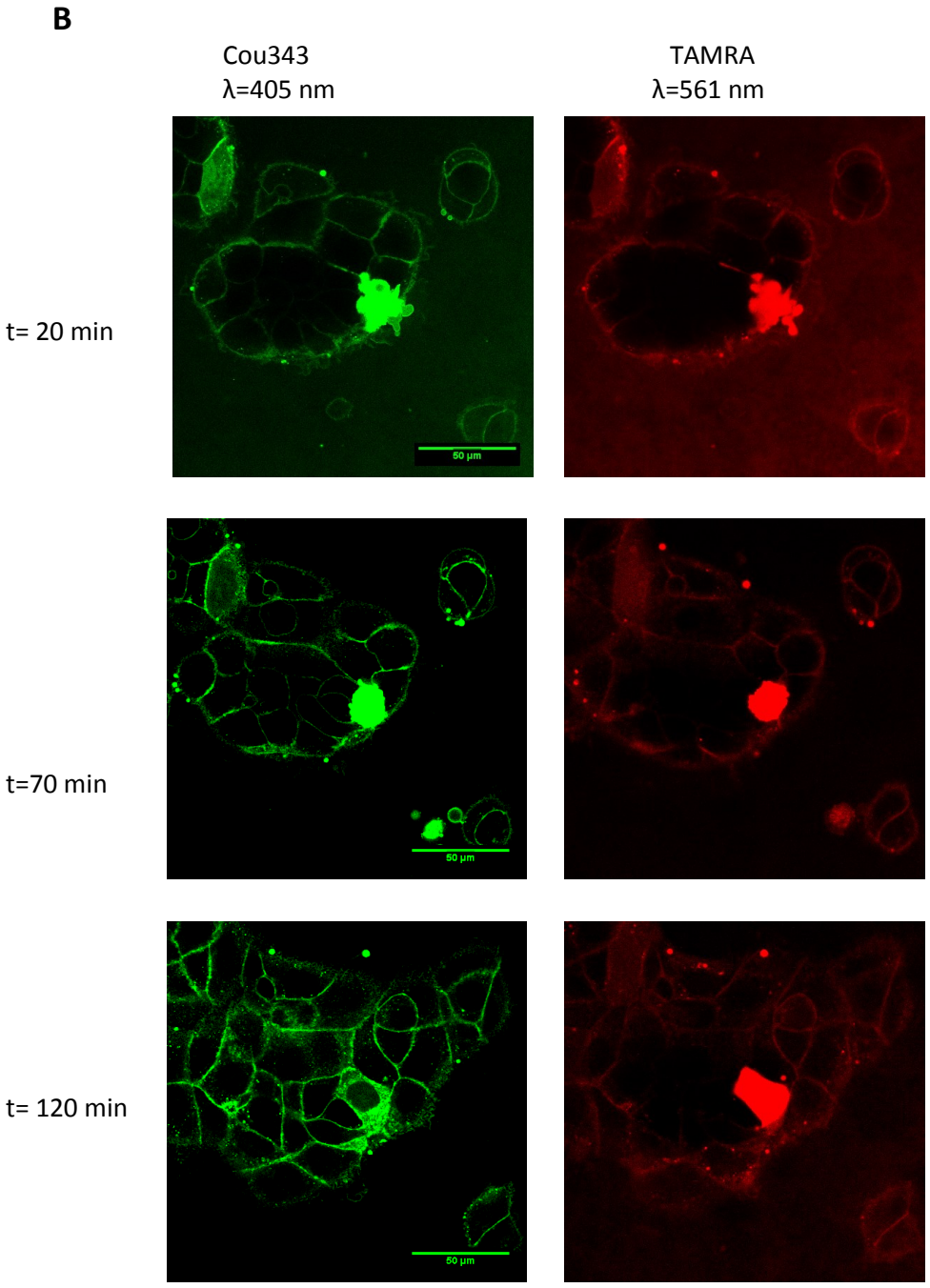

Figure 26 B: Localization of CAPRee3 on CFBE41o$^-$ cells

The cells were incubated with 2 µM of the probe and, where indicated with 50 nM mCAP3. The cells were imaged for 2 h, the images are representative for each time point. Cou343 is the donor fluorescence, TAMRA acceptor fluorescence. For each condition, 10 positions were imaged with similar cell density.

In FRET measurement setups, it is challenging to separate the signals from donor and acceptor dyes because of their spectral overlap. In our case, Cou343 has a comparably large tails which results in light emission in the range where usually acceptor fluorescence is detected. On the other hand, the

acceptor fluorophore is partially illuminated by the excitation light of the donor. As both fluorophores have to be imaged simultaneously, the overlap of the signals cannot be prevented. To calculate these effects and correct the signals mathematically, probes which have only one of the fluorophores were synthesized as donor- or acceptor-only probes. For these experiments, probes which only lack the respective fluorophores but were identical to CAPRee2 with respect to sequence. Therefore, the donor-only but also the acceptor-only probe did load on the cells similarly to the CAPRee2. The bleed through and direct excitation of the acceptor were imaged. The bleed through of Cou343 into the acceptor channel is around 10 to 15 %, thus limiting the theoretical maximal D/A ratio change. The direct excitation of TAMRA adds onto the energy transfer effect, lowering the initial D/A ratio artificially. In case of CAPRee2 and CAPRee3 for which the acceptor fragment diffused away, this phenomenon was advantageous because not only the signal due to energy transfer from the donor was lost upon cleavage but also the direct excitation from the 405 nm laser because of the spatial separation of the fragments. For the cyanin-3-based probes however, this was detrimental.

The fragments resulting from the enzymatic cleavage of CAPRee3 had been synthesized and applied to cells. The fragments were synthesized and fully characterize by Madeleine Schultz. As expected, the donor fragment, which was identical for CAPRee2 and CAPRee3, localized to the plasma membrane whereas the acceptor fragment remained in solution and did not load onto the cells (Figure 27). The acceptor fragment could be easily washed off, so that no signal was remaining after wash. The lipidated fragment did not internalize.

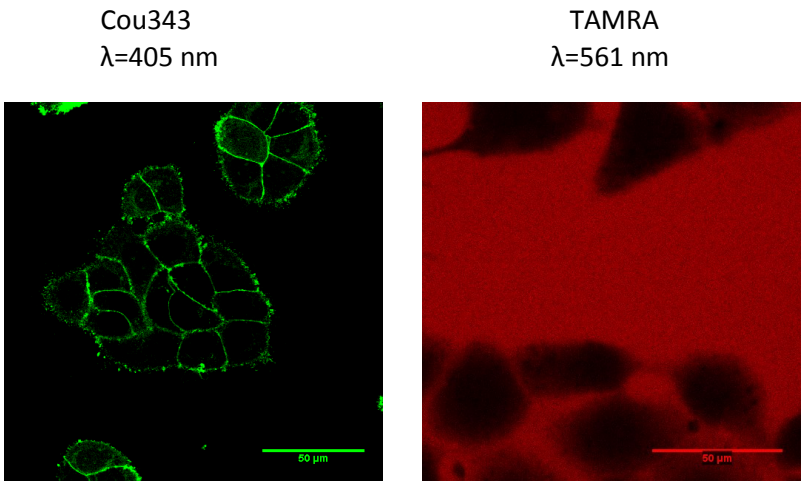

Figure 27: Localization of cleavage products of CAPRee3

The given wavelength represents the excitation wavelength for the respective image. The probe was applied at 2 µM concentration. The cells incubated with donor fragment were washed. The cells with acceptor fragment are shown unwashed. Washing removed the unbound acceptor fragment.

To summarize, CAPRee2 and especially CAPRee3 are suitable probes for the detection of enzyme activity on the surface of murine and human cells. The maximal D/A ratio change was sufficiently high to quantify changes. They localized exclusively to the plasma membrane upon addition and remained there for the time line of relevant experimental setups. Due to the higher solubility of the probe, CAPRee3 was used in the following application experiments.

2.3 Characterization of ENaC-based CAP probes

So far, the probes are based on the autoactivation cleavage site of CAP3. These probes are cleaved by CAPs as well as HAT but not by furin. Furin however has been published lately to play a crucial role in the regulation of ASL volume and other processes in the CF lung[43]. Therefore, a second class of CAPRee probes had been designed which has the CAP cleavage site in the γ-subunit of ENaC as substrate sequence (RKRK VGGS), CAPRee4 and CAPRee5. The repeat of basic residues might turn it into a furin substrate which recognizes tandem basic amino acids. The furin cleavage site in γ-ENaC however is RKRR[82] and furin prefers R in P1 in general, so that it remains to be tested whether the new probe is a target for furin.

CAPRee4 and CAPRee5 were synthesized and purified by Jonas Wilhelm and Frank Stein. CAPRee5 and modifications of it could not be synthesized efficiently for unknown reasons. When TAMRA was coupled as the first step of synthesis, no amino acids did efficiently couple to the unprotected N-terminus. The attachment of TAMRA as final step of synthesis on one hand enabled successful synthesis of the peptide, but TAMRA did not couple anymore. Therefore, the synthesis strategy was changed for CAPRee6: instead coupling TAMRA *via* amide coupling, TAMRA was coupled together with a second peg-linker moiety *via* copper-catalyzed click chemistry onto a glycine residue bearing an alkyne. TAMRA was linked to an azide functionality. In a one-pot-reaction, NHS-activated TAMRA was coupled to a peg-linker bearing an amino group on one end and an azide group on the other end. Without interim purification, by addition of copper (I) and Tris[(1-benzyl-1*H*-1,2,3-triazol-4-yl)methyl]amin (TBTA), the TAMRA derivate was coupled to the alkyne group on the C-terminal glycine. Furthermore due to the low performance of CAPRee5, the part which was tested to be less relevant for CAP recognition (P1'-P4') was changed back to the sequence used in CAPRee1-3 VVGG instead of VGGS.

The detailed structures are shown in the addendum and the methods section. The synthesis is described in section 6.2.2. Analytical data is presented in the appendix.

2.3.1 Physical properties of soluble and lipidated probes

The soluble CAPRee4 probe has been equipped with the same combination of dyes as CAPRee1. Furthermore, the two-dimensional distance between the fluorophores is also identical. The positions of Cou343 and MetOCou however were interchanged so that Cou343 was attached to the basic motive in all ENaC-based probes.

Unlike CAPRee1, the D/A ratio in the intact molecule was dependent on the probe concentration (Figure 28 A). Without the addition of enzyme, the D/A ratio remained mostly unchanged over time, but for concentrations lower than 3.33 µM, the D/A ratio increased with decreasing probe concentration (Figure 28 B). For concentrations higher than 3.33 µM, the D/A ratio did not change with increasing concentration, suggesting that intermolecular effects did not play a significant role (Figure 28 B). The maximal donor fluorescence emission was dependent on the probe concentration (Figure 28 C), i.e. higher concentrations give rise to higher final donor fluorescence intensity. The donor fluorescence intensity was also enzyme- concentration dependent to some extent (Figure 28 D), i.e. for example 2.5 and 5 nM hCAP3 gave rise to different final plateaus.

Similarly to CAPRee1, the maximal D/A ratio change was independent of the substrate in a concentration range up to about 3.33 µM. For higher concentrations, the D/A ratio change decreased significantly (Figure 28 E, F). Consequently, for CAPRee4, there was no concentration range in which the D/A ratio was completely independent of the probe concentration. This represents a strong disadvantage over CAPRee1 which is more robust to minor variability in the concentration compared to CAPRee4.

The maximal D/A ratio change at a given probe concentration (2 µM in G and 3.3 µM in H), was independent of the enzyme-concentration, both for human (Figure 28 G) and murine (Figure H) CAP3. In the direct comparison, murine CAP3 cleave the probe much faster compared to the human orthologue.

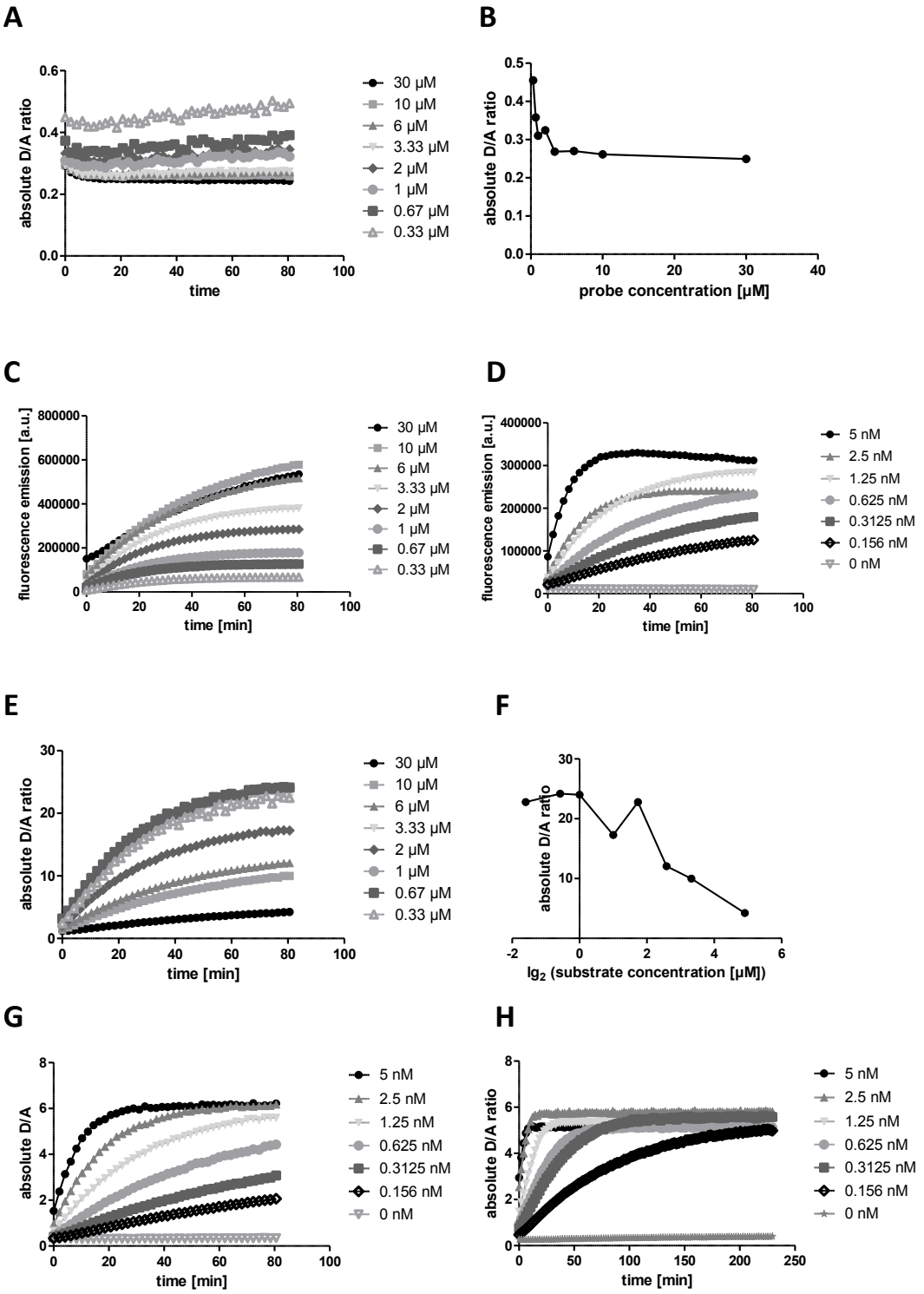

Figure 28: *In vitro* behaviour of CAPRee4

A absolute D/A ratio in absence of enzyme in dependence of probe concentration. B initial D/A ratio is substrate concentration dependent. C MetOCou fluorescence emission for different probe concentrations. D MetOCou fluorescence emission with different concentrations of hCAP3. E dependence of the maximal D/A ratio from probe concentration. E quantification of the maximal D/A ratio. F absolute D/A ratio over time upon cleavage with different concentrations of hCAP3. G absolute D/A ratio over time upon cleavage with different concentrations of mCAP3.

Each trace was measured in a single well. The data was obtained for 8 different substrate concentration from two independent dilution series and 12 different enzyme concentrations for each enzyme, pipetted from two independent dilution series.

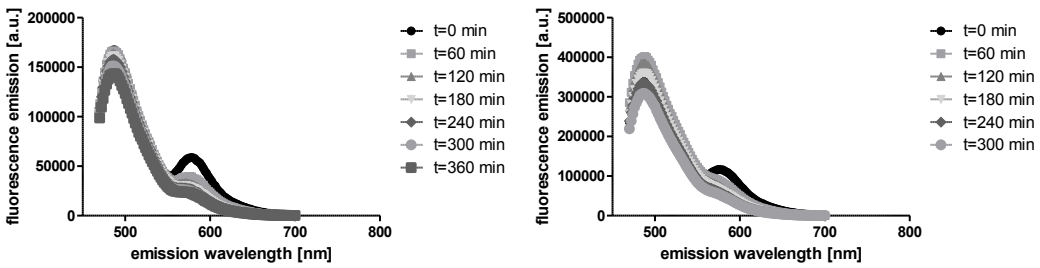

Figure 29: Emission wavescans of the lipidated probes CAPRee5 (A) and CAPRee6 (B)

The probes are cleaved by 5 nM mCAP3. The experiment was performed twice with different enzyme concentrations.

The lipidated probe CAPRee5 had a very poor performance compared to CAPRee2 and CAPRee3. Although the two-dimensional distance is similar to CAPRee2 and lower compared to CAPRee3, the sequence of four basic residues seemed to be detrimental for FRET in the lipidated probe. The initial D/A was about twice as high, resulting in a FRET ratio change of about 2. Furthermore, the donor fluorescence decreased continuously for CAPRee5 *in vitro*. This was different in cell-based experiments. On liposomes, basically no cleavage could be observed. The properties were not significantly changed for CAPRee6, which is more hydrophilic, but has an even further twodimensional distance between the fluorophores. For CAPRee6, the donor fluorescence increased for about 1 hour in these settings, but afterwards decreased rapidly. Therefore, the ratio change was very poor and thus was expected to not allow quantification of enzyme activity on the cell surface.

2.3.2 Kinetic properties and specificity towards CAPs over other proteases

Due to the poor performance of the lipidated probes with respect to FRET and maximal D/A ratio change and the undesirable behavior on the surface of cells (see section 2.3.3), the lipidated ENaC-based probes CAPRee5 and CAPRee6 require major redesign. Therefore, only the soluble probe CAPRee4 was analyzed regarding kinetics and specificity to estimate whether redesign is worth the effort. From the probes CAPRee1-3, it became clear that modifications of the dyes might have influence on the specificity and kinetic parameters so that the lipidated probes were not fully characterized.

Similarly to CAPRee1, CAPRee4 in a concentration range from 0.33 µM to 30 µM was tested for cleavage by hCAP3 and mCAP3 in 12 different concentrations. Compared to CAPRee1, the cleavage was much faster, so that the enzyme concentrations had to be dramatically reduced compared to previous experiments. For CAPRee4 and CAPRee5, the comparison is very difficult because the quantification of the cleavage was hardly possible. The maximum in donor fluorescence was reached

after 1 h compared to approximately 5 h or more for CAPRee2 and CAPRee3. It remained unclear however if full cleavage was already reached or if this was due to the poor performance of the probe. For murine CAP3, the cleavage rate was even further increased.

For the calculation of the Michaelis-constant, the linear increase of the donor fluorescence was considered. Up to 10 µM, the behavior of the probe was in line with regular Michaelis-Menten kinetics, for 30 µM, the initial reaction rate decreased by about 30 to 50 %. Most likely, this is due to product inhibition. Quantification of the Michaelis constant k_M revealed that is also in the low micromolar range, slightly lower than for CAPRee1 (Figure 30). For 1.25 nM enzyme, the calculated k_M is 1.4 µM for hCAP3 and 1.6 µM for mCAP3. The cleavage rate however was still much higher compared to CAPRee1, suggesting a high difference in the turnover number. Quantification and quantitative comparison however was not possible and would require deeper investigation. As the experiments had to be performed with recombinant enzymes, the comparison of the *in vitro* data with patient- or model system-derived numbers is anyway not possible, nor is the use of *in vitro* data for the absolute quantification of enzyme concentration on the cell surface.

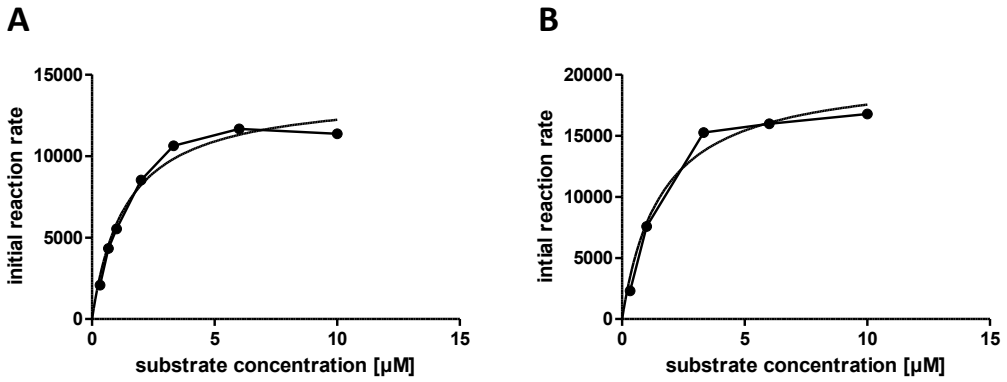

Figure 30: Kinetics of CAPRee4

A human CAP3, *B* murine CAP3; As an example shown are the results which was performed with 1.25 nM enzyme. The curves were fitted by non-linear regression to calculate v_{max} and k_M. Similar traces were obtained for 12 different enzyme concentrations for each enzyme from two independent dilution series. Each concentration was measured once.

Similarly to CAPRee1, the initial reaction rate based on the D/A ratio increase in the linear range was only in a certain range probe-concentration independent (Figure 16 F, Figure 31 A). For CAPRee4, it did not decrease with concentrations lower than 50 nM. The initial increase in D/A ratio was dependent of the probe concentration for CAPRee4 (Figure 31 A).

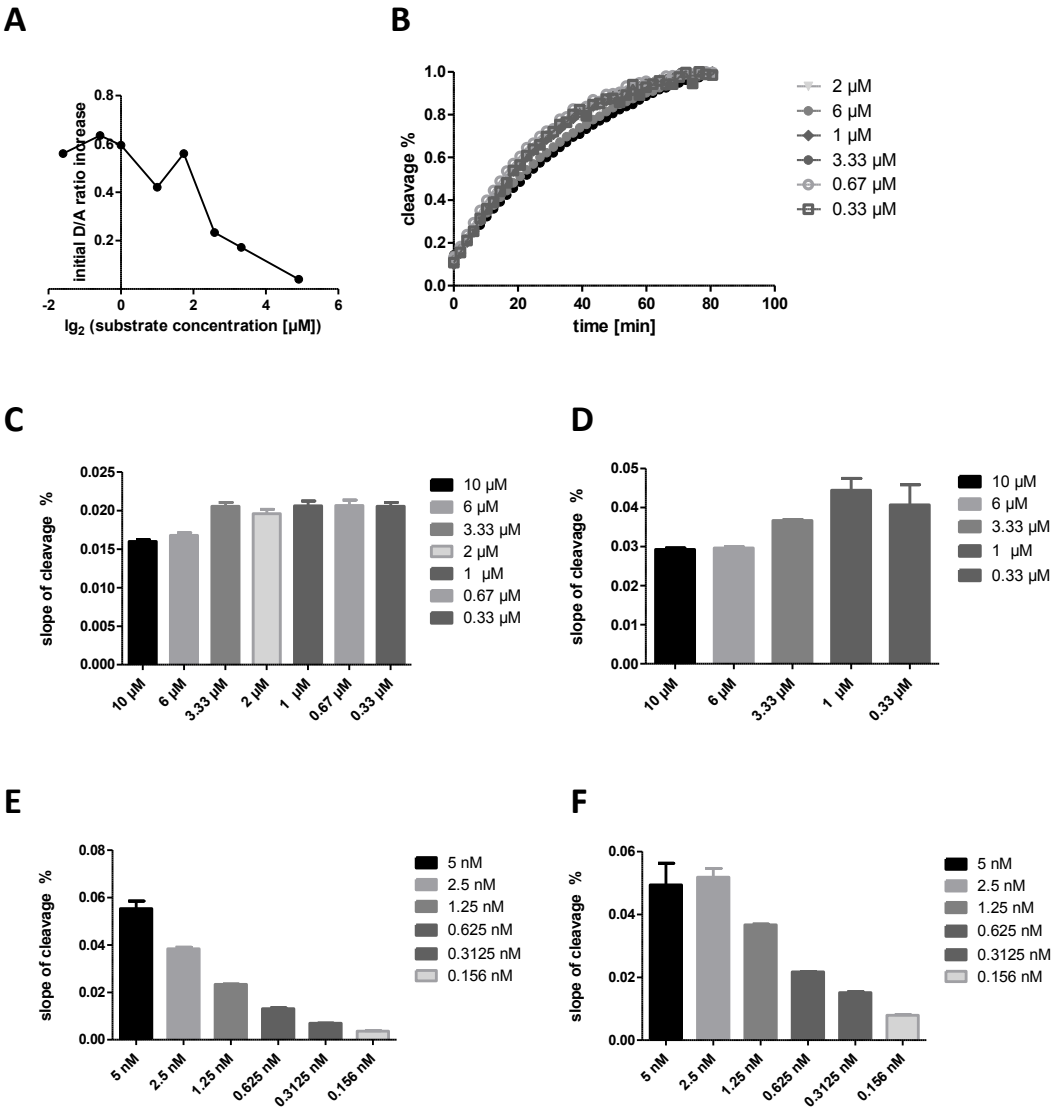

Figure 31: Quantification of enzyme activity by % cleavage

A: dependence of the initial increase in D/A ratio from the substrate concentration. B: cleavage in % calculated by normalization to negative and positive control. C: slopes of B in the first 10 min for different substrate concentrations with 1.25 nM hCAP3. D: comparable to C for 1.25 mCAP3. E: slope of % cleavage with 2 µM CAPRee4 and different concentrations of hCAP3. F: slope of % cleavage for 3.33 µM CAPRee4 and different concentrations of mCAP3.

Each concentration was measured once. Error bars indicate the error of the slope calculated by linear regression for each trace. In total 8 different probe concentrations and 12 different enzyme concentrations were tested.

As the increase as well as the maximal D/A ratio are substrate-concentration dependent, the quantification became more robust and less susceptible to pipetting errors when the read out as both normalized to positive and negative control. The cleavage % was calculated the following:

$$\%\ cleavage = \frac{\left({}^{D}/_{A} \,/\, {}^{D_{no\ enzyme}}/_{A_{no\ enzyme}}\right)}{\max\left({}^{D}/_{A}\right)}$$

with D representing the donor fluorescence emission and A the acceptor fluorescence. Max stands for the maximal value measured for the respective enzyme and substrate concentration. Consequently, the values range between 0 and 1. It was observed that for a similar concentration range compared to CAPRee1, the increase in cleavage % was independent of the substrate concentration, i.e. for concentrations lower than 3.33 µM (Figure 31 C). The slopes were not significantly different ($p>0.05$). For concentrations higher than 3.33 µM, the slope was significantly different ($p < 0.001$, for 6 µM vs. 2µM and 1 µM, $p<0.01$). Significance levels were calculated by One-way ANOVA with Bonferroni correction[90]. Similarly, for mCAP3, the increase of cleavage % was independent of the substrate concentration, i.e. all p-values are > 0.05, expect the comparison of 10 µM and 6 µM to 1 µM (Figure 31 D). The initial increase in cleavage % was significantly depending on the enzyme concentration. For hCAP3, all slopes are significantly different with $p<0.001$ exept the comparisons of 0.3125 nM with 0.625 nM and 0.156 nM (Figure 31 E). For mCAP3, there is no significant different between 5 nM and 2.5 nM, but the for lower concentrations, with the exception of 0.3125 nM compared to 0.625 nM and 0.156 nM, the slopes are significantly different. To summarize, for probes like CAPRee4, for which the D/A ratio increase and maximum are concentration-dependent, the quantification of enzyme activity by calculation of cleavage % might be an appropriate option.

CAPRee4 was also tested with respect to cleavage by other human proteases similarly to CAPRee1. Unexpectedly, the probe was not cleaved by furin at all. Furthermore, CAPRee4 was hardly cleaved by cathepsin B and human airway trypsin. Therefore, CAPRee4 had a much higher specificity towards CAPs as CAPRee1. Similarly to CAPRee1, CAPRee4 was not a substrate for cathepsin S (Figure 32). The probe was cleaved by mCAP1 and hCAP1. Murine enzymes have not been tested, expect mCAP1 and mCAP3.

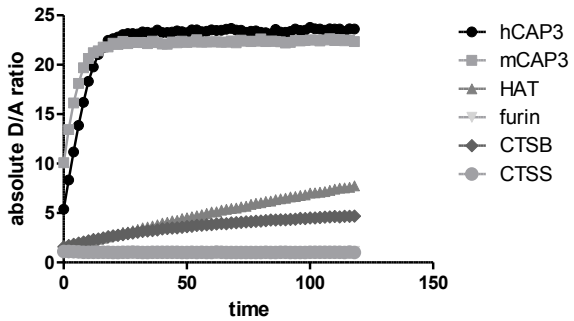

Figure 32: Specificity of CAPRee4 towards CAPs over other proteases

rmCAP3 625 pM
rhCAP3 5 nM
rhHAT 300 pM
rhFurin 100 nM
rhCTSB 20 nM
rhCTSS 100 nM

Each concentration was measured with n=1. For each enzyme, 8 different concentrations were measured. All enzymes cleaved their respective commercial substrates.

Additionally, CAPRee4 was tested on M-1 and CFBe41o$^-$ cells with broad spectrum inhibitors (Figure 33). As previously shown for CAPRee1, only the serine protease inhibitors camostat mesilate and

Pefabloc SC had significant effects on the cleavage of CAPRee4. After the measurement, all cells had been checked under the microscope for viability to exclude artefacts. For the human cell line, similarly to CAPRee1, EDTA rather increased the cleavage rate, suggesting that the probe was significantly cleaved by CAP1 which is partially inhibited by divalent cations. After incubation with Pefabloc SC, the cells died after about 3 h of incubation with the inhibitor. As the probe cannot pass the plasma membrane, the activity detected is measured as sum of surface-bound enzyme activity and activity released from the membrane during the time of the experiment.

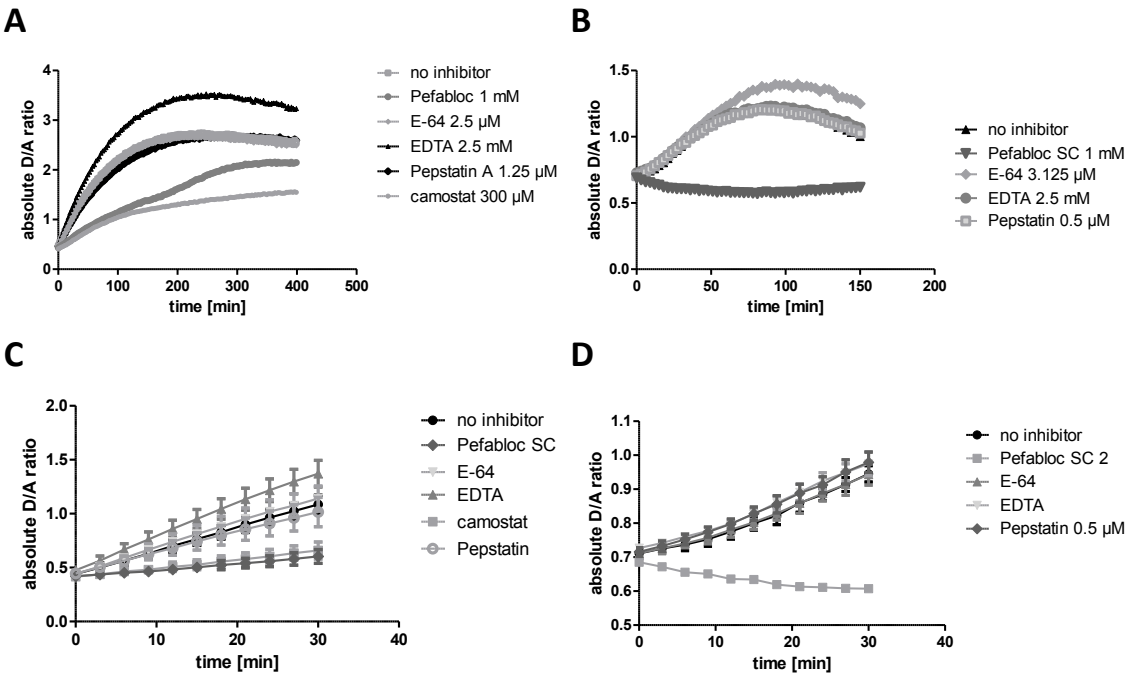

Figure 33: Specificity of CAPRee4 on CFBE41o$^-$ and M-1 cells with broad spectrum inhibitors

The cells were incubated for 20 min with the respective inhibitors. Afterwards, 2 µM CAPRee4 was added to the cells and the cleavage was measured in submerged conditions in the plate reader. The probe was dissolved in phenol red- and serum-free DMEM with 25 nM HEPES to maintain neutral buffer at atmospheric CO_2. The assay was performed at 37°C. A and B are representative traces, C and D are shown as mean ± SD, n=3 per condition. A and C: CFBE cells, B and D M-1 cells.

To summarize, the sequence of CAPRee4 seems to be very promising with respect to a highly specific a rapidly cleaved probe. As long as the fluorophores and attachment of the lipid anchor do not significantly affect the recognition, the lipidated probes might be worth further improvements.

2.3.3 Characterization of lipidated probes on murine and human cell lines

In vitro, the lipidated probes CAPRee5 and CAPRee6 were shown to have very low ratio change upon cleavage. This observation was to be confirmed in cell-based experiments and they were tested regarding the behavior on the cell surface. It should be tested how molecules behave that have one highly positively charged half of the molecule and one rather hydrophobic one. From the results, conclusions about the general design of this kind of FRET probes might be drawn.

M-1 cells were incubated with 2 µM of CAPRee5 in presence of the serine protease inhibitor camostat mesilate which should block all endogenous enzymatic activity and in presence of 7.4 nM mCAP3 to obtain full cleavage. From this data, the maximal fold change to be obtained in live cell imaging conditions was measured (Figure 34).

As expected, the fold change was very poor. Furthermore, the localization was not as desired. When incubated with camostat mesilate, a significant amount of the intact probe was internalized into vesicles and stored intracellularly. The cleaved probe however seemed to remain in the membrane. Interestingly, the probe did not seem to be cleaved by endogenous enzymes neither on M-1 cells nor on primary human nasal epithelial cells (hNEC) (Figure 35). Compared to CAPree3, the distance of the cleavage site to the lipid anchor was shorter which might impair the binding of membrane-bound enzyme activity.

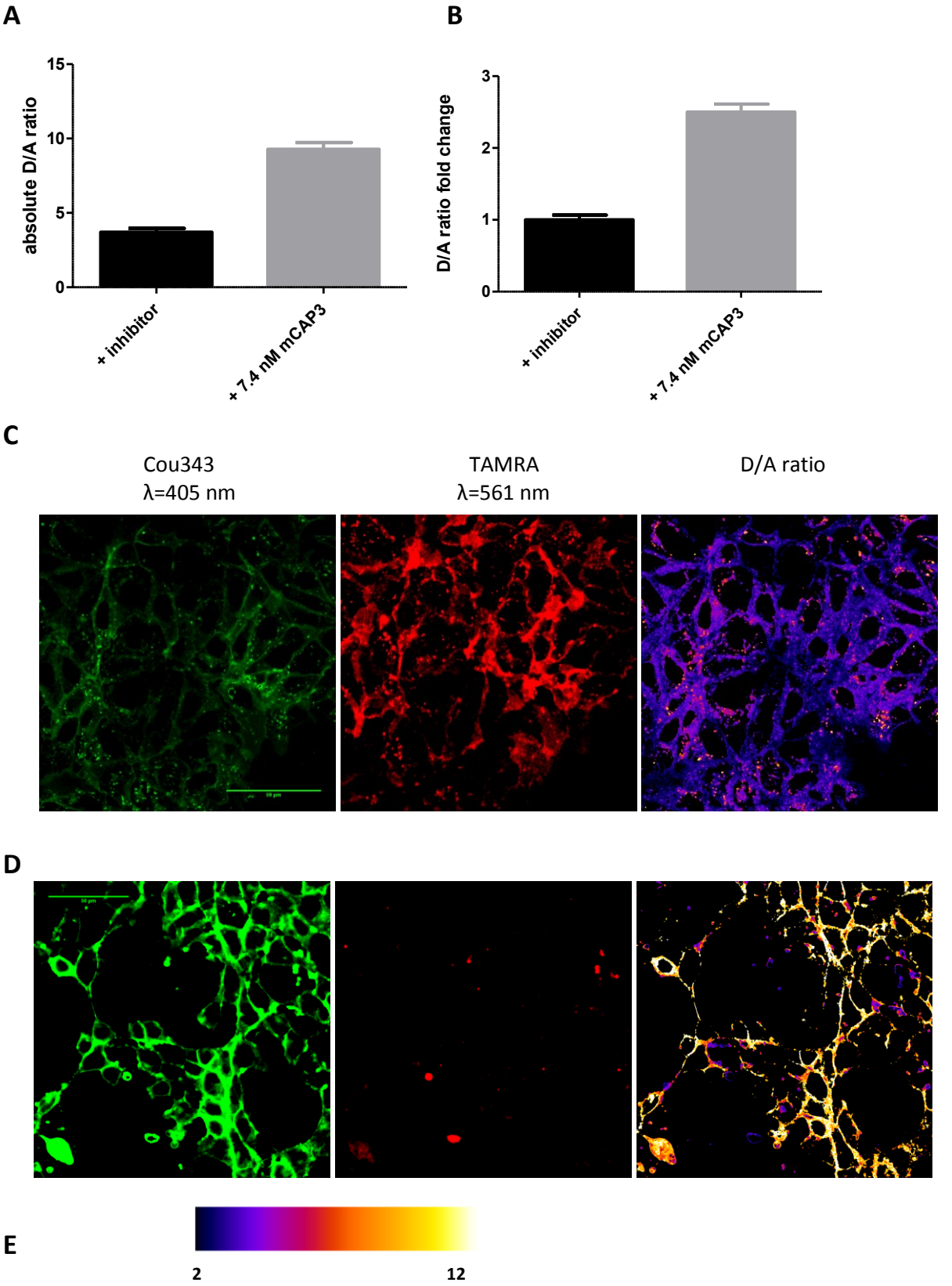

Figure 34: Localization and cleavage of CAPree5 on M-1 cells

The cells were incubated with 2 µM CAPRee5 in presence of 10 µM camostat mesilate or 7.4 nM mCAP3. A represents the absolute D/A ratio, B the maximal fold change. C represents representative images of donor and acceptor fluorophore as well as the ratio in presence of inhibitor, D in presence of mCAP3. The brightness of Cou343 and TAMRA is adjusted to the signal to show localization. The ratio is represented with the same LUT in C and D. E: LUT for D/A ratio. In A, n=15 (+ inhibitor) and n=16 (+7.4 nM mCAP3) positions. In each position was averaged from 50-100 cells each.

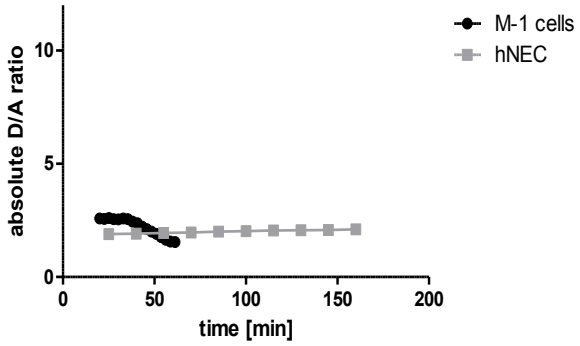

Figure 35: Cleavage of CAPRee5 on M-1 cells and hNEC

M-1 cells were incubated with 4 µM CAPRee5 and imaged without washing.

hNEC cells were incubated with 16 µM CAPRee5 for 15 min and washed with PBS prior to imaging.

For hNEC, 20 positions were imaged and averaged with each about 50-100 cells. For M-1 cells, three positions were imaged and averaged with each

As consequence of these results, the lipidated probe was modified and two additional peg-linkers were inserted. This increased the distance of the cleavage site in the two-dimensional structure to the same distance as CAPRee2 and CAPRee3. Furthermore, TAMRA was not coupled via amide coupling to a lysine residue, but it was clicked onto a glycine bearing an alkyne moiety. HPLC data revealed that the probe in total was indeed more hydrophilic. The sequence of the positions P1' to P4' was changed to the VVGG which had been used for CAPRee1-3.

On the cell surface however, the behavior remained unchanged. Both on M-1 cells, the probe was still internalized as intact molecule (Figures 36). On CFBE cells, the probe had a comparable localization.

As CAPRee2 and CAPRee3 did not show significant internalization after hours on the cell surface, the attachment of the two fluorophores and the lipid anchor are unlikely to cause the internalization. Potentially, the sequence itself triggers uptake into vesicular structures. Furthermore, the position of donor and acceptor on the molecule had been interchanged so that the combination of a highly positively charged series of amino acids close to the lipid anchor might trigger internalization.

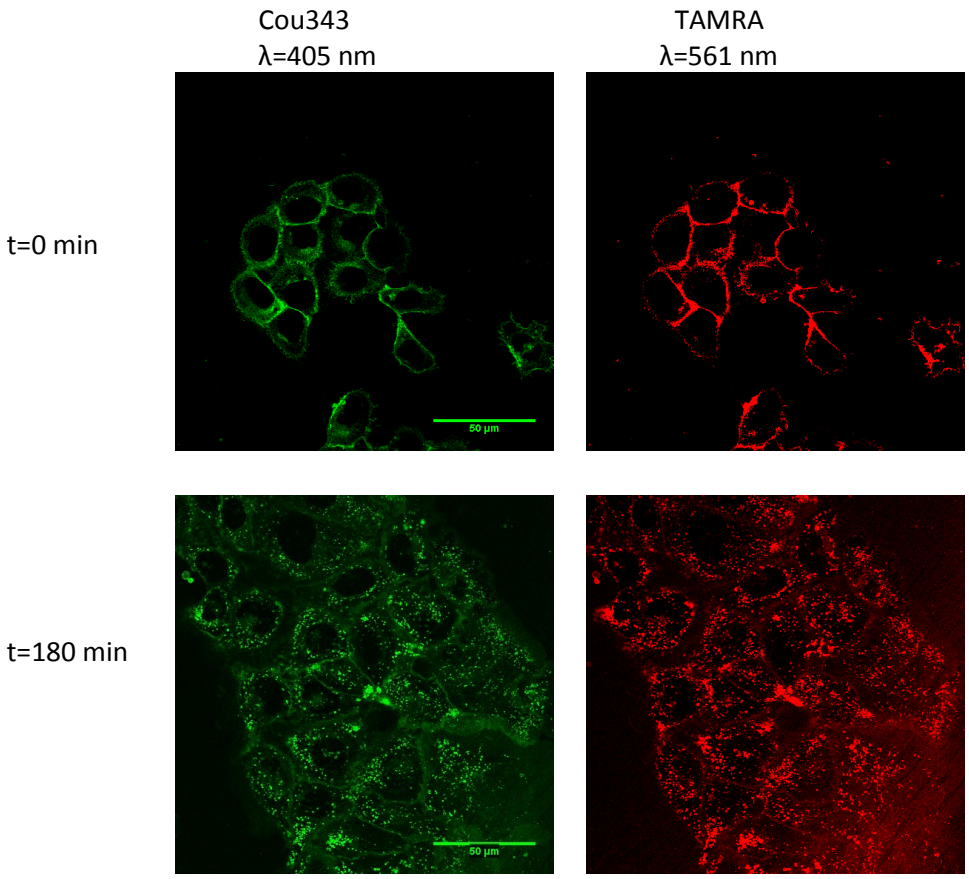

Figure 36: Localization of CAPRee6 in M-1 cells

The cells were incubated with phenol red-free and serum-free DMEM and 2 µM of CAPRee6 at 37 °C. The images are representative images from two datasets with each 20 positions. The experiments were performed on different days and different passage number of the cells.

To improve and make probe design more efficient in the future, further experiments were performed to get information about the mechanism of internalization. Therefore, the cells were kept on ice during incubation times and imaged for short periods at room temperature. Incubation at low temperature should reduce active cellular processes. In case that the cells do actively import the probe into vesicles, the internalization should be significantly reduced by temperature reduction.

Incubation of the cells with Pefabloc SC completely blocked the internalization at low temperatures (Figure 37 A), suggesting that the intact molecule was not internalized in previous experiments. The probe was slowly cleaved on the cell surface and the donor fragment was accumulating inside the cell whereas the acceptor fragment does not enter the cell (Figure 37 B). Quantification revealed that the D/A ratio marginally increased, and the ratio plasma membrane/intracellular decreased over time (Figure 37 C).

A

Cou343
λ=405 nm

TAMRA
λ=561 nm

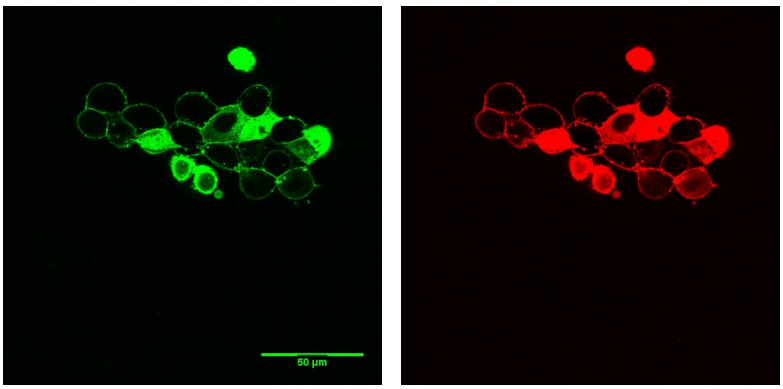

B

t= 1.5 min

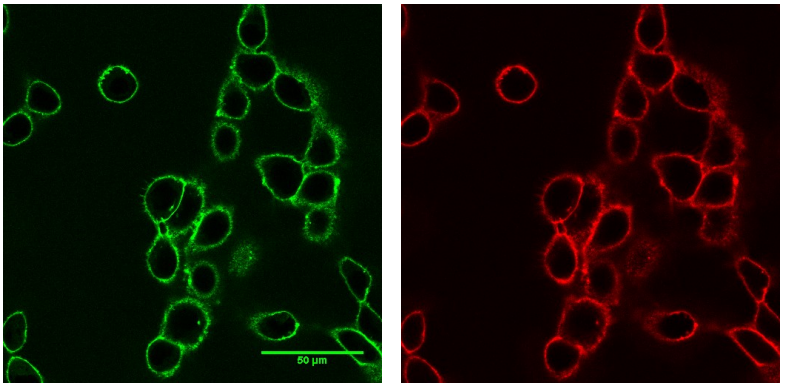

t= 38 min

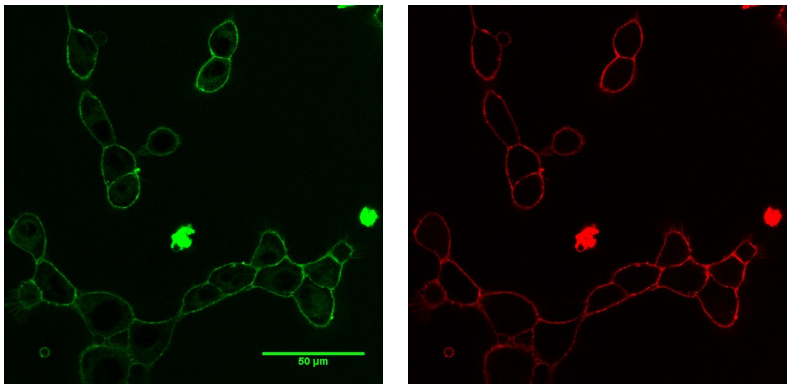

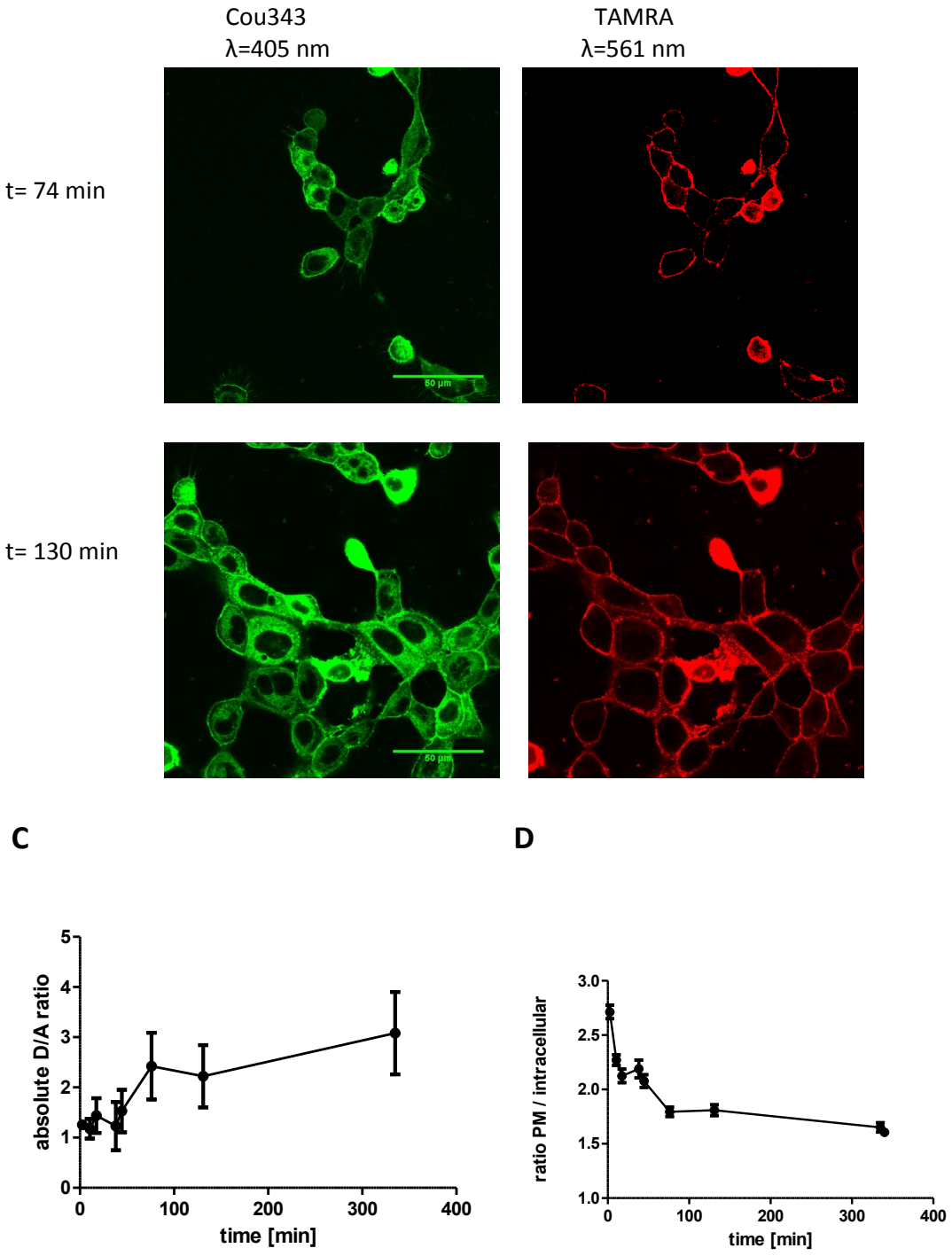

Figure 37: Localization and cleavage of CAPRee6 on M-1 cells at low temperature

The cells were incubated with 4 mM Pefabloc SC for 20 min before addition of 2 µM CAPRee6 (A) and kept on ice during incubation. In B, the cells were incubated in phenol red- and serum-free medium with 2 µM CAPRee6 on ice. The cells were imaged after 2 h (A) or at the given time points at room temperature. Change in D/A ratio (C) and change of ratio of plasma membrane and intracellular signal for Cou343 (D) was quantified. C: mean ± SD,D: mean ± SEM n=139 (t=2.5 min), n=60 (t=10.5 min), n=84 (t=17.5 min), n= 104 (t=38 min) n= 119 (t=44.5 min), n= 97 (t=76 min), n= 74 (t=131 min), n=97 (t=335 min). n is the number of cells quantified.

To find out whether the probe might be used at lower temperatures than 37 °C which are tolerated by the cells, a third series of experiments was performed at 30 °C. This is the temperature which can be maintained inside the environment box of the microscope used without cooling the system at ambient temperature. Furthermore, from experience, also primary cells tolerate 30 °C during culture and experiments.

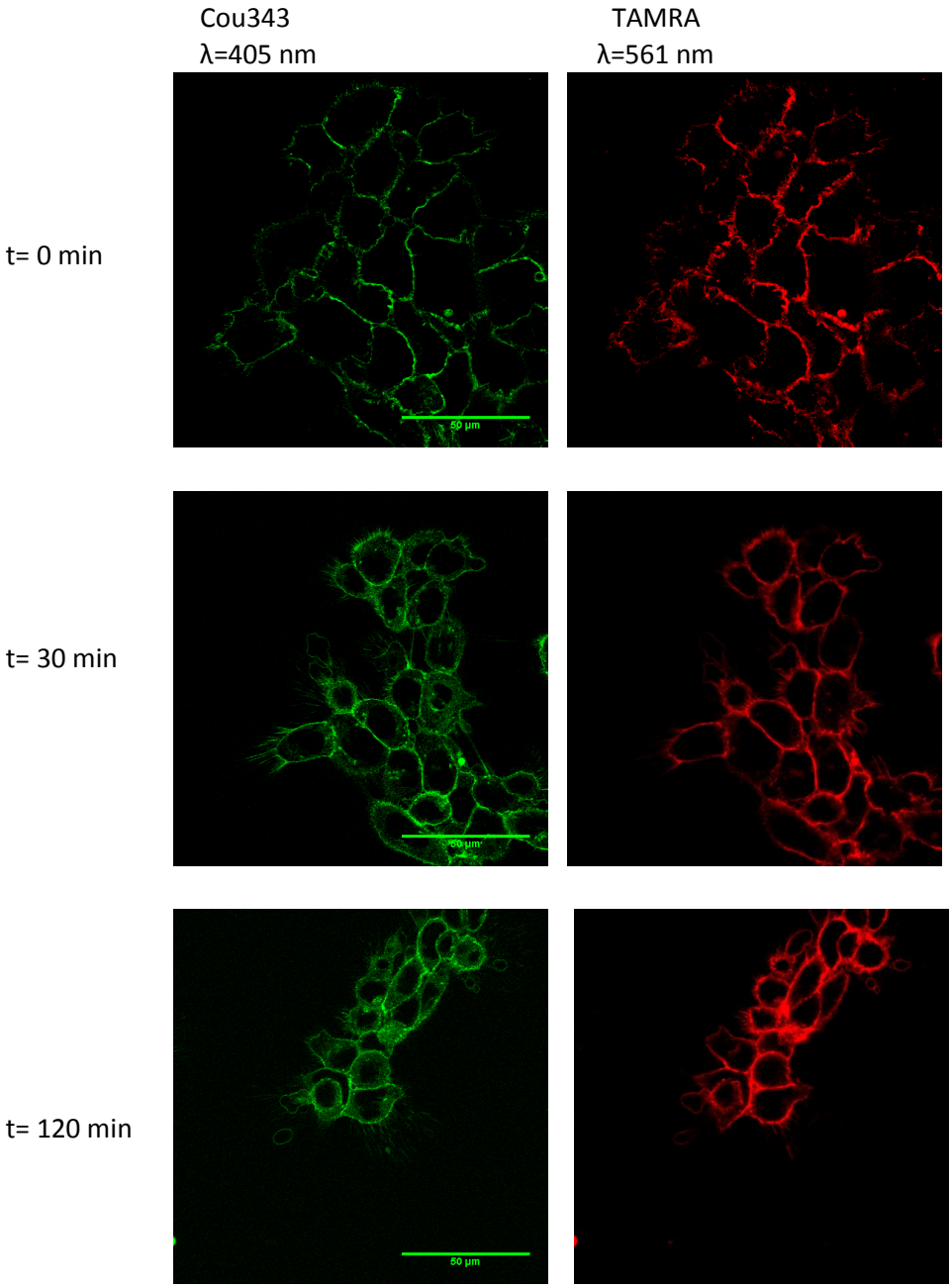

Figure 38: Localization of CAPRee6 on M-1 cells at 30 °C

The cells were incubated with 2 µM CAPRee6 for the given time points at 30 °C in 5 % CO_2. The given wavelenghs represent the excitation wavelength for the image. The images shown are representative from a dataset of 10 positions per condition.

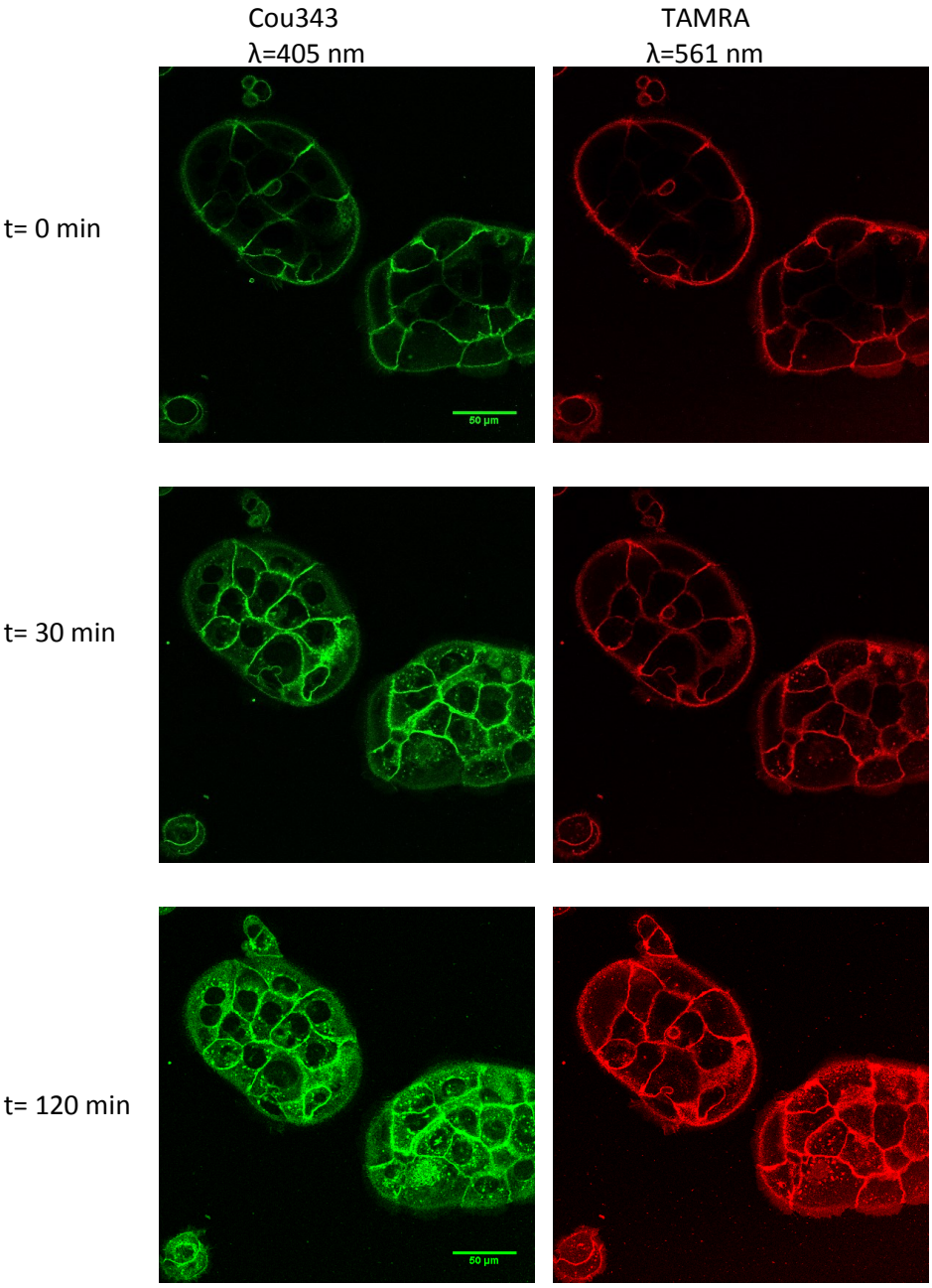

Figure 39: Localization of CAPRee6 on CFBE41o$^-$ cells at 30 °C

The cells were incubated with 2 µM CAPRee6 for the given time points at 30 °C in 5 % CO_2. The given wavelengths represent the excitation wavelengths for the series of image below. The images are representative for 10 different positions.

Figure 38 and 39 shows the results at 30 °C for M-1 cells and CFBE41o$^-$ cells. The internalization rate is much lower and more comparable to the experiment with incubation on ice for M-1 cells. For CFBE cells, the probe is still significantly internalized into vesicles. The change in localization would be ideal for a probe. The dynamic range however remains very poor in live cell imaging conditions.

Although a very small ratio change had been expected from *in vitro* data, the ratio change on the cell surface was quantified and revealed that it is indeed very low and could not be optimized significantly by modifying imaging settings.

Furthermore, in all experiments, we observed no reduction in the acceptor channel. Even with loading of the cleaved probe, we observed significant membrane staining in the acceptor channel.

Finally, for further information about the behavior of the probe, the expected fragments of CAPRee6 were synthesized and subjected to similar experimental conditions. The fragments were synthesized and fully characterize by Madeleine Schultz. Analytical data is shown in the appendix. The donor fragment was strongly internalized at 37 °C, but not at 30 °C. Interestingly, even in the absence of a lipid anchor, the acceptor fragment did efficiently load onto cells. Further investigation would be required to identify the subcellular localization. Therefore, a second factor for the poor ratio change was the fact that the acceptor fragment did not diffuse away but remained attached to the cell (Figure 40).

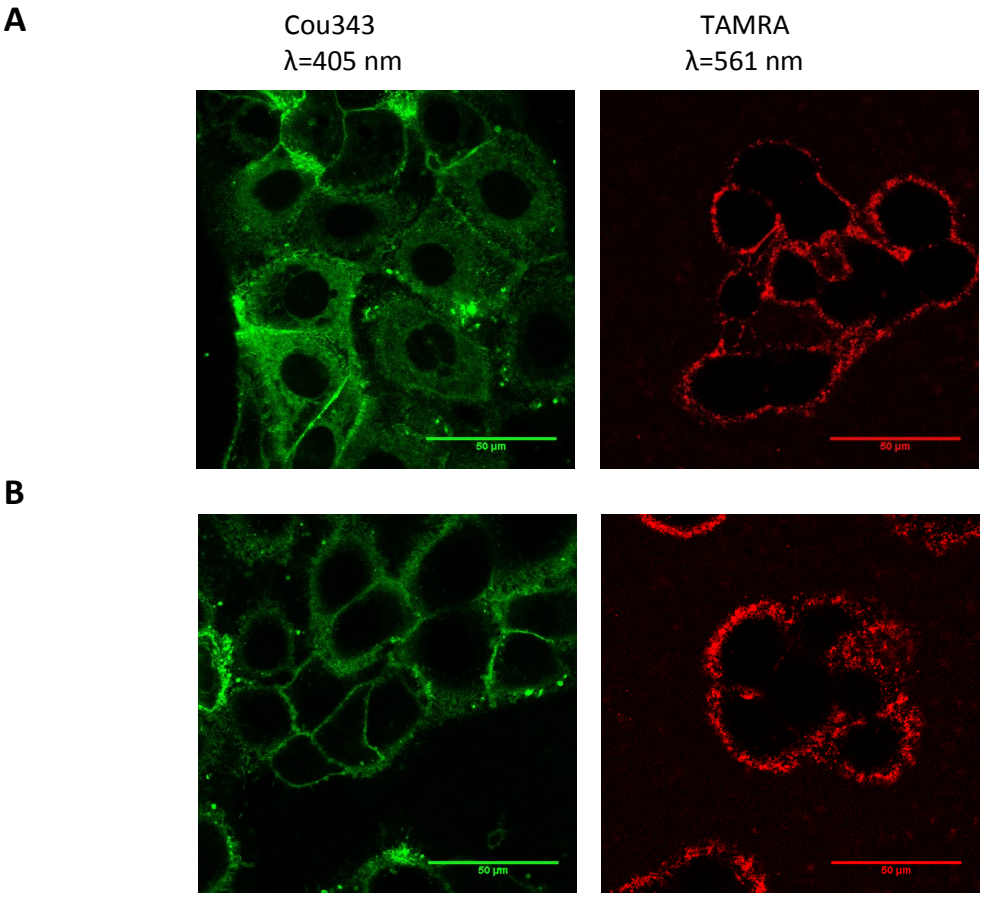

Figure 40: Localization of donor and acceptor fragment of CAPRee6 at 37 °C (A) and 30 °C (B)

The cells were loaded with 2 µM of the fragments for 15 min and washed afterwards. Imaging was performed after 30 min. The images are representative. In total, 10 positiones were images per condition.

To summarize, the lipidated CAPRee5 and CAPRee6 probes require major changes in the design. For various reasons, the current design is not useful for the purpose of design. Both the poor initial FRET as well as the internalization early on is detrimental for the use of the probes.

2.4 Application of CAP probes to murine models systems: tracheal epithelial cells isolated from βENaC-transgenic show significantly decreased CAP activity compared to wildtype C57BL/6 mice

βENaC-transgenic mice were established as a model for cystic fibrosis lung disease. By overexpression of the β-subunit in airway epithelial cells, constitutively active αβ-channels are formed that to not require proteolytic activation. Consequently, the sodium transport across the airway epithelial cells is significantly increased which leads to airway surface dehydration and mucus plugging[6, 91]. So far, it is unclear whether CAP activity is up or down regulated or unchanged in βENaC-transgenic mice.

Murine tracheal epithelial cells were isolated from 10 mice and pooled. The cells were seeded into Transwell® inserts and cultured for 2 days under submerged conditions and 8-10 days in air-liquid-interface before imaging. The cells were washed with PBS apically every second medium change and before application of CAPRee3. The supernatant was collected and incubated with CAPRee1.

Each well was washed with 100 µl PBS. The soluble CAP activity was quantified by CAPRee1 and revealed no significant difference between wild type and βENaC-transgenic animals (Figure 41 A -B). For easier handling of the samples and higher comparability, freezing is required to collect samples from several days or weeks. For the experiment, one sample was divided, one half used for enzyme quantification immediately after washing the cells, the other half was frozen for 24 h, thawed and submitted to CAP activity quantification. Freezing significantly reduced the initial increase in D/A ratio both in wild type and βENaC-transgenic samples (Figure 41 C-D). The mean difference however was not different between the groups so that freezing reduced enzyme activity in total, but did not change the difference between the samples.

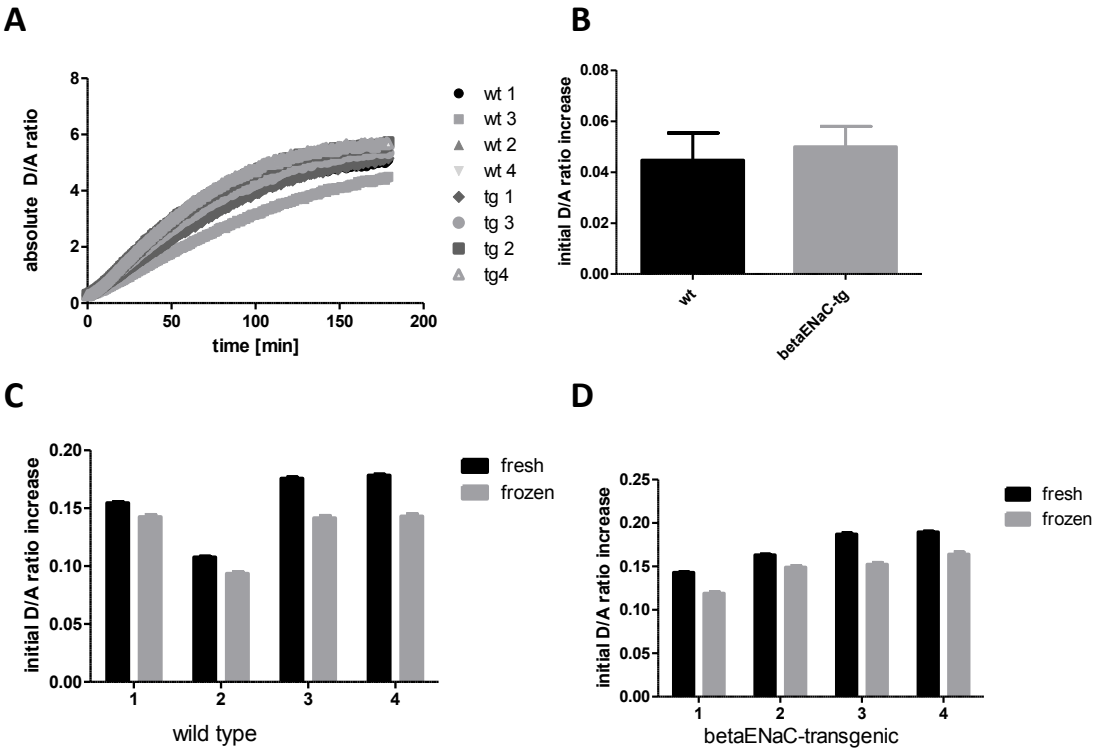

Figure 41: Soluble CAP activity of mTEC cells

A cleavage of CAPRee1 over time. B quantification of the initial increase in the first 30 min in wildtype and βENaC-transgenic samples. C comparison of fresh and frozen samples of wildtype supernatant, D comparison of fresh and frozen samples of transgenic supernatants. In A each trace is measured once. In B, the replicates per genotype (n=4) were grouped. Data is mean ± SD, n=4. In C and D, each sample was measured once. Error bars represent the error of the linear regression analysis.

To conclude, freezing samples is valid and enables the collection of higher sample numbers which can be analyzed in one experiment.

Furthermore, CAP activity was quantified on the surface of mTEC cells by CAPRee3. After washing the cells with PBS, the cells were incubated with 8 µM CAPRee3 in PBS for 15 min and washed. During imaging, the cells had full culture medium supply from the basolateral side and 20 µl PBS on the apical side. The cells were imaged with a 20x water objective. The Transwell® inserts was placed onto a cover slip which was surrounded by a special humidity chamber to maintain the humididy on the cell surface and reduced evaporation on the ASL.

Whereas wild type mTEC cleaved CAPRee3 in less than two hours on their surface, βENaC-transgenic mice had hardly any CAP activity (Figure 42 A). The initial increase was significantly different between the genotypes (Figure 42 B), the slope of the initial increase in D/A ratio was not significantly different from zero for βENaC-transgenic mTECs. Representative images of different time points are shown in Figure 42 C.

A

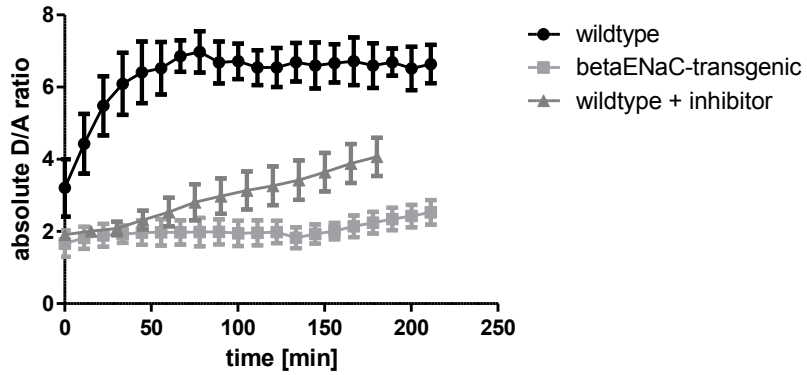

B

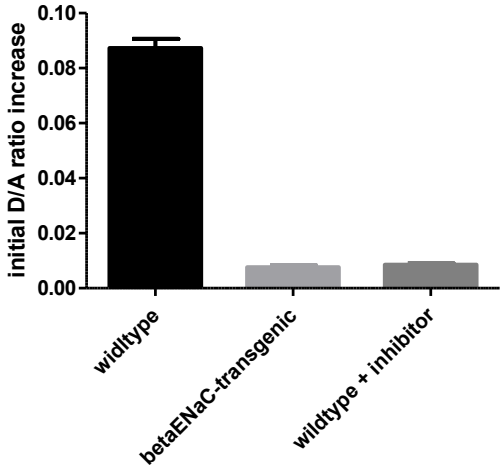

C

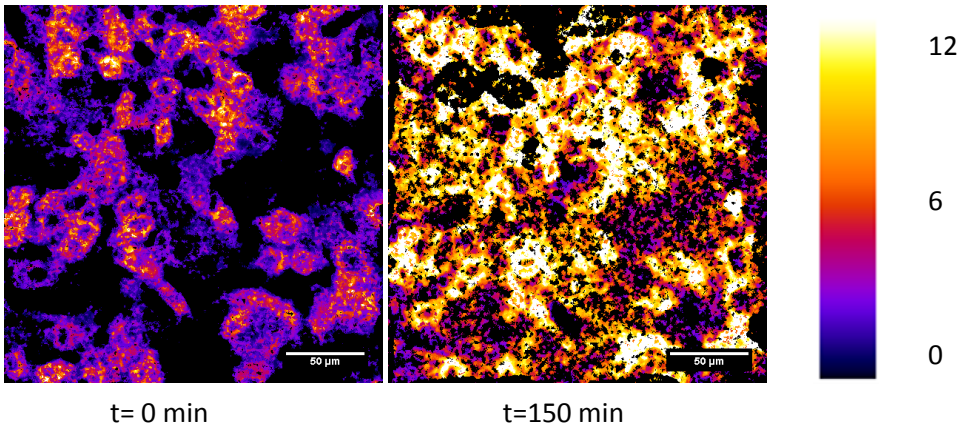

t= 0 min t=150 min

Figure 42: Surface-bound CAP activity on murine tracheal epithelial cells from wild type and βENaC-transgenic animals

The surface-bound CAP activity of mTECs was quantified with CAPRee3, comparing wild type and βENaC-transgenic animals. Furthermore, the wild type cells were incubated with 4 mM Pefabloc SC for 30 min before the experiment. All experiments were performed after 15 min preincubation with 8 µM CAPRee3. In A, two wells per condition were imaged with each 5-10 positions. Each position was considered as one measurement (n=10 wild type, n=20 for transgenic, n=15 for inhibitor). B is the slope calculated by linear regression. Error bars represent error of the fit. C shows representative image for wild type mTEC in absence of inhibitor.

transgenic. Consequently, βENaC-transgenic are no useful model to investigate CAP activity and regulation in CF lung disease because the mice behave differently compared to what is expected in human pathology. However from a biological point of view, the downregulation or inhibition of CAPs to decrease the overshooting ENaC-activity is fully plausible. The mechanism however remains to be identified.

2.5 Application of CAP probes to human samples: Increased CAP activity of CF cell lines and cultured human nasal epithelial cells isolated from CF patients compared to healthy controls

Additionally to the primary murine cells, the applicability of the CAPRee probes was tested on human cell lines. CFBE41o$^-$ cells are derived from a CF patient being homozygous for ΔF508 CFTR mutation, the most frequent mutations in the CFTR gene[92]. This cell line was used as a CF model. As healthy control cell line, a cell line derived from CFBE41o$^-$ but with stable overexpression of wild type CFTR gene was used (CFBE wt CFTR). Except CFTR, the cell lines share their genetic background which would not be the case for other bronchoepithelial cell lines like HBE, NuLi etc.

Both CFBE cell lines were seeded into a 96-well multititer plate and incubated overnight. The cells were washed with PBS to remove dead cells and soluble enzyme activity. Afterwards, 2 µM CAPRee1 in phenol red- and serum-free DMEM with 25 mM HEPES buffer was added. The assay was performed at 37 °C and atmospheric CO_2 in the plate reader.

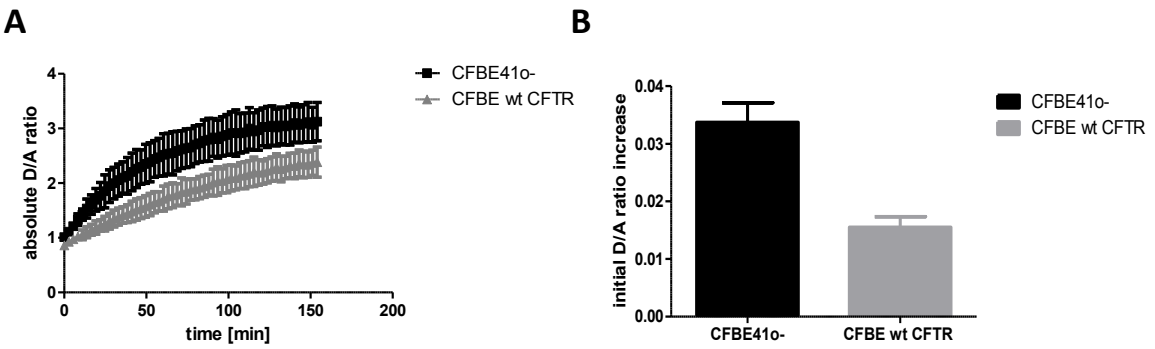

Figure 43: Quantification of CAP activity on CFBE41o$^-$ and CFBE with wild type CFTR overexpression by CAPRee1

Similarly to experiments with soluble commercial substrates, CAPRee1 can be used for the quantification of CAP activity on the cell surface and enzyme released from the cells during the experiment (A). Quantification of the initial increase in D/A ratio revealed a significantly higher enzyme activity ($p<0.0001$) (B). Data is represented as mean ± SD for n=2 for each condition (A). In B, the errors bare represent the deviation of the linear regression of the first 30 min.

Washing of the cells removes soluble enzyme activity which had been accumulated during the time of culture in the 96-well-plate. CAPRee1 was able to detect membrane-associated CAP activity together with enzyme activity that had been released to the liquid during the time of the

experiment. Quantification revealed that the CAP activity on the CF model cell line is more than 2-fold increased compared to the healthy model cell line (Figure 43).

Additionally, the lipidated probe CAPRee3 was tested in submerged conditions on both cell lines.

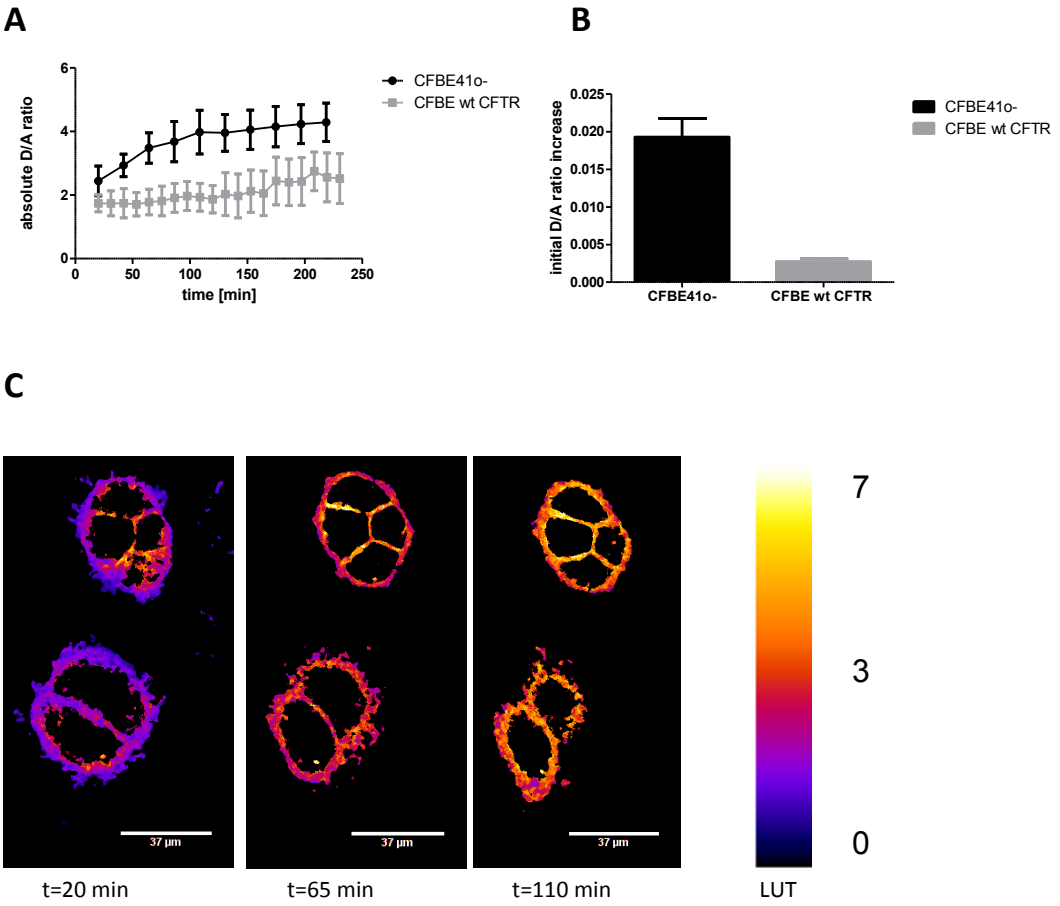

Figure 44: Quantification of CAP activity on CFBE41o- and CFBE with wilddtype CFTR overexpression by CAPRee3

CFBE cells were seeded into Lab-Tek™ dishes and cultured over night in submerged conditions. In the next day, the cells were imaged after pre-incubation with CAPRee3 for 15 min and similarly to quantification by CAPRee1, the CF model cell line has significantly increased ($p<0.0001$) CAP activity compared to the healthy control cell line. C shows a representative ratio change on CFBE41o$^-$ cells. A is shown as mean ± SD. The experiment was performed in triplicate on different days with different passage number. In each experiment, 10 positions per cell line were imaged. In each position, 10-20 cells were quantified automatically. B shows the slope calculated by linear regression, the error bars represent the error thereof. C: representative images of D/A ratio of CFBE41o$^-$ cells at the given time points.

The cells were seeded into LabTek™ dishes and incubated over night. The imaging was performed under submerged conditions in phenol red-free and serum-free DMEM at 5 % CO_2 and 37 °C. Whereas the CF model cell line CFBE41o$^-$ cleaved the probe within about 2 h, the control cell line with overexpression of wild type CFTR only showed little CAP activity (Figure 44). So far, it remains unclear whether the CAP expression levels or higher expression of inhibitors are responsible for the reduced activity and requires further investigation.

Additionally to the human cell lines, the CAP activity was investigated on human nasal epithelial cells. The cells were obtained by nasal surgery both from healthy controls and CF patients. In principle, the cells can also be collected by nasal brushing, a non-invasive and easy method. Therefore, nasal epithelial cells are an ideal system for the characterization of individual disease states. In the experiments, the question was addressed whether these cells can be used for the CAP activity quantification and whether on nasal cells, one can also observe the difference in CAP activity between CF and Non-CF samples.

After isolation, the cells were expanded in culture flasks following the protocol established and performed in our lab by Heike Scheuermann. The detailed procedure is described in the methods. Independent of the genotype, some samples were used after 2 passages without freezing. Other samples had been frozen after the first passage and after thawing, they were directly seeded into 24-well Transwell® filter inserts. Paired experiments revealed no significant difference between passage 1 and passage 2 so that passage 2 was used for all following experiments because of easier handling and higher cell numbers.

Similarly to mTEC cells, hNEC were imaged on the Transwell® filter inserts in the humidity chamber at 37 °C with full culture medium supply from the basolateral side. The imaging was performed with a 40x oil objective which is able to do adaptive focus control despite the large distance of the cells to the objective. Due to the high signal of the membrane in the DRAQ5 channel, focusing on the nuclei was not possible.

Representative images of localization of the probe in x-y and x-z direction of donor and acceptor are shown in Figure 45. The probe localizes homogenously to the plasma membrane without significant internalization into vesicles or inner membranes. Consequently, it is not required to focus on the apical membrane. This would be highly disadvantageous due to inhomogeneity of cell height and loss of focus due to minor drifts in the focal plane. This however cannot be avoided during 10 h of imaging time and movement of the stage to different imaging positions. Inhibition of cleavage revealed that CAP activity could be completely blocked by addition of 4 mM Pefabloc SC® both to the apical and basolateral baths (Figure 45 B). The difference in the slope of the initial increase in D/A ratio was highly significant ($p<0.0001$).

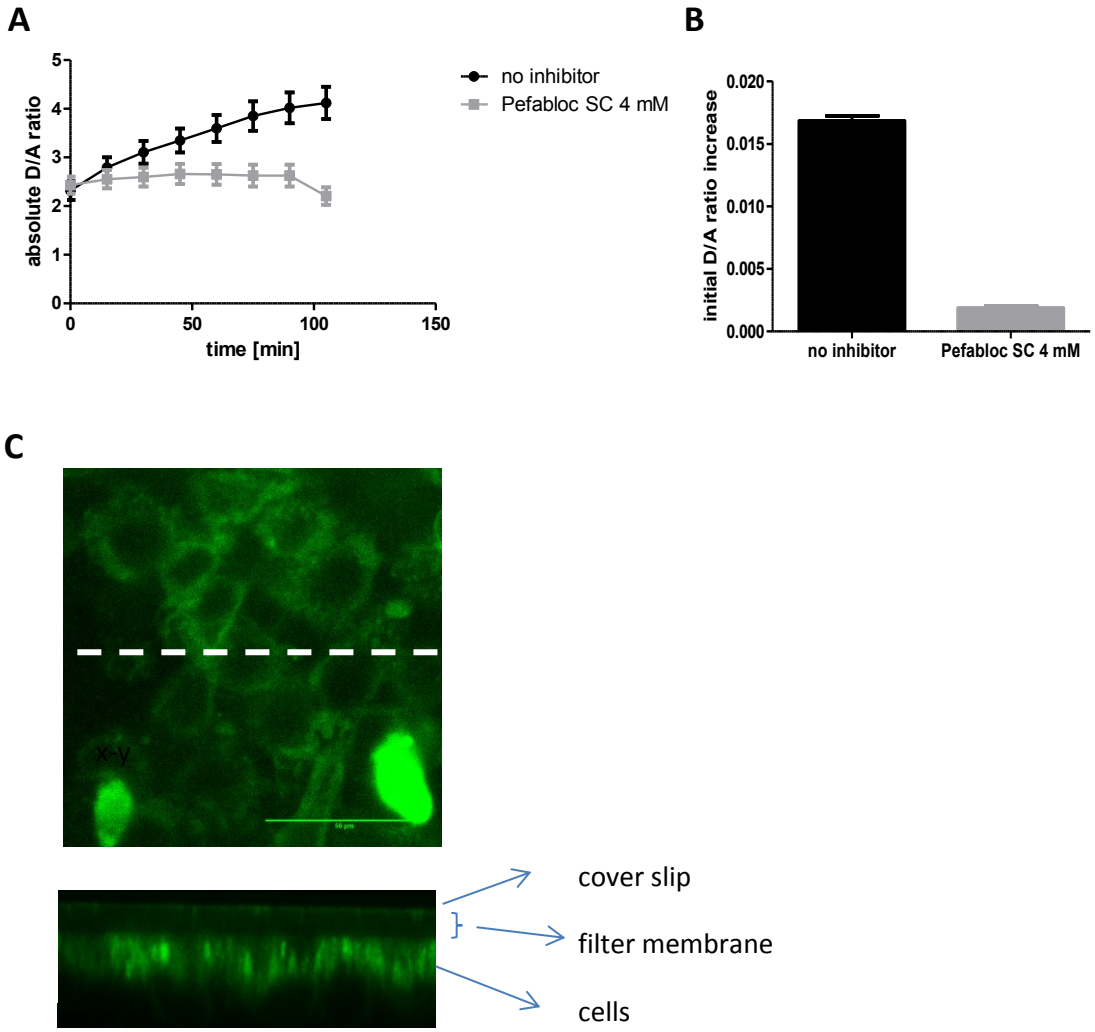

Figure 45: Cleavage of CAPRee3 on hNEC in absence and presence of serine protease inhibitor Pefabloc SC®

The cells were preincubated basolaterally and apically for 30 min with 4 mM of Pefabloc SC®. Afterwards, CAPRee3 was incubated in presence of inhibitor for 15 min. Then, the cells were washed apically, fresh PBS with inhibitor was added and the cells were imaged. Both wells were derived from batch of cells and imaged on the same day. The activity is strongly reduced, however the slope for cells incubated with inhibitor is still significantly different from zero ($p=0.043$. The difference between the slopes is highly significant ($p<0.0001$). C shows a representative image of the donor fluorescence in x-y an x-z direction. For A, in each well, 20 positions were imaged with each about 50 cells. The D/A ratio calculated per ROI was averaged per position. B represents the slope calculated for the first 60 min in both conditions. The error bar represents the error of the slope. C shows a representative image with 40 x magnification. Scale bar represents 50 µM.

For the comparison, four healthy controls and four CF samples were tested. All samples were measured in duplicate; however one had to be excluded due to technical issues. Because of the low CAP activity on nasal cells in general, the imaging time was extended to 10 h for the latest experiments. 20 positions were sequentially imaged every 15 min. All data sets were corrected for exact timing, i.e. the correction of the time due to the shift in imaging and the different times before starting the imaging process.

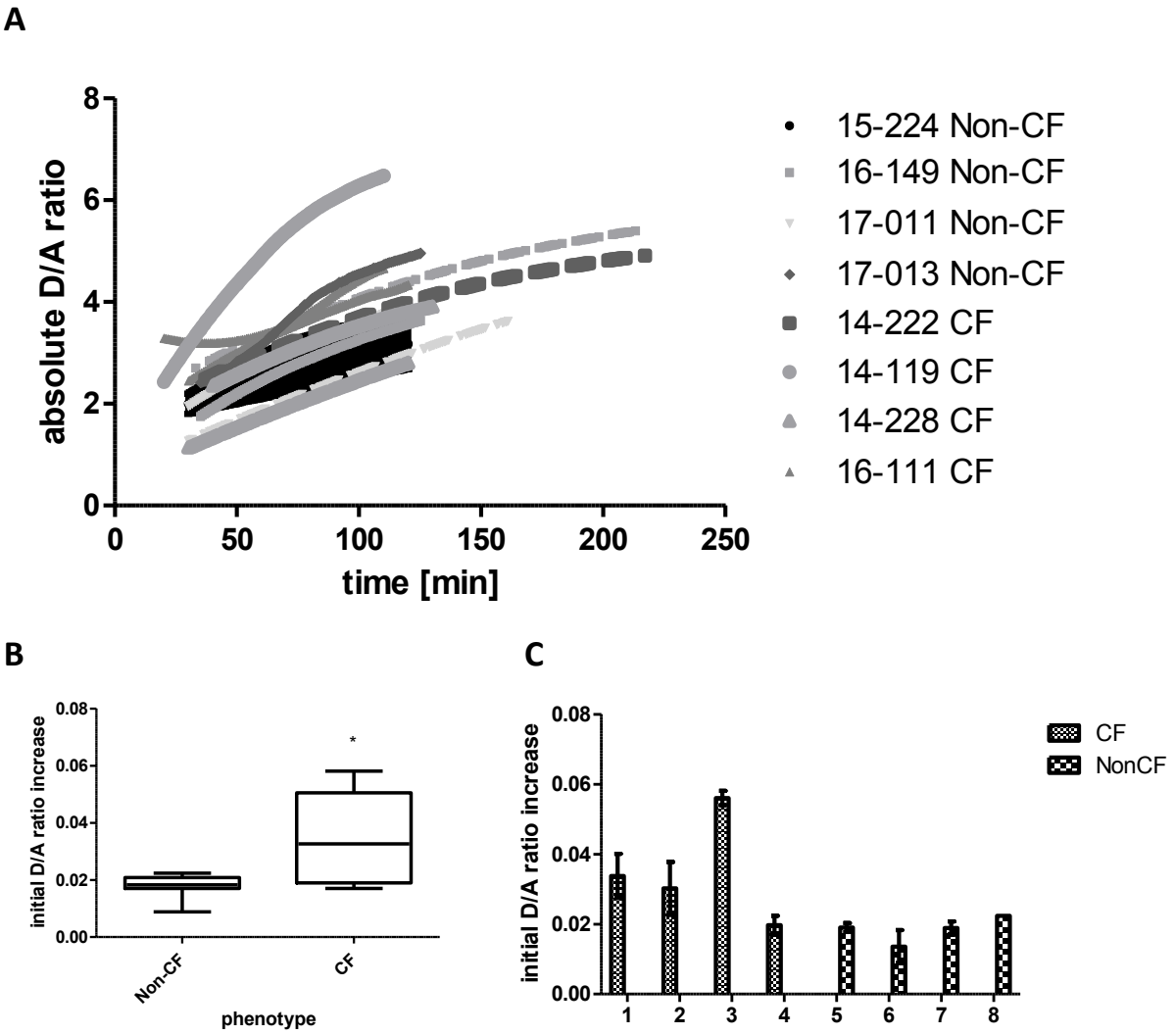

Figure 46: Quantification of CAP activity on healthy and CF hNEC

The cells were cultured on Transwell® filter inserts in ALI for at least 8 days. Two wells per patient were imaged. The cells were incubated with 16 µM CAPRee3 for 15 min and washed. During imaging, the cells had basolateral full medium supply and 20 µl PBS on the apical side.

A shows the interpolated traces of two wells for each individual. Each well was imaged in 20 positions with approximately 50 cells per position. B represents the quantification of the initial increase of the D/A ratio in the first 60 min shown as Whiskers Plot from minimum to maximum values. Each well was considered as individual sample. The difference between Non-CF and CF is significant (p=0.02). C represents the averaged D/A ratio increase of two wells for each individual.

After imaging, the initial increase in D/A ratio was quantified for each well by choosing the linear time individually for each sample. A minimum of 60 min of imaging, i.e. 4 time points measured, was set as minimum requirement. Figure 46 A shows the overview of the mean D/A ratio traces per patient. Quantification revealed that the initial increase in Non-CF control samples was very low and without strong variability. The CF group however was more heterogeneous and had a higher mean CAP activity. Considering each well as individual sample (n=15), the difference between the CF and Non-CF samples was statistically significant (p=0.02) (Figure 46 B). Averaging the initial D/A ratio

increase for each patient weakened the statistics, due to the lower sample number. The strong trend towards increased CAP activity remains (p=0.08) (Figure 46 C).

To conclude, CAPRee3 was able to detect increased CAP activity in nasal epithelial cells derived from CF patients compared to healthy controls. So far, no conclusion could be drawn whether a specific mutation or a combination of those are responsible for increased CAP activity or whether this is due to inflammatory stimuli from the diseased CF lung. In my cohort, all patients bear one allele ΔF508 mutated CFTR and one other mutation, partially unknown. The regulation of CAP activity will require further investigation.

3. Discussion

In cystic fibrosis, the ion transport balance is disrupted by the lack of a functional CFTR chloride channel. Although the mechanism remains under discussion, not only chloride secretion across the epithelium, but also sodium transport across lung epithelial cells is altered. Due to increased sodium absorption, the water homeostasis is disrupted and consequently the viscosity of the airway surface liquid is dramatically increased, resulting in mucus plugging and reduced ciliary beating. As a consequence, chronic infection and inflammation manifest in the CF lung[4].

The mechanism of how the activity of epithelial sodium channels is increased is not understood so far. Similarly to the βENaC mouse model, mutations in human αENaC-subunit lead to a cystic fibrosis-like lung disease[93]. These mutations might also play a role in CF caused by mutations in the CFTR gene. Furthermore, the inhibition of ENaC by CFTR itself is under discussion. In *Xenopus* oocytes, it has been described that normal CFTR, in contrast to CFTR with ΔF508 mutation, is able to associate with ENaC and prevent the α- and γ-subunit from cleavage by proteases[94]. The proteolytic activation of ENaC might be one of the most relevant processes in increasing ENaC activity in various tissues, including the lung. Recent studies with inhibitors show that either by protecting ENaC from cleavage or by blocking protease activity, ASL dehydration and ciliary beating can be significantly improved [43, 78]. Clearly, channel-activating proteases play a major role in the pathophysiology but their regulation in different diseases remains unclear. Therefore, a novel FRET probe was developed that enables the quantification of enzyme activity on the surface of cells cultured in submerged or air-liquid-interface conditions. Additionally, the probes should be usable both in murine and human samples.

3.1 Physical and biochemical properties of FRET probes

For the quantification of CAP activity, two sets of CAP activity probes have been synthesized and tested for the physical behavior *in vitro* and on cells. The first set was based on the autoactivation cleavage site of human CAP3, the second set was based on the CAP cleavage site in the γ-subunit of human ENaC. To improve the performance of the probe, but also to increase knowledge about general design of such FRET probes, several small modifications on the soluble probe CAPRee1 were synthesized and compared to CAPRee1. Minor changes like the replacement of arginine by lysine do not significantly affect the FRET in the intact molecule (Figure 11). However not only the increase in distance between the fluorophores affect the D/A ratio but also extension of the peptide backbone outside the core structure between the fluorophores has significant effect on the D/A ratio in the intact molecule. Notably, the effects of modifications are not always comparable between the

soluble and lipidated probe. Whereas the insertion of additional four ethylene glycol units was detrimental for FRET in the soluble probe CAPRee1, this was not the case for the lipidated probes CAPRee2 and CAPRee3 (Figure 10 and Figure 11). The sequence of four basic amino acids in the ENaC-based probes CAPRee4-6 removed the initial FRET in the lipidated probes CAPRee5 and 6 but not in the soluble CAPRee4 (Figures 26 and 27). So far, little is known about the three-dimensional structure of these short peptides which are equipped with two fluorophores. The amino acid sequence of CAPRee1-3 is derived from the autoactivation cleavage site of human CAP3 but there is not structural information available for this region. The murine enzyme with a very similar sequence has never been crystallized and this is true for the structure of ENaC, the basis for the CAP probes 4-6. Structure prediction for peptides by OMICS_28421 suggest a linear model which is very unlikely as described before[95]. Furthermore, the comparison of lipidated and soluble probes, CAPRee4 and CAPRee5/6 point to a significant influence of the fluorophores on the secondary structure of the FRET probe. Our data suggest that a lot of positive charges significantly affect the FRET efficiency of Cou343 and TAMRA, but not of MetOCou and Cou343. It is well known that the environment, e.g. the amino acid sequence in proximity, and also positive charges have an impact on the fluorescence of small molecules[96-97]. Nevertheless, predictions of the ideal combination cannot be drawn from our data so that it remains to be tested for the design of FRET reporters for other enzymes. Highly positively charged molecules however should be avoided.

The choice of fluorophores as FRET pair has been further tested (Figures 11, 20, 21, 22). Interestingly, the tested cyanin-3 derivative behaved well as acceptor fluorophore for FRET efficiency and gave the highest dynamic range on fixed cells, but performed poorly in cell- based assays. For unknown reasons, the acceptor fragment is localized to dot-shaped structures, suggesting the internalization into vesicles or endosomes. Preliminary experiments with a further red-shifted FRET reporter which was equipped with TAMRA and a mono-sulfonated cyanine-5 derivative suggest that this is an inherent problem of the cyanine dyes which are very sticky to membrane structures. Unpublished data by M. Schultz in the Schultz group point into a similar direction. Consequently, this class of fluorophores seems not to be suitable for FRET probes which are localized to the plasma membrane and require diffusion of the cyanine-bearing cleavage fragment. As the localization of the acceptor fragment with TAMRA does not show this behavior at all, this is clearly not related to the sequence. Further, it also does not seem to be related to hydrophilicity of the dye in general, because the acceptor fragment with Dy485-XL which is even sulfonated and according to HPLC less lipophilic, behaves similarly (Figure 21).

3.2 Specificity of soluble and lipidated probes

In general, the specificity should be determined by the amino acid sequence, i.e. mediated by the binding of amino acid side chains into the catalytic center of the enzyme. Flanking moieties like linkers, fluorophores and the lipid anchor should not significantly affect the specificity, at least not in theory.

The specificity is affected by at least two important factors: the affinity of the substrate to the enzyme (k_M) and the catalytic turn over (k_{cat}). For human and murine CAP3, partially also CAP1, the k_M was calculated and was in the high nanomolar to low micromolar range for CAPRee1, CAPRee3 and CAPRee4. Due to the experimental setup, k_{cat} was not easily accessible. It was observed however that CAPRee4 was faster processed by human and murine CAP3 more than 100 fold faster compared to CAPRee1. The lipidated analogs of CAPRee1 are even slower processed. This suggests a huge difference in k_{cat}.

With respect to specificity, this leads to the conclusion that CAPRee4 was much more specific towards CAPs over other proteases, as the cleavage rate of other proteases is not comparably increased (Figure 15, 29). For the lipidated probe CAPRee3, enzymes that efficiently bind the aa sequence in CAPRee1, are apparently hindered to cleave CAPRee3, either because of the lipid or the fluorophores in their respective position and orientation. Further experiments with minor modifications of the FRET probe are required to identify the reasons, first, why the lipidated probe is cleaved much slower in general and, second, why it is not recognized by some enzymes anymore.

Considering the structure of our probes, it is not entirely unexpected that the fluorophores do matter. Especially for the lipidated probe, the mass of fluorophores and lipid anchor reach about 50 % of the total molecule mass. Nevertheless, this effect has been ignored and was never carefully tested before[10, 76-77]. The current data clearly show that the modification of the fluorophores without modification of the amino acid sequence increases specificity towards CAPs over the other tested enzymes. However, this might not be the case for other enzymes that were not tested.

Published recognition sequences e.g. for CAP1 did not improve the cleavage of the probe by CAP1 which might actually be due to the fact that the fluorophore composition was different. Consequently, all probes have to be characterized in all variants to determine which should be used for a specific enzyme. So far, the effect of additional linkers or the addition of small amino acid residues has not been tested but this will also be necessary because they might change the distance of the fluorophore from the cleavage site in the FRET probe or enable or disable the binding of the fluorophores into hydrophobic pockets of the active center.

On one hand, this observation strongly increases the complexity of the design of FRET probes offering chances to create probes that are selective for the target enzymes over other enzymes that recognize similar sequences or are highly promiscuous like CTSB. Although for CTSB, the amino acid sequence can be highly variable, it nonetheless did not recognize CAPRee3 at all. No cleavage is observed, not even for very high enzyme concentrations.

On the other hand, it also questions the concept of substrate sequence optimization. In principle, fluorophores significantly contribute to substrate specificity. Therefore, it is questionable whether small modifications in the amino acid sequence can improve or diminish specificity, if the binding is mostly mediated by the fluorophore or the lipid anchor. To answer these open questions, structural analysis of a complex of the target enzyme with a soluble and a lipidated version of our FRET probes would be highly interesting. Regarding the contribution of the fluorophores to specificity as a chance for the design of FRET probes which avoids cleavage by promiscuous protein-degrading proteases, the structural insights contribute to more efficient and more specific design.

Studies with broad spectrum inhibitors however revealed that for studies on airway epithelial cells independent of their origin, the specificity of the FRET probes described in this work is high enough, also for CAPRee1 and CAPRee3 (Figure 16). For application in sputum supernatants of CF patients in which the NE activity is very high, the readout of CAP activity was only possible with addition of NE inhibitor. Interestingly, in contrast to purified NE from human blood, CF sputum supernatants were not able to cleave the modified CAPRee1*. The reasons for that remain to be investigated.

3.3 Effects of amino acid sequence on localization

For the desired application, the lipidated FRET probe has to anchor into the outer leaflet of the plasma membrane and has to remain there for the time frame of the experiment which has been shown to be at least 2-3 h. For primary human cells, experiments were performed up to 10 h. The design of a probe which fulfills this criterion is challenging, especially due the circumstance that there is very little knowledge about the mechanism that triggers internalization of these peptidic, lipidated structures. So far, it seems to be clear that it can be dependent on the fluorophore composition. For the previously established probes LaRee and Nemo, it was affected by the amino acid sequence[76-77].

In contrast to CAPRee2 and 3, CAPRee5 and 6 are internalized into dot-shaped structures, most likely vesicles. Whereas CAPRee2 and 3 are stable on the plasma membrane for hours and the donor fragment remains there without significant internalization, CAPRee5 and 6 are rapidly taken up by the cell. Reduction of the incubation temperature reduced the internalization significantly, suggesting active cellular machinery that triggers internalization. Nevertheless, it remains to be

answered how the amino acid sequence and fluorophore position determines the fate of the reporter both before and after cleavage. Although CAPRee3 and 6 share one part of the sequence, the localization is entirely different. Consequently, most likely the basic motive in CAPRee6 is crucial for cell entry. Peptides that are able to penetrate into cells, so called cell-permeable peptides (CPP) or protein transduction peptides have a common feature: they are amphiphilic, i.e. they have a hydrophobic and a hydrophilic part. All of our reporters, but especially CAPRee5/6, fulfill this criterion. Naturally occurring CPP are often highly positively charged molecules, also a central feature of CAPree4-6[98-99]. However, they are longer compared to our probes and require α-helical structures[99]. All lipidated CAPREee probes are amphiphilic and have a number of positive charges, with the highest charges in the probes 5 and 6. The donor fragment of CAPRee2 and 3 however is overall uncharged which might prevent internalization. It remains unclear however, how CAPRee2 and CAPRee3 as intact molecules as well as their lipidated donor fragments can actually escape from regular membrane turnover. They remain in the plasma membrane for several hours without significant internalization.

Addition of only the lipidated donor fragment of CAPRee6 however led to instantaneous internalization into the cytoplasm of the cell at 37 °C. This fragment is highly positively charged and hydrophilic on one end (C-terminal), due to the lipid anchor and donor fluorophore very hydrophobic on the other end which was sufficient to enable cell entry. Observation of entry of the donor fragment after probe cleavage might be masked by the high amount of uncleaved probe inside the cell which is no longer accessible to enzymatic cleavage. In the intact molecule, these properties might be sufficient to trigger endocytosis into vesicles. Redesign of the probe is required to overcome the internalization of the intact molecule as well as the poor FRET efficiency. So far, it cannot be conclusively said, how negative charges affect the internalization of our probes. The addition of negative charges by including several aspartic acid residues however had detrimental effects on the FRET ratio of CAPRee1_d, so that it has not been tested for the lipidated probe so far. The addition of negative charges by sulfonic acid moieties has been shown to be very efficient in keeping molecules at the plasma membrane so that sulfonated dyes or unnatural amino acids in the sequence might help to prevent internalization which is triggered by the sequence[100].

3.4 Analysis of kinetic properties of the CAPRee probes and consequences for assay design

Commercially available protease substrates are usually designed as fluorogenic substrates, consisting of a fluorophore and a quencher which are linked by a small number of amino acids for specific recognition. Cleavage results in a strong increase in fluorescence. The fluorescence however is

affected by various factors like the microenvironment of the molecule, the pH, the probe concentration etc. [101] The CAPRee probes are designed with two fluorophores instead to obtain a ratiometric readout which should control for some of these factors. In case of the lipidated probes, the spatial separation of the two fluorophores gives an additional readout. Ideally, ratiometric FRET probes give a concentration independent readout. Figures 13 and 26 show that this is only partially the case.

Commercial substrates have to be used in high concentrations to overcome the substrate concentration dependent increase in the reaction rate which occurs for concentrations around the Michaelis constant. Therefore, they are ideally used in concentrations of 10x k_M in order to work in the concentration range of saturation of the enzyme. This is not possible with our FRET probes due to a lack of aqueous solubility. Calculations for k_M for the soluble probe CAPRee1 show that it is in the low micromolar range for all CAPs. For the lipidated probes, it seems to be lower but the calculation is only by approximation because concentrations in the saturation range, i.e. higher than 4 µM cannot be tested due to solubility and precipitation artefacts.

Interestingly, the D/A ratio does not follow Michaelis Menten kinetics. For CAPRee1, the increase in D/A ratio was mostly independent of the substrate concentration. For very low and high concentrations, the D/A ratio increase was decreased compared to the plateau (Figure 13). Therefore, the D/A ratio increase was ideal because it was very robust to small experimental inaccuracies.

In contrast, this was not the case for CAPRee4 (Figure 26 and 27) for which both the initial D/A ratio in the intact molecule as well as the maximal D/A ratio upon cleavage depended on the probe concentration. Therefore, the D/A ratio increase was not exclusively dependent on the enzyme concentration anymore, but is also dependent on the probe concentration. This could be overcome by normalization of the D/A ratio to both negative and positive control (Figure 28), e.g. by calculation of the cleavage in %. By normalization to both initial D/A ratio and maximal D/A ratio, the slope of the % cleavage was exclusively dependent on enzyme concentration. Therefore, it also represents an adequate measure for enzyme activity. For the lipidated probes however, this requirement would be highly disadvantageous. Because of longer incubation times before the start of imaging and different background due to different origin of samples, the minimum for each sample was not easily experimentally accessible. Extrapolation from the slope might be an adequate way. Furthermore, the design of a caged version of our probes might be another option. The addition of a photolabile protecting group for example on the arginine residue in P1 of CAPRee3 might disable the recognition and cleavage by CAPs. Therefore, the cells could be incubated and washed without cleavage of the probe. Only upon illumination, the cleavable probe is released and can be tackled by the enzymes.

The protection of an arginine residue however requires elaborate chemistry[102]. Preliminary data obtained from CAPRee1_a which has a lysine in P1 suggests that the replacement of R by K might be an option that keeps both dynamic range and specificity of the probe. A lysine residue would be comparably easy to photocage and is even commercially available as Fmoc - Lys(4,5 - dimethoxy - 2 - nitro - benzyloxycarbonyl) – OH. The insertion of an amino acid that is photocaged requires a red shifted fluorophore combination that has very little absorbance in the UV-range. Such a combination has not been successfully established so far in our lab. Initial tests with TAMRA and a mono-sulfonated Cyanin-5 derivate failed.

Apart from difficulties to determine the initial FRET ratio on the specimen, the determination of the maximal D/A ratio in live cell imaging experiments was also not easy to achieve because of an inherent problem of the target enzymes: high concentrations or long incubation with CAPs will have a similar effect as incubation with trypsin – rounding up of the cells and detachment from the solid surface. Therefore, for samples with low enzyme activity like primary nasal cells of healthy control subjects, determination of kinetics of cleavage is highly time- consuming and difficult to obtain accurate data.

In addition to the problem, that the D/A ratio increase might not be probe concentration-independent, for the lipidated probe CAPRee3, the maximal donor fluorescence which was reached in the plateau was not only dependent on the probe concentration. For mCAP3, the fluorescence intensity in the plateau depended on the enzyme concentration (Figure 14) so that apparently, the probe was never fully cleaved. Therefore, no plateau was reached for this particular enzyme. For hCAP3 and HAT however, the final D/A ratio was independent of the enzyme concentration. This suggests that mCAP3 but not hCAP3 and HAT are subjected to product inhibition. As the enzyme tested are only recombinantly expressed catalytic subunits, the results might not be directly transferable to endogenous enzymes. Artefacts due to precipitation seem to be unlikely because the behavior is independent of the probe concentration and happens similarly with low probe concentrations but only depends on the ratio between enzyme und substrate concentrations. Further investigation is required to understand the mechanism.

To summarize, several factors can influence the D/A ratio. Analysis of a large data set with known enzyme and probe concentrations showed that the quantification of the initial increase of the D/A ratio is a very robust measure for enzyme concentration and is always highly significantly correlated ($p < 0.0001$). The slope was always calculated by linear regression of at least 4 time points and over at least 30 min, for primary cells 60 min. The results are highly robust and are not significantly affected by the absolute D/A ratio values at the beginning of the experiment or the final plateau if it is reached during imaging. Absolute quantification of the enzyme concentration however is not easily

possible due to significant differences between the recombinantly expressed catalytic subunit or the full molecule which is endogenously expressed in the tested cell lines and airway epithelial cells.

3.5 Increased CAP activity in CF – cell lines and human nasal epithelial cells

To test whether the CAPRee probes are useful research tools, they were applied in systems where one could speculate about the biological answer. As proof-of-concept, CAPRee1 and CAPRee3 were tested on primary murine tracheal epithelial cells and human nasal epithelial cells. Both cell systems are easily accessible so that they could also be the basis for future applications. As a first validation of the CAPRee probes, they were used in CF context, where CAP activity is abnormally regulated.

So far, it was not clear how CAPs are regulated in the murine CF model which has been established by Mall *et al* [6]. Mice that overexpress β-subunit of ENaC show a lung phenotype that is comparable to the human disease. MTECs from transgenic animals and littermate control wildtype mice were isolated and cultured for 14 days in ALI. It could be clearly shown that mTECs from βENaC- transgenic mice have significantly reduced CAP activity compared to wildtype littermate controls which had not been observed previously. It is known that the mice still have protease-sensitive αβγ-channels so it seems consistent that the protease activity is reduced to minimum to limit ENaC activity as far as possible. This would be in line with what is expected in a system where the regulation of protease activity is not disrupted. Therefore, it would be interesting to study CAP regulation comparing wild type and βENaC-transgenic. One challenge for this research is the lack of suitable CAP-knockout models. As described in the introduction, CAPs are crucial for survival and development of the animals so that a systemic knockout of the proteases is not possible. So far, in the existing CAP1 – knockout model with conditional deletion in the lung, alveolar cells lack CAP1 whereas the βENaC-transgene is expressed in Club cells[6, 19]. It is completely unclear how a double mutant mouse might behave.

None of the CFTR mutant mouse strains show a lung phenotype comparable to human CF lung disease. Murine nasal tissue is comparable to human bronchial airways with respect to tissue composition and electric properties[103]. Therefore, potentially nasal cells of CFTR-knockout mice could also be used to study CAP activity.

Several studies have shown that CAP activity is abnormally regulated in CF[21-22,104]. Therefore, the CAPRee probes were tested to see whether they are able to detect the increased CAP activity in the CF cell line CFBE41o$^-$ and the corresponding healthy control which expressed wildtype CFTR. Both CAPRee1 and CAPRee3 were able to detect the significantly increased enzyme activity in CF cells. The difference, however, was only about 2.5 fold, due to the fact that the healthy control also has

enzyme activity. This is in contrast to FRET probes for inflammatory proteases which are absent or inactive in healthy controls[51,105].

Human nasal epithelial cells are emerging in CF research on the way to personalized treatment of the disease. They are very easily accessible by nasal brushing or nasal surgery. Culturing protocols have been established in many labs so that their use is becoming more and more popular. So far, the cells were used as *ex vivo*, patient-derived testing system for CFTR modulator and corrector drugs. Protocols for the detection of electrophysiological properties have been established and the cells are nowadays well characterized so that personalized treatments can be tested[106]. Due to the low invasiveness of the procedure to obtain hNECs, both healthy controls and diseased people can be subjected to the procedure, repeatedly without significant side-effects. This allows higher sample numbers and can improve statistics.

So far, human nasal epithelial cells have not been used in studies that investigate CAP activity. We cultured the cells in ALI conditions mimicking the *in vivo* situation. The quantification of CAP activity by CAPRee3 revealed that on cells derived from CF patients, CAP activity is increased. Whereas the healthy control samples show very little variability, CAP activity was very variable among the CF samples. When treating each well as individual sample, the increase in the CF samples was statistically significant. However, only four patients each with two wells were tested and included into the statistics. Averaging both samples per patient resulted in loss of significance, due to the low sample number and high variability of the patients.

The proof-of-concept experiments that CAP activity can be quantified on hNEC cells despite long imaging times and challenging microcopy set ups set the stage for studying CAP activity and CAP regulation in human systems. Data obtained from model systems, either cell lines or murine tissue, can be validated *ex vivo* in a human system.

4. Conclusion

In this work, the design, characterization and early application of fluorescent reporters for the quantification of CAP activity were described. Two different approaches for the design of the substrate sequence and optimization were tested as well as the modification of acceptor fluorophores to improve performance.

Whereas the probes which were based on one of the most relevant physiological targets, ENaC, were shown to have comparably performance, the approach taking the autoactivation cleavage site of CAP3 as substrate sequence resulted in useful FRET probes. These probes were shown to be a suitable tool for CAP quantification in human and murine samples. Among the different lipidated probes tested, CAPRee3 is the best performing probe with respect specificity, localization and dynamic range upon cleavage. The probe is highly stable in the plasma membrane which enables quantification of even very low concentrations by imaging over several hours. Whereas the donor fragment remains to be bound in the plasma membrane, the acceptor fragment diffuses into the fluid on top of the cells, resulting in spatial separation of the dyes and loss of FRET. Due to very good aqueous solubility, the probe can be loaded onto cells in higher concentrations compared to CAPRee2. Therefore, staining of cells cultured in ALI is efficient and homogenous. The specificity is even better compared to the soluble analog CAPRee1 which has the same amino acid sequence.

For CAPRee1 and CAPRee3, the change in D/A ratio is very robust towards little aberrations that result from pipetting errors or efficiency in loading of the probe onto the cell membrane. Over a large concentration range, the increase in D/A ratio is only probe concentration dependent. This is very advantageous compared to commercial protease substrates which have to be used in high concentrations which however reduces the sensitivity. CAPRee1 and CAPRee3 can be used in the low micromolar to nanomolar range without being susceptible concentration variability. Furthermore, the quantification of enzyme activity by the lipidated CAPRee3 is independent of the cell number. Especially for cells that are cultured for several days up to weeks, the number of cells in the final experiment can vary significantly between different specimens. CAPRee3 is the first tool which enables the detection of CAP activity in a spatially resolved manner and on a single cell level. The activity of individual cells can be quantified which has not been possible so far. Therefore, the number of cells per specimen does not affect the quantification of enzyme activity which has been a critical drawback so far.

To date, FRET sensors were applied in fixed samples and only very preliminary live cell imaging experiments were performed. From a technical perspective, live cell imaging is more challenging but also gives rise to new opportunities. Elaborate protocols for imaging of primary cells for several hours

without significant impact on the cells have been established to enable the spatially resolved quantification of CAP activity on primary cells for the first time. The detection of enzyme activity measured over time gives a more robust signal compared to the quantification of individual time points. Single time points might be excluded without severe loss of information. Especially for precious clinical samples, this is beneficial.

In addition to the use of lipidated FRET probes in microscopy, the soluble probes have been successfully used in fluorescence plate reader assays which could in principle be done on cells that had been grown in Transwell® or Snapwell® inserts. The latter might enable the quantification of CAP activity and the detection of electric currents in the Ussing chamber from the same sample. This combination is not possible on inverted microscopes because Snapwell®-inserts are not transparent to the imaging light.

The ability to detect CAP activity on cells that are grown on Transwell® filter inserts will also enable the simultaneous detection of the ASL height. This has not been possible so far with fluorogenic substrates that are commercially available. The combined measurement of CAP activity and ASL height might reveal new insights about how these processes are coupled in health and disease.

To conclude, the FRET reporters developed in this work are novel research tools that will open various opportunities in the field of CAP activity and regulation research that have been impossible so far due to major technical limitations. Furthermore, the question whether CAPs might be relevant biomarkers for the stage and progression of chronic lung diseases, including CF, COPD or pulmonary fibrosis, can be further investigated.

The applicabilty of the same probes to human und murine samples will facilitate the transfer from murine to human. In CF, but not limited to that disease, the characterization of CAP activity in *ex vivo* might also be an interesting tool on the way to personalized medicine. Quantification of CAP activity on patient speciment *ex vivo*, such as nasal epithelial cells, might discrimate patients that profit from serine protease inhibitor treatment from those who do not benefit from the drug. So far, CAP activity has not been measured on nasal epithelial cells so far.

5. Outlook

So far, little is known about the regulation of CAP activity in CF and COPD. As previously described, CAP activity is increased in CF but the mechanism remains unclear. For COPD, the importance of CAPs is unknown und remains to be investigated. The combination of quantifiying RNA, protein and enzyme activity levels of CAPs as well as their cognate inhibitors might reveal at which level the protease activity is regulated in health and disease.

From different areas of research, including gastrointestinal diseases or skin development, several factors have been suggested that might influence CAP activity. Inflammatory cytokines have been published to down-regulate CAP1 activity in the gut[107]. The application of our CAPRee probes might reveal how these stimuli affect CAP activity in the lung. In CF, CAP activity is potentially increased in presence of inflammatory cytokines[108]. Another report which used the murine M-1 cell line describes that interleukin (IL)-6 increases ENaC activity and CAP1 expression levels[109]. IL-6 has been reported to be increased in CF[110]. CAPRee probes can be an important research tool in disecting the stages from RNA expression, translation and activation of the proteases. This might results additional knowlegde about the pathophysiological processes in CF and potentially reveal new therapeutic strategies. So far, it remains unclear, whether CAPs could be an interesting therapeutic target. As previously described, so far selective inhibtiors have not been designed which might be one of the greatest obstacles for CAPs as target. Therefore, an upsteam regulator of CAPs might lead to reduced side effects compared to the direct targeting of the proteases. For their identification, the use of our CAPRee probes might be an adequate tool.

Clinical studies including different parameters of the CF or COPD lung disease which are established biomarkers such as FEV_1% predicted, or the identification of the CFTR mutation of the respective patient could be performed to investigate whether the CAPRee probes might be useful biomarkers.

Additionally, the application of the FRET probes is not limited to CF. As described in the introduction, CAPs have been published to assiociated with pulmonary fibrosis, developmental defects in the skin as well as cancer development and progression[28,40, 111]. In COPD, the role of CAPs has not been assessed so far.

Especially in the context of cancer, the lipdiated CAP probes could give great insights because of their spatial resolution. Potentially not only the amount of enzyme, but also the activity and localization of

activity are useful biomarkers for the progression of the disease. Such an investigation has not been possible so far.

To summarize, CAPRee probes might be useful tools in different fields of research. They offer the unique chance to quantify CAP activity in a spatially and temperally resolved manner and will be helpful on the way to personalized treatment in different disease context.

6. Material and Methods

6.1 Material

Standard solvents for peptide synthesis were purchased from Fluka, Sigma-Aldrich (Steinheim, Germany) and Novabiochem (Darmstadt, Germany). Anhydrous 1-Hydroxybenzotriazole (HOBt), 2-(1H-Benzotriazole-1-yl)-1,1,3,3-tetramethyluronium hexafluorophosphate (HBTU), Fmoc-Lys(Mtt) Wang resin and Fmoc-amino acids were from Novabiochem. [2-[2-(Fmoc-amino)ethoxy]ethoxy]acetic acid (Fmoc-OcO2-OH; peg-linker), Fmoc-Lys(Palm)-OH and Fmoc-Lys-Wang resin were from Iris Biotech (Marktredwitz, Germany). Coumarin 343 was purchased from Acros Organics (Geel, Belgium). 7-methoxycoumarin-3-carboxylic acid, palmitoic acid and COMU were from Sigma-Aldrich. 5,6-Carboxytetramethylrhodamine-N-succimidyl ester (TAMRA-NHS) was from Primetech LLC (Minsk, Belarus) or Anaspec. Cyanin-3 was purchased from Lumiprobe (Hannover, Germany), Dy485-XL from Dyomics (Jena, Germany).

Cell culture media and supplements for the CFBE cell lines, HL-60, mTECs and PBS were ordered from Gibco/Thermo Fisher Scientific, for the hNEC cells from PromoCell and for M-1 cells from ATCC. Equipment for cell culture and microtiter plates were from Corning.

Recombinant enzymes and commercial protease substrates were purchased from R&D systems; NE was purchased from Merck Millipore (Darmstadt, Germany).

6.2 Methods

6.2.1 Chemical synthesis and purification of individual probes

All probes were synthesized by Fmoc-based solid phase peptide synthesis on a Wang resin, pre-loaded with an α-Fmoc–ε-unprotected lysine residue (CAPRee1-5), α-Fmoc-Asp(OtBu) residue (CAPRee1_b), α -Fmoc-Arg (Pbf) residue (acceptor fragment CAPRee3), α-Fmoc–ε-Mtt protected lysine residue (donor fragment CAPree6) or α -Fmoc-propargyl-Gly residue (CAPree6). Before the start of the synthesis, the resin was swollen for 30 min in Dimethylformamide (DMF) or DMF/Dichloromethane (DCM) mixture. Fmoc deprotection was performed in 40 % piperidine in DMF for 3 min, followed by 12 min 20 % piperidine in DMF. The step was repeated once. Between all coupling and deprotection steps, the resin was washed with 1 ml DMF for 1 min with continuous shaking. This step was repeated four times. All amino acids of the CAPRee1-3 probes were coupled using 5 equivalents of the respective amino acid, 5 equi. HBTU, 5 equi. HOBt and 10 equi.

diisopropylethylamin (DIPEA) in DMF twice for 40 min at room temperature on a Syro peptide synthesizer. CAPRee4 and 5 were synthesized using an identical protocol manually. CAPRee6 was partially synthesized on the automated synthesizer, i.e. the Val and Gly residues were coupled automatically, the Arg and Lys residues were coupled manually to increase the yield. The detailed coupling protocol is given below for each probe.

After complete synthesis, the probe was cleaved from the resin and fully deprotected with 95 % trifluoroacetic acid (TFA), 2.5 % tri-isopropyl-silane and 2.5 % water and precipitated from ice-cold diethyl ether. After centrifugation, it was once washed in ice cold either and dried over night or under argon flow.

Purification was performed by HPLC, using an acetonitrile (ACN) gradient in water. Analytical HPLC was performed on a NUCLEODUR C18 ec 5 µm, 4 mm x 250 mm, Macherey Nagel, Düren, Germany) column, semipreparative HPLC was performed on Discovery Bio Wide Pore C18 column (10 µm, 25 cm x 21.2 mm, SUPELCO, Sigma-Aldrich) The detailed information for the gradient is given below. To improve performance, 0.5% TFA was added to both solvents. Characterization was achieved by ESI mass spectrometry, including high resolution mass spectrometry for the most important probes. The fragments were additionally characterized by NRM.

Due to the sensitivity of the Coumarin343 towards remaining TFA after freeze-drying, all probes were immediately dissolved in DMSO and kept at -20°C for storage. Quality checks were performed regularly to confirm the integrity of the samples.

The concentration of the DMSO stocks was measured using the absorbance of Coumarin343 (extinction coefficient ε=44140 L*mol-1*cm-1) in ethanol.

6.2.2 Detailed structures and procedures:

CAPRee1:

Expected mass: 1584.73 Da
$[M+1]^{+}$ exp. 1585.75, 1585.79 $[M+2]^{2+}$ exp. 793.38, found 793.30/792.90, $[M+3]^{3+}$ exp. 529.25, found 529.25

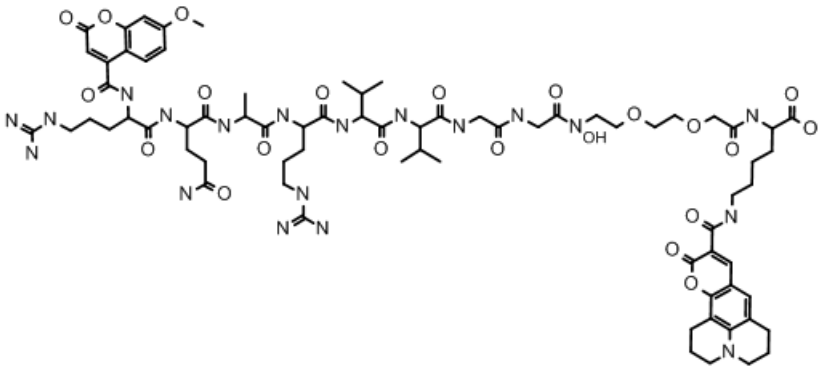

Synthesis:

1. Coupling of Cou3432: equiv. of dye, 3 equi. of (1-Cyano-2-ethoxy-2-oxoethylidenaminooxy)dimethylamino-morpholino-carbenium-hexafluorophosphat (COMU) and 6 equi. of DIPEA in DMF/DCM 1:3 ratio for 2 h. The step was repeated once.
2. Synthesis of the aa sequence and peg-linker
3. Coupling of MetOCou: 2 equiv. of dye, 3 equi. of COMU and 6 equi. of DIPEA in DMF for 2 h. The step was repeated once

Purification:

30-70 % ACN in water

CAPRee1_a:

Expected mass: 1557.72 Da

[M+1]+ exp. 1558.72, not found [M+2]2+ exp. 779.36 , found 779.35 [M+3]3+ exp. 519.90, found 519.95 [M+4]4+ exp. 390.18, found 390.05

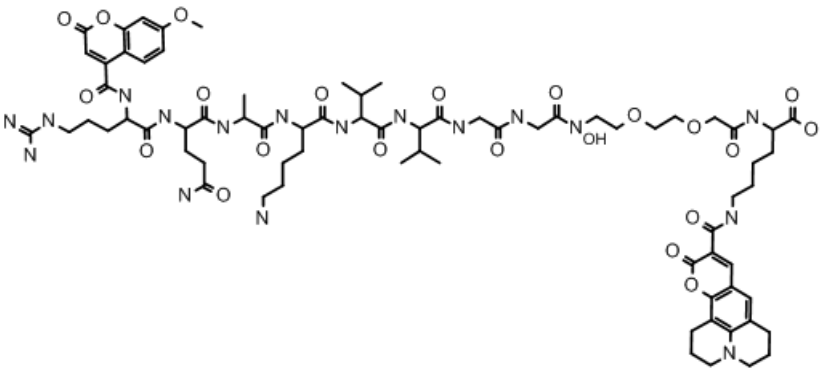

Synthesis and Purification identical to CAPree1

CAPRee1_b:

Expected mass: 1913.99 Da
$[M+1]^{+}$ exp. 1913.99, not found; $[M+2]^{2+}$ exp. 958.00, found 965.70, $[M+3]^{3+}$ exp. 639.00, found 644.40

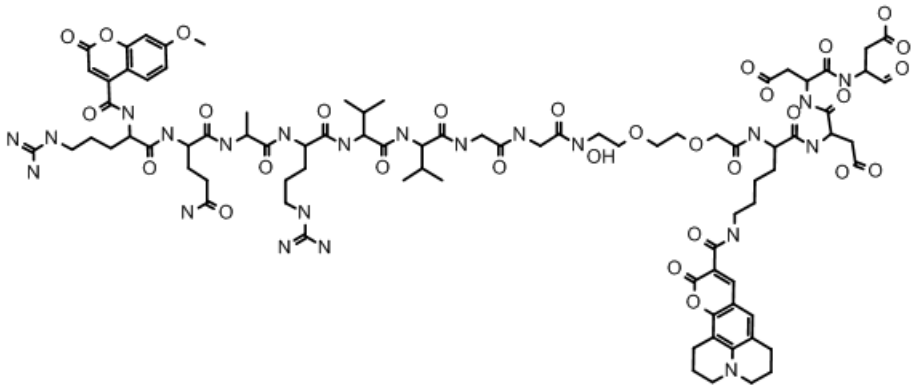

Synthesis:

- Use of α-Fmoc-Asp(OtBu) Wang resin
- Automatic coupling of 2 additional Asp residues
- Coupling of α-Fmoc-ε-Mtt- protected lysine manually
- Cleavage of ε-Mtt protecting group by 1 % TFA and 5 % TIS in DCM, change of cleavage cocktail every 15 min 6 times
- Coupling of Cou343: equiv. of dye, 3 equi. of COMU and 6 equi. of DIPEA in DMF/DCM 1:3 ratio for 2 h. The step was repeated once.
- Automatic coupling of the aa sequence and peg-linker
- Coupling of MetOCou: 2 equiv. of dye, 3 equi. of COMU and 6 equi. of DIPEA in DMF for 2 h. The step was repeated once.

Purification:

30-70 % ACN in water

CAPRee1_c:

Expected mass: 1729.88 Da
$[M+1]^{+}$ exp. 1730.88, not found; $[M+2]^{2+}$ exp. 865.94, found 865.85 $[M+3]^{3+}$ exp. 577.62, found 577.55$[M+4]^{4+}$ exp. 43.47, found 433.45

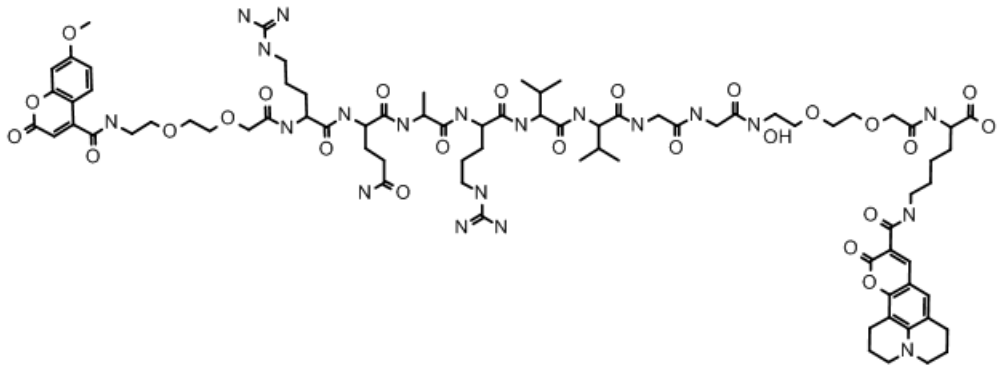

Synthesis and purification identical to CAPRee1

CAPRee1_d:

Expected mass: 1686.73 Da
$[M+1]^{+}$ exp. 1687.73, not found; $[M+2]^{2+}$ exp. 844.16, found 843.1, $[M+3]^{3+}$ exp. 563.10, found 562.64, $[M+4]^{4+}$ exp. 422.75, found 422.15

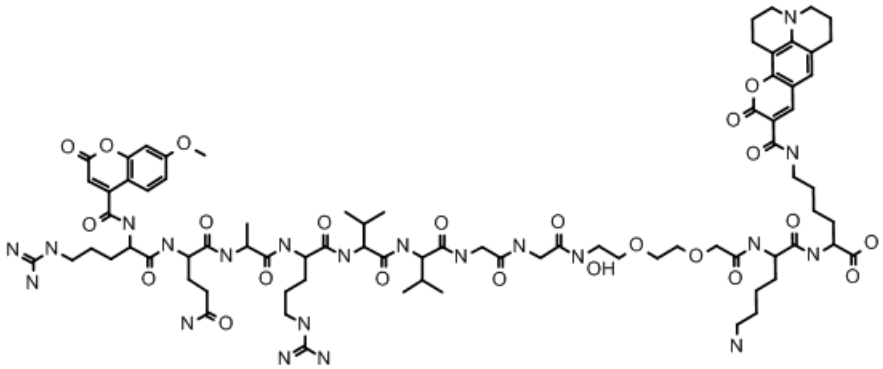

Synthesis and purification identical to CAPRee1, the additional lysine had already been coupled on the resin

CAPRee2:

Expected mass: 2161.58 Da
$[M+1]^{+}$ exp. 2162.78, not found; $[M+2]^{2+}$ exp. 1081.79, found 1081.86 /1081.62, $[M+3]^{3+}$ exp. 721.53, found 721.41/721.42 $[M+4]^{4+}$ exp. 541.36, found 541.39

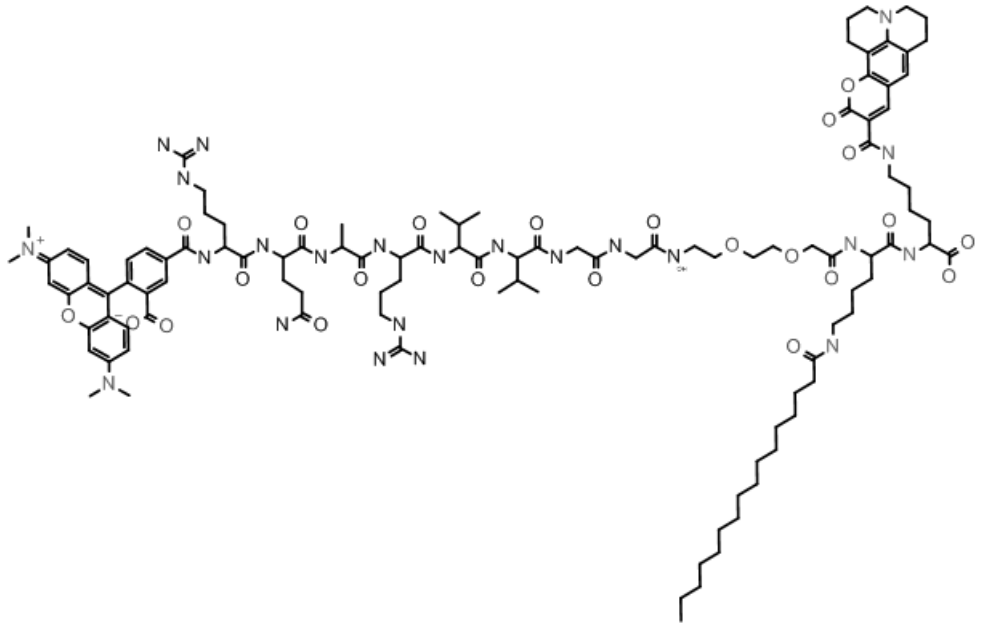

Synthesis:

- Coupling of Cou343: 2 equiv. of dye, 3 equi. of COMU and 6 equi. of DIPEA in DMF/DCM 1:3 ratio for 2 h. The step is repeated once
- Capping of unreacted amino groups by 10 % acetic anhydride in pyridine for 10 min
- Couling of palmitoylated lysine, using 3 equi. of the amino acid, 3 equi. of COMU and 6 equi. of DIPEA in DMF/DCM in 1:3 ratio for 2 h
- Coupling of the amino acids and peg linkers
- Coupling of TAMRA as NHS derivative with 1.1 equi. dye and 2 equi. DIPEA in DMF

Purification:

50-100 % ACN in water

CAPRee2_a:

Expected mass: 2161.58 Da
$[M+1]^{+}$ exp. 2162.78, not found; $[M+2]^{2+}$ exp. 1081.79, found 1081.86 /1081.62, $[M+3]^{3+}$ exp. 721.53, found 721.41/721.42 $[M+4]^{4+}$ exp. 541.36, found 541.39

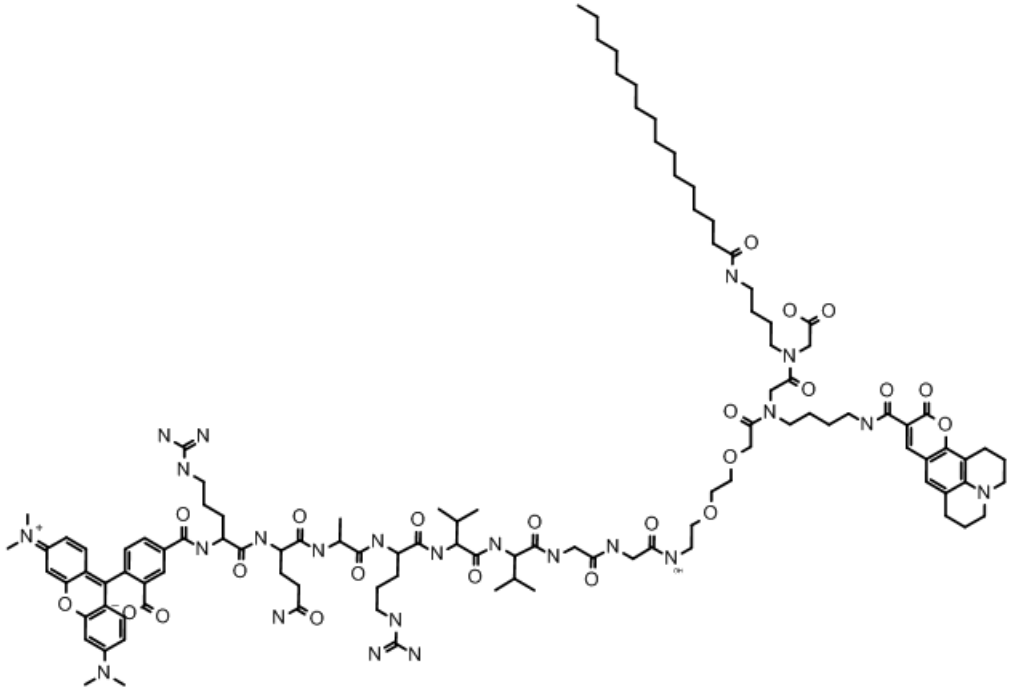

Synthesis:

- Coupling of palmitic acid onto the free ε-amino group with 5 equi. palmitic acid, 5 equi. HBTU, 5 equi. HOBt and 10 equi. DIPEA in DMF/DMC 1:3 for 2 h. The step was repeated once
- Coupling of α-Fmoc-ε-Mtt- protected lysine manually
- Cleavage of ε-Mtt protecting group by 1 % TFA and 5 % TIS in DCM, change of cleavage cocktail every 15 min 6 times
- Coupling of Cou343: equiv. of dye, 3 equi. of COMU and 6 equi. of DIPEA in DMF/DCM 1:3 ratio for 2 h. The step was repeated once.
- Automatic coupling of the aa sequence and peg-linker
- Coupling of TAMRA as NHS derivative with 1.1 equi. dye and 2 equi. DIPEA in DMF

Purification:

50-100 % ACN in water

CAPRee2_b:

Expected mass: 2237.74 Da
$[M+1]^+$ exp. 2238.74, not found; $[M+2]^{2+}$ exp. 1119.87, found 1117.63

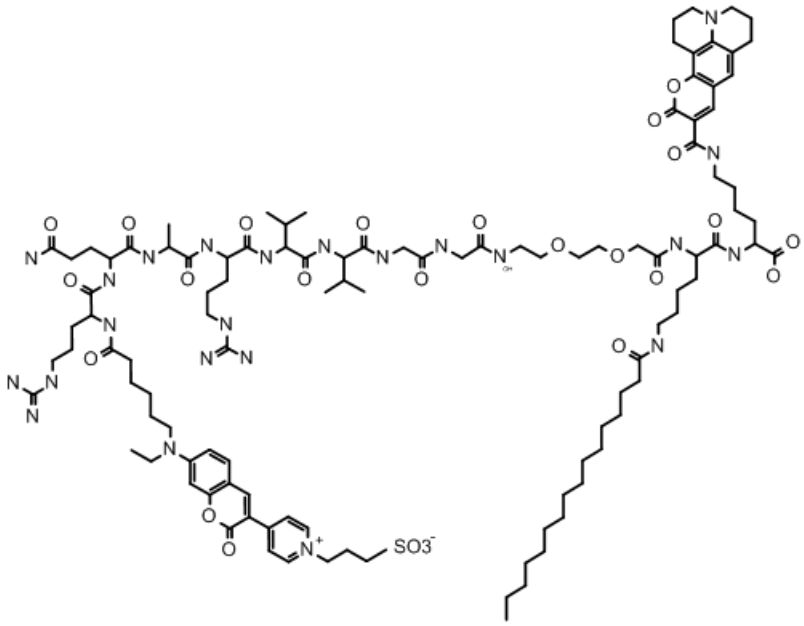

Synthesis:

- Coupling of Cou343: 2 equiv. of dye, 3 equi. of COMU and 6 equi. of DIPEA in DMF/DCM 1:3 ratio for 2 h. The step is repeated once
- Capping of unreacted amino groups by 10 % acetic anhydride in pyridine for 10 min
- Couling of palmitoylated lysine, using 3 equi. of the amino acid, 3 equi. of COMU and 6 equi. of DIPEA in DMF/DCM in 1:3 ratio for 2 h
- Coupling of the amino acids and peg linkers
- Coupling of Dy485-XL as NHS derivative with 1 equi. dye and 2 equi. DIPEA in DMF

Purification:

50-100 % ACN in water

CAPRee2_c:

Expected mass: 2190.78 Da
$[M+1]^{+}$ exp. 2191.78, not found; $[M+2]^{2+}$ exp. 1095.39, found 1095.50 /1094.68, $[M+3]^{3+}$ exp. 730.26, found 730.10/730.122 $[M+4]^{4+}$ exp. 547.70, found 547.95

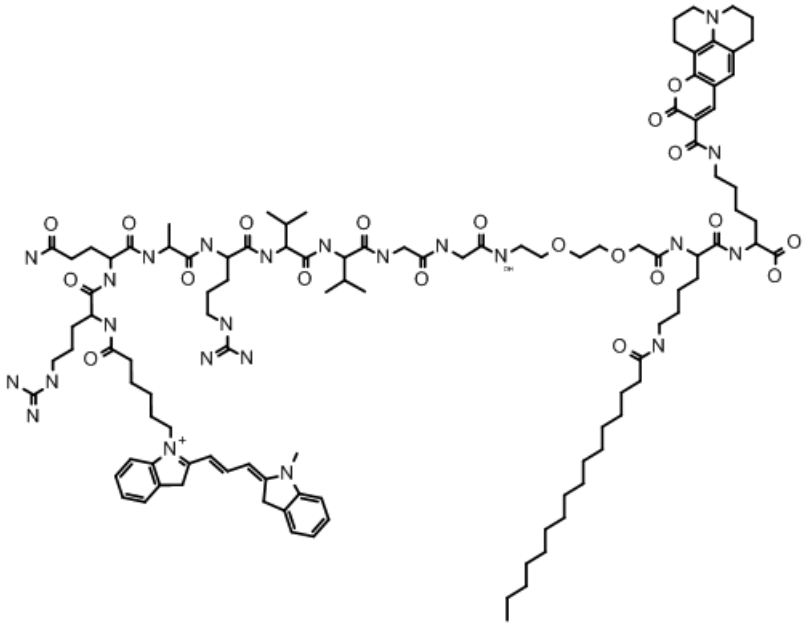

Synthesis:

- Coupling of Cou343: 2 equiv. of dye, 3 equi. of COMU and 6 equi. of DIPEA in DMF/DCM 1:3 ratio for 2 h. The step is repeated once.
- Capping of unreacted amino groups by 10 % acetic anhydride in pyridine for 10 min
- Couling of palmitoylated lysine, using 3 equi. of the amino acid, 3 equi. of COMU and 6 equi. of DIPEA in DMF/DCM in 1:3 ratio for 2 h
- Coupling of the amino acids and peg linkers
- Coupling of Cyanin-3 as NHS derivative with 1.5 equi. dye and 2 equi. DIPEA in DMF

Purification:

50-100 % ACN in water

CAPRee3:

Expected mass: 2306.74 Da
$[M+1]^{+}$ exp. 2307.74, not found; $[M+2]^{2+}$ exp. 1154.37, found 1154.24/1154.16, $[M+3]^{3+}$ exp. 769.91, found 769.75/769.77 $[M+4]^{4+}$ exp. 577.69, found 577.61

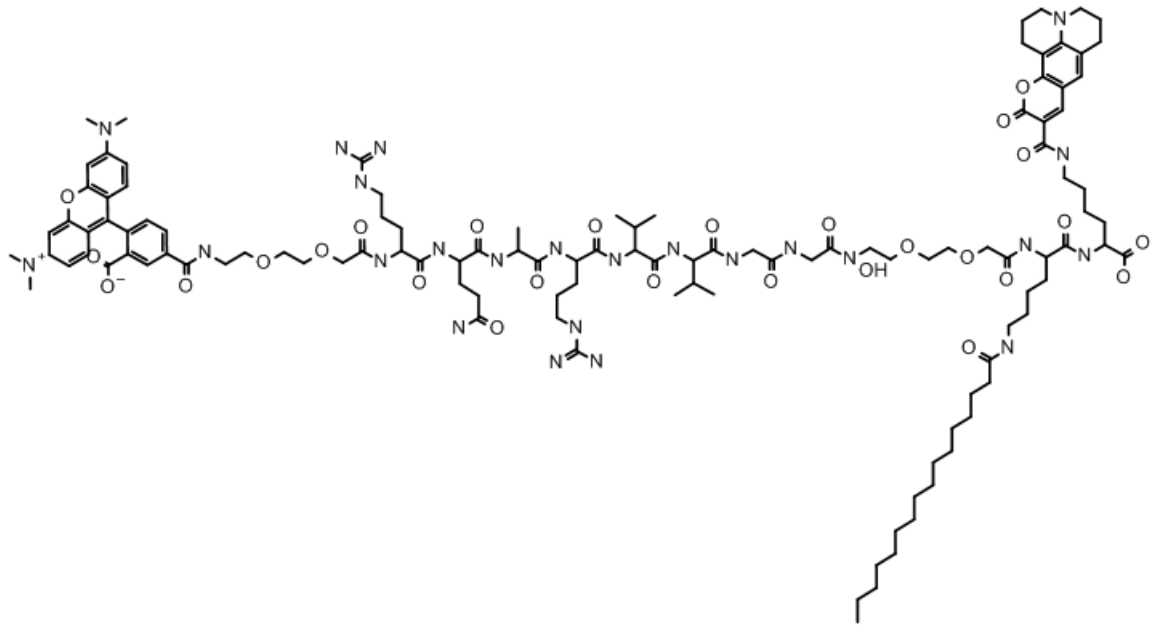

Synthesis and purification identical to CAPRee2

CAPRee4:

The probe was designed by Verena Rickert-Zacharias and synthesized by Jonas Wilhelm and Frank Stein.

Expected mass: 1629.81 Da
$[M+1]^{+}$ exp. 1630.81, not found; $[M+2]^{2+}$ exp. 815.91, found 815.55, $[M+3]^{3+}$ exp. 544.27, found 544.05

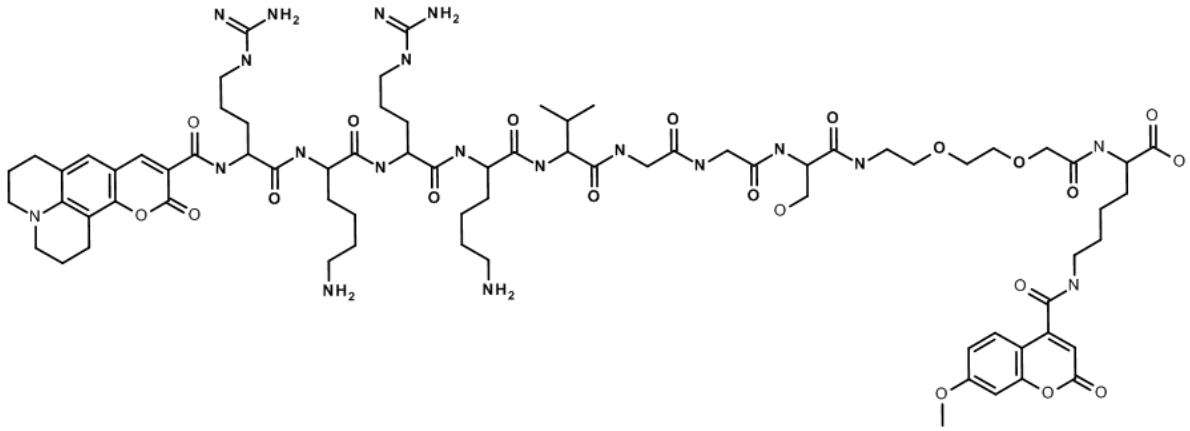

Synthesis:

- Cleavage of ε-Mtt protecting group by 1 % TFA and 5 % TIS in DCM, change of cleavage cocktail every 15 min 6 times
- Coupling of MetOCou: equiv. of dye, 3 equi. of COMU and 6 equi. of DIPEA in DMF/DCM 1:3 ratio for 2 h. The step was repeated once.
- Manual synthesis of the peptide backbone
- Coupling of Cou343: 2 equiv. of dye, 3 equi. of COMU and 6 equi. of DIPEA in DMF/DCM 1:3 ratio for 2 h. The step is repeated once.

Purification: 30-70 % ACN in water

CAPRee5:

The probe was designed by Verena Rickert-Zacharias and synthesized by Jonas Wilhelm and Frank Stein.

Expected mass: 2206.76 Da
$[M+1]^{+}$ exp. 2207.76, not found; $[M+2]^{2+}$ exp. 1104.38, found 1104.20, $[M+3]^{3+}$ exp. 736.59, found 736.70, $[M+4]^{4+}$ exp. 552.49, found 552.65

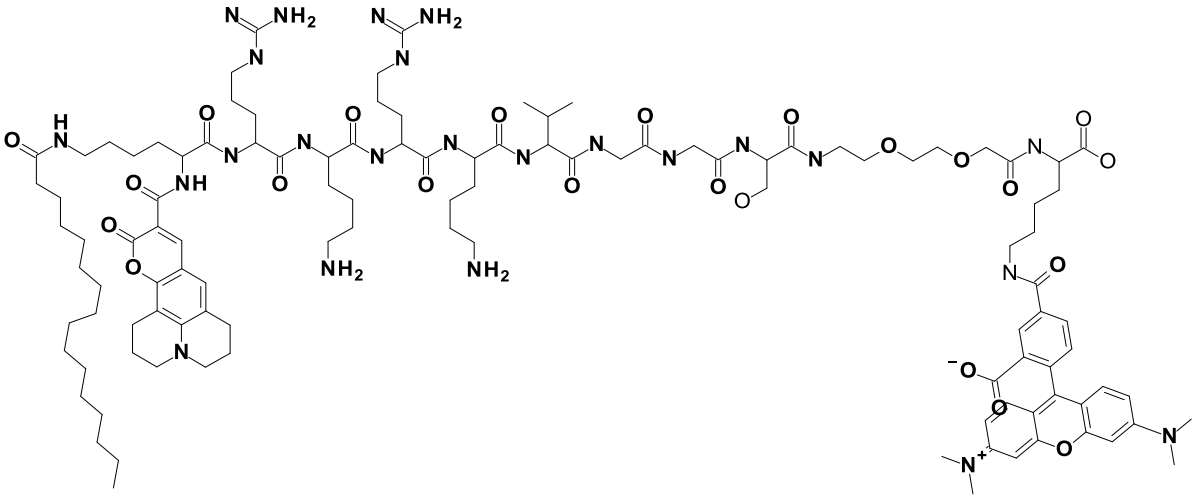

Synthesis:

- Coupling of TAMRA as NHS derivative with 1.1 equi. dye and 2 equi. DIPEA in DMF
- Manual synthesis of the aa sequence
- Couling of palmitoylated lysine, using 3 equi. of the amino acid, 3 equi. of COMU and 6 equi. of DIPEA in DMF/DCM in 1:3 ratio for 2 h
- Coupling of Cou343: 2 equiv. of dye, 3 equi. of COMU and 6 equi. of DIPEA in DMF/DCM 1:3 ratio for 2 h. The step is repeated once

Purification: 50-100% ACN in water

CAPRee6:

Expected mass: 2504.0 Da

$[M+1]^+$ exp. 2505, not found; $[M+2]^{2+}$ exp. 1253, found 1254.00, $[M+3]^{3+}$ exp. 835.67, found 836.25

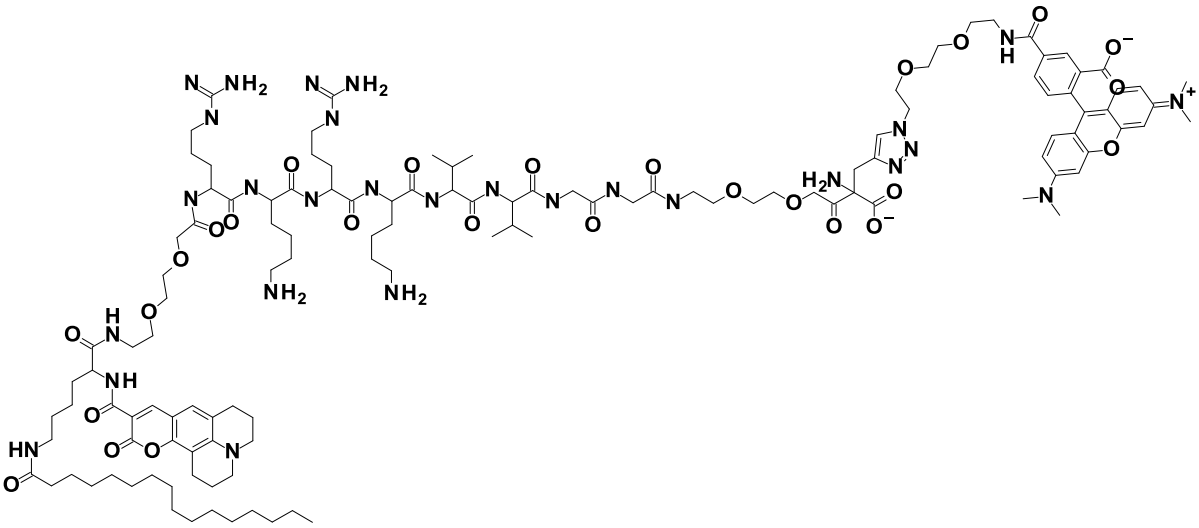

Synthesis:

- Coupling of the aa sequence and peg-linkers on the Fmoc-propargyl-glycine Wang resin, Val and Gly automatically, Arg and Lys manually
- Couling of palmitoylated lysine, using 3 equi. of the amino acid, 3 equi. of COMU and 6 equi. of DIPEA in DMF/DCM in 1:3 ratio for 2 h
- Coupling of Cou343: 2 equiv. of dye, 3 equi. of COMU and 6 equi. of DIPEA in DMF/DCM 1:3 ratio for 2 h. The step is repeated once
- Coupling of 1-Amino-11-azido-3,6,9-trioxaundecane (1.2 equi. of peptide) and 5,6-TAMRA-NHS (1.3 equi. of peptide) with 2 equi. DIPEA in DMF
- Click of peptide with TAMRA-peg-azide with 1/3 equi. of azide and 0.5 equi. of Tris[(1-benzyl-1*H*-1,2,3-triazol-4-yl)methyl]amin)

Purification: 30-70 % ACN in water

Fragments of the probes CAPRee3 and CAPree6

All fragments were designed by Verena Rickert-Zacharias, synthesized and fully characterized by Madeleine Schultz. TAMRA-peg-azide was designed by Victoria Halls and synthesized by Madeleine Schultz. High resolution mass spectrometry was done as service in the OCI, University of Heidelberg, Germany.

Acceptor fragment CAPRee3:

Expected mass: 1086.53 Da
$[M+H]^+$ exp. 1087.53, found 1087.53 $[M+2]^+$ exp. 544.76, found 544.27

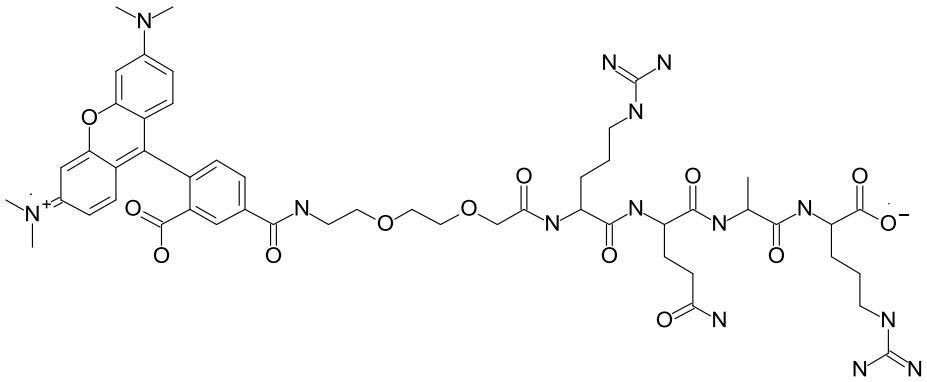

Synthesis:

- Coupling of the amino acids manually on an α-Fmoc-Arg(Pbf) Wang resin
- Coupling of TAMRA-NHS with 1.1 equi. and 2 equi. DIPEA

Donor fragment CAPRee3:

Expected mass: 1237.77 Da
$[M+1]^+$ exp. 1238.77, found 1238.79

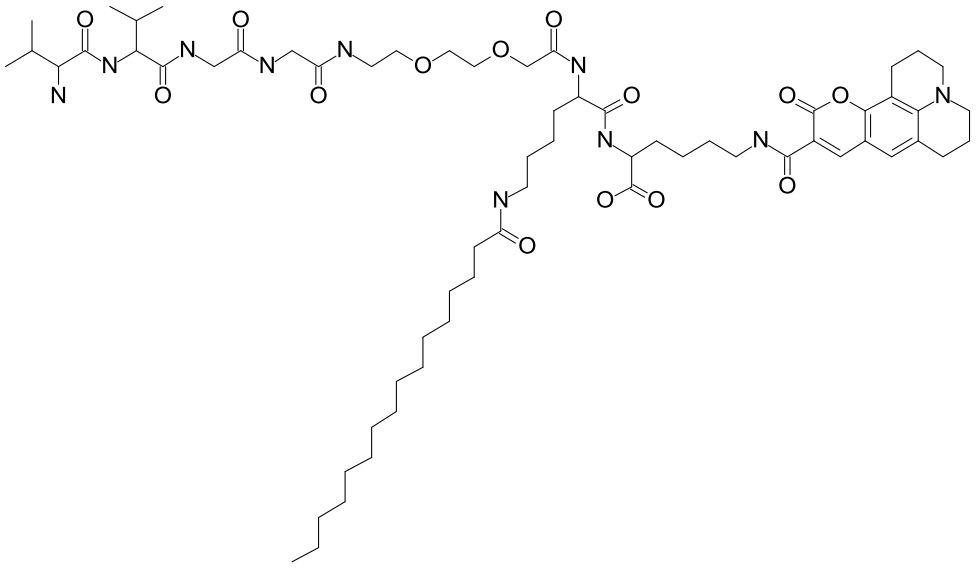

Synthesis and Purification:

Identical to CAPRee3, amino acids coupled manually

Detailed structure of with **TAMRA-peg-azide**:

Expected mass: 700.3095, found: 700.3102

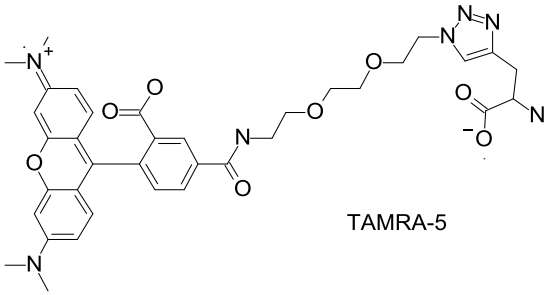

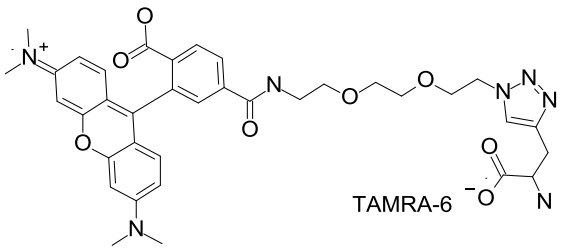

Acceptor fragment CAPRee6:

Expected mass: 1156.56 Da
$[M+1]^{+}$ exp. 1157.56, found 1157.56, $[M+2]^{2+}$ exp. 579.78, found 579.28

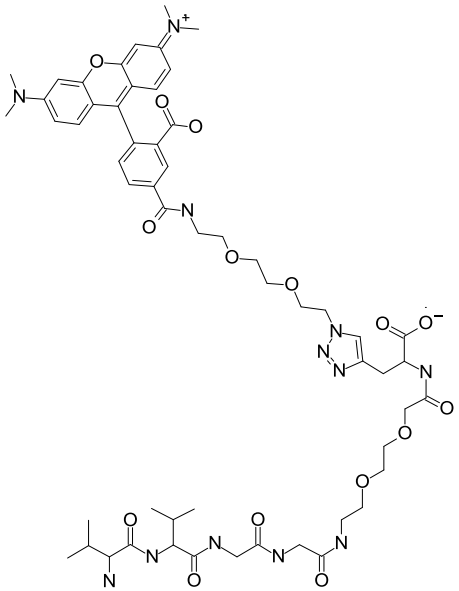

Synthesis and Purification similar to CAPRee6 up to Val in P1', amino acids coupled manually

Donor fragment CAPRee6:

Expected mass: 1364.898 Da
$[M+1]^+$ exp. 1365.898, found 1365.901, $[M+2]^{2+}$ exp. 683.449, found 682.45

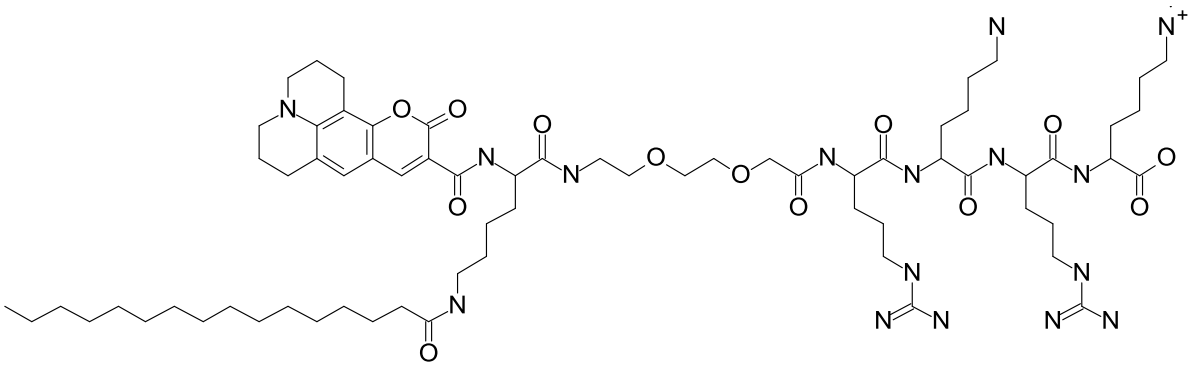

Synthesis:

- Use of α-Fmoc-ε-Mtt lysine Wang resin
- Manual coupling of the amino acids
- Couling of palmitoylated lysine, using 3 equi. of the amino acid, 3 equi. of COMU and 6 equi. of DIPEA in DMF/DCM in 1:3 ratio for 2 h
- Coupling of Cou343: 2 equiv. of dye, 3 equi. of COMU and 6 equi. of DIPEA in DMF/DCM 1:3 ratio for 2 h. The step is repeated once
-

6.2.3 *In vitro* characterization

6.2.3.1 Characterization with recombinant enzymes

The *in vitro* characterization of the probes was performed with recombinant human and murine enzymes. All experiments were performed in a Perkin Elmer EnSpire® multimode plate reader at 37°C and atmospheric CO_2. We performed emission wavescans with a fixed excitation wavelength of 354 nm for the soluble and 440 nm for the lipidated probes. The detected emission wavelength range was from 380 nm to 600 nm for the soluble and from 470 nm to 700 nm. In order to obtain ratiometric measurements, the step size was increased to 90 nm, resulting in measurements at 400 nm and 490 nm for the soluble, and 490 nm and 580 nm for the lipidated probes.

The FRET probes were diluted from DMSO stock solutions with final DMSO concentration up to 0.1 % in assay buffer. As long as not indicated otherwise, the final probe concentration was 2 µM. The enzyme concentrations varied depending on the given and measured enzyme activity, so that the latter one was comparable between different enzymes. The assay was performed in the recommended buffer composition, however regardless the pH unless stated otherwise, because we observed an unexpected decrease of the donor-to-acceptor ratio after cleavage in basic conditions. As this effect was exclusively pH-dependent, the pH was kept in neutral conditions (6.7-7.4) for all enzymes.

The assay was started by addition of enzyme or substrate just before the microtiter plate was put into the plate reader.

6.2.3.2 Characterization with broad spectrum inhibitors on M-1 and CFBE41o- cells

For cell-based experiments, the cells were trypsinized, washed with PBS and counted. Per well, 30 000 cells were seeded and incubated over night to reach 90-100% confluency. Before the experiment, the cells were once washed with DMEM without addition of FCS, antibiotics/antimycotics and phenol red, but with the addition of 25 mM HEPES buffer to maintain the pH at atmospheric CO_2. The inhibitors were dissolved from water or DMSO stocks, according to the manufacturer's recommendations, in DMEM and incubated for 20 min on the cells at room temperature. The probe was added at 2 µM concentration in DMEM with 25 mM HEPES buffer.

6.2.3.3 Liposome preparation

Liposomes were prepared by extrusion with an Avanti Mini Extruder. The extruder was cleaned and assembled according to the supplier's protocol. The liposomes were formed to a final concentration of 3.8 mM liposome in assay buffer (50 nM Tris-HCl, 0.05% Brij-35 in water) with 90% 1,2-Dioleoyl-sn-glycero-3-phosphocholine (DOPC) and 10 % 1,2-dioleoyl-sn-glycero-3-phospho-L-serine. The lipids were dissolved in chloroform which was removed under slow argon flow and. Afterwards, the dried lipids were rehydrated in buffer, preheated to 62°C, and shaked in a horizontal shaker for 1 h at 62°C. Whatman filter papers and the Whatman 400 nm filter membrane were equilibrated in buffer and after assembly, the extruder was heated to 62 °C. To avoid bubbles, the filter papers and filter membrane were again equilibrated with buffer. Afterwards, the liposomes were extruded by pushing the liquid 41 times through the filter membrane. The quality and size of the liposomes was checked by dynamic light scattering. The liposomes were smaller than expected with an average size of 320 nm.

Buffers:

mCAP1, mCAP3, hCAP1, hCAP3, HAT, trypsin: 50 mM Tris, 0.05% (w/v) Brij 35

CTSB: Activation Buffer: 25 mM MES, 5 mM DTT; Assay Buffer: 25 mM MES; dilution to 10 µg/mL in Activation Buffer, incubation at room temperature for 15 minutes, dilution to the desired concentrations

CTSS: Assay Buffer, 50 mM NaOAc, 5 mM DTT, 250 mM NaCl; dilution to 10 µg/mL in Assay Buffer , incubation at room temperature for 2 hours, dilution to the desired concentrations

Furin: 1 mM $CaCl_2$, 50 mM Tris, 0.05% (w/v) Brij 35

NE: 100 mM Tris-HCl, pH 7.5, 500 mM NaCl

MMP12: 50 mM Tris, 10 mM $CaCl_2$, 150 mM NaCl, 0.05% (w/v) Brij-35, pH 7.5 (TCNB); activation by adding APMA to a final concentration of 1 mM and incubating at 37 °C for 24 hours

Commercial substrates: Cat.# refers to R&D systems

mCAP1, mCAP3, hCAP1, hCAP3, HAT, trypsin: Boc-QAR-AMC Fluorogenic Peptide Substrate (Cat. # ES014)

CTSB: Z-LR-AMC Fluorogenic Peptide Substrate (Cat.# ES008)

CTSS: MCA-Arg-Pro-Lys-Pro-Val-Glu-NVAL-Trp-Arg-Lys(DNP)-NH2 (Cat.# ES002)

Furin: p-Glu-Arg-Thr-Lys-Arg-AMC (Cat. # ES013)

NE: MeOSuc-AAPV-AMC (Cat. # 324740, Calbiochem)

MMP-12: MCA-Lys-Pro-Leu-Gly-Leu-DPA-Ala-Arg-NH_2 (Cat.# ES012)

6.2.4 Cell culture

6.2.4.1 Cell lines

CFBE41o$^-$ and the corresponding cell line stably overexpressing wild type CTFR were kindly provided by Dr. D.C. Gruenert, Cal. Pacific Med. Cent. Res. Inst. The cells were cultured in 15 ml of Minimum Essential Medium supplemented with 10 % Fetal Bovine Serine (FBS), 1 % L-Glutamine and 1 % penicillin/streptomycin in T-75 culture flask. The cells were subcultured with a ratio of 1:5 every five days with interim medium chance after 2 days of culture.

The murine cell line M-1 has been purchased from ATCC as well as all culture media and supplements. The cell line was cultured in 15 ml of DMEM: F-12 Medium (ATCC® 30-2006), supplemented with 5 % FBS (ATCC® 30-2020) and 0.005 mM dexamethasone. The subculturing was performed according to the supplier's protocol every 2 to 3 days in a ratio of 1:3.

HL60 cells were cultured by Dario Frey according to the supplier's protocols in Iscove's Modified Dulbecco's Medium with 20 % FBS in T-75 culture flasks. Cell density was maintained between 1 x 10^5 and 1 x 10^6 viable cells/mL. The medium was renewed every 2-3 days by addition of 2/3 fresh medium to 1/3 of the cell suspension.

HEK cells were cultured by Jan-Erik Hoffmann in high glucose Dulbecco's modified Eagle's Medium containing 10% FBS and 1 % penicillin/streptomycin in 10 cm dishes. The cells were subcultered by addition of trypsin in a ratio of 1:10 every 2-3 days.

6.2.4.2 Primary cells

6.2.4.2.1 Murine tracheal epithelial cells

The cells were prepared and cultured by Ayca Seyhan Agircan.

The killing of wild type C57BL/6 mice and the breeding and killing of βENaC-transgenic animals was approved by the local animal welfare authorities (Regierungspräsidium, Karlsruhe, Germany). Mice were housed in a specific pathogen-free animal facility with free access to food and water. The mice were killed by the application of an overdose of ketamine/xylacin. The trachea was freed from

surrounding vessels, muscle and connective tissue *in situ* and put into collection medium (DMEM:F-12 1:1, 1x Pen/Strep). After isolation 10 tracheas were pooled and washed in PBS.

The tissue was transferred to dissociation medium (PBS Ca^{2+}/Mg^{2+} free, 43 mM $NaHCO_3$, 6.25 nM FeN_3O_9, 1 µM sodium pyruvate, 0.6x Pen/Strep, 1.4 mg/ml Protease E, 0.1 mg/ml DNAse I) and incubated over night at 4 °C. The temperature was increased to 37 °C for 1 hour before the dissociation reaction was stopped by addition of 1 % heat-inactivated FBS. The sample was filtered through a 100 µm cell strainer, rinsed with 10 ml culture medium and the fractions were pooled. After centrifugation at 1300 rpm for 10 min, the cell pellet was resuspended in 5 ml culture medium and seeded onto a 10 cm petri dish. To remove contaminating fibroblasts, the cell suspension was incubated for 2 h at 37 °C. The medium with airway epithelial cells was carefully removed. The cells were counted, centrifuged and resuspended to a density of 600 000 cells/500 µl. In each 12-well Transwell® culture insert, 500 µl of cell suspension were added apically, 2 ml of culture medium basolaterally. After 48 h, the medium was changed basolaterally, the apical medium was removed to start the air-liquid-interface culture. The medium was changed every other day, the cells were washed with PBS every second medium change. The cells were used in experiments after 14 to 21 days after start of ALI culture.

6.2.4.2.2 Human nasal epithelial cells

The cells were obtained by medical personal in the Kopfklinik, University Hospital, Heidelberg. The isolation and culture was done by Heike Scheuermann.

Human nasal cells were obtained from CF patients or Non-CF controls during nasal surgery. The tissue sample was washed in PBS to remove remaining blood. Afterwards, the tissue was cut into small pieces (~ 3 mm) in fresh PBS and transferred to 20 ml dissociation medium, supplemented with 1.4 mg/ml protease E and 0.1 mg/ml DNAse I. After overnight incubation at 4°C, the dissociation was stopped by the addition of 5 ml heat-inactivated FBS. The cells were filtered through a 100 µm cell strainer. For maximum cell recovery, the samples is washed with 10 ml culture medium, filtered through the same cell trainer again and pooled. Afterwards, the cells were centrifuged at 1300 rpm for 10 min. In case of remaining red blood cells, the cells were resuspended in red-blood-cell lysis buffer, incubated for 5 min and centrifuged at 1300 rpm for 5 min again.

After discarding the supernatant, the cells were suspended in 5 ml of culture medium and seeded into a 10 cm tissue culture dish. To separate fibroblasts from airway epithelial cells, the cells were incubated for 2 h at 37°C. Under these conditions, fibroblasts adhere. The medium with the

remaining airway epithelial cells was transferred to a fresh falcon tube and the cells were counted. After 10 min centrifugation at 1300 rpm, the cells were resuspended in culture medium.

The cells were expanded in a T-75 culture flask seeding 100 000 – 200 000 cells per flask in presence of Rho-Associated Protein Kinase inhibitor.

The cells were seeded at a density of 100 000 cells/50 µl into 24-well Transwell® culture inserts. In the basolateral medium reservoir, 600 µl of culture medium were added. Every two days, the culture medium was changed, the day in-between, 15 µl of supplement mix was added to the culture medium. 48 h after seeding, the apical medium was removed and air-liquid-interface culture started.

The experiments were performed after 14 to 21 days of culture.

6.2.5 Microscopy

All experiments were conducted on a Leica TCS SP8 confocal microscope. The microscope was equipped with an environment chamber (EMBL, Heidelberg) that enables the performance of experiments at 37°C and 5 % CO2. Furthermore, the use of a special humidity chamber for Transwell® culture inserts prevented the evaporation of low liquid volumes on the apical side of cells cultured in air-liquid-interface conditions.

For the excitation of the donor fluorophore Coumarin343 of the lipidated probes, we used the 405 nm UV laser in earlier experiments (CAPRee2, CAPRee2_a, CAPRee2_b, CAPRee2_c) and later 458 nm laser line of an Argon laser (CAPRee3, CAPRee5, CAPRee6). Direct excitation of the acceptor fluorophore TAMRA was performed with an diode pumped solid state (DPSS) laser at 561 nm, the nuclear stain DRAQ5 was excited with an helium-neon-laser line at 633 nm. For the detection of donor and acceptor fluorophores, we used the hybrid detectors with gates from 470 nm to 510 nm at a gain of 150 and 570 nm to 630 nm with a gain of 200. The nuclear stain was detected with a photomultiplier tube (PMT) between 650 nm and 715 nm with a gain of 650. The laser power was adjusted to staining efficiency and brightness of the signal.

For imaging in submerged conditions, the cells were trypsinized, washed, counted and seeded in 8-well LabTek® dishes with a density of 30 000 cells per well. After over night incubation, the cells were washed in DMEM without serum, antibiotics/antimycotics or phenol red. The cells were incubated with 2 µM probe and 10 µM DRAQ5 in DMEM for 5 min, then washed and fresh DMEM was added. The cells were imaged with a HC PL APO CS2 63x/1.40 OIL objective.

For fixed cells, the cells were stained in suspension with 1 µM of the probe, as stated in the results section, in presence or absence of the given concentration of enzyme or inhibitors. After incubation,

the cells were spinned down onto a glass slide using a Cytospin centrifuge (Thermo Fisher Scientific) with 1000 rpm for 5 min. The cells were washed once with PBS and stained in 4 % formaldehyde in PBS. The cells were embedded with Fluoromount (Sigma Aldrich, Germany).

Cultured murine tracheal epithelial cells and human nasal epithelial cells were imaged after air-liquid-interface culture on Transwell® inserts. For loading, the probe was added apically in 100 µl PBS at a concentration of 16 µM for 15 min at room temperature. After incubation, the PBS was removed; the cells were washed twice in 100 µl PBS and 20 µl PBS were added for the imaging procedure. The Transwell® inserts was placed onto a glass cover slip which was part of a special humidity chamber which prevented evaporation of low, apical liquid volumes. Basolaterally, the cells were incubated in 500 µl full culture medium. Every position was imaged every 15 min, reducing the amount of light on the cells to minimum. As our probes do not show significant toxicity to the cells, the cells do survive several hours of imaging.

Human cells were imaged with a HC PL APO CS2 40x/1.30 OIL objective, murine tracheal epithelial cells with a HC PL APO CS2 20x/0.75 IMM water objective.

6.2.6 Image and data analysis

The image analysis was performed in Fiji using FluoQ (published by Frank Stein *et al*.). The cells were segmented by a semi-automated process using DRAQ5 nuclear stain and a voronoi algorithm. The threshold for the signal was set semi-automated. The Macro automatically calculates the mean intensities for donor and acceptor signals as well as the ratio between them. The calculated mean was taken for quantification of enzyme activity[112].

Data handling and calculation of slopes was performed in R (Version 3.3.3). Graphics and statistical analysis was done in GraphPad Prism 5 (GraphPad Software Inc., La Jolla, CA, USA).

6.2.7 Statistical analysis

Statistical analysis was done in GraphPad. Unless indicated otherwise, bar charts are displayed as mean ± SEM. The initial increase in fluorescence or D/A ratio was done by linear regression analysis. Statistical analysis was performed with one-way ANOVA and Bonferroni multiple comparison test. For the comparison of two groups, we used an unpaired t-test. $p < 0.05$ was accepted to indicate statistical significance for the human nasal cell data.

7. References

1. Gaillard, E. A.; Kota, P.; Gentzsch, M.; Dokholyan, N. V.; Stutts, M. J.; Tarran, R., Regulation of the epithelial Na+ channel and airway surface liquid volume by serine proteases. *Pflugers Archiv : European Journal of Physiology* **2010,** *460* (1), 1-17.
2. Kleyman, T. R.; Carattino, M. D.; Hughey, R. P., ENaC at the cutting edge: regulation of epithelial sodium channels by proteases. *The Journal of Biological Chemistry* **2009,** *284* (31), 20447-51.
3. Boucher, R. C., Airway surface dehydration in cystic fibrosis: pathogenesis and therapy. *Annual Review of Medicine* **2007,** *58*, 157-70.
4. Elborn, J. S., Cystic fibrosis. *Lancet (London, England)* **2016,** *388* (10059), 2519-2531.
5. Welsh, M. J., Ramsey, B.W., Accurso, F. & Cutting, G.R., *The Metabolic & Molecular Bases of Inherited Disease* McGraw-Hill: New York, 2001.
6. Mall, M.; Grubb, B. R.; Harkema, J. R.; O'Neal, W. K.; Boucher, R. C., Increased airway epithelial Na+ absorption produces cystic fibrosis-like lung disease in mice. *Nature Medicine* **2004,** *10*, 487.
7. Kleyman, T. R.; Myerburg, M. M.; Hughey, R. P., Regulation of ENaCs by proteases: An increasingly complex story. *Kidney International* **2006,** *70* (8), 1391-2.
8. Ray, E. C.; Kleyman, T. R., Cutting it out: ENaC processing in the human nephron. *Journal of the American Society of Nephrology : JASN* **2015,** *26* (1), 1-3.
9. Yu, J. X.; Chao, L.; Chao, J., Prostasin is a novel human serine proteinase from seminal fluid. Purification, tissue distribution, and localization in prostate gland. *The Journal of Biological Chemistry* **1994,** *269* (29), 18843-8.
10. Shipway, A.; Danahay, H.; Williams, J. A.; Tully, D. C.; Backes, B. J.; Harris, J. L., Biochemical characterization of prostasin, a channel activating protease. *Biochemical and Biophysical Research Communications* **2004,** *324* (2), 953-63.
11. Rickert, K. W.; Kelley, P.; Byrne, N. J.; Diehl, R. E.; Hall, D. L.; Montalvo, A. M.; Reid, J. C.; Shipman, J. M.; Thomas, B. W.; Munshi, S. K.; Darke, P. L.; Su, H. P., Structure of human prostasin, a target for the regulation of hypertension. *The Journal of Biological Chemistry* **2008,** *283* (50), 34864-72.
12. Zhu, H.; Guo, D.; Li, K.; Yan, W.; Tan, Y.; Wang, X.; Treiber, F. A.; Chao, J.; Snieder, H.; Dong, Y., Prostasin: a possible candidate gene for human hypertension. *American Journal of Hypertension* **2008,** *21* (9), 1028-33.
13. Malsure, S.; Wang, Q.; Charles, R. P.; Sergi, C.; Perrier, R.; Christensen, B. M.; Maillard, M.; Rossier, B. C.; Hummler, E., Colon-specific deletion of epithelial sodium channel causes sodium loss and aldosterone resistance. *Journal of the American Society of Nephrology : JASN* **2014,** *25* (7), 1453-64.
14. Donaldson, S. H.; Hirsh, A.; Li, D. C.; Holloway, G.; Chao, J.; Boucher, R. C.; Gabriel, S. E., Regulation of the epithelial sodium channel by serine proteases in human airways. *The Journal of Biological Chemistry* **2002,** *277* (10), 8338-45.
15. Hummler, E.; Dousse, A.; Rieder, A.; Stehle, J. C.; Rubera, I.; Osterheld, M. C.; Beermann, F.; Frateschi, S.; Charles, R. P., The channel-activating protease CAP1/Prss8 is required for placental labyrinth maturation. *PLoS One* **2013,** *8* (2), e55796.
16. Leyvraz, C.; Charles, R. P.; Rubera, I.; Guitard, M.; Rotman, S.; Breiden, B.; Sandhoff, K.; Hummler, E., The epidermal barrier function is dependent on the serine protease CAP1/Prss8. *The Journal of Cell Biology* **2005,** *170* (3), 487-96.
17. Peters, D. E.; Szabo, R.; Friis, S.; Shylo, N. A.; Uzzun Sales, K.; Holmbeck, K.; Bugge, T. H., The membrane-anchored serine protease prostasin (CAP1/PRSS8) supports epidermal development and postnatal homeostasis independent of its enzymatic activity. *The Journal of Biological Chemistry* **2014,** *289* (21), 14740-9.

18. Vallet, V.; Chraibi, A.; Gaeggeler, H. P.; Horisberger, J. D.; Rossier, B. C., An epithelial serine protease activates the amiloride-sensitive sodium channel. *Nature* **1997,** *389* (6651), 607-10.
19. Planes, C.; Randrianarison, N. H.; Charles, R. P.; Frateschi, S.; Cluzeaud, F.; Vuagniaux, G.; Soler, P.; Clerici, C.; Rossier, B. C.; Hummler, E., ENaC-mediated alveolar fluid clearance and lung fluid balance depend on the channel-activating protease 1. *EMBO Molecular Medicine* **2010,** *2* (1), 26-37.
20. Tong, Z.; Illek, B.; Bhagwandin, V. J.; Verghese, G. M.; Caughey, G. H., Prostasin, a membrane-anchored serine peptidase, regulates sodium currents in JME/CF15 cells, a cystic fibrosis airway epithelial cell line. *American Journal of Physiology. Lung Cellular and Molecular Physiology* **2004,** *287* (5), L928-35.
21. Tarran, R.; Trout, L.; Donaldson, S. H.; Boucher, R. C., Soluble mediators, not cilia, determine airway surface liquid volume in normal and cystic fibrosis superficial airway epithelia. *Journal of General Physiology* **2006,** *127* (5), 591-604.
22. Myerburg, M. M.; McKenna, E. E.; Luke, C. J.; Frizzell, R. A.; Kleyman, T. R.; Pilewski, J. M., Prostasin expression is regulated by airway surface liquid volume and is increased in cystic fibrosis. *American Journal of Physiology. Lung Cellular and Molecular Physiology* **2008,** *294* (5), L932-41.
23. Garcia-Caballero, A.; Dang, Y.; He, H.; Stutts, M. J., ENaC proteolytic regulation by channel-activating protease 2. *Journal of General Physiology* **2008,** *132* (5), 521-35.
24. García-Caballero, A.; Dang, Y.; He, H.; Stutts, M. J., ENaC Proteolytic Regulation by Channel-activating Protease 2. *The Journal of General Physiology* **2008,** *132* (5), 521-535.
25. Passero, C. J.; Mueller, G. M.; Myerburg, M. M.; Carattino, M. D.; Hughey, R. P.; Kleyman, T. R., TMPRSS4-dependent activation of the epithelial sodium channel requires cleavage of the gamma-subunit distal to the furin cleavage site. *American Journal of Physiology. Renal Physiology* **2012,** *302* (1), F1-8.
26. Andreasen, D.; Vuagniaux, G.; Fowler-Jaeger, N.; Hummler, E.; Rossier, B. C., Activation of epithelial sodium channels by mouse channel activating proteases (mCAP) expressed in Xenopus oocytes requires catalytic activity of mCAP3 and mCAP2 but not mCAP1. *Journal of the American Society of Nephrology : JASN* **2006,** *17* (4), 968-76.
27. Keppner, A.; Andreasen, D.; Merillat, A. M.; Bapst, J.; Ansermet, C.; Wang, Q.; Maillard, M.; Malsure, S.; Nobile, A.; Hummler, E., Epithelial Sodium Channel-Mediated Sodium Transport Is Not Dependent on the Membrane-Bound Serine Protease CAP2/Tmprss4. *PLoS One* **2015,** *10* (8), e0135224.
28. Cohen, A. S.; Khalil, F. K.; Welsh, E. A.; Schabath, M. B.; Enkemann, S. A.; Davis, A.; Zhou, J. M.; Boulware, D. C.; Kim, J.; Haura, E. B.; Morse, D. L., Cell-surface marker discovery for lung cancer. *Oncotarget* **2017,** *8* (69), 113373-113402.
29. Valero-Jimenez, A.; Zuniga, J.; Cisneros, J.; Becerril, C.; Salgado, A.; Checa, M.; Buendia-Roldan, I.; Mendoza-Milla, C.; Gaxiola, M.; Pardo, A.; Selman, M., Transmembrane protease, serine 4 (TMPRSS4) is upregulated in IPF lungs and increases the fibrotic response in bleomycin-induced lung injury. *PLoS One* **2018,** *13* (3), e0192963.
30. de Aberasturi, A. L.; Calvo, A., TMPRSS4: an emerging potential therapeutic target in cancer. *British Journal of Cancer* **2015,** *112* (1), 4-8.
31. Lee, Y.; Ko, D.; Min, H. J.; Kim, S. B.; Ahn, H. M.; Lee, Y.; Kim, S., TMPRSS4 induces invasion and proliferation of prostate cancer cells through induction of Slug and cyclin D1. *Oncotarget* **2016,** *7* (31), 50315-50332.
32. Li, X. M.; Liu, W. L.; Chen, X.; Wang, Y. W.; Shi, D. B.; Zhang, H.; Ma, R. R.; Liu, H. T.; Guo, X. Y.; Hou, F.; Li, M.; Gao, P., Overexpression of TMPRSS4 promotes tumor proliferation and aggressiveness in breast cancer. *International Journal of Molecular Medicine* **2017,** *39* (4), 927-935.
33. Tanabe, L. M.; List, K., The role of type II transmembrane serine protease-mediated signaling in cancer. *The FEBS Journal* **2017,** *284* (10), 1421-1436.
34. Shi, Y. E.; Torri, J.; Yieh, L.; Wellstein, A.; Lippman, M. E.; Dickson, R. B., Identification and characterization of a novel matrix-degrading protease from hormone-dependent human breast cancer cells. *Cancer Research* **1993,** *53* (6), 1409-15.

35. Cao, J.; Cai, X.; Zheng, L.; Geng, L.; Shi, Z.; Pao, C. C.; Zheng, S., Characterization of colorectal-cancer-related cDNA clones obtained by subtractive hybridization screening. *Journal of Cancer Research and Clinical Oncology* **1997,** *123* (8), 447-51.
36. List, K.; Haudenschild, C. C.; Szabo, R.; Chen, W.; Wahl, S. M.; Swaim, W.; Engelholm, L. H.; Behrendt, N.; Bugge, T. H., Matriptase/MT-SP1 is required for postnatal survival, epidermal barrier function, hair follicle development, and thymic homeostasis. *Oncogene* **2002,** *21* (23), 3765-79.
37. List, K.; Szabo, R.; Wertz, P. W.; Segre, J.; Haudenschild, C. C.; Kim, S.-Y.; Bugge, T. H., Loss of proteolytically processed filaggrin caused by epidermal deletion of Matriptase/MT-SP1. *The Journal of Cell Biology* **2003,** *163* (4), 901-910.
38. List, K.; Currie, B.; Scharschmidt, T. C.; Szabo, R.; Shireman, J.; Molinolo, A.; Cravatt, B. F.; Segre, J.; Bugge, T. H., Autosomal ichthyosis with hypotrichosis syndrome displays low matriptase proteolytic activity and is phenocopied in ST14 hypomorphic mice. *The Journal of Biological Chemistry* **2007,** *282* (50), 36714-23.
39. Buzza, M. S.; Netzel-Arnett, S.; Shea-Donohue, T.; Zhao, A.; Lin, C. Y.; List, K.; Szabo, R.; Fasano, A.; Bugge, T. H.; Antalis, T. M., Membrane-anchored serine protease matriptase regulates epithelial barrier formation and permeability in the intestine. *Proceedings of the National Academy of Sciences of the United States of America* **2010,** *107* (9), 4200-5.
40. Bardou, O.; Menou, A.; François, C.; Duitman, J. W.; von der Thüsen, J. H.; Borie, R.; Sales, K. U.; Mutze, K.; Castier, Y.; Sage, E.; Liu, L.; Bugge, T. H.; Fairlie, D. P.; Königshoff, M.; Crestani, B.; Borensztajn, K. S., Membrane-anchored Serine Protease Matriptase Is a Trigger of Pulmonary Fibrogenesis. *American Journal of Respiratory and Critical Care Medicine* **2016,** *193* (8), 847-860.
41. Thomas, G., Furin at the cutting edge: from protein traffic to embryogenesis and disease. *Nature Reviews. Molecular Cell Biology* **2002,** *3* (10), 753-766.
42. Thibodeau, P. H.; Butterworth, M. B., Proteases, cystic fibrosis and the epithelial sodium channel (ENaC). *Cell and tissue research* **2013,** *351* (2), 309-23.
43. Reihill, J. A.; Walker, B.; Hamilton, R. A.; Ferguson, T. E.; Elborn, J. S.; Stutts, M. J.; Harvey, B. J.; Saint-Criq, V.; Hendrick, S. M.; Martin, S. L., Inhibition of Protease-Epithelial Sodium Channel Signaling Improves Mucociliary Function in Cystic Fibrosis Airways. *American Journal of Respiratory and Critical Care Medicine* **2016,** *194* (6), 701-10.
44. Patel, A. B.; Chao, J.; Palmer, L. G., Tissue kallikrein activation of the epithelial Na channel. *American Journal of Physiology - Renal Physiology* **2012,** *303* (4), F540-F550.
45. Picard, N.; Eladari, D.; El Moghrabi, S.; Planes, C.; Bourgeois, S.; Houillier, P.; Wang, Q.; Burnier, M.; Deschenes, G.; Knepper, M. A.; Meneton, P.; Chambrey, R., Defective ENaC processing and function in tissue kallikrein-deficient mice. *The Journal of Biological Chemistry* **2008,** *283* (8), 4602-11.
46. Svenningsen, P.; Hinrichs, G. R.; Zachar, R.; Ydegaard, R.; Jensen, B. L., Physiology and pathophysiology of the plasminogen system in the kidney. *Pflugers Archiv : European Journal of Physiology* **2017,** *469* (11), 1415-1423.
47. Menou, A.; Duitman, J.; Flajolet, P.; Sallenave, J. M.; Mailleux, A. A.; Crestani, B., Human airway trypsin-like protease, a serine protease involved in respiratory diseases. *American Journal of Physiology. Lung Cellular and Molecular Physiology* **2017,** *312* (5), L657-l668.
48. Sales, K. U.; Hobson, J. P.; Wagenaar-Miller, R.; Szabo, R.; Rasmussen, A. L.; Bey, A.; Shah, M. F.; Molinolo, A. A.; Bugge, T. H., Expression and genetic loss of function analysis of the HAT/DESC cluster proteases TMPRSS11A and HAT. *PLoS One* **2011,** *6* (8), e23261.
49. Menou, A.; Flajolet, P.; Duitman, J.; Justet, A.; Moog, S.; Jaillet, M.; Tabeze, L.; Solhonne, B.; Garnier, M.; Mal, H.; Mordant, P.; Castier, Y.; Cazes, A.; Sallenave, J. M.; Mailleux, A. A.; Crestani, B., Human airway trypsin-like protease exerts potent, antifibrotic action in pulmonary fibrosis. *FASEB journal : official publication of the Federation of American Societies for Experimental Biology* **2018,** *32* (3), 1250-1264.
50. Gehrig, S.; Duerr, J.; Weitnauer, M.; Wagner, C. J.; Graeber, S. Y.; Schatterny, J.; Hirtz, S.; Belaaouaj, A.; Dalpke, A. H.; Schultz, C.; Mall, M. A., Lack of Neutrophil Elastase Reduces Inflammation, Mucus Hypersecretion, and Emphysema, but Not Mucus Obstruction, in Mice with

Cystic Fibrosis–like Lung Disease. *American Journal of Respiratory and Critical Care Medicine* **2014,** *189* (9), 1082-1092.
51. Dittrich, A. S.; Kuhbandner, I.; Gehrig, S.; Rickert-Zacharias, V.; Twigg, M.; Wege, S.; Taggart, C. C.; Herth, F.; Schultz, C.; Mall, M. A., Elastase activity on sputum neutrophils correlates with severity of lung disease in cystic fibrosis. *The European respiratory journal* **2018,** *51* (3).
52. Adebamiro, A.; Cheng, Y.; Rao, U. S.; Danahay, H.; Bridges, R. J., A Segment of γ ENaC Mediates Elastase Activation of Na(+) Transport. *The Journal of General Physiology* **2007,** *130* (6), 611-629.
53. Caldwell, R. A.; Boucher, R. C.; Stutts, M. J., Neutrophil elastase activates near-silent epithelial Na+ channels and increases airway epithelial Na+ transport. *American Journal of Physiology-Lung Cellular and Molecular Physiology* **2005,** *288* (5), L813-L819.
54. Weldon, S.; McNally, P.; McAuley, D. F.; Oglesby, I. K.; Wohlford-Lenane, C. L.; Bartlett, J. A.; Scott, C. J.; McElvaney, N. G.; Greene, C. M.; McCray, P. B.; Taggart, C. C., miR-31 Dysregulation in Cystic Fibrosis Airways Contributes to Increased Pulmonary Cathepsin S Production. *American Journal of Respiratory and Critical Care Medicine* **2014,** *190* (2), 165-174.
55. Kesimer, M.; Kirkham, S.; Pickles, R. J.; Henderson, A. G.; Alexis, N. E.; Demaria, G.; Knight, D.; Thornton, D. J.; Sheehan, J. K., Tracheobronchial air-liquid interface cell culture: a model for innate mucosal defense of the upper airways? *American journal of physiology. Lung cellular and molecular physiology* **2009,** *296* (1), L92-l100.
56. Haerteis, S.; Krappitz, M.; Bertog, M.; Krappitz, A.; Baraznenok, V.; Henderson, I.; Lindstrom, E.; Murphy, J. E.; Bunnett, N. W.; Korbmacher, C., Proteolytic activation of the epithelial sodium channel (ENaC) by the cysteine protease cathepsin-S. *Pflugers Archiv : European Journal of Physiology* **2012,** *464* (4), 353-65.
57. Tan, C. D.; Hobbs, C.; Sameni, M.; Sloane, B. F.; Stutts, M. J.; Tarran, R., Cathepsin B contributes to Na+ hyperabsorption in cystic fibrosis airway epithelial cultures. *Journal of Physiology* **2014,** *592* (23), 5251-68.
58. Alli, A. A.; Song, J. Z.; Al-Khalili, O.; Bao, H. F.; Ma, H. P.; Alli, A. A.; Eaton, D. C., Cathepsin B is secreted apically from Xenopus 2F3 cells and cleaves the epithelial sodium channel (ENaC) to increase its activity. *The Journal of Biological Chemistry* **2012,** *287* (36), 30073-83.
59. Netzel-Arnett, S.; Currie, B. M.; Szabo, R.; Lin, C. Y.; Chen, L. M.; Chai, K. X.; Antalis, T. M.; Bugge, T. H.; List, K., Evidence for a matriptase-prostasin proteolytic cascade regulating terminal epidermal differentiation. *The Journal of Biological Chemistry* **2006,** *281* (44), 32941-5.
60. Buzza, M. S.; Martin, E. W.; Driesbaugh, K. H.; Desilets, A.; Leduc, R.; Antalis, T. M., Prostasin is required for matriptase activation in intestinal epithelial cells to regulate closure of the paracellular pathway. *The Journal of Biological Chemistry* **2013,** *288* (15), 10328-37.
61. Friis, S.; Uzzun Sales, K.; Godiksen, S.; Peters, D. E.; Lin, C. Y.; Vogel, L. K.; Bugge, T. H., A matriptase-prostasin reciprocal zymogen activation complex with unique features: prostasin as a non-enzymatic co-factor for matriptase activation. *The Journal of Biological Chemistry* **2013,** *288* (26), 19028-39.
62. Szabo, R.; Hobson, J. P.; Christoph, K.; Kosa, P.; List, K.; Bugge, T. H., Regulation of cell surface protease matriptase by HAI2 is essential for placental development, neural tube closure and embryonic survival in mice. *Development (Cambridge, England)* **2009,** *136* (15), 2653-63.
63. Fan, B.; Brennan, J.; Grant, D.; Peale, F.; Rangell, L.; Kirchhofer, D., Hepatocyte growth factor activator inhibitor-1 (HAI-1) is essential for the integrity of basement membranes in the developing placental labyrinth. *Developmental Biology* **2007,** *303* (1), 222-30.
64. Szabo, R.; Uzzun Sales, K.; Kosa, P.; Shylo, N. A.; Godiksen, S.; Hansen, K. K.; Friis, S.; Gutkind, J. S.; Vogel, L. K.; Hummler, E.; Camerer, E.; Bugge, T. H., Reduced prostasin (CAP1/PRSS8) activity eliminates HAI-1 and HAI-2 deficiency-associated developmental defects by preventing matriptase activation. *PLoS Genetics* **2012,** *8* (8), e1002937.
65. Phin, S.; Marchand-Adam, S.; Fabre, A.; Marchal-Somme, J.; Bantsimba-Malanda, C.; Kataoka, H.; Soler, P.; Crestani, B., Imbalance in the pro-hepatocyte growth factor activation system in bleomycin-induced lung fibrosis in mice. *American Journal of Respiratory Cell and Molecular Biology* **2010,** *42* (3), 286-93.

66. Menou, A.; Duitman, J.; Crestani, B., The impaired proteases and anti-proteases balance in Idiopathic Pulmonary Fibrosis. *Matrix Biology* **2018**.
67. Twigg, M. S.; Brockbank, S.; Lowry, P.; FitzGerald, S. P.; Taggart, C.; Weldon, S.; #xe9; ad, The Role of Serine Proteases and Antiproteases in the Cystic Fibrosis Lung. *Mediators of Inflammation* **2015,** *2015*, 10.
68. Myerburg, M. M.; Butterworth, M. B.; McKenna, E. E.; Peters, K. W.; Frizzell, R. A.; Kleyman, T. R.; Pilewski, J. M., Airway surface liquid volume regulates ENaC by altering the serine protease-protease inhibitor balance: a mechanism for sodium hyperabsorption in cystic fibrosis. *The Journal of Biological Chemistry* **2006,** *281* (38), 27942-9.
69. Fan, B.; Wu, T. D.; Li, W.; Kirchhofer, D., Identification of hepatocyte growth factor activator inhibitor-1B as a potential physiological inhibitor of prostasin. *The Journal of Biological Chemistry* **2005,** *280* (41), 34513-20.
70. Marlor, C. W.; Delaria, K. A.; Davis, G.; Muller, D. K.; Greve, J. M.; Tamburini, P. P., Identification and cloning of human placental bikunin, a novel serine protease inhibitor containing two Kunitz domains. *The Journal of Biological Chemistry* **1997,** *272* (18), 12202-8.
71. Kim, C. S.; Ahmad, S.; Wu, T.; Walton, W. G.; Redinbo, M. R.; Tarran, R., SPLUNC1 is an allosteric modulator of the epithelial sodium channel. *FASEB journal : official publication of the Federation of American Societies for Experimental Biology* **2018**, fj201701126R.
72. Zhou, R.; Patel, S. V.; Snyder, P. M., Nedd4-2 catalyzes ubiquitination and degradation of cell surface ENaC. *The Journal of Biological Chemistry* **2007,** *282* (28), 20207-12.
73. Garland, A. L.; Walton, W. G.; Coakley, R. D.; Tan, C. D.; Gilmore, R. C.; Hobbs, C. A.; Tripathy, A.; Clunes, L. A.; Bencharit, S.; Stutts, M. J.; Betts, L.; Redinbo, M. R.; Tarran, R., Molecular basis for pH-dependent mucosal dehydration in cystic fibrosis airways. *Proceedings of the National Academy of Sciences of the United States of America* **2013,** *110* (40), 15973-8.
74. Ghiran, I. C., Introduction to fluorescence microscopy. *Methods in Molecular Biology (Clifton, N.J.)* **2011,** *689*, 93-136.
75. Ishikawa-Ankerhold, H. C.; Ankerhold, R.; Drummen, G. P., Advanced fluorescence microscopy techniques--FRAP, FLIP, FLAP, FRET and FLIM. *Molecules (Basel, Switzerland)* **2012,** *17* (4), 4047-132.
76. Cobos-Correa, A.; Trojanek, J. B.; Diemer, S.; Mall, M. A.; Schultz, C., Membrane-bound FRET probe visualizes MMP12 activity in pulmonary inflammation. *Nature Chemical Biology* **2009,** *5*, 628.
77. Gehrig, S.; Mall, M. A.; Schultz, C., Spatially Resolved Monitoring of Neutrophil Elastase Activity with Ratiometric Fluorescent Reporters. *Angewandte Chemie International Edition* **2012,** *51* (25), 6258-6261.
78. Scott, D. W.; Walker, M. P.; Sesma, J.; Wu, B.; Stuhlmiller, T. J.; Sabater, J. R.; Abraham, W. M.; Crowder, T. M.; Christensen, D. J.; Tarran, R., SPX-101 Is a Novel Epithelial Sodium Channel-targeted Therapeutic for Cystic Fibrosis That Restores Mucus Transport. *American Journal of Respiratory and Critrical Care Medicine* **2017,** *196* (6), 734-744.
79. Zhou, Z.; Treis, D.; Schubert, S. C.; Harm, M.; Schatterny, J.; Hirtz, S.; Duerr, J.; Boucher, R. C.; Mall, M. A., Preventive but not late amiloride therapy reduces morbidity and mortality of lung disease in betaENaC-overexpressing mice. *American Journal of Respiratory and Critical Care Medicin* **2008,** *178* (12), 1245-56.
80. List, K.; Bugge, T. H.; Szabo, R., Matriptase: Potent Proteolysis on the Cell Surface. *Molecular Medicine* **2006,** *12* (1-3), 1-7.
81. Caldwell, R. A.; Boucher, R. C.; Stutts, M. J., Neutrophil elastase activates near-silent epithelial Na+ channels and increases airway epithelial Na+ transport. *American Journal of Physiology. Lung Cellular and Molecular Physiology* **2005,** *288* (5), L813-9.
82. Bruns, J. B.; Carattino, M. D.; Sheng, S.; Maarouf, A. B.; Weisz, O. A.; Pilewski, J. M.; Hughey, R. P.; Kleyman, T. R., Epithelial Na+ channels are fully activated by furin- and prostasin-dependent release of an inhibitory peptide from the gamma-subunit. *The Journal of Biological Chemistry* **2007,** *282* (9), 6153-60.

83. Li, G.; Jia, J.; Ji, K.; Gong, X.; Wang, R.; Zhang, X.; Wang, H.; Zang, B., The neutrophil elastase inhibitor, sivelestat, attenuates sepsis-related kidney injury in rats. *International Journal of Molecular Medicine* **2016,** *38* (3), 767-75.
84. Kawabata, K.; Suzuki, M.; Sugitani, M.; Imaki, K.; Toda, M.; Miyamoto, T., ONO-5046, a novel inhibitor of human neutrophil elastase. *Biochemical and Biophysical Research Communications* **1991,** *177* (2), 814-20.
85. Cornish-Bowden, A., One hundred years of Michaelis–Menten kinetics. *Perspectives in Science* **2015,** *4*, 3-9.
86. Hinrichs, G. R.; Michelsen, J. S.; Zachar, R.; Friis, U. G.; Svenningsen, P.; Birn, H.; Bistrup, C.; Jensen, B. L., Albuminuria in kidney transplant recipients is asscioated with increased urinatry serine proteases and activation of the epithelial sodium channel. *American Journal of Physiology. Renal Physiology* **2018**.
87. Steensgaard, M.; Svenningsen, P.; Tinning, A. R.; Nielsen, T. D.; Jorgensen, F.; Kjaersgaard, G.; Madsen, K.; Jensen, B. L., Apical serine protease activity is necessary for assembly of a high-resistance renal collecting duct epithelium. *Acta Physiologica* **2010,** *200* (4), 347-59.
88. Svenningsen, P.; Uhrenholt, T. R.; Palarasah, Y.; Skjodt, K.; Jensen, B. L.; Skott, O., Prostasin-dependent activation of epithelial Na+ channels by low plasmin concentrations. *American Journal of Physiology. Regulatory, Integrative and Comparative Physiology* **2009,** *297* (6), R1733-41.
89. Liu, L.; Hering-Smith, K. S.; Schiro, F. R.; Hamm, L. L., Serine protease activity in m-1 cortical collecting duct cells. *Hypertension (Dallas, Tex. : 1979)* **2002,** *39* (4), 860-4.
90. Ranstam, J., Multiple P-values and Bonferroni correction. *Osteoarthritis and Cartilage* **2016,** *24* (5), 763-764.
91. Zhou, Z.; Duerr, J.; Johannesson, B.; Schubert, S. C.; Treis, D.; Harm, M.; Graeber, S. Y.; Dalpke, A.; Schultz, C.; Mall, M. A., The ENaC-overexpressing mouse as a model of cystic fibrosis lung disease. *Journal of Cystic Fibrosis : Official Journal of the European Cystic Fibrosis Society* **2011,** *10 Suppl 2*, S172-82.
92. Ehrhardt, C.; Collnot, E. M.; Baldes, C.; Becker, U.; Laue, M.; Kim, K. J.; Lehr, C. M., Towards an in vitro model of cystic fibrosis small airway epithelium: characterisation of the human bronchial epithelial cell line CFBE41o. *Cell and Rissue Research* **2006,** *323* (3), 405-15.
93. Azad, A. K.; Rauh, R.; Vermeulen, F.; Jaspers, M.; Korbmacher, J.; Boissier, B.; Bassinet, L.; Fichou, Y.; des Georges, M.; Stanke, F.; De Boeck, K.; Dupont, L.; Balascakova, M.; Hjelte, L.; Lebecque, P.; Radojkovic, D.; Castellani, C.; Schwartz, M.; Stuhrmann, M.; Schwarz, M.; Skalicka, V.; de Monestrol, I.; Girodon, E.; Ferec, C.; Claustres, M.; Tummler, B.; Cassiman, J. J.; Korbmacher, C.; Cuppens, H., Mutations in the amiloride-sensitive epithelial sodium channel in patients with cystic fibrosis-like disease. *Human Mutation* **2009,** *30* (7), 1093-103.
94. Gentzsch, M.; Dang, H.; Dang, Y.; Garcia-Caballero, A.; Suchindran, H.; Boucher, R. C.; Stutts, M. J., The cystic fibrosis transmembrane conductance regulator impedes proteolytic stimulation of the epithelial Na+ channel. *The Journal of Biological Chemistry* **2010,** *285* (42), 32227-32.
95. Derreumaux, P.; Mousseau, N., Coarse-grained protein molecular dynamics simulations. *The Journal of Chemical Physics* **2007,** *126* (2), 025101.
96. Chen, L.; McBranch, D. W.; Wang, H.-L.; Helgeson, R.; Wudl, F.; Whitten, D. G., Highly sensitive biological and chemical sensors based on reversible fluorescence quenching in a conjugated polymer. *Proceedings of the National Academy of Sciences* **1999,** *96* (22), 12287.
97. Alston, R. W.; Lasagna, M.; Grimsley, G. R.; Scholtz, J. M.; Reinhart, G. D.; Pace, C. N., Peptide sequence and conformation strongly influence tryptophan fluorescence. *Biophysical Journal* **2008,** *94* (6), 2280-7.
98. Guo, Z.; Peng, H.; Kang, J.; Sun, D., Cell-penetrating peptides: Possible transduction mechanisms and therapeutic applications. *Biomedical Reports* **2016,** *4* (5), 528-534.
99. Joliot, A.; Prochiantz, A., Transduction peptides: from technology to physiology. *Nature Cell Biology* **2004,** *6* (3), 189-96.
100. Yushchenko, D. A.; Nadler, A.; Schultz, C., Manipulating cell signaling with subcellular spatial resolution. *Cell cycle* **2016,** *15* (8), 1023-4.

101. Lemke, E. A.; Schultz, C., Principles for designing fluorescent sensors and reporters. *Nature Chemical Biology* **2011,** *7*, 480.
102. Nikola, P.; Albert, B.; Max, K.; Ralf, Z.; Nathalie, P.; Günther, B.; Armin, B., Application of the Guanidine–Acylguanidine Bioisosteric Approach to Argininamide-Type NPY Y2 Receptor Antagonists. *ChemMedChem* **2011,** *6* (9), 1727-1738.
103. Wilke, M.; Buijs-Offerman, R. M.; Aarbiou, J.; Colledge, W. H.; Sheppard, D. N.; Touqui, L.; Bot, A.; Jorna, H.; De Jonge, H. R.; Scholte, B. J., Mouse models of cystic fibrosis: Phenotypic analysis and research applications. *Journal of Cystic Fibrosis* **2011,** *10*, S152-S171.
104. Nimishakavi, S.; Besprozvannaya, M.; Raymond, W. W.; Craik, C. S.; Gruenert, D. C.; Caughey, G. H., Activity and inhibition of prostasin and matriptase on apical and basolateral surfaces of human airway epithelial cells. *American Journal of Physiology. Lung Cellular and Molecular Physiology* **2012,** *303* (2), L97-106.
105. Trojanek, J. B.; Cobos-Correa, A.; Diemer, S.; Kormann, M.; Schubert, S. C.; Zhou-Suckow, Z.; Agrawal, R.; Duerr, J.; Wagner, C. J.; Schatterny, J.; Hirtz, S.; Sommerburg, O.; Hartl, D.; Schultz, C.; Mall, M. A., Airway Mucus Obstruction Triggers Macrophage Activation and Matrix Metalloproteinase 12–Dependent Emphysema. *American Journal of Respiratory Cell and Molecular Biology* **2014,** *51* (5), 709-720.
106. Muller, L.; Brighton, L. E.; Carson, J. L.; Fischer, W. A., 2nd; Jaspers, I., Culturing of human nasal epithelial cells at the air liquid interface. *Journal of Visualized Experiments : JoVE* **2013,** (80).
107. Buzza, M. S.; Johnson, T. A.; Conway, G. D.; Martin, E. W.; Mukhopadhyay, S.; Shea-Donohue, T.; Antalis, T. M., Inflammatory cytokines down-regulate the barrier-protective prostasin-matriptase proteolytic cascade early in experimental colitis. *The Journal of Biological Chemistry* **2017,** *292* (26), 10801-10812.
108. Bonfield, T. L.; Panuska, J. R.; Konstan, M. W.; Hilliard, K. A.; Hilliard, J. B.; Ghnaim, H.; Berger, M., Inflammatory cytokines in cystic fibrosis lungs. *American Journal of Respiratory and Critical Care Medicine* **1995,** *152* (6 Pt 1), 2111-8.
109. Li, K.; Guo, D.; Zhu, H.; Hering-Smith, K. S.; Hamm, L. L.; Ouyang, J.; Dong, Y., Interleukin-6 stimulates epithelial sodium channels in mouse cortical collecting duct cells. *American Journal of Physiology. Regulatory, Integrative and Comparative Physiology* **2010,** *299* (2), R590-5.
110. Nixon, L. S.; Yung, B.; Bell, S. C.; Stuart Elborn, J.; Shale, D. J., Circulating Immunoreactive Interleukin-6 in Cystic Fibrosis. *American Journal of Respiratory and Critical Care Medicine* **1998,** *157* (6), 1764-1769.
111. Kanemaru, A.; Yamamoto, K.; Kawaguchi, M.; Fukushima, T.; Lin, C. Y.; Johnson, M. D.; Camerer, E.; Kataoka, H., Deregulated matriptase activity in oral squamous cell carcinoma promotes the infiltration of cancer-associated fibroblasts by paracrine activation of protease-activated receptor 2. *International Journal of Cancer* **2017,** *140* (1), 130-141.
112. Stein, F.; Kress, M.; Reither, S.; Piljic, A.; Schultz, C., FluoQ: a tool for rapid analysis of multiparameter fluorescence imaging data applied to oscillatory events. *ACS Chemical Biology* **2013,** *8* (9), 1862-8.

8. Appendix

CAPRee1:

Expected mass: 1584.73 Da
$[M+1]^+$ exp. 1585.75, 1585.79 $[M+2]^{2+}$ exp. 793.38, found 793.30/792.90, $[M+3]^{3+}$ exp. 529.25, found 529.25

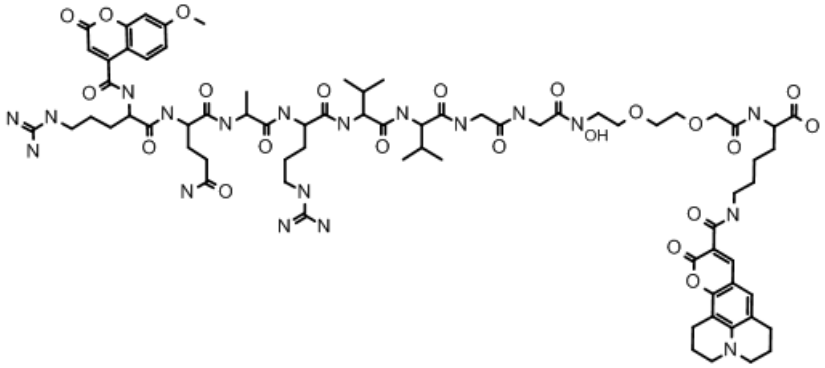

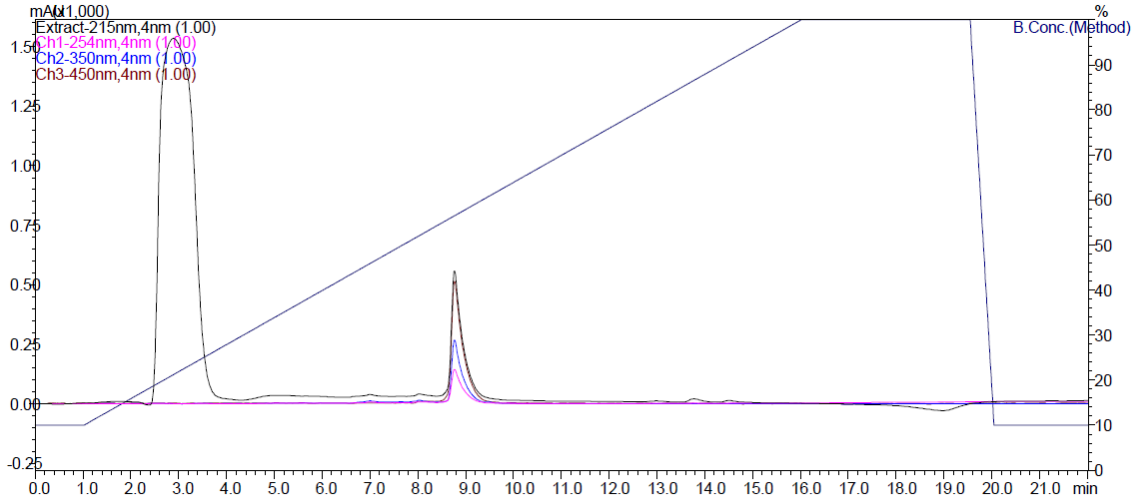

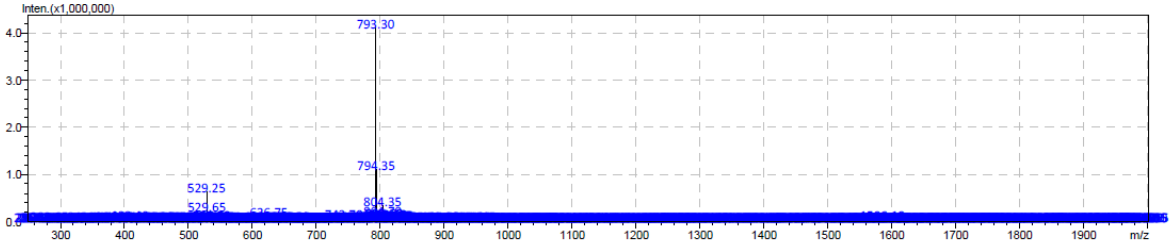

Analysis Info

Analysis Name	D:\Data\Schultz_EMBL\icr29464_000001.d	Acquisition Date	1/16/2018 2:48:22 PM
Method	ESI pos HPmix 200-1800	Instrument	ICR Apex-Qe
Sample Name	CAPS5	Operator	D.Lang
Comment	Schultz, AK Schultz (EMBL): CAPS5 in MeOH		

Acquisition Parameters

Accumulations	16	Collision Gas Flow Rate	0.5 L/sec	Capillary Entrance	4200.0 V
Broadband Low Mass	173.2 m/z	Collision Energy	0.5 eV	Calibration Date	Tue Jan 2 09:15:53 2018
Broadband High Mass	2500.0 m/z	Collision Cell RF	1200.0 V		
Data Acquisition Size	2097152	Q1 Resolution	5.0		
		Q1 Mass	200.000 m/z		

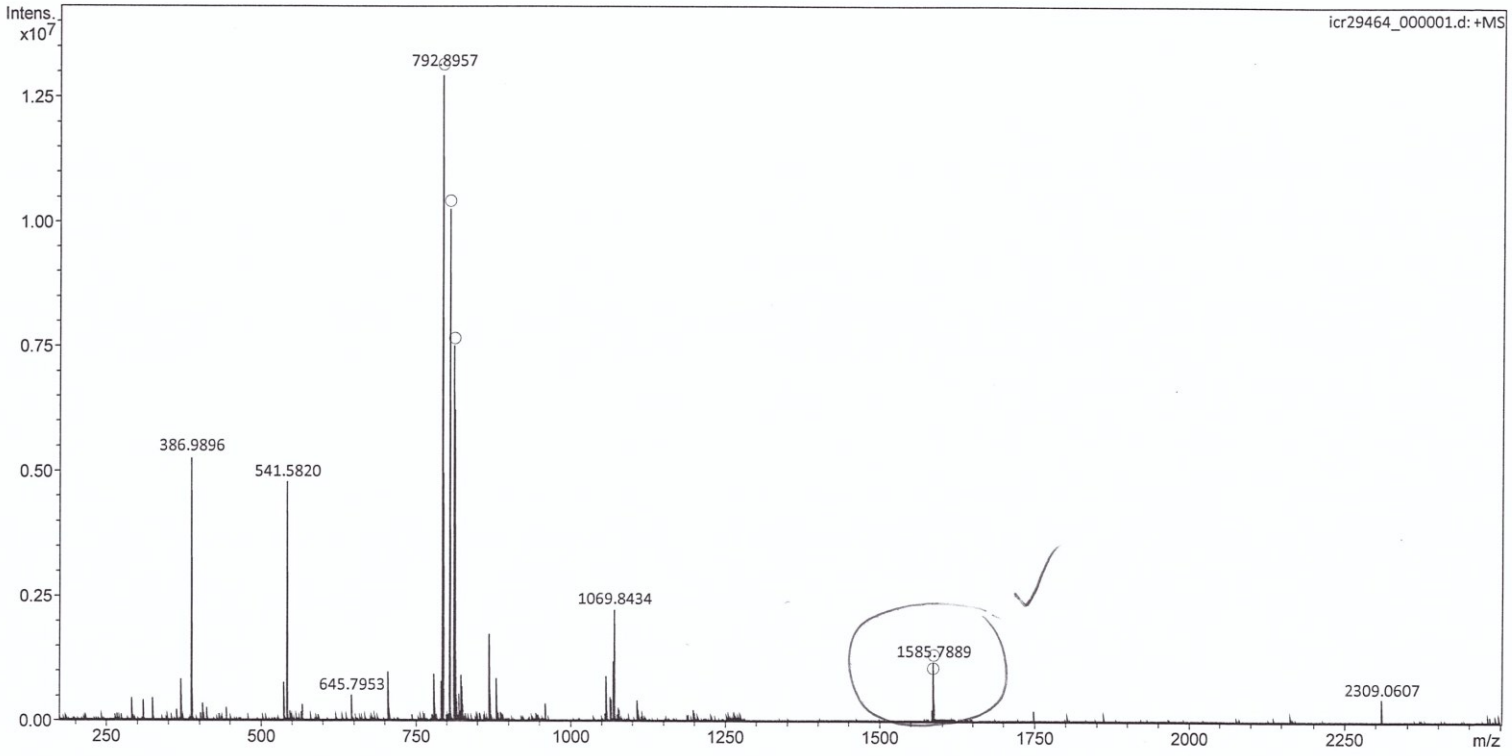

Spectrum Display Report Bruker Compass DataAnalysis 4.3 printed: 1/16/2018 2:56:33 PM Page 1 of 1

Analysis Info

Analysis Name	D:\Data\Schultz_EMBL\icr29464_000001.d	Acquisition Date	1/16/2018 2:48:22 PM
Method	ESI pos HPmix 200-1800	Instrument	ICR Apex-Qe
Sample Name	CAPS5	Operator	D.Lang
Comment	Schultz, AK Schultz (EMBL): CAPS5 in MeOH		

Acquisition Parameters

Accumulations	16	Collision Gas Flow Rate	0.5 L/sec	Capillary Entrance	4200.0 V
Broadband Low Mass	173.2 m/z	Collision Energy	0.5 eV	Calibration Date	Tue Jan 2 09:15:53 2018
Broadband High Mass	2500.0 m/z	Collision Cell RF	1200.0 V		
Data Acquisition Size	2097152	Q1 Resolution	5.0		
		Q1 Mass	200.000 m/z		

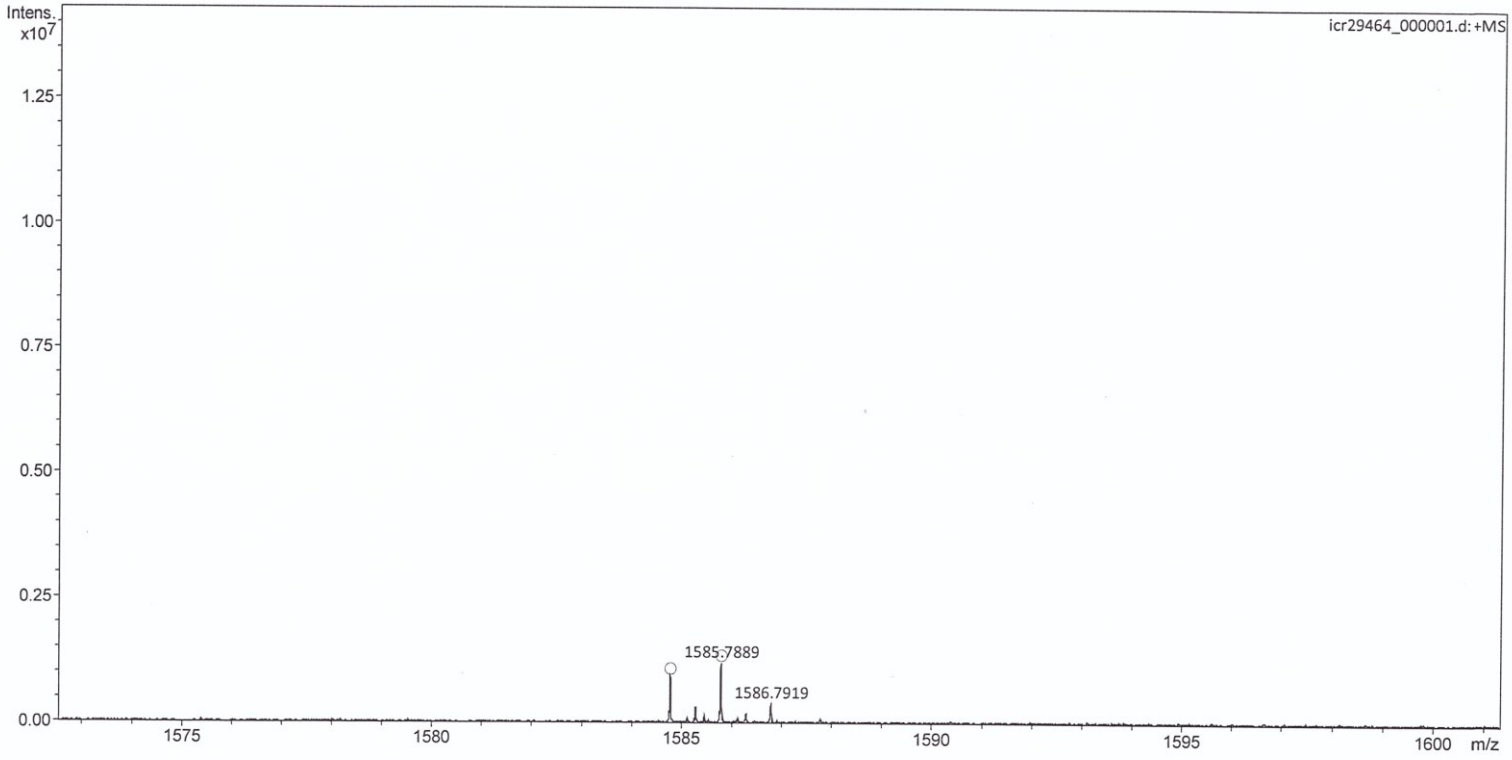

Spectrum Display Report Bruker Compass DataAnalysis 4.3 printed: 1/16/2018 2:58:17 PM Page 1 of 1

Analysis Info

Analysis Name	D:\Data\Schultz_EMBL\icr29464_000001.d	Acquisition Date	1/16/2018 2:48:22 PM
Method	ESI pos HPmix 200-1800	Instrument	ICR Apex-Qe
Sample Name	CAPS5	Operator	D.Lang
Comment	Schultz, AK Schultz (EMBL): CAPS5 in MeOH		

Acquisition Parameters

Accumulations	16	Collision Gas Flow Rate	0.5 L/sec	Capillary Entrance	4200.0 V
Broadband Low Mass	173.2 m/z	Collision Energy	0.5 eV	Calibration Date	Tue Jan 2 09:15:53 2018
Broadband High Mass	2500.0 m/z	Collision Cell RF	1200.0 V		
Data Acquisition Size	2097152	Q1 Resolution	5.0		
		Q1 Mass	200.000 m/z		

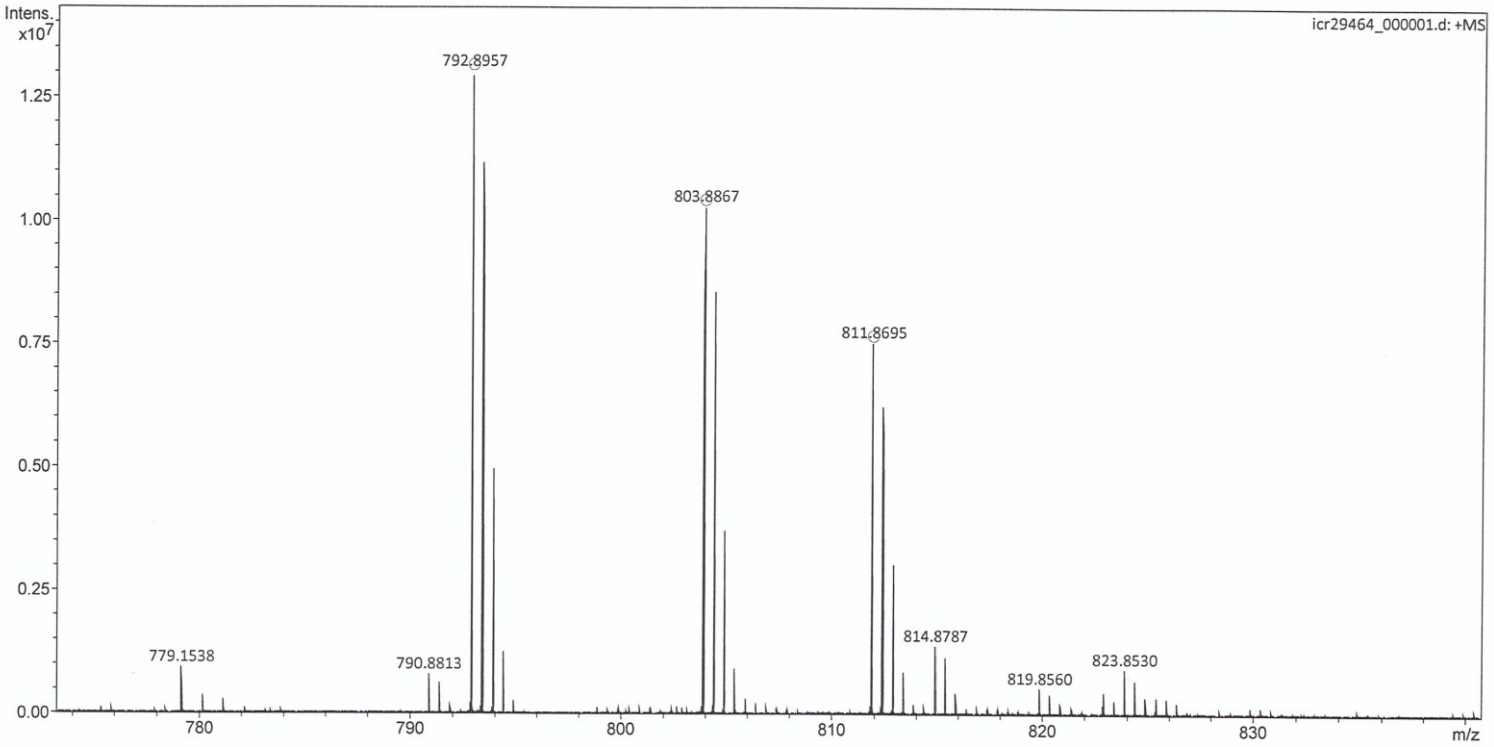

Spectrum Display Report Bruker Compass DataAnalysis 4.3 printed: 1/16/2018 2:57:25 PM Page 1 of 1

Mass Spectrum Formula Report

Analysis Info

Analysis Name D:\Data\Schultz_EMBL\icr29464_000001.d

Acquisition Date 1/16/2018 2:48:22 PM

Comment Schultz, AK Schultz (EMBL): CAPS5 in MeOH

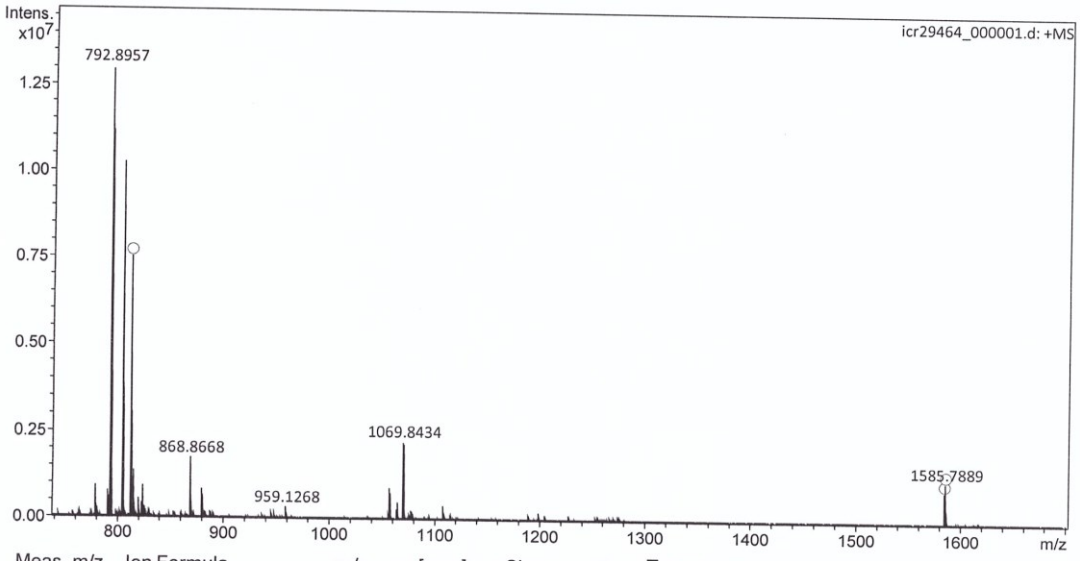

Meas. m/z	Ion Formula	m/z	err [ppm]	mSigma	rdb	e⁻ Conf	N-Rule
792.8957	C73H107N19O21	792.8939	-2.3	30.8	30.0	even	ok
	C74H103N23O17	792.8946	-1.5	38.9	35.0	even	ok
	C73H87N41O3	792.8952	-0.7	54.5	51.0	even	ok
803.8867	C70H105N21O23	803.8841	-3.3	30.1	29.0	even	ok
	C75H105N19O21	803.8861	-0.8	53.7	33.0	even	ok
811.8695	C73H101N21O22	811.8710	1.8	36.8	34.0	even	ok
	C80H97N21O17	811.8680	-1.9	76.5	43.0	even	ok
1584.7873	C72H90N37O7	1584.7818	-3.5	131.0	46.5	even	ok
	C73H86N41O3	1584.7832	-2.6	131.7	51.5	even	ok
	C73H102N25O16	1584.7931	3.6	134.8	35.5	even	ok
	C74H102N23O17	1584.7819	-3.4	135.9	35.5	even	ok
	C72H106N21O20	1584.7918	2.8	136.5	30.5	even	ok
1585.7889	C73H107N19O21	1585.7883	-0.3	316.1	30.0	odd	ok
	C73H87N41O3	1585.7910	1.3	347.9	51.0	odd	ok

Bruker Compass DataAnalysis 4.3 printed: 1/16/2018 2:56:20 PM Page 1 of 1

CAPRee1_a:

Expected mass: 1557.72 Da
$[M+1]^{+}$ exp. 1558.72, not found $[M+2]^{2+}$ exp. 779.36 , found 779.35 $[M+3]^{3+}$ exp. 519.90, found 519.95 $[M+4]^{4+}$ exp. 390.18, found 390.05

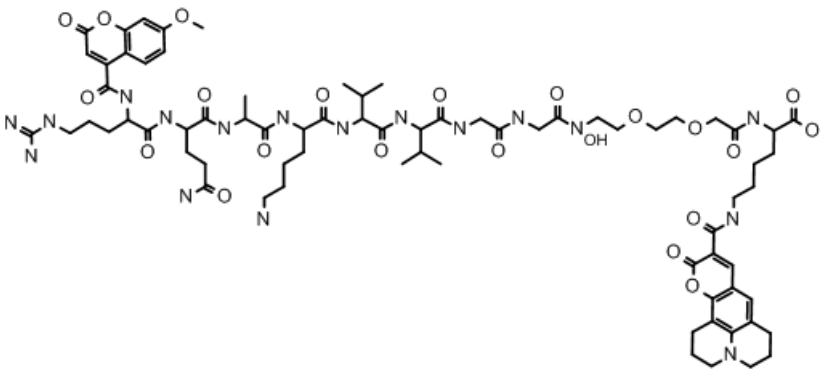

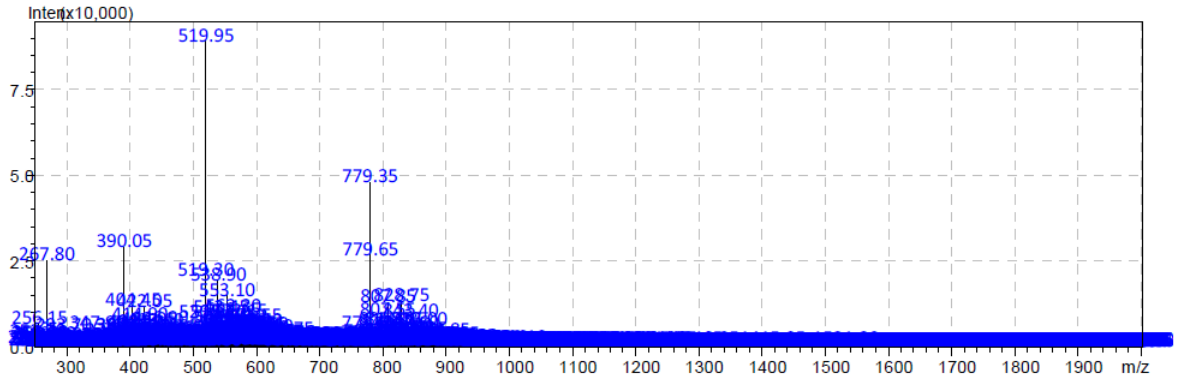

CAPRee1_b:

Expected mass: 1913.99 Da
$[M+1]^{+}$ exp. 1913.99, not found; $[M+2]^{2+}$ exp. 958.00, found 965.70, $[M+3]^{3+}$ exp. 639.00, found 644.40

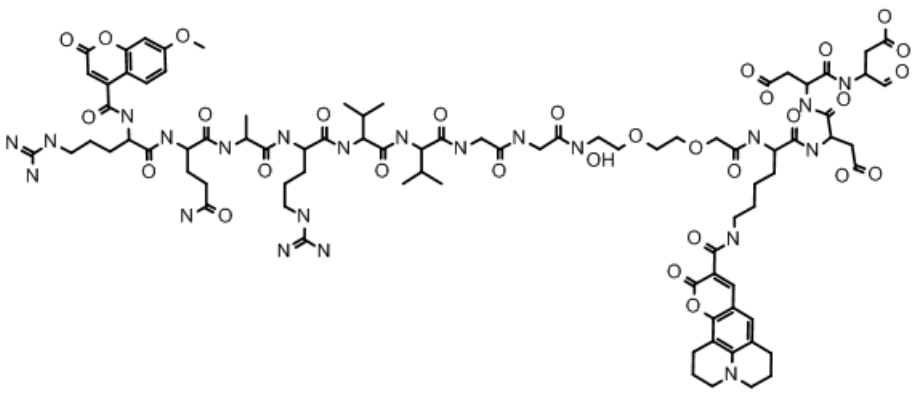

CAPRee1_c:

Expected mass: 1729.88 Da

$[M+1]^{+}$ exp. 1730.88, not found; $[M+2]^{2+}$ exp. 865.94, found 865.85 $[M+3]^{3+}$ exp. 577.62, found 577.55$[M+4]^{4+}$ exp. 43.47, found 433.45

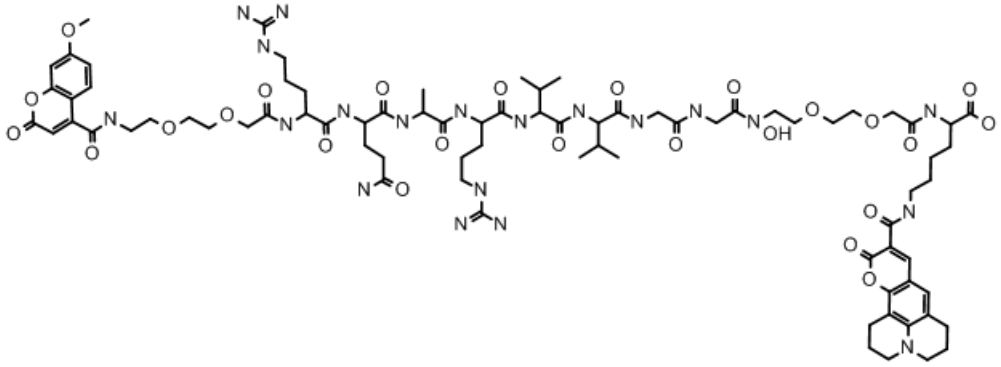

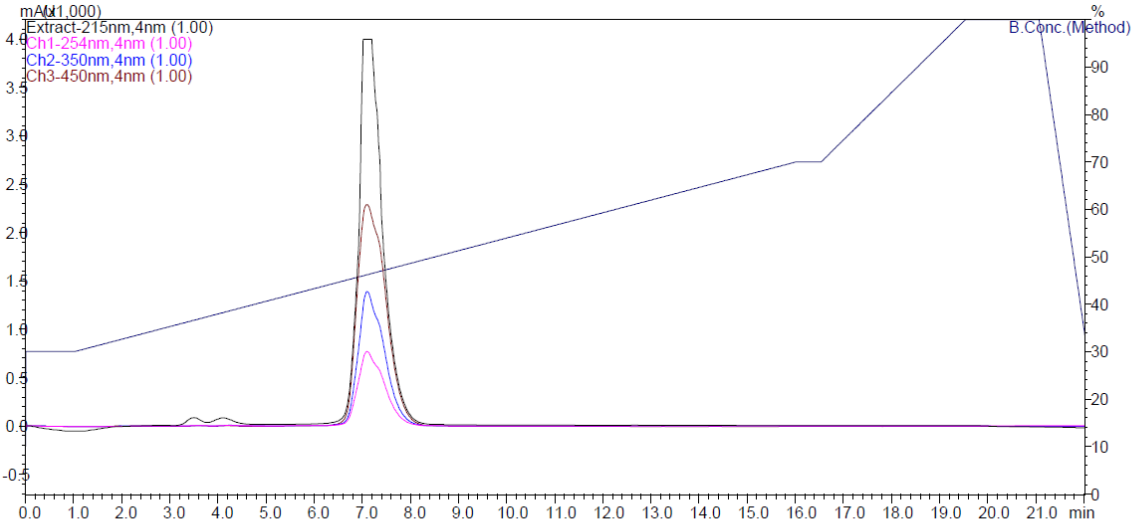

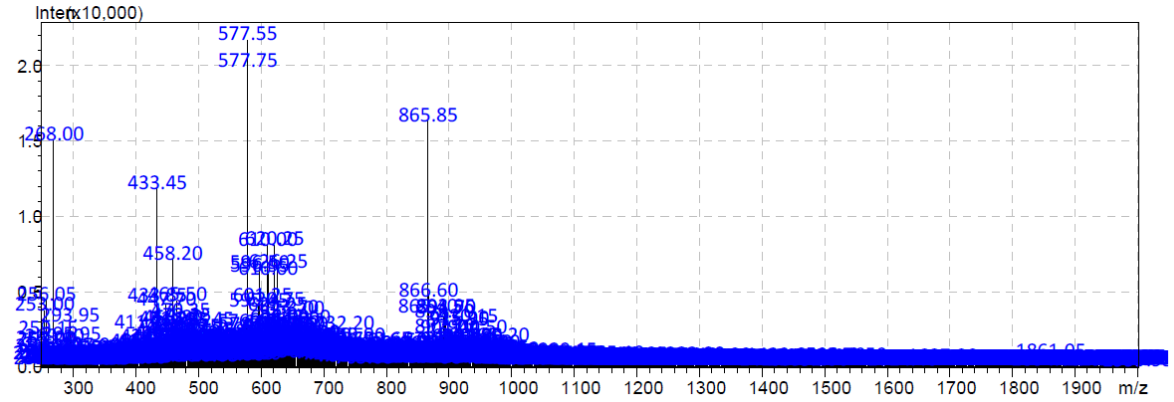

CAPRee1_d:

Expected mass: 1686.73 Da
$[M+1]^{+}$ exp. 1687.73, not found; $[M+2]^{2+}$ exp. 844.16, found 843.1, $[M+3]^{3+}$ exp. 563.10, found 562.64, $[M+4]^{4+}$ exp. 422.75, found 422.15

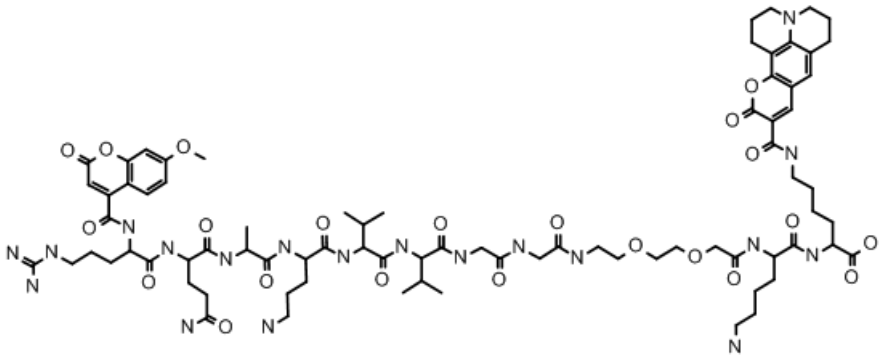

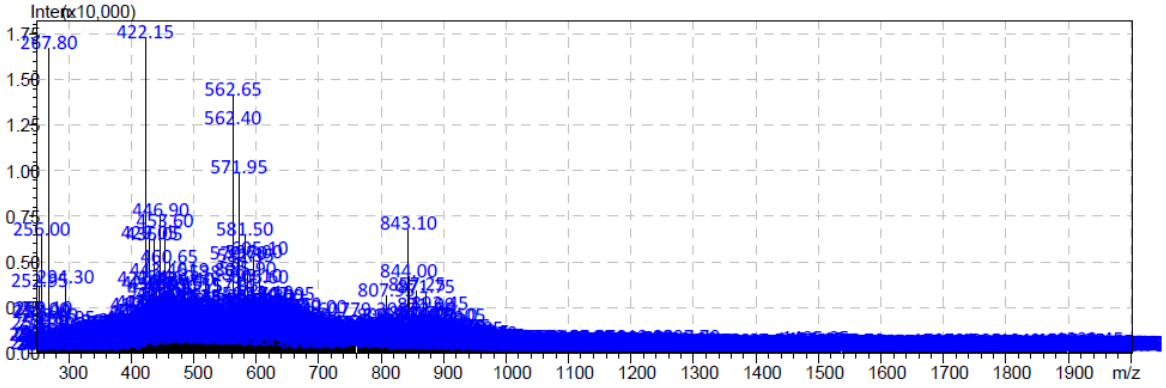

CAPRee2:

Expected mass: 2161.58 Da
$[M+1]^{+}$ exp. 2162.78, not found; $[M+2]^{2+}$ exp. 1081.79, found 1081.86 /1081.62, $[M+3]^{3+}$ exp. 721.53, found 721.41/721.42 $[M+4]^{4+}$ exp. 541.36, found 541.39

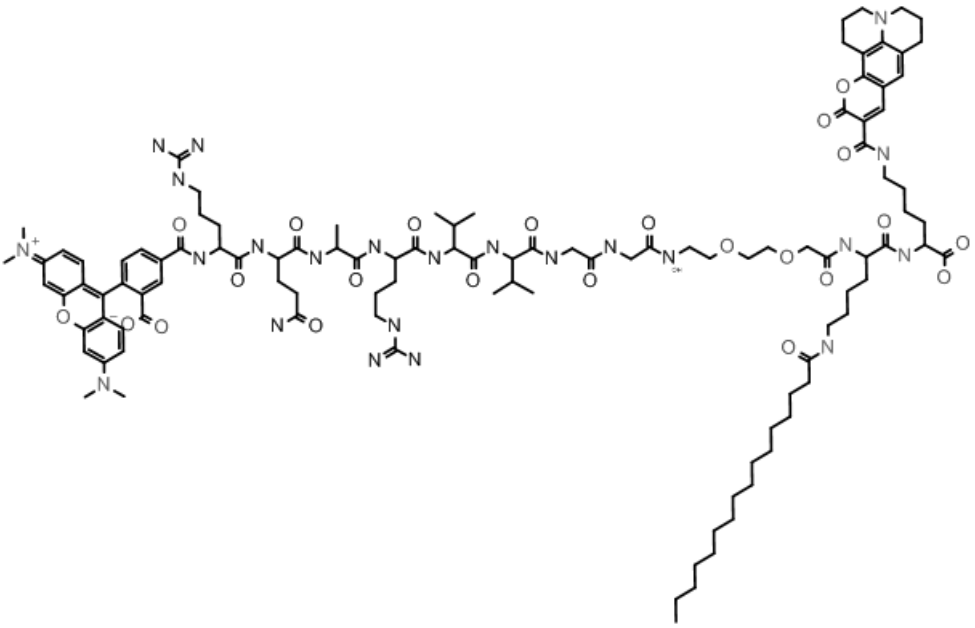

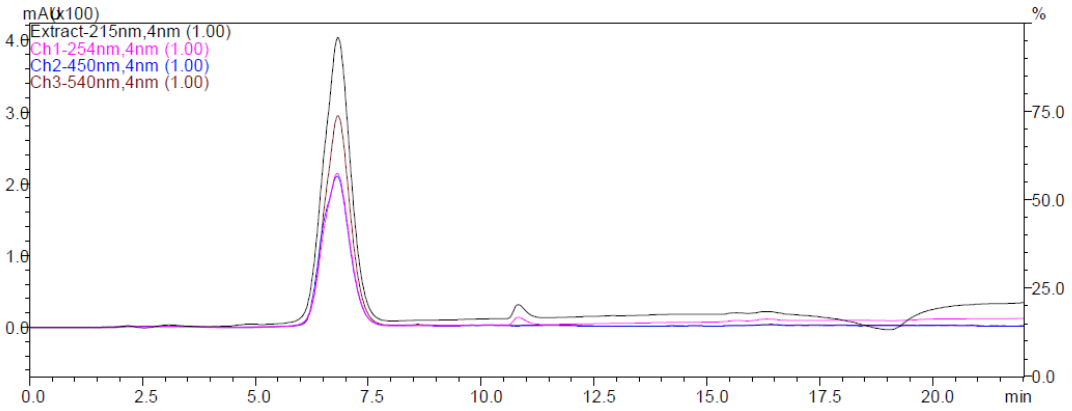

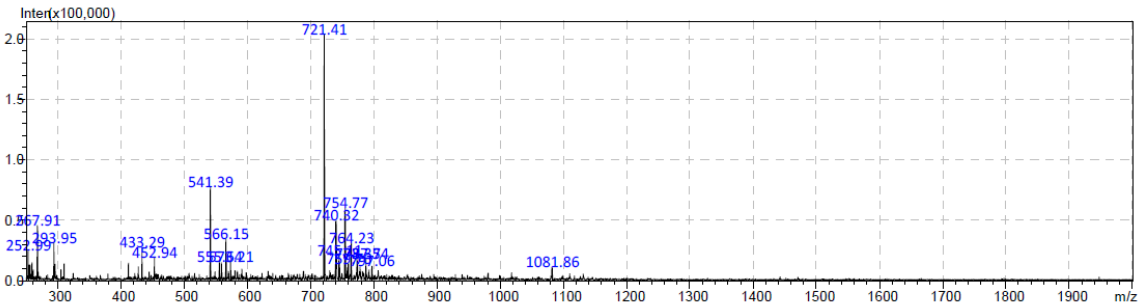

CAPRee2_a:

Expected mass: 2161.58 Da
$[M+1]^{+}$ exp. 2162.78, not found; $[M+2]^{2+}$ exp. 1081.79, not found, $[M+3]^{3+}$ exp. 721.53, found 721.41/721.42, $[M+4]^{4+}$ exp. 541.36, found 541.55

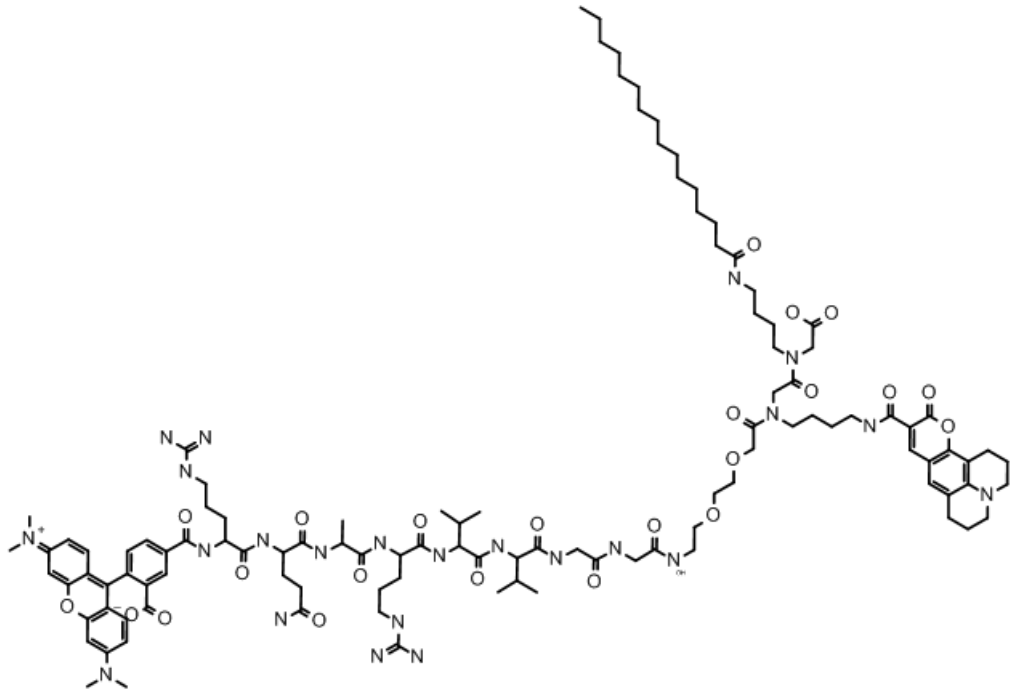

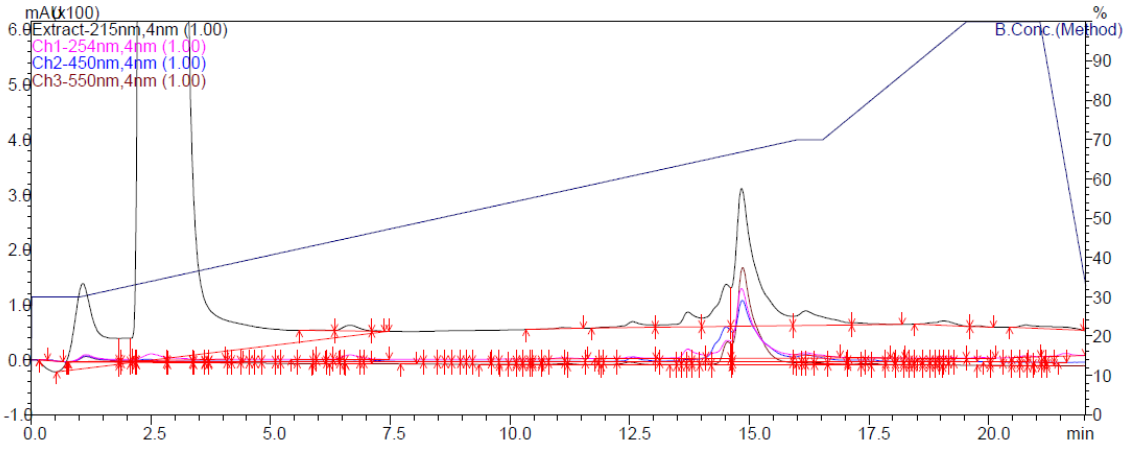

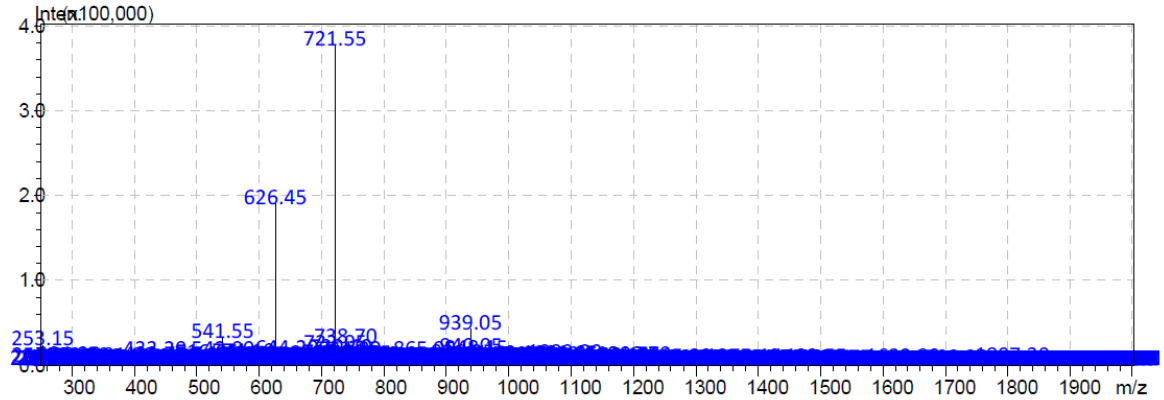

CAPRee2_b:

Expected mass: 2237.74 Da
$[M+1]^{+}$ exp. 2238.74, not found; $[M+2]^{2+}$ exp. 1119.87, found 1117.63

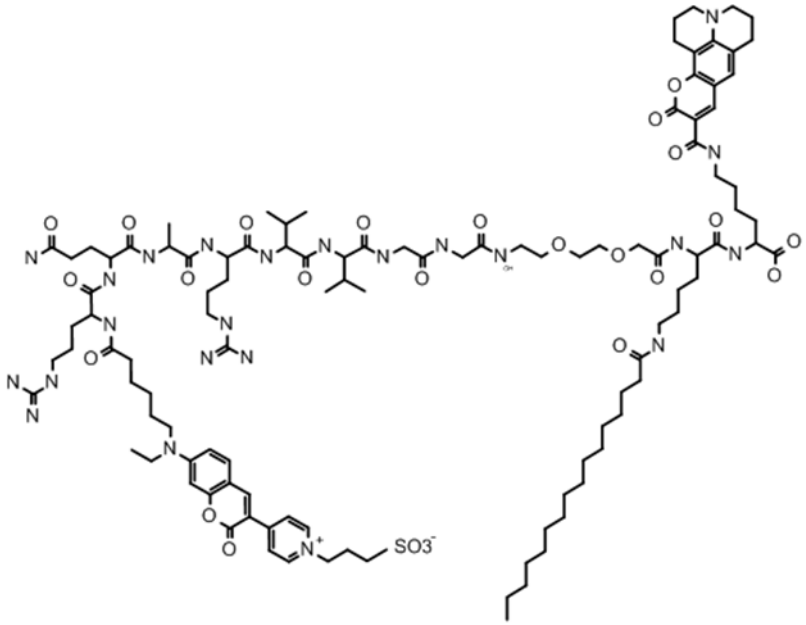

Analysis Info

Analysis Name	D:\Data\Schultz_EMBL\icr29468_000002.d	Acquisition Date	1/17/2018 8:53:59 AM
Method	ESI pos HPmix 500-3000	Instrument	ICR Apex-Qe
Sample Name	CAPS25	Operator	I.Mitsch
Comment	Schultz, Schultz/EMBL: CAPS25 in MeOH		

Acquisition Parameters

Accumulations	16	Collision Gas Flow Rate	0.4 L/sec	Capillary Entrance	4400.0 V
Broadband Low Mass	389.7 m/z	Collision Energy	0.5 eV	Calibration Date	Tue Jan 2 09:21:14 2018
Broadband High Mass	3500.0 m/z	Collision Cell RF	1700.0 V		
Data Acquisition Size	2097152	Q1 Resolution	10.0		
		Q1 Mass	400.000 m/z		

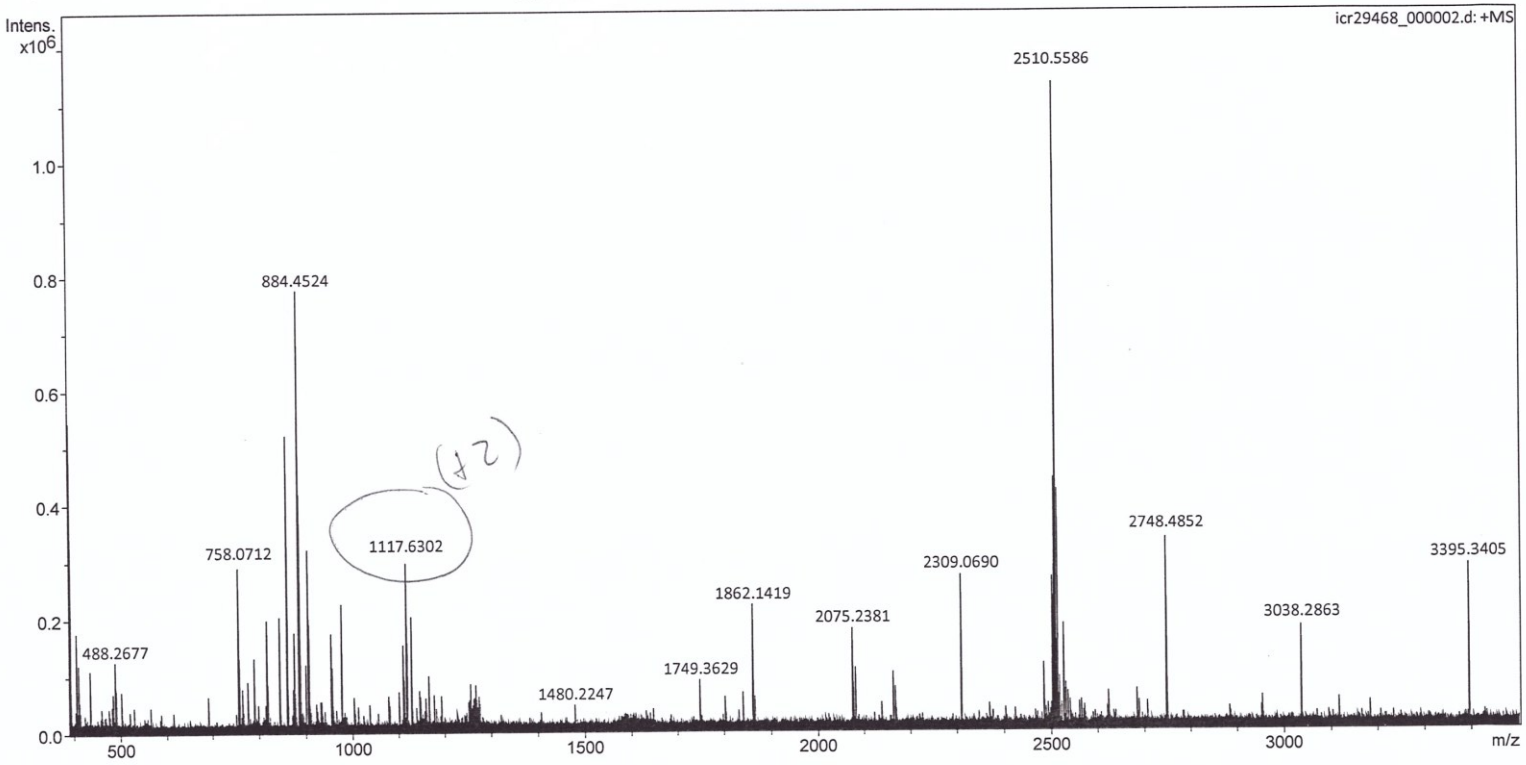

Mass Spectrum Formula Report

Analysis Info Acquisition Date 1/17/2018 8:53:59 AM

Analysis Name D:\Data\Schultz_EMBL\icr29468_000002.d

Comment Schultz, Schultz/EMBL: CAPS25 in MeOH

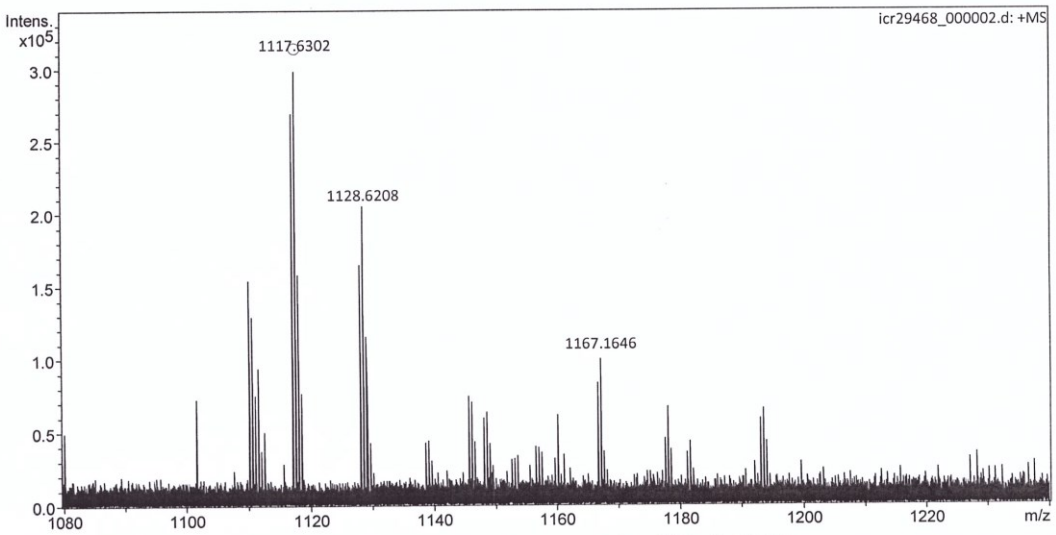

Meas. m/z	Ion Formula	m/z	err [ppm]	mSigma	rdb	e⁻ Conf	N-Rule
1117.6302	C109H172N23O25S	1117.6302	0.0	294.1	35.5	odd	ok

CAPRee2_c:

Expected mass: 2190.78 Da
$[M+1]^{+}$ exp. 2191.78, not found; $[M+2]^{2+}$ exp. 1095.39, found 1095.50 /1094.68, $[M+3]^{3+}$ exp. 730.26, found 730.10/730.122 $[M+4]^{4+}$ exp. 547.70, found 547.95

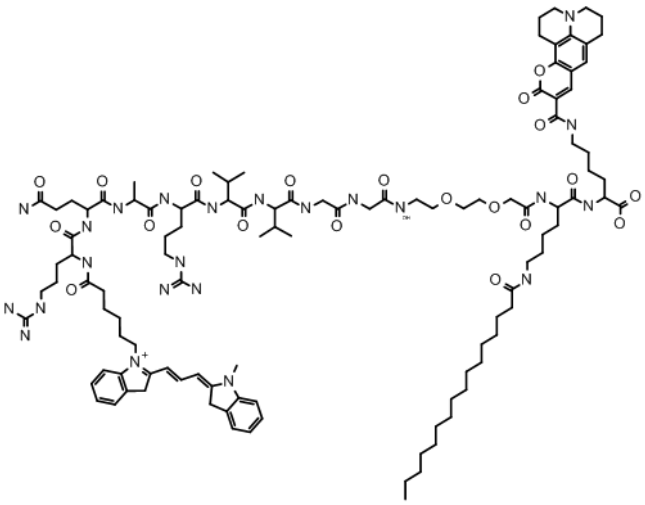

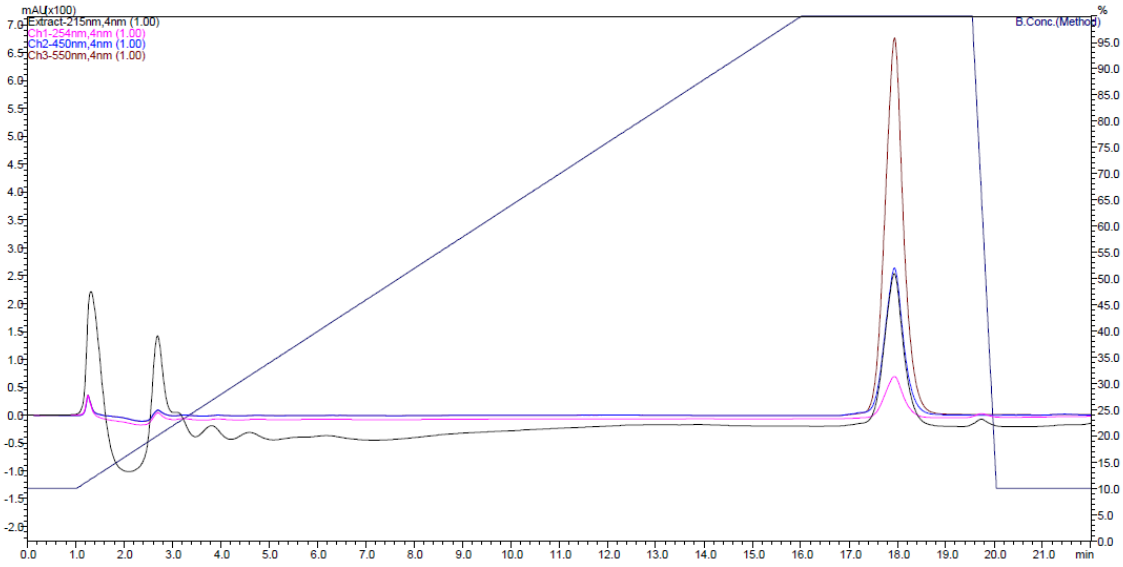

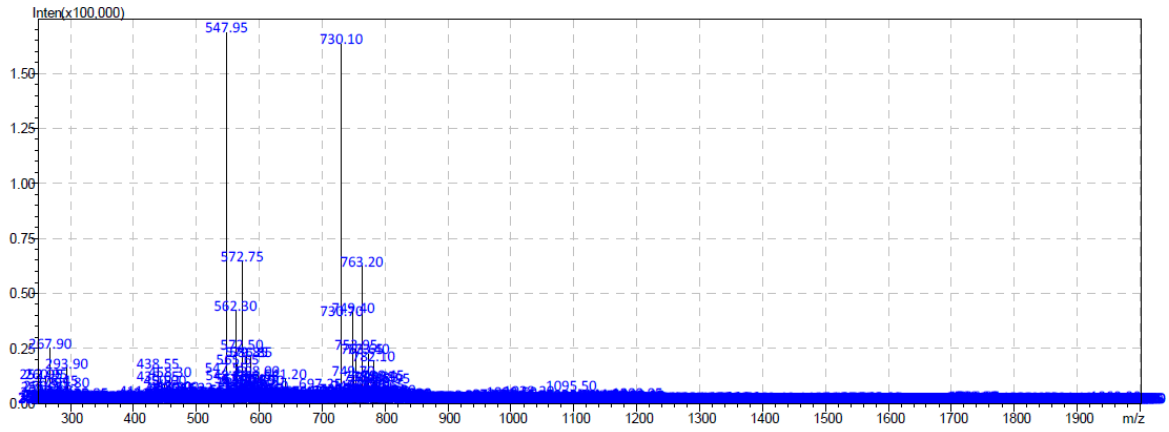

Analysis Info

Analysis Name	D:\Data\Schultz_EMBL\icr29467_000001.d	Acquisition Date	1/17/2018 8:27:36 AM
Method	ESI pos HPmix 500-3000	Instrument	ICR Apex-Qe
Sample Name	CAPS24	Operator	I.Mitsch
Comment	Schultz, Schultz/EMBL: CAPS24 in MeOH		

Acquisition Parameters

Accumulations	16	Collision Gas Flow Rate	0.4 L/sec	Capillary Entrance	4400.0 V
Broadband Low Mass	389.7 m/z	Collision Energy	0.5 eV	Calibration Date	Tue Jan 2 09:21:14 2018
Broadband High Mass	3500.0 m/z	Collision Cell RF	1700.0 V		
Data Acquisition Size	2097152	Q1 Resolution	10.0		
		Q1 Mass	400.000 m/z		

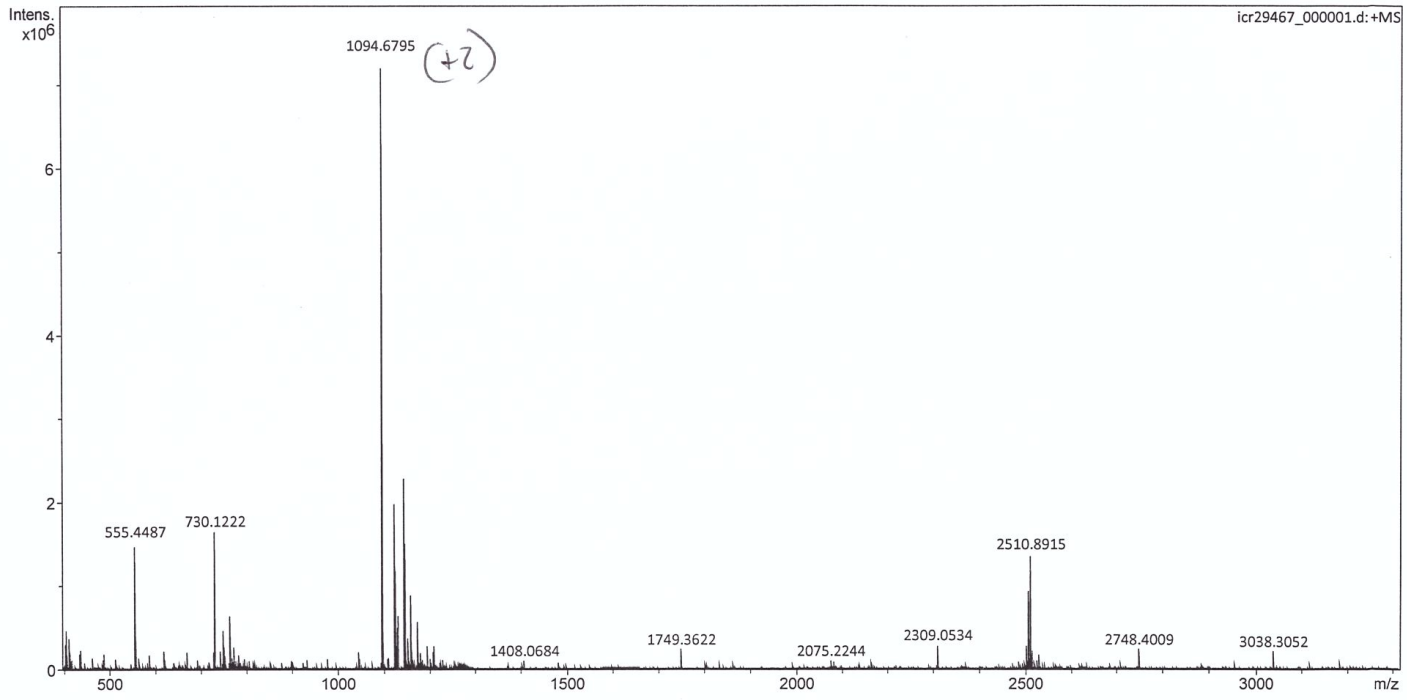

Analysis Info

Analysis Name	D:\Data\Schultz_EMBL\icr29467_000001.d	Acquisition Date	1/17/2018 8:27:36 AM
Method	ESI pos HPmix 500-3000	Instrument	ICR Apex-Qe
Sample Name	CAPS24	Operator	I.Mitsch
Comment	Schultz, Schultz/EMBL: CAPS24 in MeOH		

Acquisition Parameters

Accumulations	16	Collision Gas Flow Rate	0.4 L/sec	Capillary Entrance	4400.0 V
Broadband Low Mass	389.7 m/z	Collision Energy	0.5 eV	Calibration Date	Tue Jan 2 09:21:14 2018
Broadband High Mass	3500.0 m/z	Collision Cell RF	1700.0 V		
Data Acquisition Size	2097152	Q1 Resolution	10.0		
		Q1 Mass	400.000 m/z		

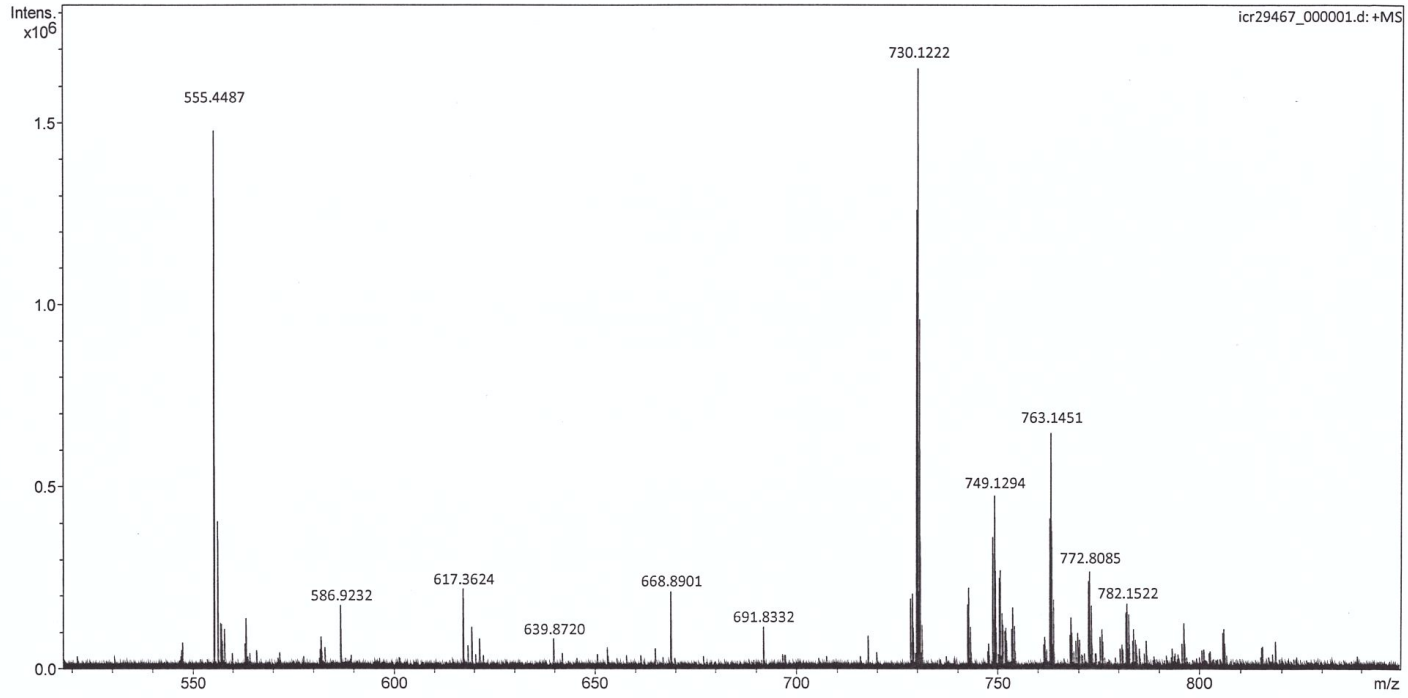

Analysis Info

Analysis Name	D:\Data\Schultz_EMBL\icr29467_000001.d	Acquisition Date	1/17/2018 8:27:36 AM
Method	ESI pos HPmix 500-3000	Instrument	ICR Apex-Qe
Sample Name	CAPS24	Operator	I.Mitsch
Comment	Schultz, Schultz/EMBL: CAPS24 in MeOH		

Acquisition Parameters

Accumulations	16	Collision Gas Flow Rate	0.4 L/sec	Capillary Entrance	4400.0 V
Broadband Low Mass	389.7 m/z	Collision Energy	0.5 eV	Calibration Date	Tue Jan 2 09:21:14 2018
Broadband High Mass	3500.0 m/z	Collision Cell RF	1700.0 V		
Data Acquisition Size	2097152	Q1 Resolution	10.0		
		Q1 Mass	400.000 m/z		

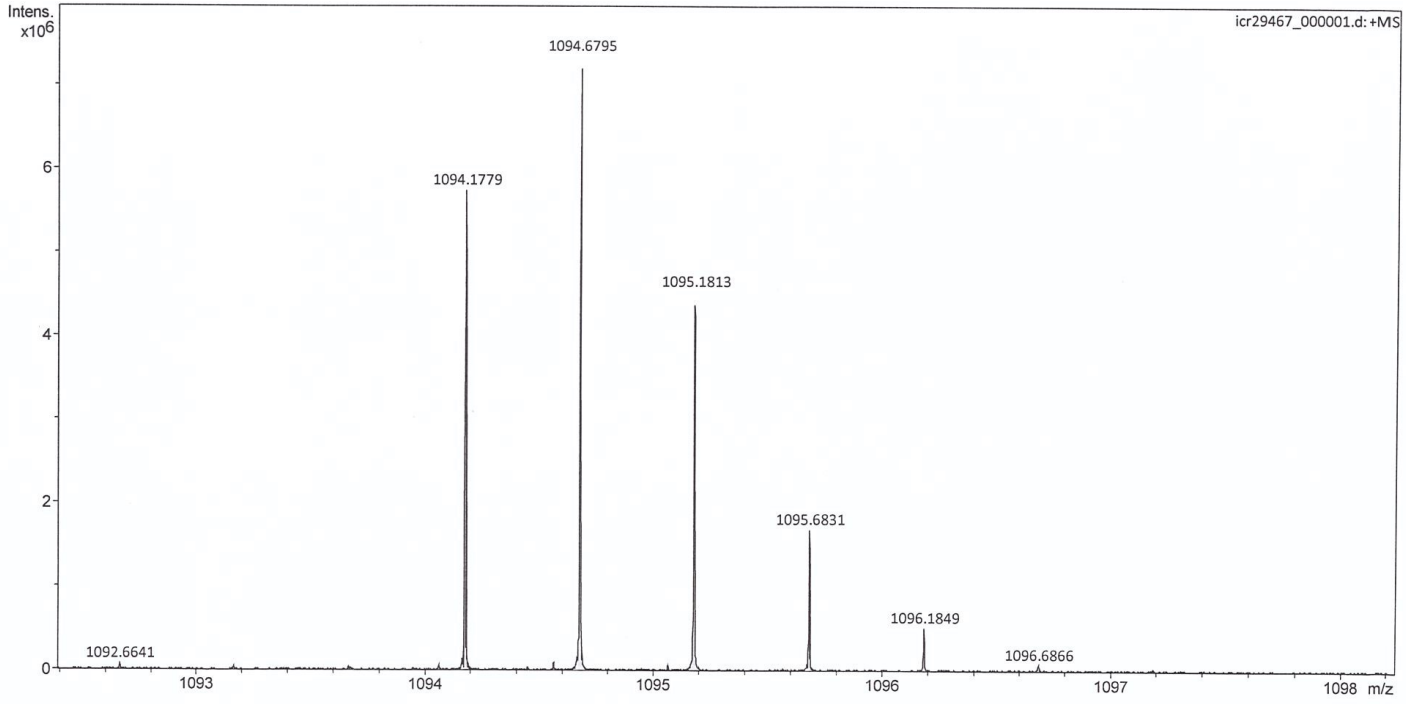

Spectrum Display Report Bruker Compass DataAnalysis 4.3 printed: 1/17/2018 8:31:05 AM Page 1 of 1

Mass Spectrum Formula Report

Analysis Info

Analysis Name	D:\Data\Schultz_EMBL\icr29467_000001.d	Acquisition Date	1/17/2018 8:27:36 AM
Comment	Schultz, Schultz/EMBL: CAPS24 in MeOH		

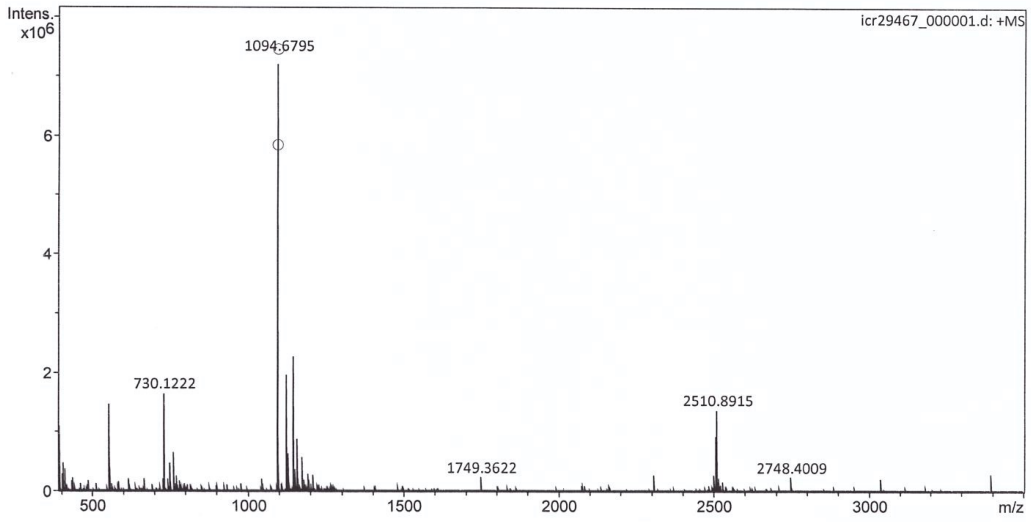

Meas. m/z	Ion Formula	m/z	err [ppm]	mSigma	rdb	e⁻ Conf	N-Rule
1094.1779	C114H177N23O20	1094.1765	-1.3	59.0	38.0	even	ok
1094.6795	C114H177N23O20	1094.1765	-1.4	59.0	38.0	even	ok
	C114H178N23O20	1094.6804	0.8	291.6	37.5	odd	ok

CAPRee3:

Expected mass: 2306.74 Da
$[M+1]^{+}$ exp. 2307.74, not found; $[M+2]^{2+}$ exp. 1154.37, found 1154.24/1154.16, $[M+3]^{3+}$ exp. 769.91, found 769.75/769.77 $[M+4]^{4+}$ exp. 577.69, found 577.61

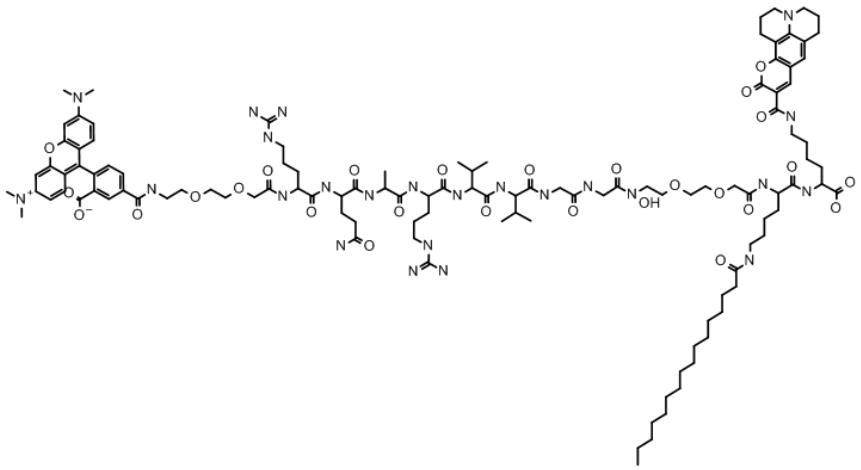

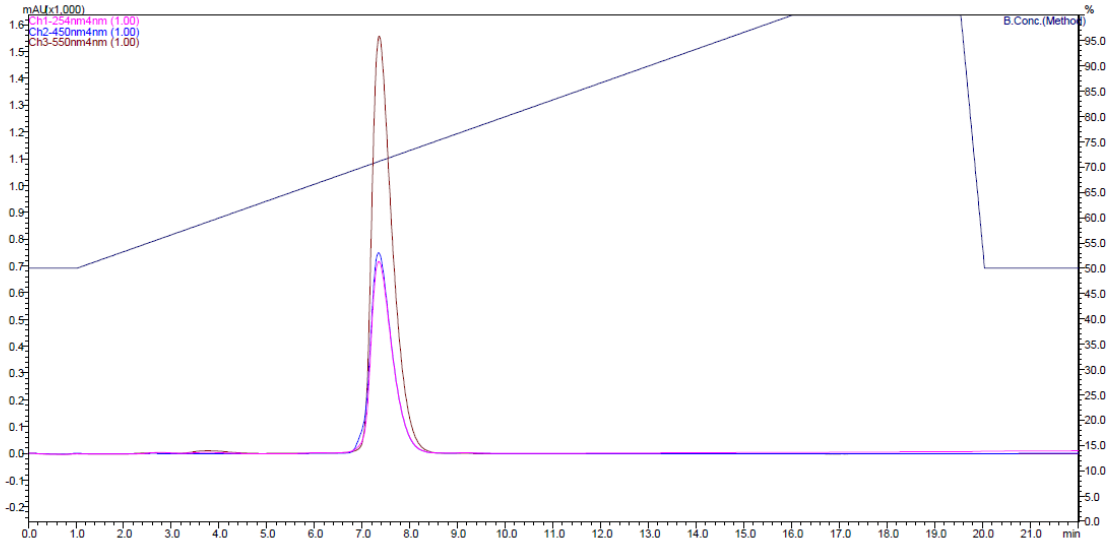

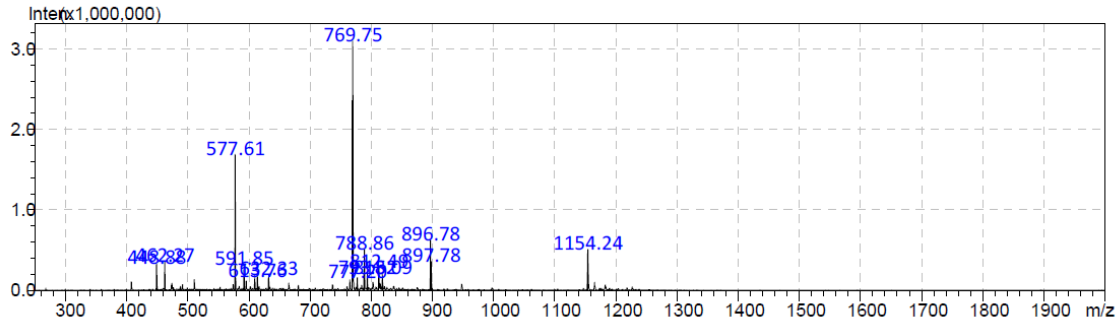

Analysis Info

Analysis Name	D:\Data\Schultz_EMBL\icr29470_000002.d	Acquisition Date	1/17/2018 9:22:26 AM
Method	ESI pos HPmix 500-3000	Instrument	ICR Apex-Qe
Sample Name	CAPS35	Operator	I.Mitsch
Comment	Schultz, Schultz/EMBL: CAPS35 in MeOH		

Acquisition Parameters

Accumulations	16	Collision Gas Flow Rate	0.4 L/sec	Capillary Entrance	4400.0 V
Broadband Low Mass	389.7 m/z	Collision Energy	0.5 eV	Calibration Date	Tue Jan 2 09:21:14 2018
Broadband High Mass	3500.0 m/z	Collision Cell RF	1700.0 V		
Data Acquisition Size	2097152	Q1 Resolution	10.0		
		Q1 Mass	400.000 m/z		

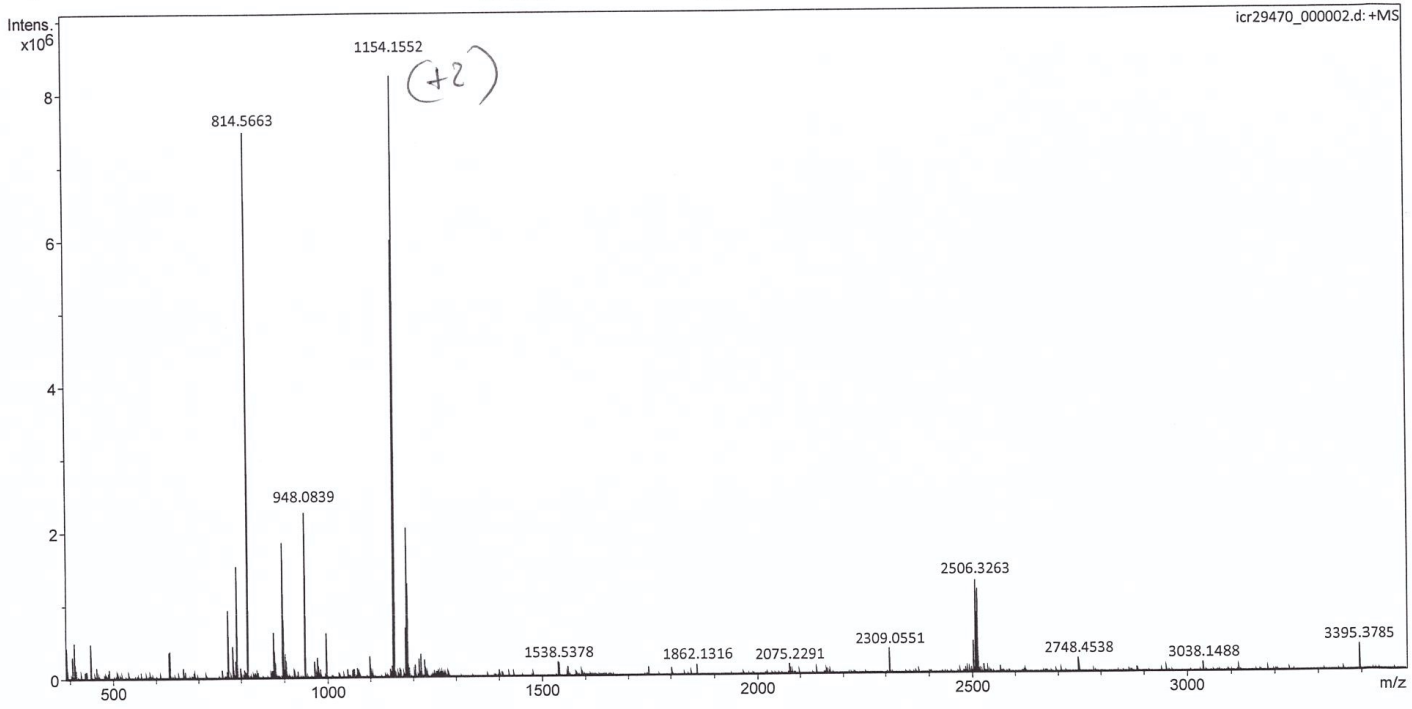

Spectrum Display Report Bruker Compass DataAnalysis 4.3 printed: 1/17/2018 9:24:38 AM Page 1 of 1

Analysis Info

Analysis Name	D:\Data\Schultz_EMBL\icr29470_000002.d	Acquisition Date	1/17/2018 9:22:26 AM
Method	ESI pos HPmix 500-3000	Instrument	ICR Apex-Qe
Sample Name	CAPS35	Operator	I.Mitsch
Comment	Schultz, Schultz/EMBL: CAPS35 in MeOH		

Acquisition Parameters

Accumulations	16	Collision Gas Flow Rate	0.4 L/sec	Capillary Entrance	4400.0 V
Broadband Low Mass	389.7 m/z	Collision Energy	0.5 eV	Calibration Date	Tue Jan 2 09:21:14 2018
Broadband High Mass	3500.0 m/z	Collision Cell RF	1700.0 V		
Data Acquisition Size	2097152	Q1 Resolution	10.0		
		Q1 Mass	400.000 m/z		

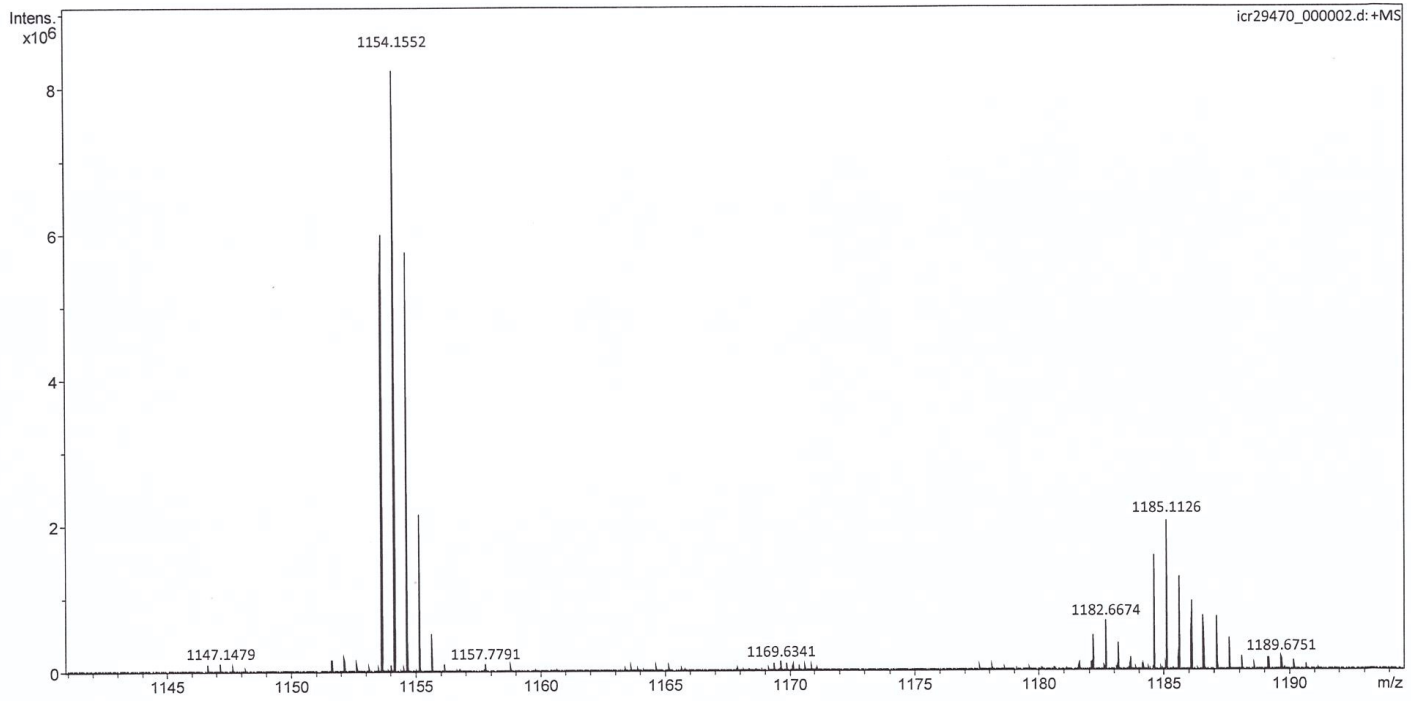

Mass Spectrum Formula Report

Analysis Info

Analysis Name	D:\Data\Schultz_EMBL\icr29470_000002.d	Acquisition Date	1/17/2018 9:22:26 AM
Comment	Schultz, Schultz/EMBL: CAPS35 in MeOH		

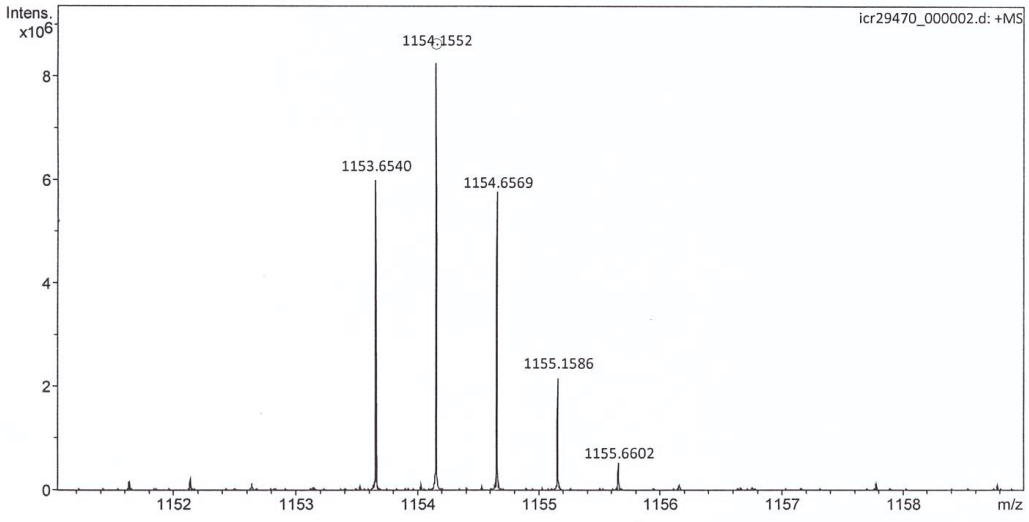

Meas. m/z	Ion Formula	m/z	err [ppm]	mSigma	rdb	e⁻ Conf	N-Rule
1154.1552	C115H175N24O26	1154.1549	-0.3	283.7	40.5	odd	ok

CAPRee4:

Expected mass: 1629.81 Da
$[M+1]^{+}$ exp. 1630.81, not found; $[M+2]^{2+}$ exp. 815.91, found 815.55, $[M+3]^{3+}$ exp. 544.27, found 544.05

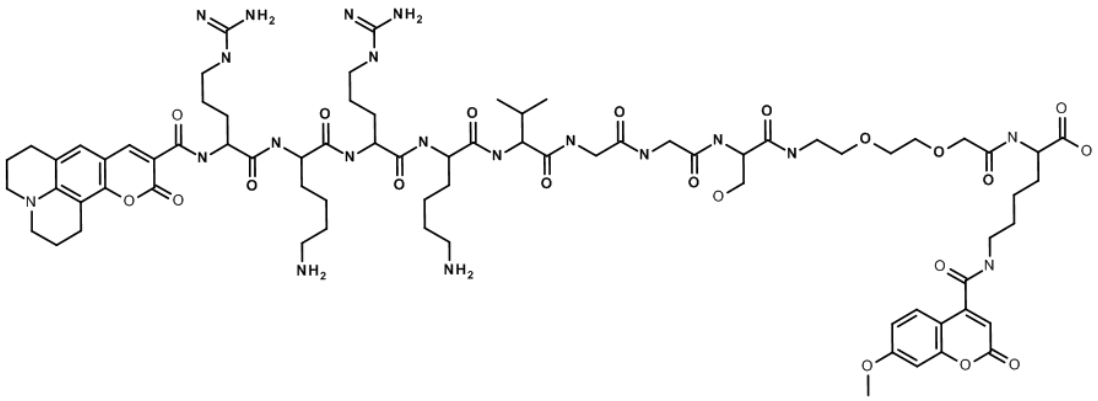

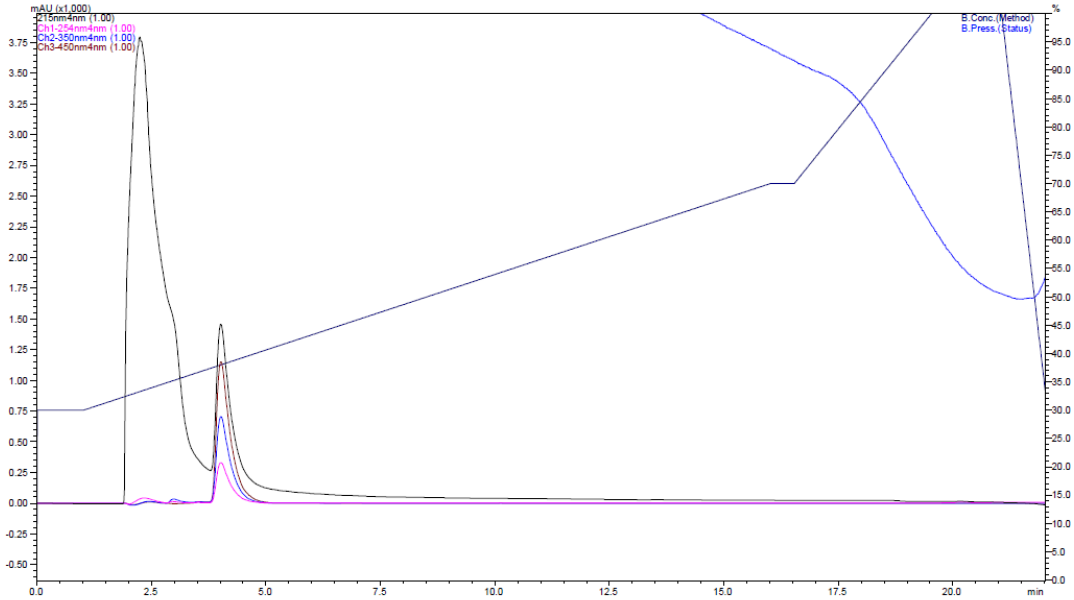

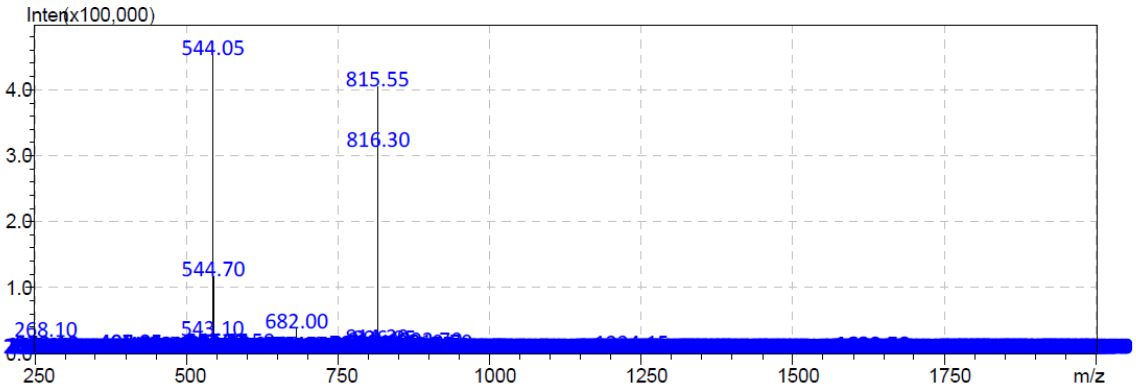

CAPRee5:

Expected mass: 2206.76 Da
$[M+1]^{+}$ exp. 2207.76, not found; $[M+2]^{2+}$ exp. 1104.38, found 1104.20, $[M+3]^{3+}$ exp. 736.59, found 736.70, $[M+4]^{4+}$ exp. 552.49, found 552.65

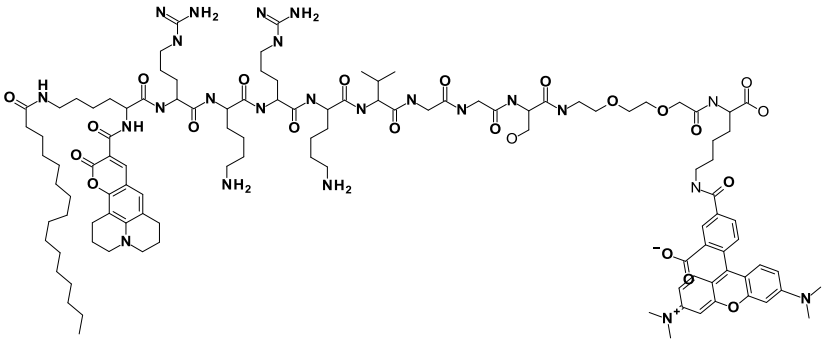

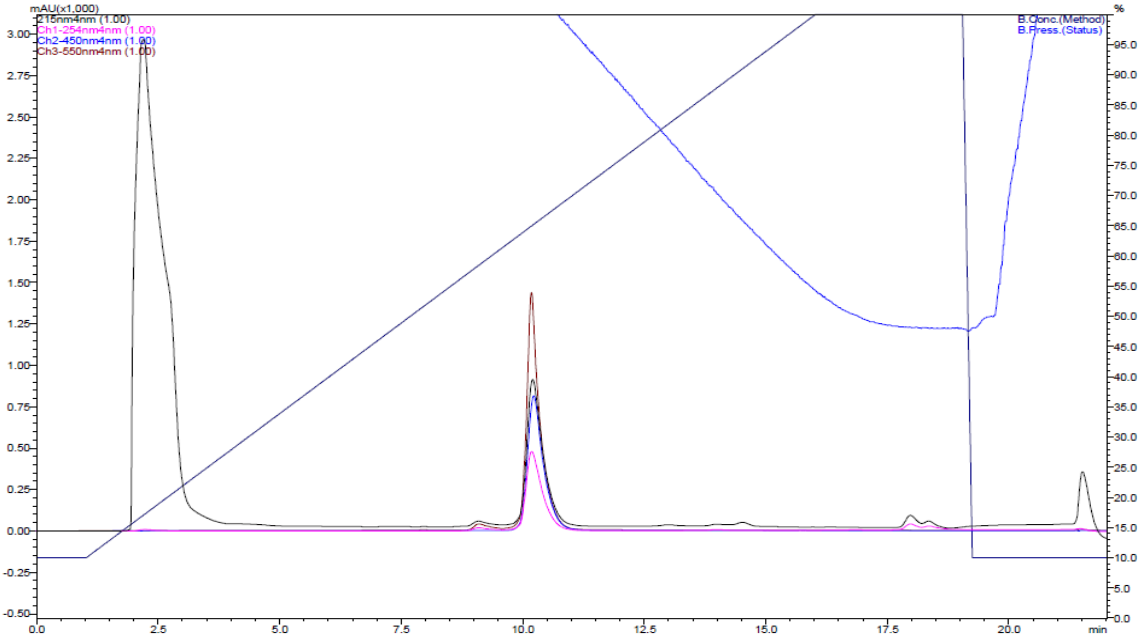

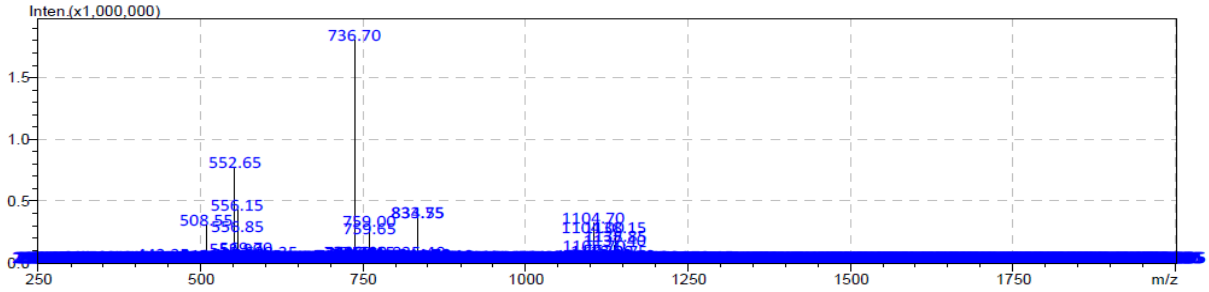

CAPRee6:

Expected mass: 2504.0 Da

$[M+1]^{+}$ exp. 2505, not found; $[M+2]^{2+}$ exp. 1253, found 1254.00, $[M+3]^{3+}$ exp. 835.67, found 836.25

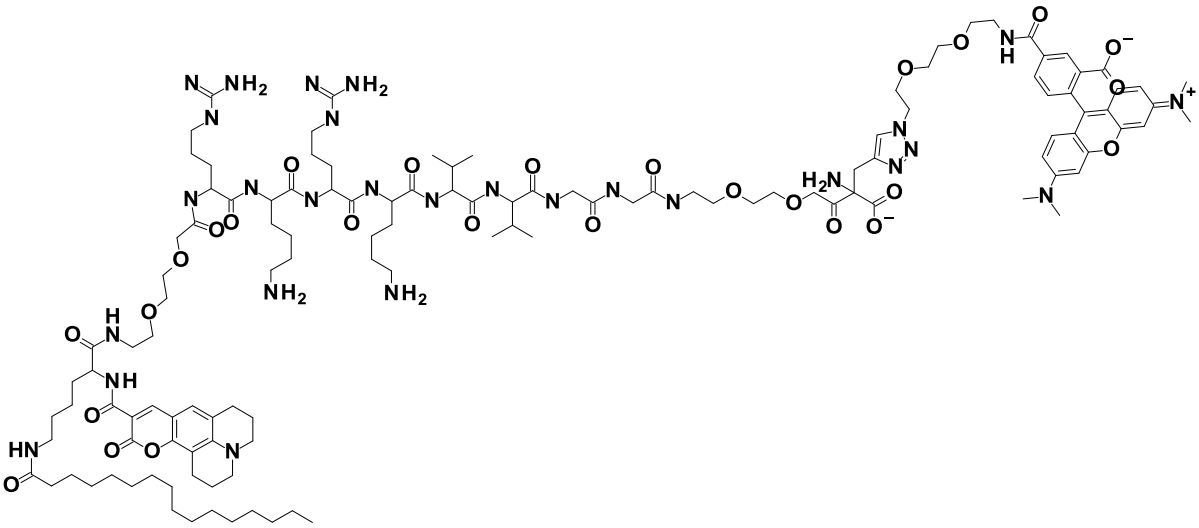

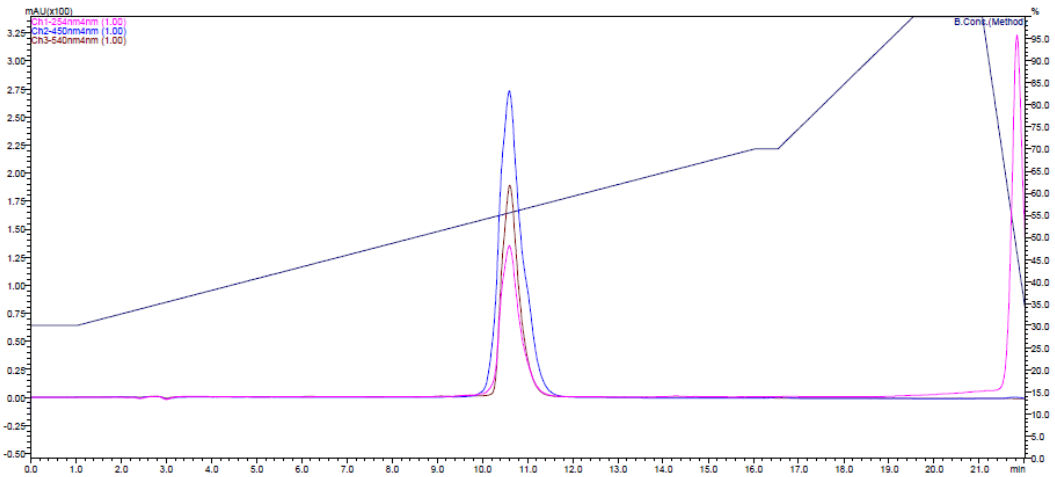

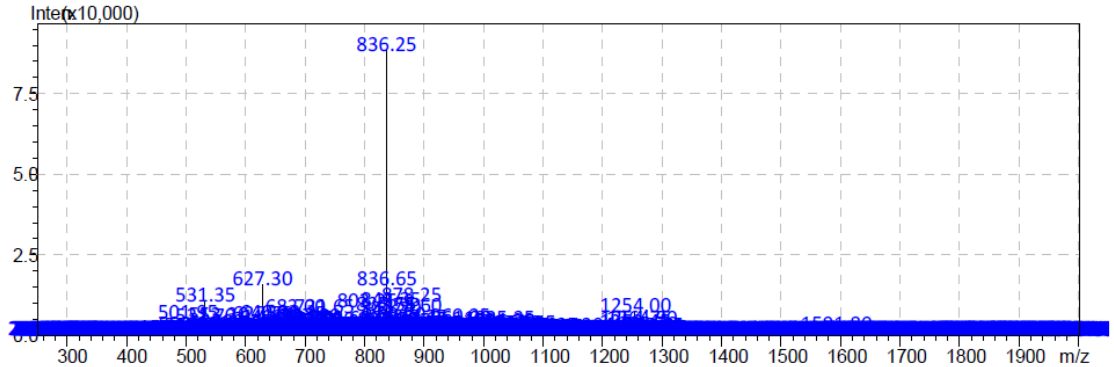

Acceptor fragment CAPRee3:

Expected mass: 1086.53 Da

$[M+H]^+$ exp. 1087.53, found 1087.53 $[M+2]^+$ exp. 544.76, found 544.27

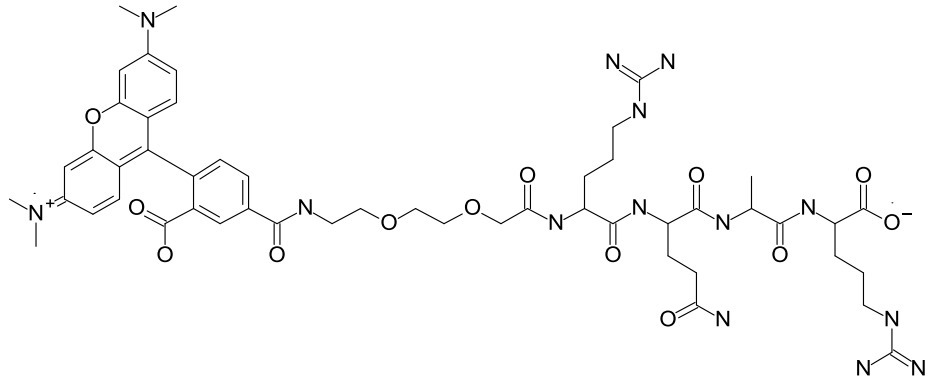

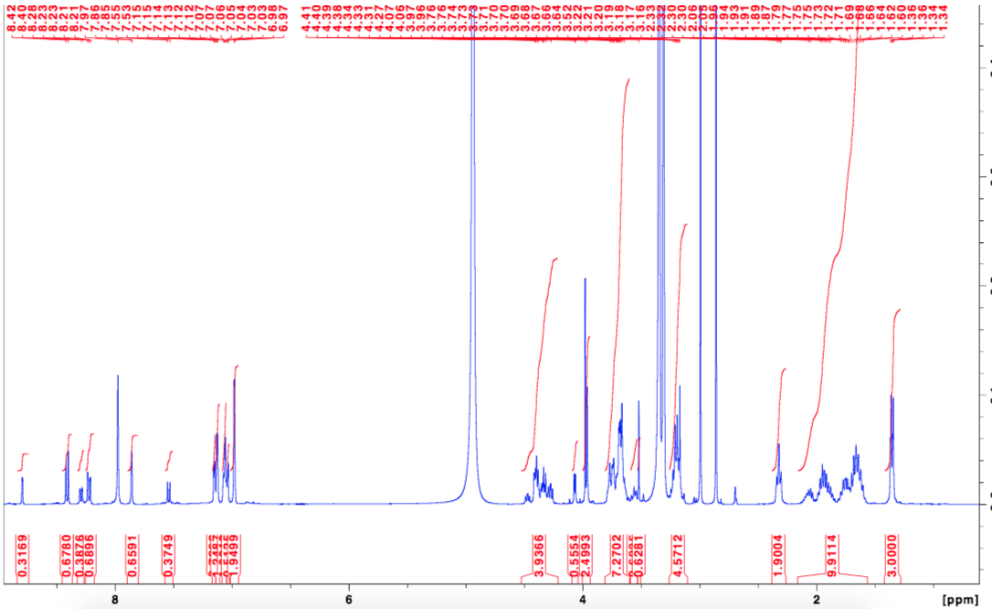

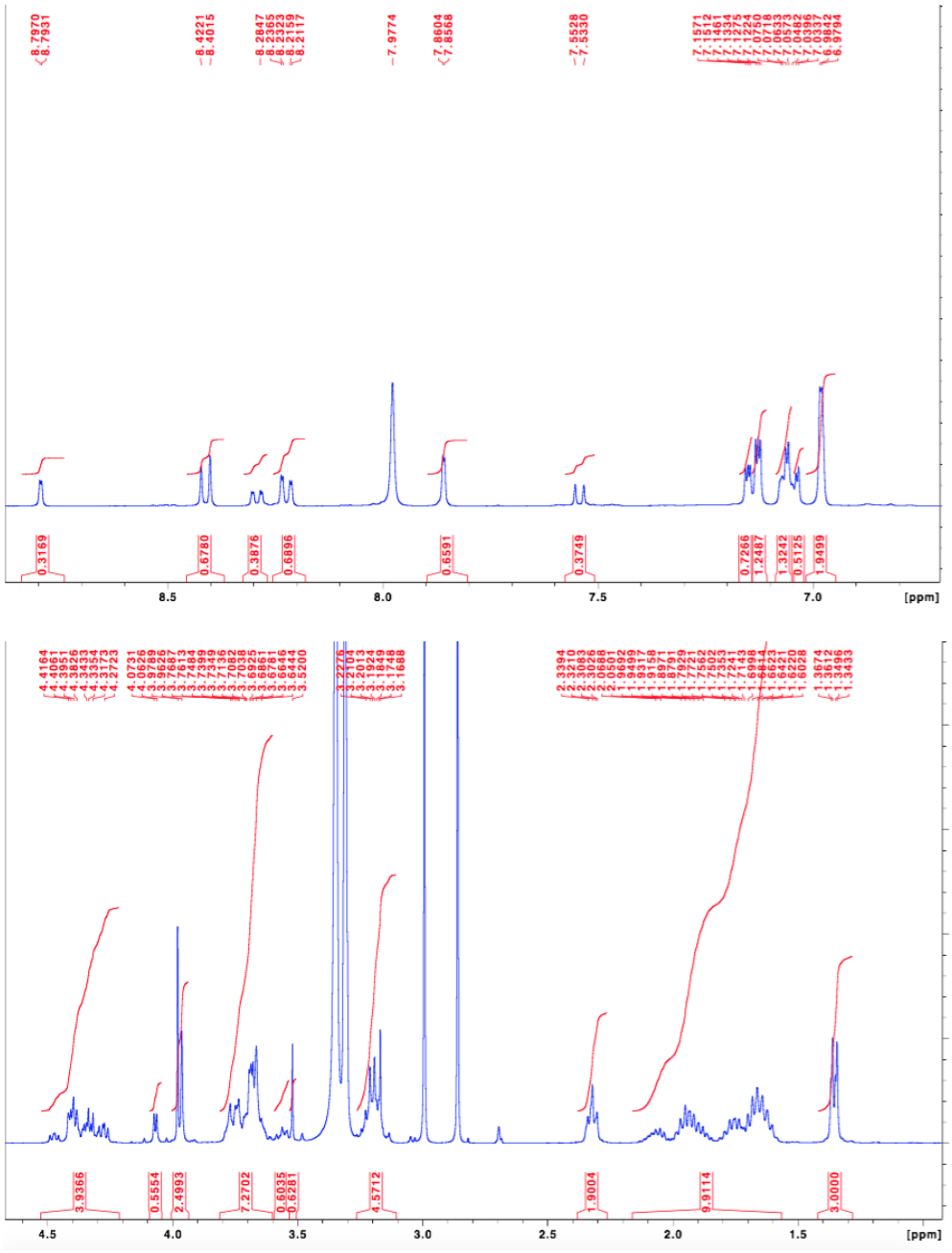

^{1}H NMR spectrum (MeOD, 400 MHz): δ 8.79 (d, $^{4}J_{HH}$ = 1.6 Hz, 0.3H, TAMRA-5'), 8.41 (d, $^{3}J_{HH}$ = 8.2 Hz, 0.7H, TAMRA-6'), 8.29 (dd, $^{3}J_{HH}$ = 8.0 Hz, $^{4}J_{HH}$ = 1.8 Hz, 0.3H, TAMRA-5'), 8.22 (dd, $^{3}J_{HH}$ = 8.2 Hz, $^{4}J_{HH}$ = 1.7 Hz, 0.7H, TAMRA-6'), 7.86 (d, $^{4}J_{HH}$ = 1.4 Hz, 0.7H, TAMRA-6'), 7.54 (d, $^{3}J_{HH}$ = 8.0 Hz, 0.3H, TAMRA-5'), 7.17-6.96 (m, 6H, TAMRA-5' and TAMRA-6'), 4.5-4.2 (m, 4H, α-CH of Arg, Gln, Ala), 3.98 (s, 2H, OCH_2CON), 3.80-3.60 (m, 8H, peg), 3.4 (12 NMe_2 protons of TAMRA obscured by proteomethanol in NMR solvent), 3.25-3.15 (m, 4H, NCH_2 of Arg), 2.32 (t, $^{3}J_{HH}$ = 7.5 Hz, 2H, CH_2CO of Gln), 2.14 - 1.57 (m, 10H, CH_2 of Arg, Gln), 1.35 (d, $^{3}J_{HH}$ = 7.2 Hz, 3H, CH_3 of Ala).

VRZ1

Analysis Info

Analysis Name	D:\Data\Schultz_EMBL\icr29045_000001.d	Acquisition Date	11/22/2017 3:18:56 PM
Method	ESI pos HPmix 200-1800	Instrument	ICR Apex-Qe
Sample Name	MS402	Operator	I.Mitsch
Comment	M. Schultz, EMBL/Schultz: MS402 in MeOH		

Acquisition Parameters

Accumulations	16	Collision Gas Flow Rate	0.5 L/sec	Capillary Entrance	4200.0 V
Broadband Low Mass	173.2 m/z	Collision Energy	0.5 eV	Calibration Date	Wed Oct 25 09:25:50 2017
Broadband High Mass	2500.0 m/z	Collision Cell RF	1200.0 V		
Data Acquisition Size	2097152	Q1 Resolution	5.0		
		Q1 Mass	200.000 m/z		

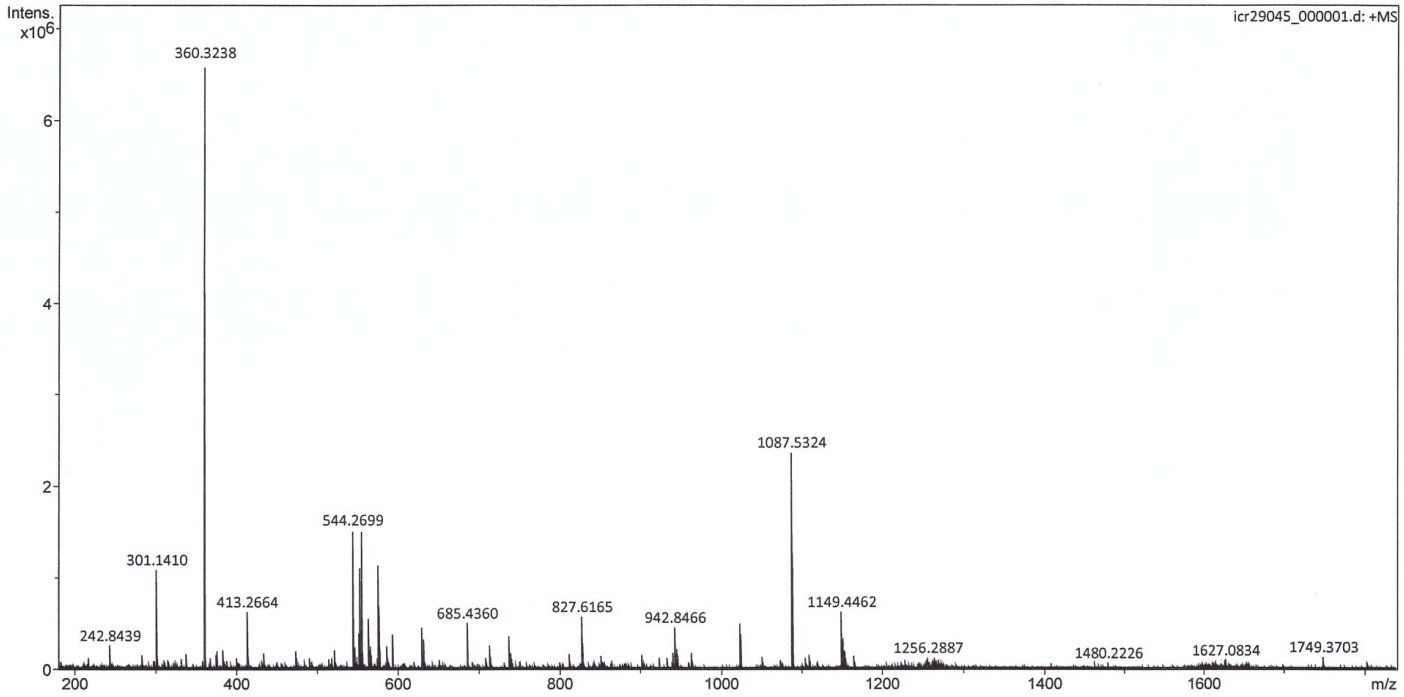

Mass Spectrum Formula Report

Analysis Info

Analysis Name D:\Data\Schultz_EMBL\icr29045_000001.d

Comment M. Schultz, EMBL/Schultz: MS402 in MeOH

Acquisition Date 11/22/2017 3:18:56 PM

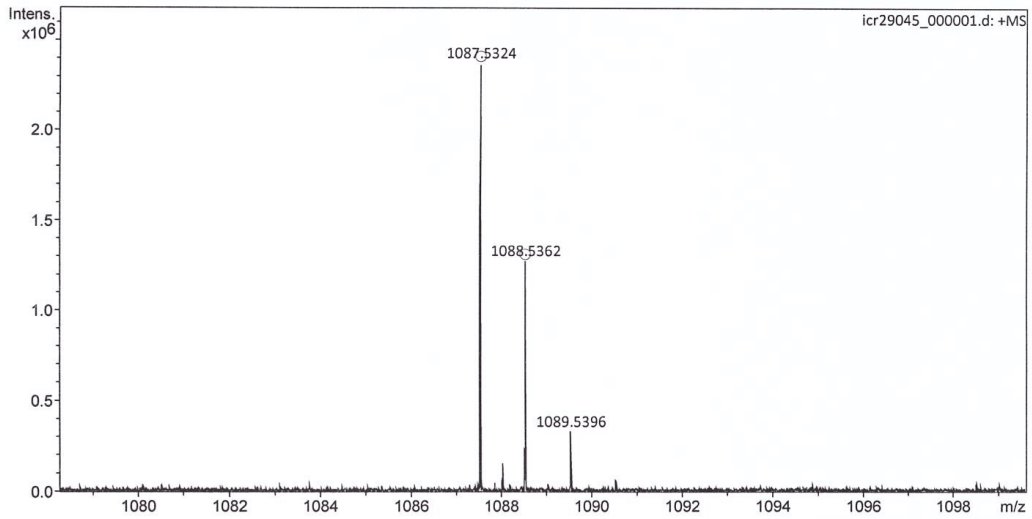

Meas. m/z	Ion Formula	m/z	err [ppm]	mSigma	rdb	e⁻ Conf	N-Rule
1087.5324	C52H77N7O18	1087.5320	-0.4	51.7	18.0	odd	ok
	C52H67N18O9	1087.5333	0.9	62.3	28.5	even	ok
	C52H57N29	1087.5346	2.1	83.8	39.0	odd	ok
1088.5362	C52H78N7O18	1088.5398	3.3	182.9	17.5	even	ok

Donor fragment CAPRee2 und 3:

Expected mass: 1237.77 Da

$[M+1]^+$ exp. 1238.77, found 1238.79

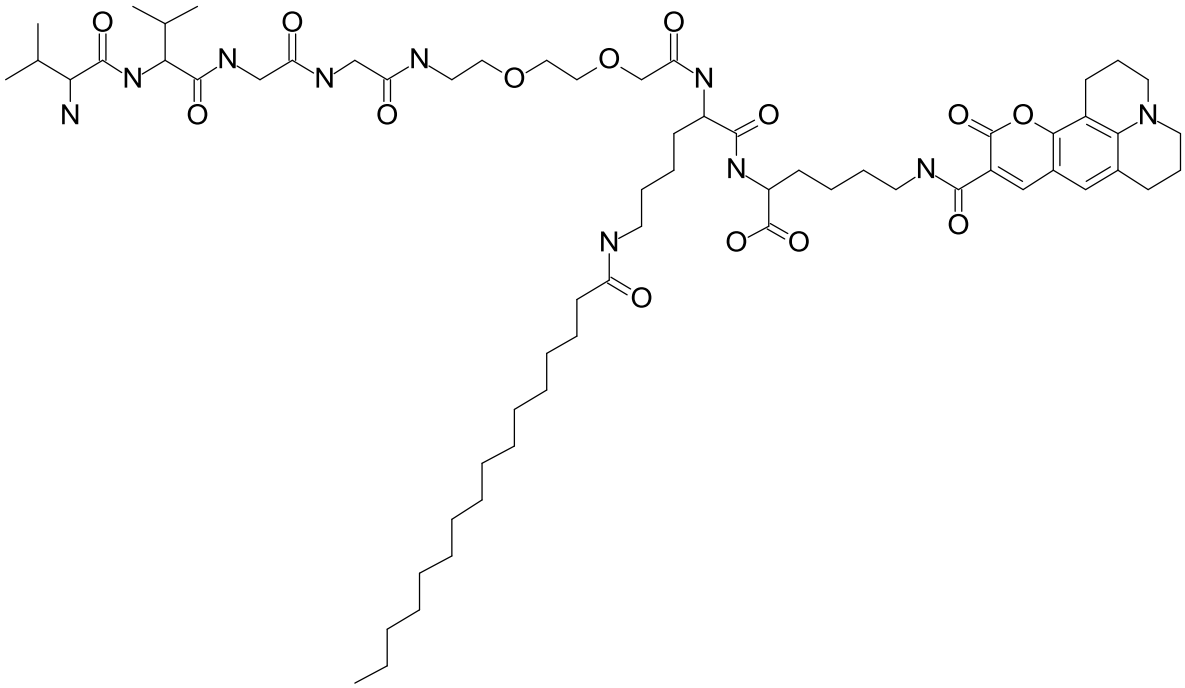

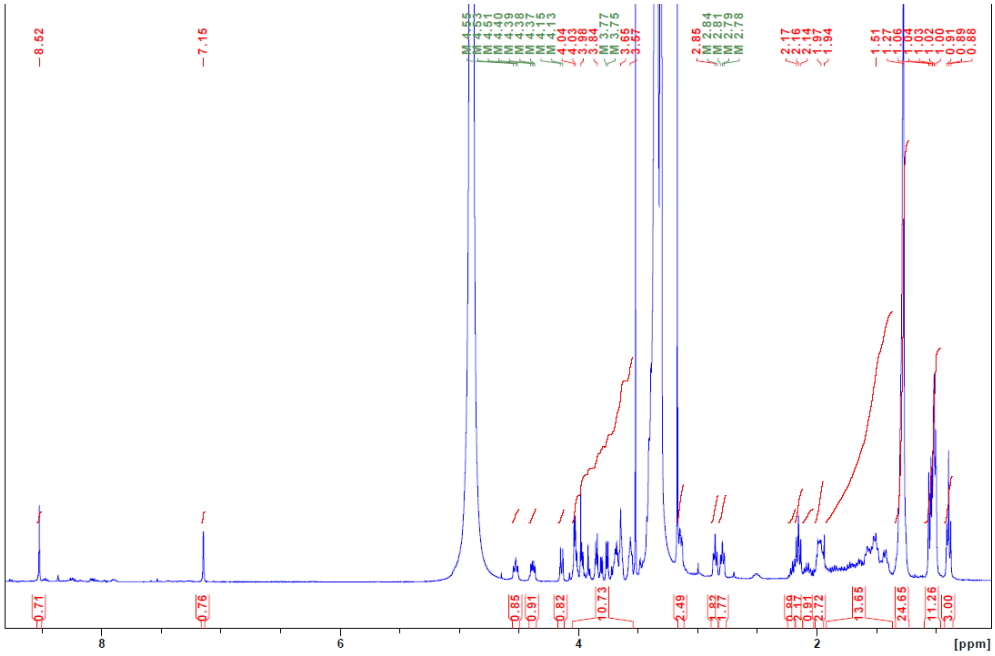

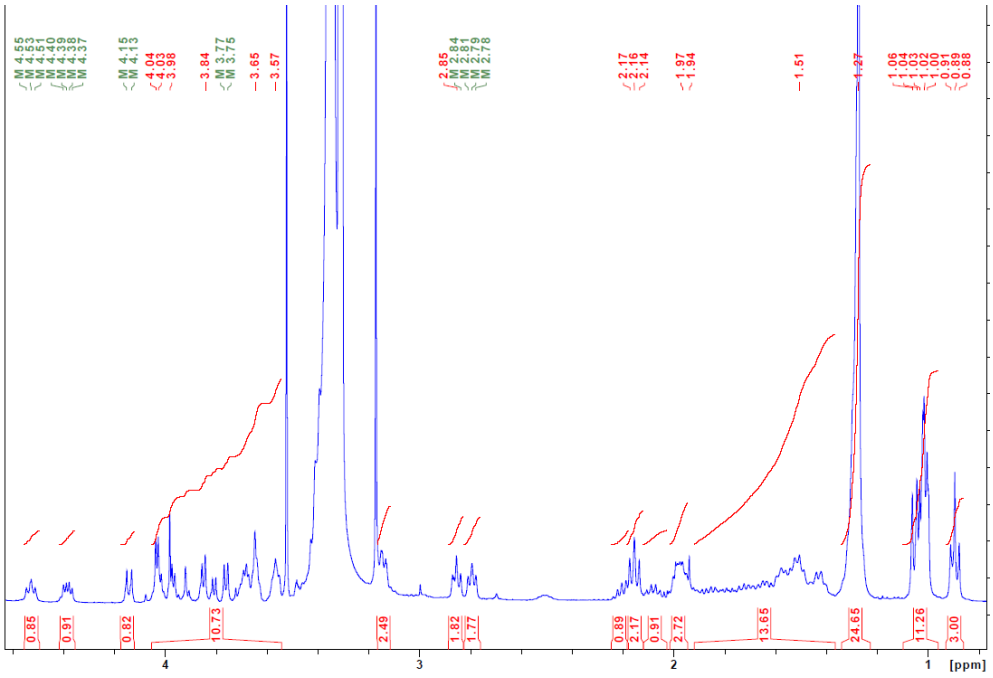

^{1}H NMR spectrum (MeOD, 400 MHz): δ 8.52 (s, 1H, C_4H of Cou), 7.15 (s, 1H, C_5H of Cou), 4.53 (br t, $^{3}J_{HH}$ = 8 Hz, 1H, α-CH of Lys), 4.38 (dd, $^{3}J_{HH}$ = 9 Hz, $^{3}J_{HH}$ = 5 Hz, 1H, α-CH of Lys), 4.14 (d, $^{3}J_{HH}$ = 7 Hz, 1H, α-CH of Val), 4.05 - 3.3 (m, 15H, CH_2 of Gly, peg, OCH_2CON; α-CH of Val; obscured by solvent), 3.4 (m, 4H, NCH_2 of Cou; obscured by solvent), 3.15 (partially obscured m, 4H, NCH_2 of Lys), 2.85 (t, $^{3}J_{HH}$ = 6 Hz, 2H, CH_2 of Cou), 2.7 (t, $^{3}J_{HH}$ = 6 Hz, 2H, CH_2 of Cou), 2.2 (m, 1H, CH of Val), 2.15 (t, $^{3}J_{HH}$ = 7 Hz, 2H, CH_2CO of Palm), 2.1 (m, 1H, CH of Val), 1.95 (m, 4H, CH_2 of Cou), 1.9 - 1.4 (m, 14H, CH_2 of Lys, Palm), 1.27 (br, 24H, CH_2 of Palm), 1.1 - 1.0 (m, 12H, CH_3 of Val), 0.89 (t, $^{3}J_{HH}$ = 7 Hz, 3H, CH_3 of Palm).

Analysis Info

Analysis Name	D:\Data\Schultz_EMBL\icr29463_000001.d	Acquisition Date	1/16/2018 2:36:02 PM
Method	ESI pos HPmix 200-1800	Instrument	ICR Apex-Qe
Sample Name	MS407	Operator	D.Lang
Comment	Schultz, AK Schultz (EMBL): MS407 in MeOH		

Acquisition Parameters

Accumulations	16	Collision Gas Flow Rate	0.5 L/sec	Capillary Entrance	4200.0 V
Broadband Low Mass	173.2 m/z	Collision Energy	0.5 eV	Calibration Date	Tue Jan 2 09:15:53 2018
Broadband High Mass	2500.0 m/z	Collision Cell RF	1200.0 V		
Data Acquisition Size	2097152	Q1 Resolution	5.0		
		Q1 Mass	200.000 m/z		

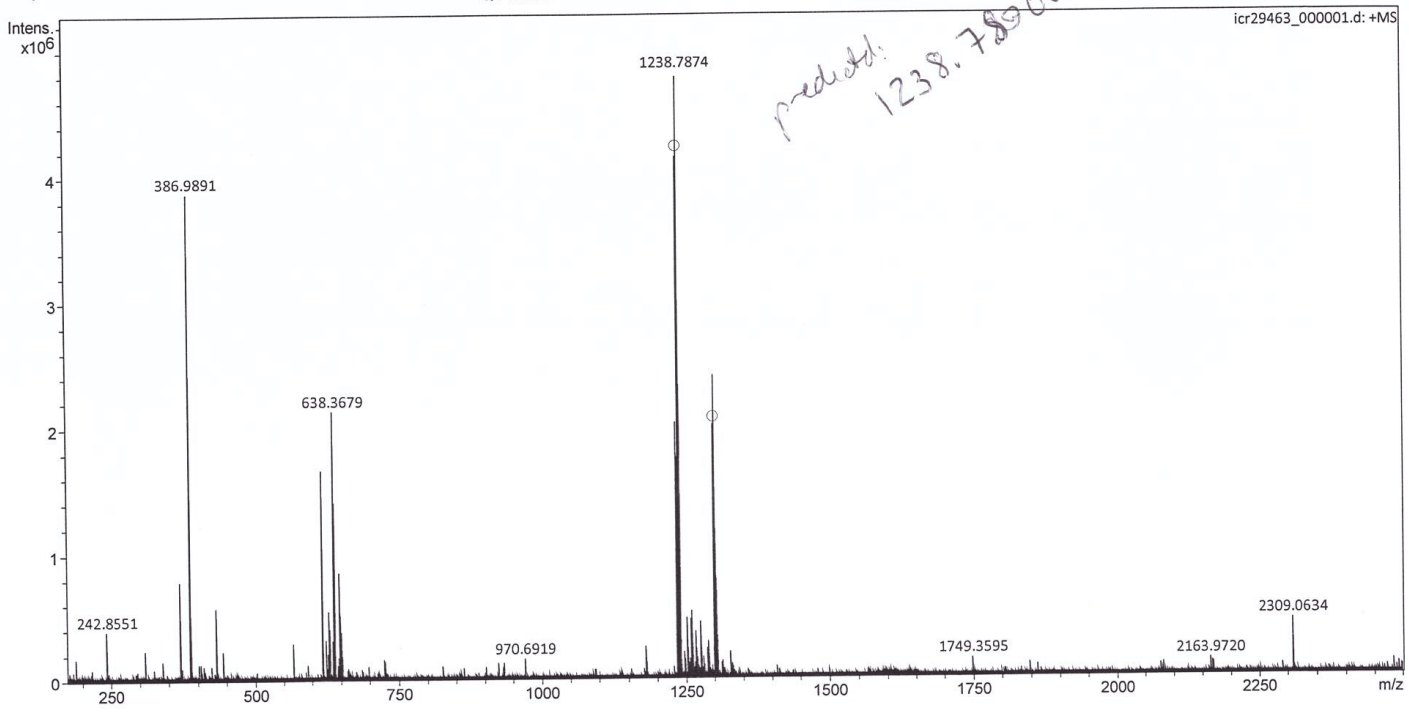

Mass Spectrum Formula Report

Analysis Info Acquisition Date 1/16/2018 2:36:02 PM

Analysis Name D:\Data\Schultz_EMBL\icr29463_000001.d

Comment Schultz, AK Schultz (EMBL): MS407 in MeOH

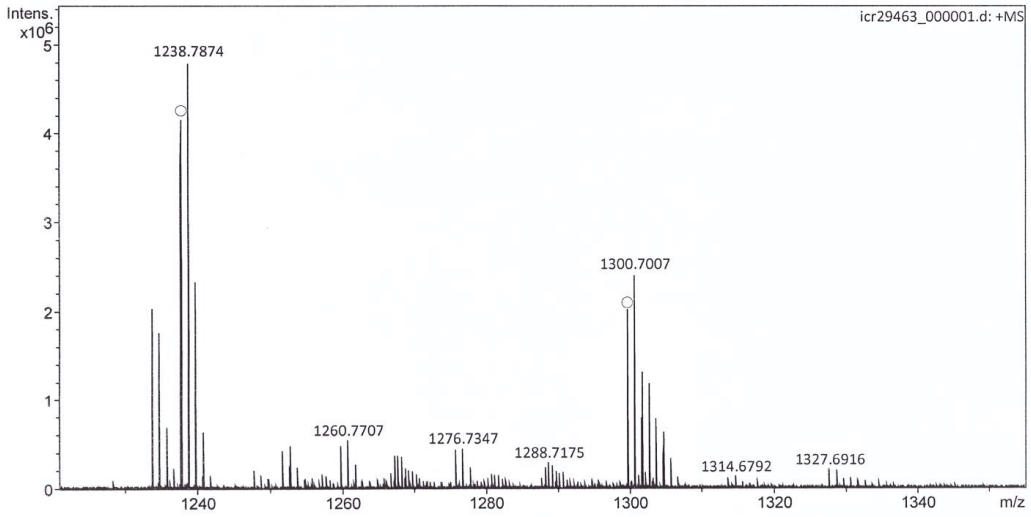

Meas. m/z	Ion Formula	m/z	err [ppm]	mSigma	rdb	e⁻ Conf	N-Rule
1237.7828	C64H105N10O14	1237.7806	-1.8	152.6	17.5	even	ok
1299.6964	C65H95N12O16	1299.6984	1.5	277.0	24.5	even	ok
	C60H95N14O18	1299.6943	-1.6	294.0	20.5	even	ok

TAMRA-peg-azide:

Expected mass: 700.3095, found: 700.3102

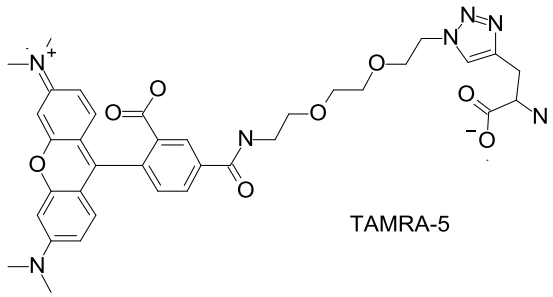

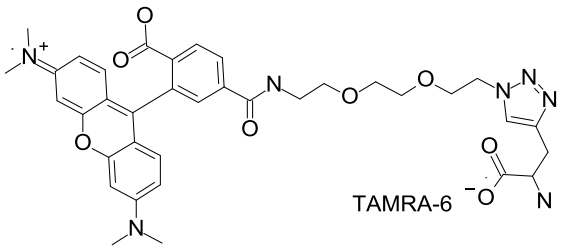

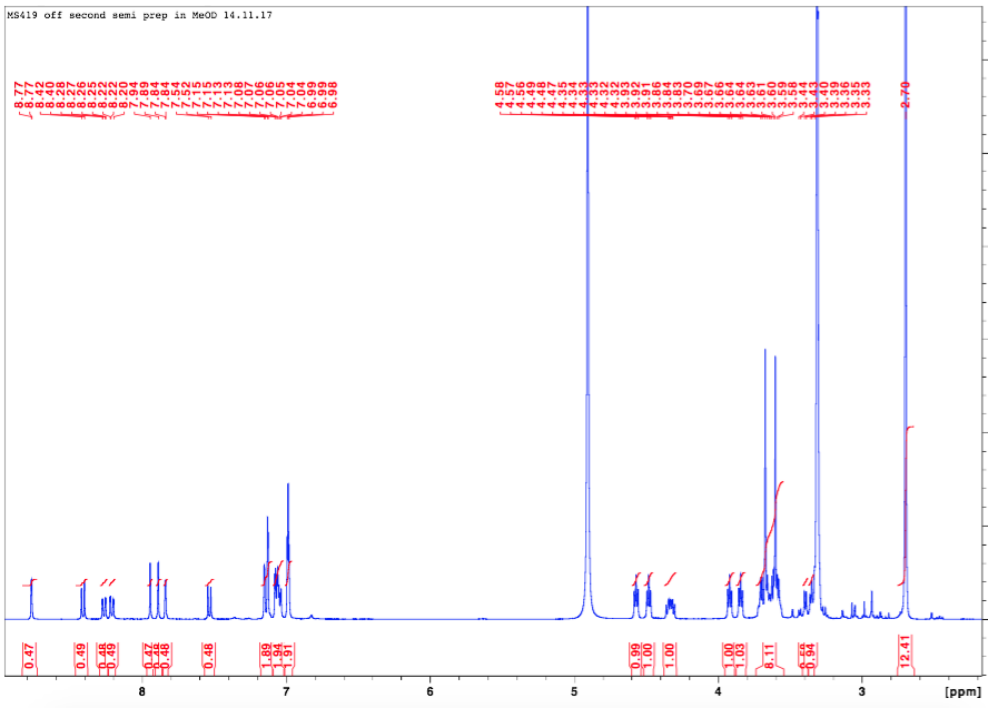

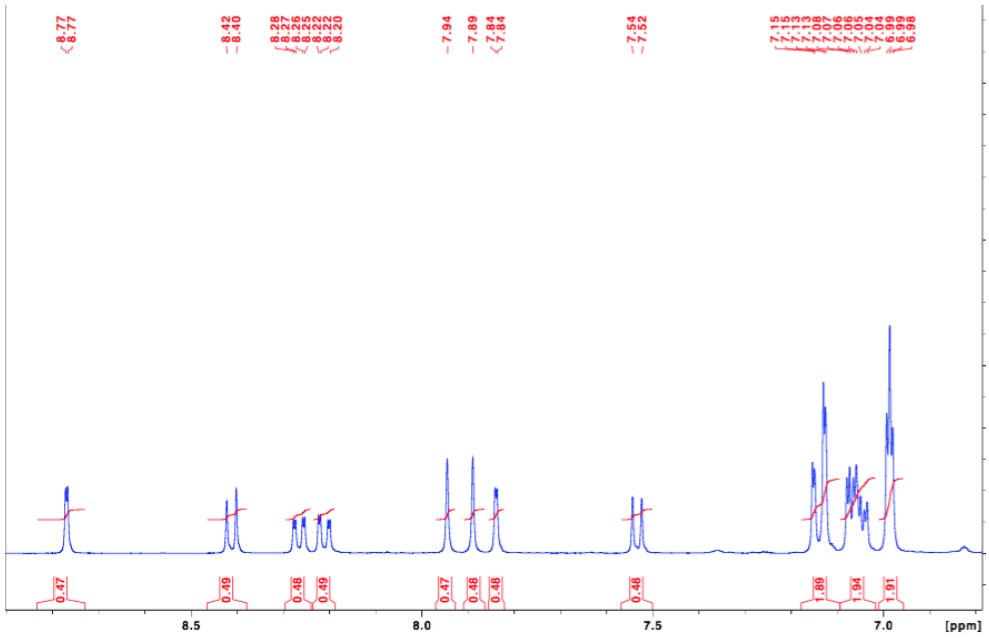

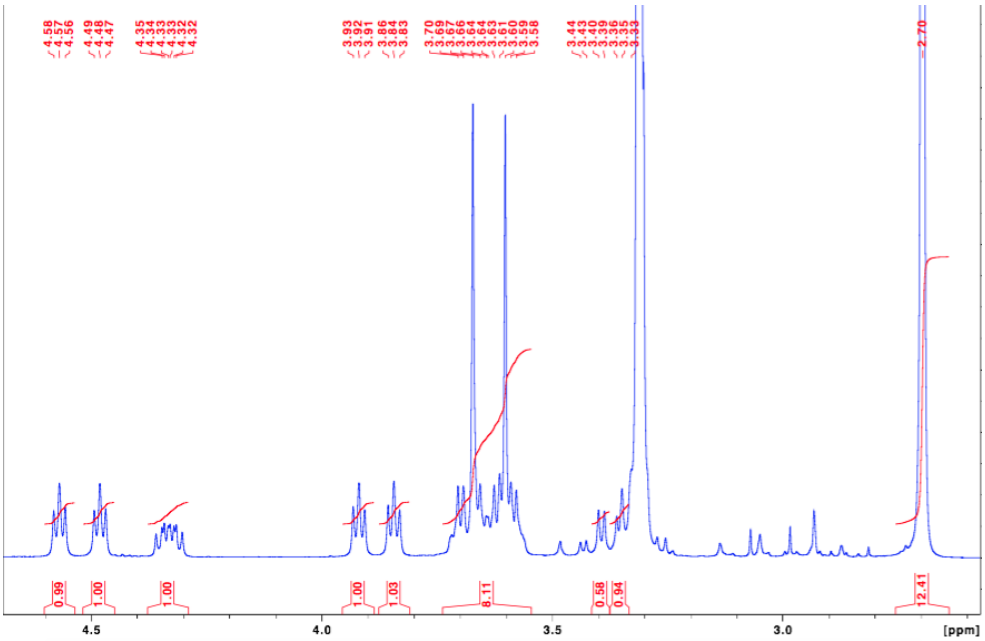

^{1}H NMR spectrum (MeOD, 400 MHz): δ 8.77 (d, $^{4}J_{HH}$ = 2 Hz, 0.5H, TAMRA isomer), 8.41 (d, $^{3}J_{HH}$ = 8 Hz, 0.5H, TAMRA isomer), 8.26 (dd, $^{3}J_{HH}$ = 8 Hz, $^{4}J_{HH}$ = 2 Hz, 0.5H, TAMRA isomer), 8.21 (dd, $^{3}J_{HH}$ = 8 Hz, $^{4}J_{HH}$ = 2 Hz, 0.5H, TAMRA isomer), 7.94 (s, 0.5H, ring N_3CCH isomer), 7.89 (s, 0.5H, ring N_3CCH isomer), 7.84 (d, $^{4}J_{HH}$ = 2 Hz, 0.5H, TAMRA isomer), 7.53 (d, $^{3}J_{HH}$ = 8 Hz, 0.5H, TAMRA isomer), 7.15 (m, 2H, TAMRA both isomers), 7.06 (m, 2H, TAMRA both isomers), 6.99 (pseudo t, 2H, TAMRA both isomers), 4.57 (t, $^{3}J_{HH}$ = 5 Hz, 1H, N_3CH_2 isomer), 4.48 (t, $^{3}J_{HH}$ = 5 Hz, 1H, N_3CH_2 isomer), 4.30 - 4.36 (m, 1H, Prg-αCH both isomers), 3.92 (t, 1H, $^{3}J_{HH}$ = 5 Hz, $N_3CH_2C\underline{H}_2$ isomer), 3.84 (t, $^{3}J_{HH}$ = 5 Hz, 1H, $N_3CH_2C\underline{H}_2$ isomer), 3.75 - 3.5 (m, 8H, remaining pegCH$_2$), 3.44 - 3.3 (partially obscured by methanol, m, 2H, Prg-CH$_2$ both isomers), 2.7 (s, 12H, TAMRA-Me both isomers).

Acceptor fragment CAPRee6:

Expected mass: 1156.56 Da

$[M+1]^{+}$ exp. 1157.56, found 1157.56, $[M+2]^{2+}$ exp. 579.78, found 579.28

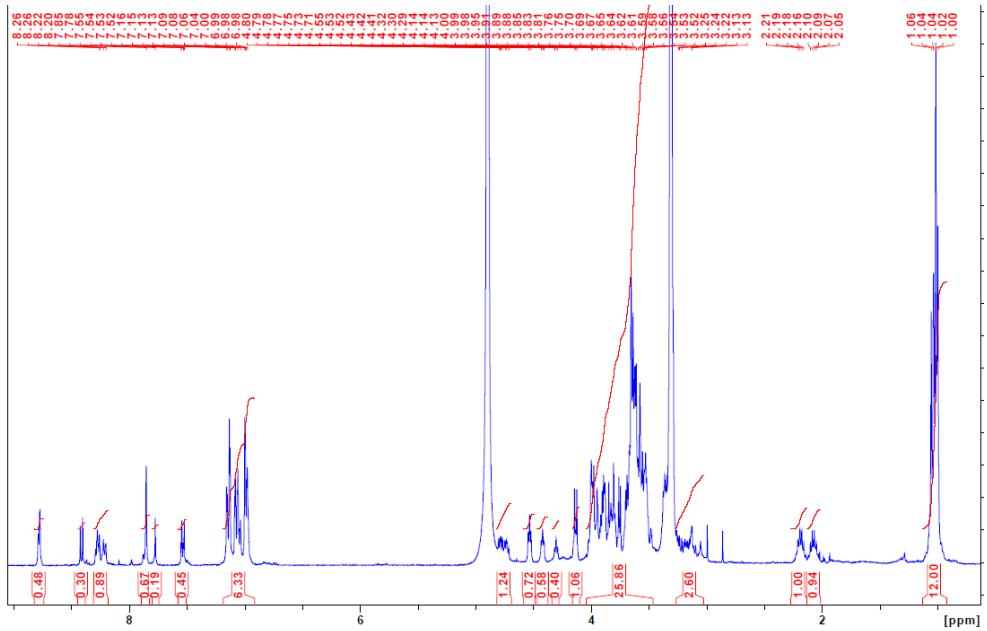

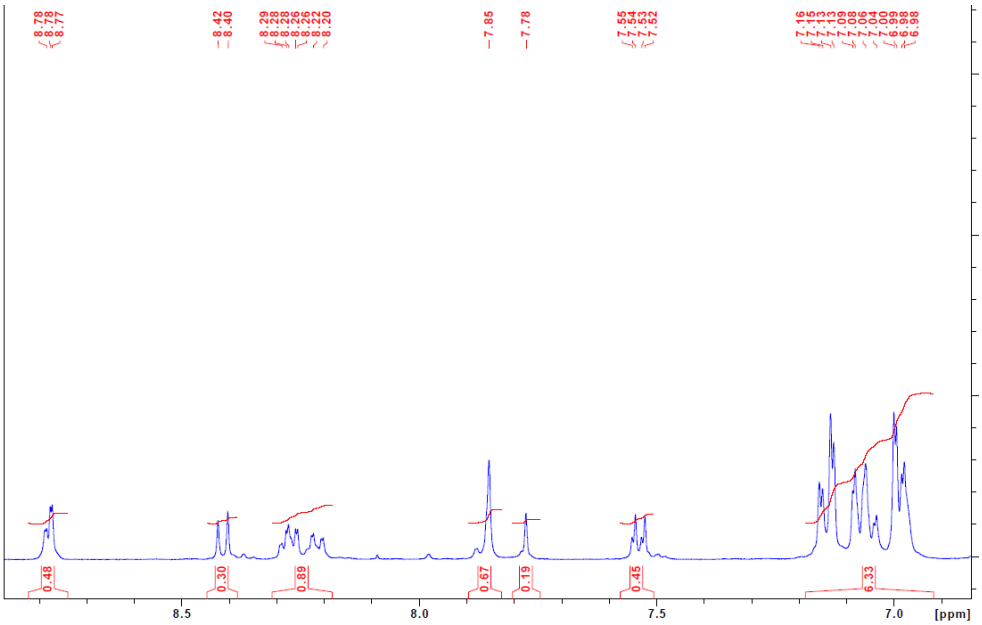

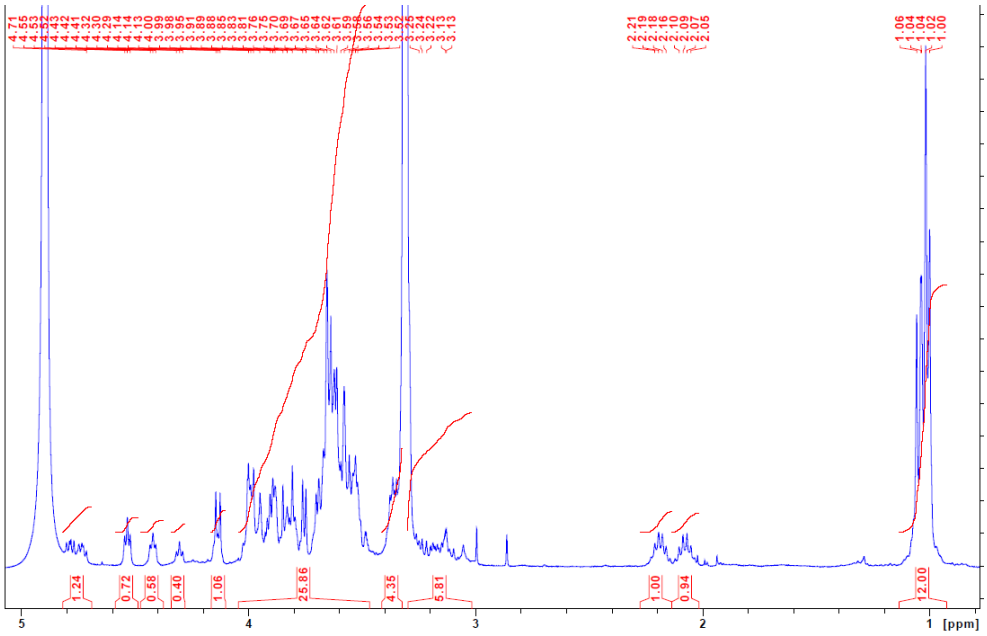

^{1}H NMR spectrum (MeOD, 400 MHz): δ 8.78 (m, 0.6H, TAMRA isomer), 8.40 (d, $^{3}J_{HH}$ = 8 Hz, 0.4H, TAMRA isomer), 8.26 (m, 1H, TAMRA both isomers), 7.85 (s, 1H, ring $N_3CC\underline{H}$), 7.78 (s, 0.4H, TAMRA isomer), 7.53 (m, 0.6H, TAMRA isomer), 7.2 - 6.9 (m, 6H, TAMRA both isomers), 4.75 (m, 1H, α-CH of Prg, both isomers), 4.53 (t, $^{3}J_{HH}$ = 5 Hz, 1H, N_3CH_2 isomers), 4.42 (t, $^{3}J_{HH}$ = 5 Hz, 0.6H, N_3CH_2 isomer), 4.30 (t, $^{3}J_{HH}$ = 5 Hz, 0.4H, N_3CH_2 isomer), 4.14 (d, $^{3}J_{HH}$ = 8 Hz, 1H, α-CH of Val), 4.0 - 3.5 (m, 25H, CH_2 of Gly, peg, OCH_2CON; α-CH of Val), 3.3-3.0 (m, 14H, Prg-CH_2 both isomers and NMe_2 protons of TAMRA obscured by solvent), 2.19 (heptet, $^{3}J_{HH}$ = 6.5 Hz, 1H, Val-CH), 2.08 (heptet, $^{3}J_{HH}$ = 7 Hz, 1H, Val-CH), 1.05 - 0.95 (m, 12H, Val-CH_3).

VR74

Analysis Info

Analysis Name	D:\Data\Schultz_EMBL\icr29072_000001.d	Acquisition Date	11/24/2017 9:24:55 AM
Method	ESI pos HPmix 200-1800	Instrument	ICR Apex-Qe
Sample Name	MS404	Operator	I.Mitsch
Comment	M.Schultz,EMBL/Schultz: MS404 in MeOH		

Acquisition Parameters

Accumulations	16	Collision Gas Flow Rate	0.5 L/sec	Capillary Entrance	4200.0 V
Broadband Low Mass	173.2 m/z	Collision Energy	0.5 eV	Calibration Date	Wed Oct 25 09:25:50 2017
Broadband High Mass	2500.0 m/z	Collision Cell RF	1200.0 V		
Data Acquisition Size	2097152	Q1 Resolution	5.0		
		Q1 Mass	200.000 m/z		

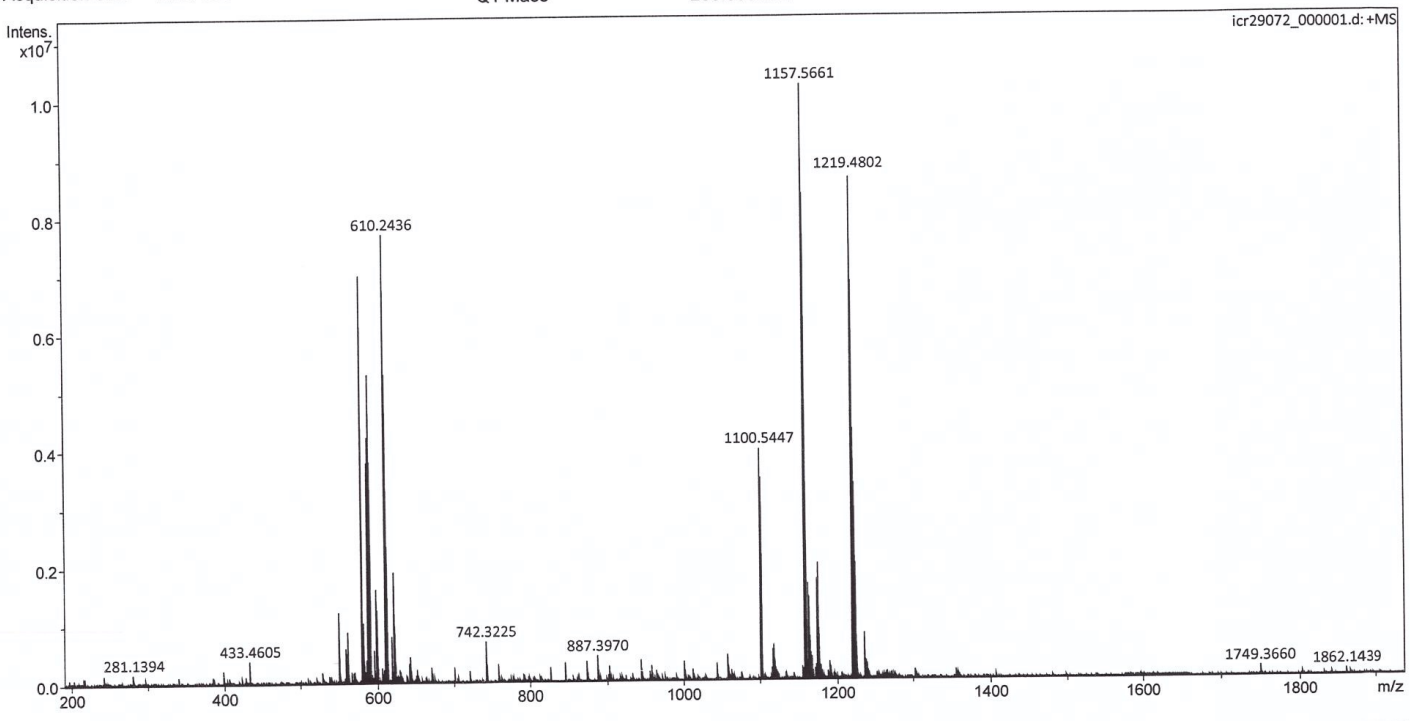

Analysis Info

Analysis Name	D:\Data\Schultz_EMBL\icr29072_000001.d	Acquisition Date	11/24/2017 9:24:55 AM
Method	ESI pos HPmix 200-1800	Instrument	ICR Apex-Qe
Sample Name	MS404	Operator	I.Mitsch
Comment	M.Schultz,EMBL/Schultz: MS404 in MeOH		

Acquisition Parameters

Accumulations	16	Collision Gas Flow Rate	0.5 L/sec	Capillary Entrance	4200.0 V
Broadband Low Mass	173.2 m/z	Collision Energy	0.5 eV	Calibration Date	Wed Oct 25 09:25:50 2017
Broadband High Mass	2500.0 m/z	Collision Cell RF	1200.0 V		
Data Acquisition Size	2097152	Q1 Resolution	5.0		
		Q1 Mass	200.000 m/z		

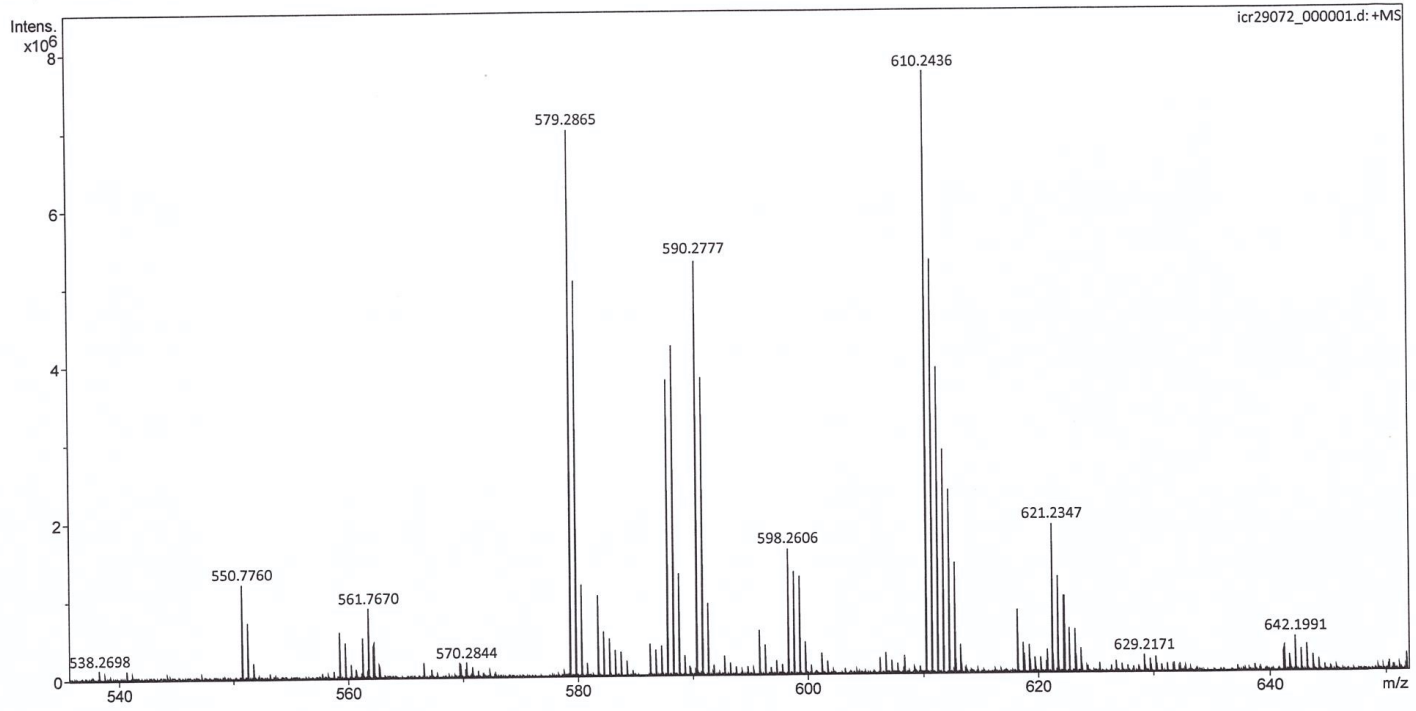

Spectrum Display Report Bruker Compass DataAnalysis 4.3 printed: 11/24/2017 9:29:15 AM Page 1 of 1

Analysis Info

Analysis Name	D:\Data\Schultz_EMBL\icr29072_000001.d	Acquisition Date	11/24/2017 9:24:55 AM
Method	ESI pos HPmix 200-1800	Instrument	ICR Apex-Qe
Sample Name	MS404	Operator	I.Mitsch
Comment	M.Schultz,EMBL/Schultz: MS404 in MeOH		

Acquisition Parameters

Accumulations	16	Collision Gas Flow Rate	0.5 L/sec	Capillary Entrance	4200.0 V
Broadband Low Mass	173.2 m/z	Collision Energy	0.5 eV	Calibration Date	Wed Oct 25 09:25:50 2017
Broadband High Mass	2500.0 m/z	Collision Cell RF	1200.0 V		
Data Acquisition Size	2097152	Q1 Resolution	5.0		
		Q1 Mass	200.000 m/z		

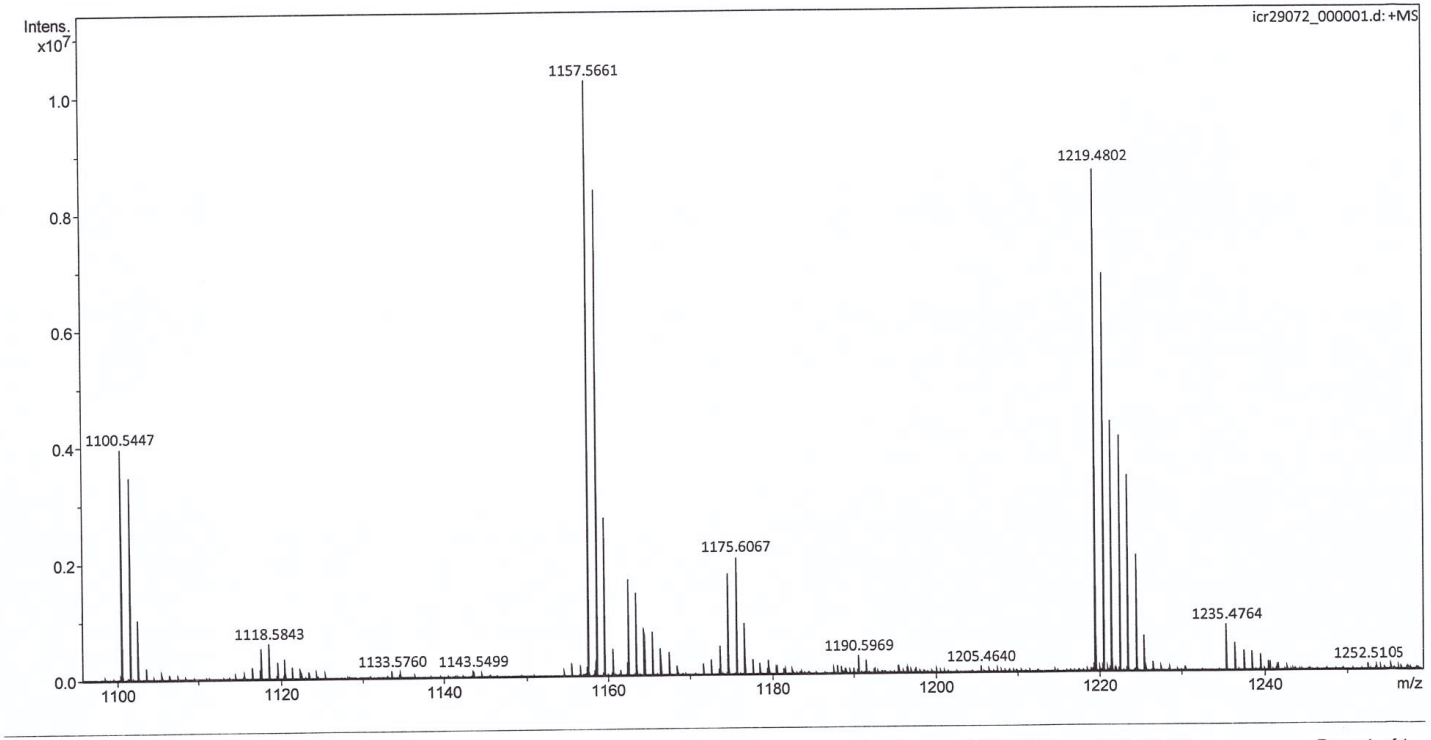

Spectrum Display Report Bruker Compass DataAnalysis 4.3 printed: 11/24/2017 9:29:29 AM Page 1 of 1

Donor fragment CAPRee6:

Expected mass: 1364.898 Da

$[M+1]^+$ exp. 1365.898, found 1365.901, $[M+2]^{2+}$ exp. 683.449, found 682.45

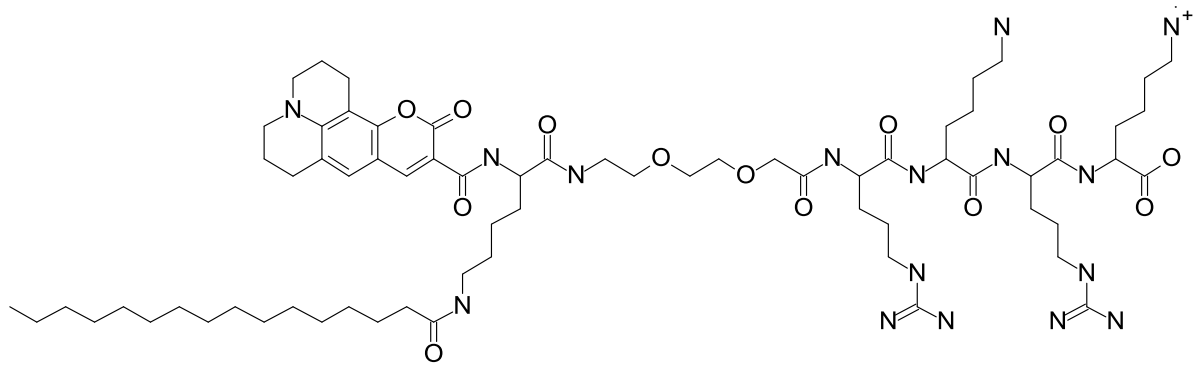

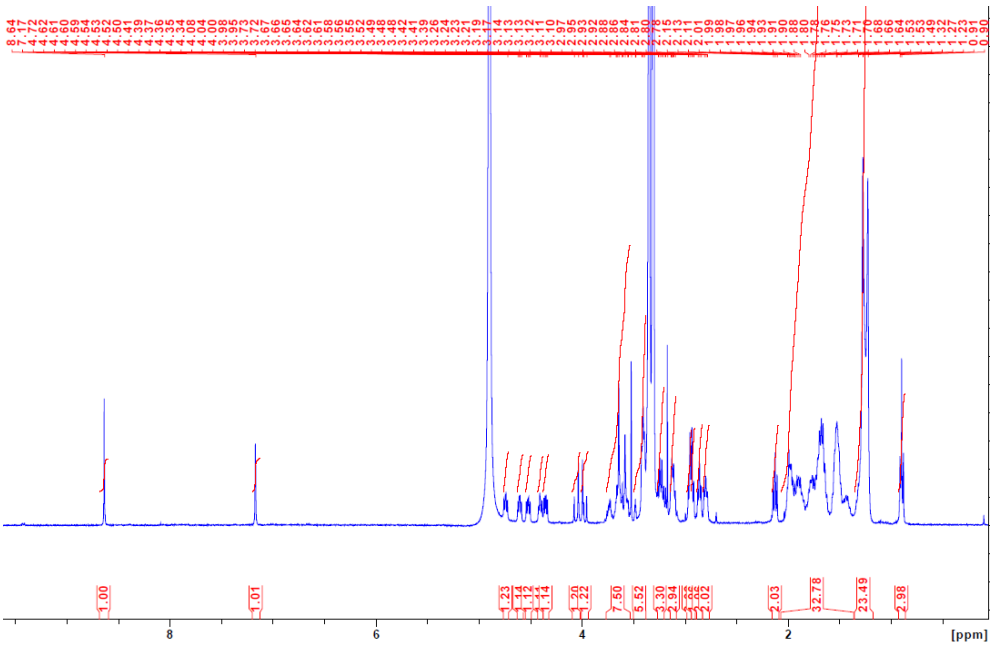

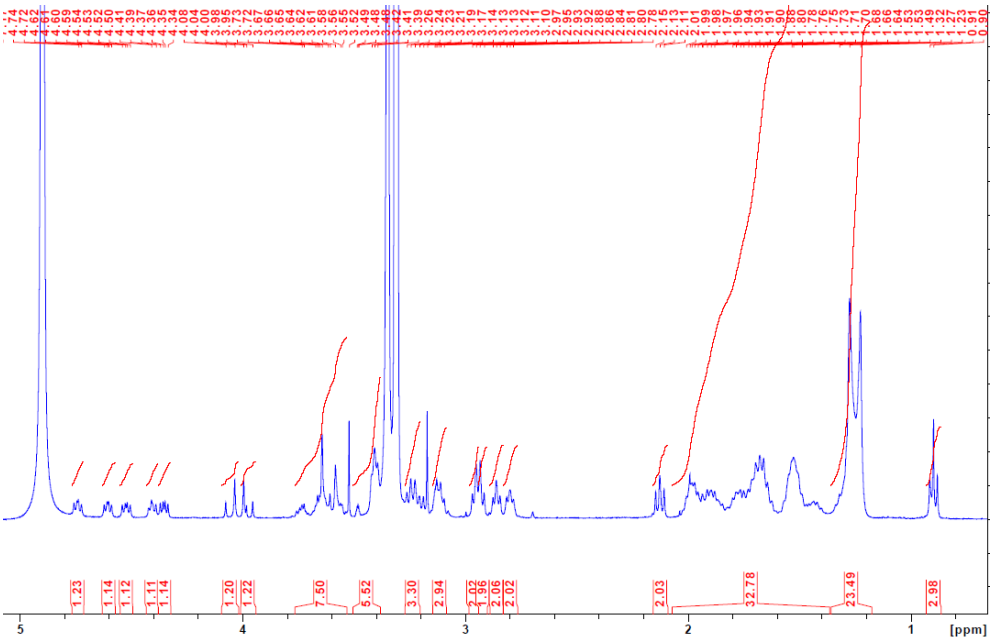

^{1}H NMR spectrum (MeOD, 400 MHz): δ 8.64 (s, 1H, C_4H of Cou), 7.17 (s, 1H, C_5H of Cou), 4.72 (dd, $^{3}J_{HH}$ = 8 Hz, $^{3}J_{HH}$ = 6 Hz, 1H, α-CH), 4.61 (dd, $^{3}J_{HH}$ = 8 Hz, $^{3}J_{HH}$ = 5 Hz, 1H, α-CH), 4.52 (dd, $^{3}J_{HH}$ = 9 Hz, $^{3}J_{HH}$ = 5 Hz, 1H, α-CH), 4.40 (unresolved dd, $^{3}J_{HH}$ = 8 Hz, 1H, α-CH), 4.35 (dd, $^{3}J_{HH}$ = 9 Hz, $^{3}J_{HH}$ = 5 Hz, 1H, α-CH), 4.05 (d, $^{2}J_{HH}$ = 16 Hz, 1H, OCH_2CON), 3.97 (d, $^{2}J_{HH}$ = 16 Hz, 1H, OCH_2CON), 3.8 - 3.3 (m, 12H, peg; NCH_2 of Cou), 3.3 - 3.1 (m, 6H, NCH_2 of Arg and (Palm)Lys), 2.96 (t, $^{3}J_{HH}$ = 7 Hz, 2H, NCH_2 of Lys), 2.92 (t, $^{3}J_{HH}$ = 7 Hz, 2H, NCH_2 of Lys), 2.86 (t, $^{3}J_{HH}$ = 6 Hz, 2H, CH_2 of Cou), 2.80 (t, $^{3}J_{HH}$ = 6 Hz, 2H, CH_2 of Cou), 2.12 (t, $^{3}J_{HH}$ = 7 Hz, 2H, CH_2CO of Palm), 2.0 - 1.7 (m, 32H, CH_2 of Cou, Arg, Lys, Palm), 1.3 - 1.2 (m, 24H, Palm), 0.9 (t, $^{3}J_{HH}$ = 7 Hz, 3H, CH_3 of Palm).

Analysis Info

Analysis Name	D:\Data\Schultz_EMBL\icr29073_000001.d	Acquisition Date	11/24/2017 9:38:01 AM
Method	ESI pos HPmix 200-1800	Instrument	ICR Apex-Qe
Sample Name	MS409	Operator	I.Mitsch
Comment	M.Schultz,EMBL/Schultz: MS409 in MeOH		

Acquisition Parameters

Accumulations	16	Collision Gas Flow Rate	0.5 L/sec	Capillary Entrance	4200.0 V
Broadband Low Mass	173.2 m/z	Collision Energy	0.5 eV	Calibration Date	Wed Oct 25 09:25:50 2017
Broadband High Mass	2500.0 m/z	Collision Cell RF	1200.0 V		
Data Acquisition Size	2097152	Q1 Resolution	5.0		
		Q1 Mass	200.000 m/z		

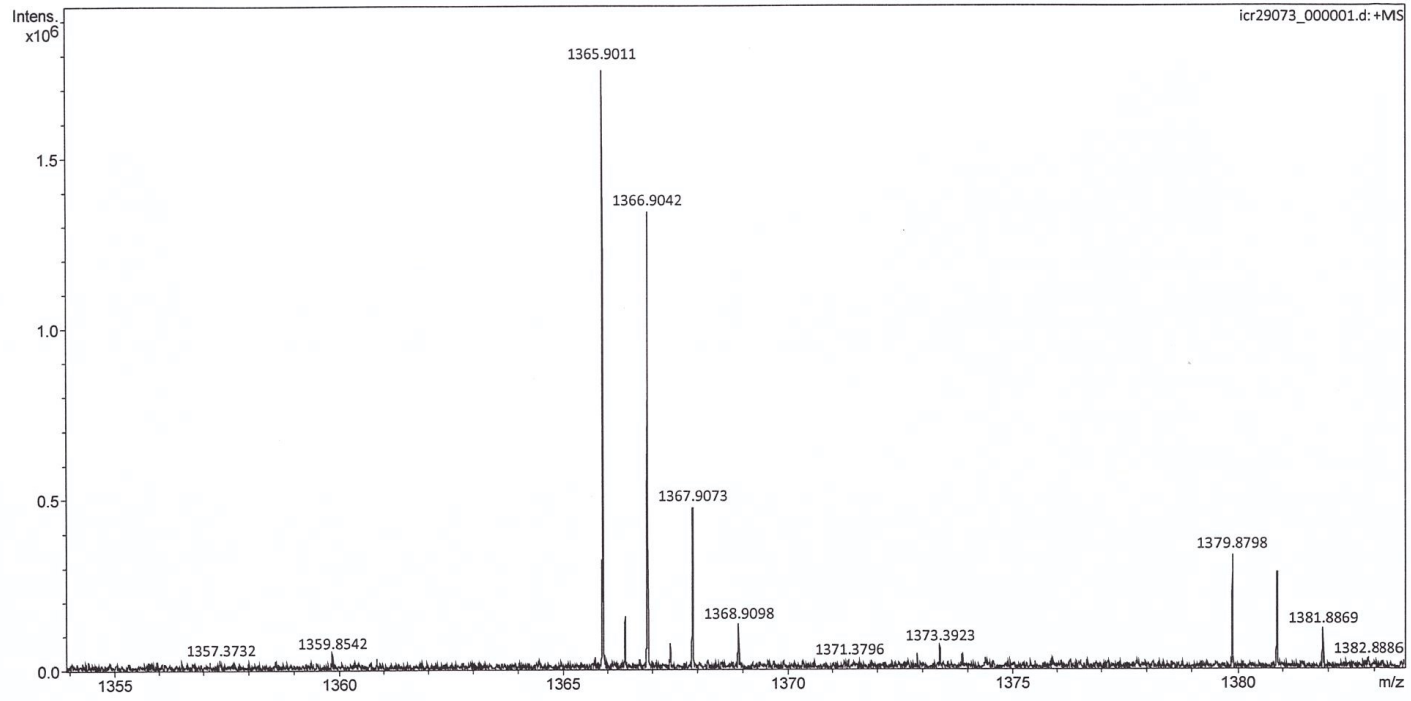

Spectrum Display Report Bruker Compass DataAnalysis 4.3 printed: 11/24/2017 9:40:47 AM Page 1 of 1

VRZ3

Analysis Info

Analysis Name	D:\Data\Schultz_EMBL\icr29073_000001.d	Acquisition Date	11/24/2017 9:38:01 AM
Method	ESI pos HPmix 200-1800	Instrument	ICR Apex-Qe
Sample Name	MS409	Operator	I.Mitsch
Comment	M.Schultz,EMBL/Schultz: MS409 in MeOH		

Acquisition Parameters

Accumulations	16	Collision Gas Flow Rate	0.5 L/sec	Capillary Entrance	4200.0 V
Broadband Low Mass	173.2 m/z	Collision Energy	0.5 eV	Calibration Date	Wed Oct 25 09:25:50 2017
Broadband High Mass	2500.0 m/z	Collision Cell RF	1200.0 V		
Data Acquisition Size	2097152	Q1 Resolution	5.0		
		Q1 Mass	200.000 m/z		

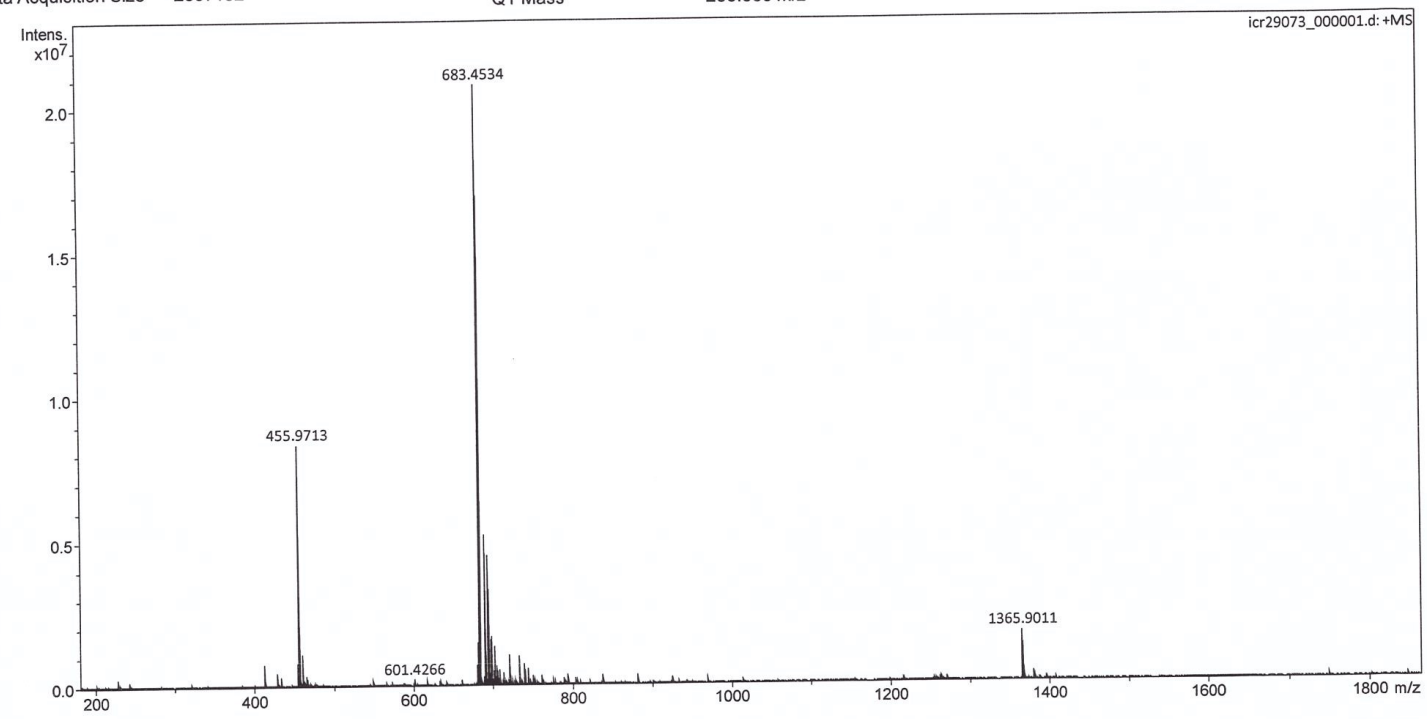

Spectrum Display Report Bruker Compass DataAnalysis 4.3 printed: 11/24/2017 9:40:15 AM Page 1 of 1

Mass Spectrum Formula Report

Analysis Info

Analysis Name	D:\Data\Schultz_EMBL\icr29073_000001.d	Acquisition Date	11/24/2017 9:38:01 AM
Comment	M.Schultz,EMBL/Schultz: MS409 in MeOH		

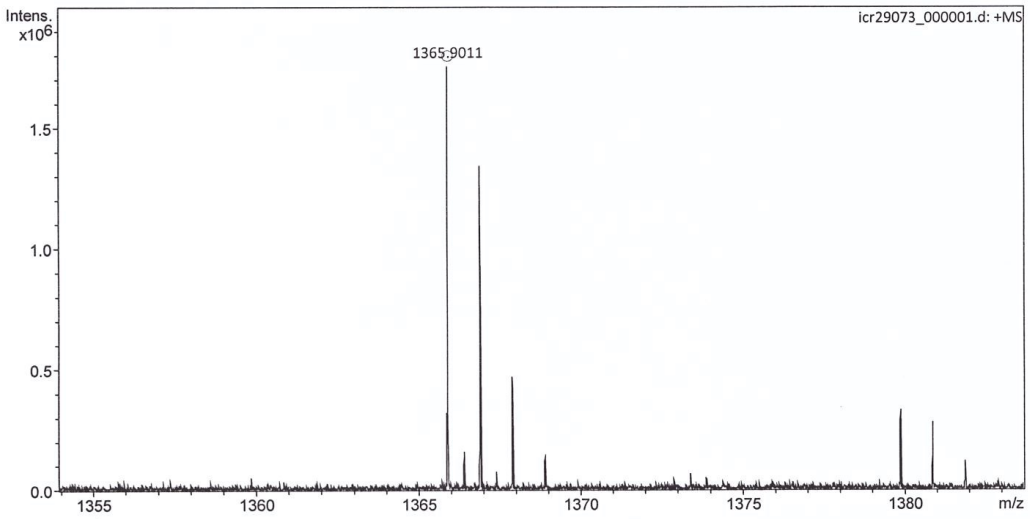

Meas. m/z	Ion Formula	m/z	err [ppm]	mSigma	rdb	e⁻ Conf	N-Rule
1365.9011	C68H127N5O22	1365.8967	-3.2	60.7	8.0	odd	ok
	C68H8NO33	1365.8973	-2.8	65.0	65.5	even	ok
	C68H117N16O13	1365.8981	-2.3	66.0	18.5	even	ok
	C68H107N27O4	1365.8994	-1.3	74.8	29.0	odd	ok

Bruker Compass DataAnalysis 4.3 printed: 11/24/2017 9:43:00 AM Page 1 of 1

Publications

Rickert V., Haefeli W.E., and Weiss J. (2014). Pharmacokinetic interaction profile of riociguat, a new soluble guanylate cyclase stimulator, in vitro. Pulm Pharmacol Ther. 2014 Aug;28(2):130-7.

Rickert-Zacharias V., Schultz C. and Mall M.A. (2016). A Protease Inhibitor Tackles Epithelial Sodium Channels in Cystic Fibrosis. Am. J. Respir. Crit. Care Med. 194(6):650-652. (Editorial)

Dittrich A.S., Kühbandner I., Gehrig S., Rickert-Zacharias V., Twigg M., Wege S., Taggart C.C., Herth F., Schultz C. and Mall M.A. (2018) Elastase activity on sputum neutrophils correlates with severity of lung disease in cystic fibrosis. Eur Respir J 51(3)

Manuscript submitted/in preparation

Rickert-Zacharias V., Schultz M., Mall M.A. and Schultz C.

Acknowledgements

I want to thank my supervisors Dr. Carsten Schultz and Prof. Dr. Marcus Mall for their support during my entire PhD, for sharing their expertise and their ideas and critical thinking on the progress of the project.

I want to thank the members of both labs for the inspiring atmosphere in the labs and support with technical questions. Special thanks to Dr. Madeleine Schultz who had always friendly ear for all kinds of chemical questions and supported my work with synthesis of probe fragments as well as their full characterization and the submission of all other samples to the High Resolution Mass Spectrometry Facility at the OCI Heidelberg. Further thanks to Dr. Frank Stein who was a great support with image and data analysis. Together with Jonas Wilhelm, he synthesized and purified the probes CAPRee4 and 5. Heike Scheuermann thankfully cultured human nasal epithelial cells as well as supported the culture of cell lines. Thanks to Marko Lampe and A Aliaksandr Halavatyi for their support with the microscope.

Many thanks to my TAC members Dr. Anne-Claude Gavin, Dr. Marko Kaksonen and Prof. Dr. Ralf Bartenschlager their interest in my work and their helpful suggestions during TAC meetings.

Außerdem danke ich meinem Mann Marko für die großartige Unterstützung während meiner Arbeit und meinen Kindern Emilia und Silas, die mein Leben reicher machen.

Addendum: Overview of all structures

CAPRee1:

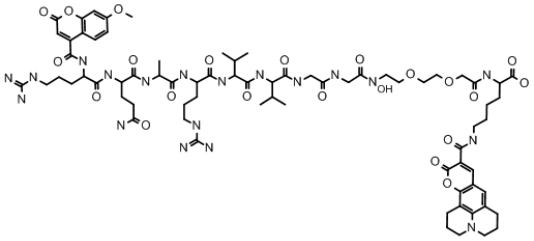

CAPree1_a:

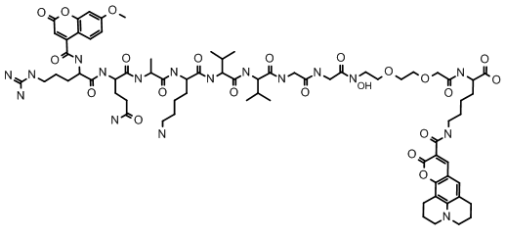

CAPRee1_b:

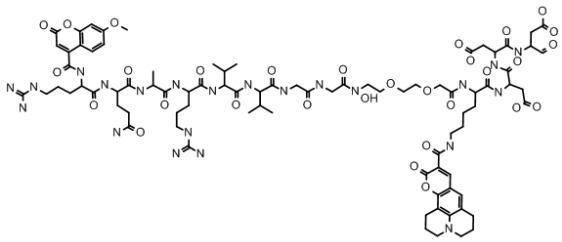

CAPRee1_c:

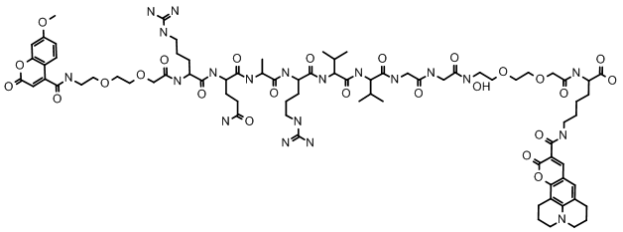

CAPRee1_d:

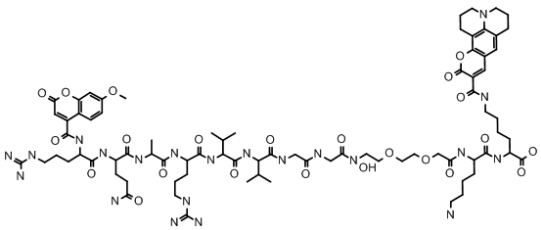

CAPRee2:

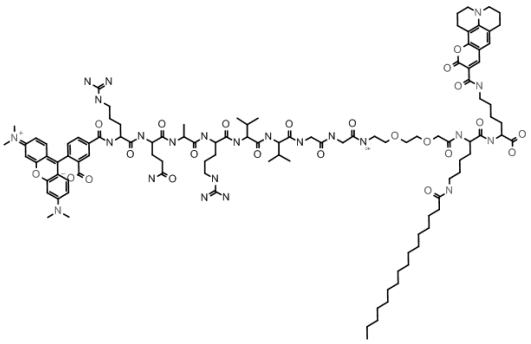

CAPRee2_a:

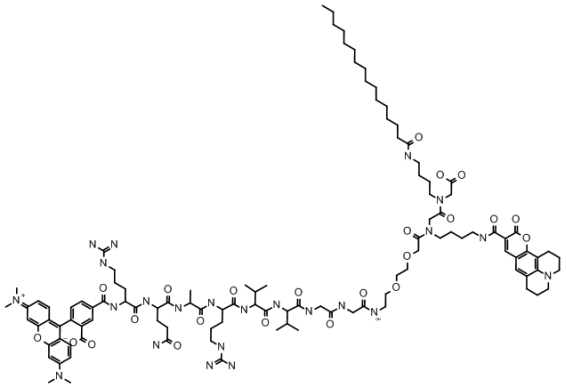

CAPRee2_b

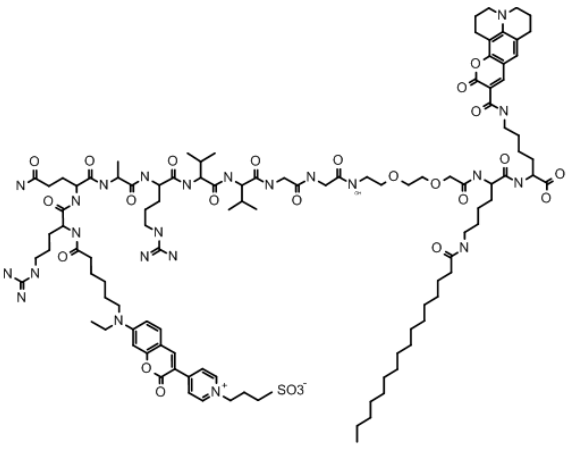

CAPRee2_c:

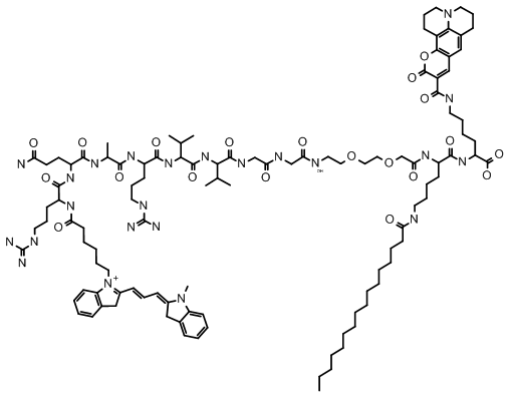

CAPRee3:

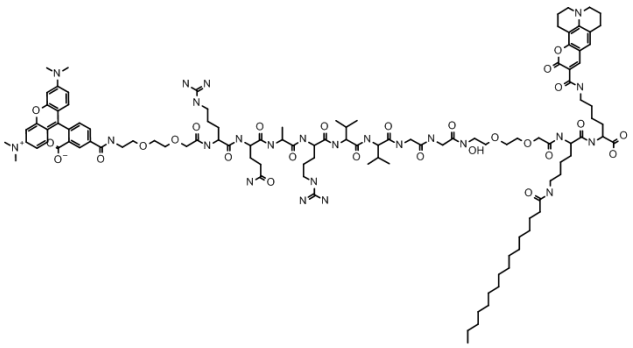

CAPRee4:

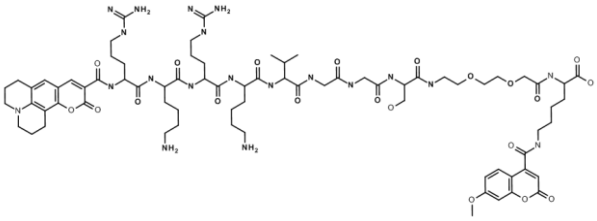

CAPRee5:

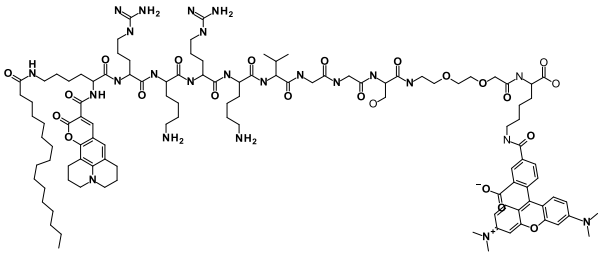

CAPRee6: